# Applied Nanotechnology & Nanotoxicology

*Book of Abstracts*

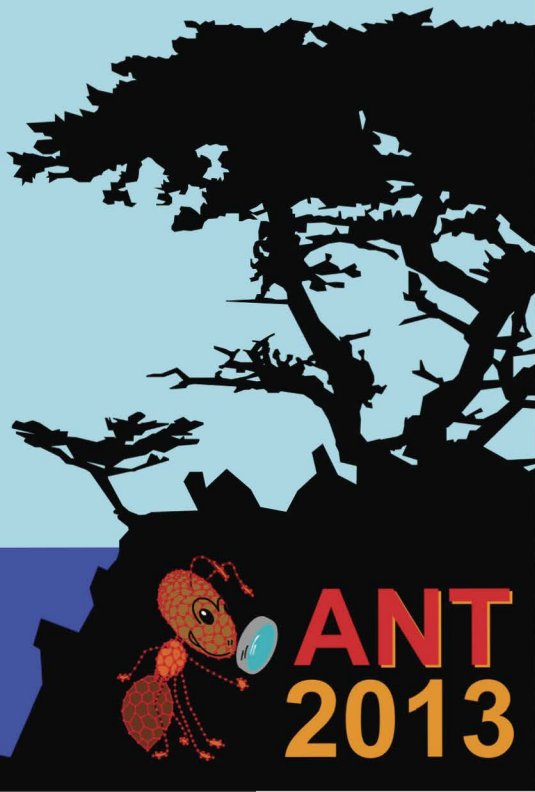

2nd International School-Conference
August 15-19, 2013, Lake Baikal (Listvyanka), Russia

ANT 2013

Boreskov Institute of Catalysis SB RAS
Far Eastern Federal University
Institute of Cytology and Genetics SB RAS
Institute for Hydrocarbons Processing SB RAS
National Research Irkutsk State Technical University
Baikal Museum ISC SB RAS
Competence Center “Catalysts for power efficient technologies”


# Second International School-Conference
# “Applied Nanotechnology & Nanotoxicology”

**Listvyanka, Baikal Lake, Irkutsk Region, Russia**
**August 15-19, 2013**

# BOOK OF ABSTRACTS

ISBN 978-5-9902557-8-4


**Novosibirsk, 2013**

УДК 544+546+57.04+615
ББК 24.1+24.5+28.4+52

**Second International School-Conference "Applied Nanotechnology & Nanotoxicology"**, August 15-19, 2013, Listvyanka, Baikal Lake, Irkutsk Region, Russia: Book of Abstracts, ed.: Dr. Aleksey Vedyagin, Boreskov Institute of Catalysis SB RAS, Novosibirsk, Russia, 192 p., ISBN 978-5-9902557-8-4

В надзаг.: Boreskov Institute of Catalysis SB RAS
Far Eastern Federal University
Institute of Cytology and Genetics SB RAS
Institute for Hydrocarbons Processing SB RAS
National Research Irkutsk State Technical University
Baikal Museum ISC SB RAS
Competence Center "Catalysts for power efficient technologies"

**Перевод заглавия:**
Вторая Международная школа-конференция "Прикладная нанотехнология и нанотоксикология", Тезисы докладов

The book contains the abstracts on following topics:

**1. Nanotechnology**
- Synthesis of novel nanostructured materials
- Unique physicochemical features of nanostructures
- Characterization methods for nanoparticles
- Nanosize effects in catalysis
- Nanotechologies for green chemistry and clean energy

**2. Nanotoxicology**
- Toxicology of nanoparticles
- Toxicity of purified and non-purified nanomaterials, oxidative stress and antioxidants
- Tissue specific response to nanoparticles
- Recognition and clearance of nanoparticles
- Individual resistance/susceptibility to nanocontamination
- Animal models in nanotoxicology



**ISBN 978-5-9902557-8-4**

**School-Conference Organizers:**

*Boreskov Institute of Catalysis SB RAS*

*Far Eastern Federal University*

*Institute of Cytology and Genetics SB RAS*

*Institute for Hydrocarbons Processing SB RAS*

*National Research Irkutsk State Technical University*

*Baikal Museum ISC SB RAS*

*Competence Center "Catalysts for power efficient technologies"*

**Financial Support:**

*Russian Foundation for Basic Research*

*Bruker Corporation*

*LLC "Company SocTrade"*

*Postnova Analytics GmbH*

*LLC "Reolgrade Service"*

**Informational Support:**


*Journal "Nanotechnologies in Russia"*

**International Program Committee:**
Valery I. Bukhtiyarov (Chair) *BIC SB RAS (Novosibirsk, Russia)*
Mikhail P. Moshkin (Co-Chair) *ICG SB RAS (Novosibirsk, Russia)*
Mikhail V. Alfimov *Nanotechnologies in Russia, Editor-in-Chief (Moscow, Russia)*
Anna A. Shvedova *West Virginia University (Morgantown, USA)*
Vladimir A. Likholobov *IHP SB RAS (Omsk, Russia)*
Liliya M. Fatkhutdinova *Medical University (Kazan, Russia)*
Tatiana A. Tkacheva *RIOH RAMS (Moscow, Russia)*
Kirill S. Golohvast *FEFU (Vladivostok, Russia)*
Aleksey A. Vedyagin *BIC SB RAS (Novosibirsk, Russia)*
Ilya V. Mishakov *BIC SB RAS (Novosibirsk, Russia)*
Yuri P. Meshalkin *ILP SB RAS (Novosibirsk, Russia)*
Alexandr V. Lavrenov *IHP SB RAS (Omsk, Russia)*
Alexandr N. Gul'kov *FEFU (Vladivostok, Russia)*

**Organizing Committee:**
Aleksey A. Vedyagin (Chair) *BIC SB RAS (Novosibirsk, Russia)*
Ilya V. Mishakov (Co-Chair) *BIC SB RAS (Novosibirsk, Russia)*
Elena V. Zelynskaya *ISTU (Irkutsk, Russia)*
Dmitry Shlyapin *IHP SB RAS (Omsk, Russia)*
Olga T. Rusinek *Baikal Museum ISC SB RAS (Listvyanka, Russia)*
Maxim O. Kazakov *IHP SB RAS (Omsk, Russia)*
Maxim S. Mel'gunov *BIC SB RAS (Novosibirsk, Russia)*
Elena A. Mel'gunova *BIC SB RAS (Novosibirsk, Russia)*
Eugeny V. Starokon *BIC SB RAS (Novosibirsk, Russia)*
Nataliya N. Leonteva *IHP SB RAS (Omsk, Russia)*
Tatiana V. Chernyshova *IHP SB RAS (Omsk, Russia)*
Tatyana A. Komnik *BIC SB RAS (Novosibirsk, Russia)*
Yuri I. Bauman *BIC SB RAS (Novosibirsk, Russia)*

**Secretariat:**
Irina V. Tokareva *BIC SB RAS (Novosibirsk, Russia)*
Dmitry V. Krasnikov *BIC SB RAS (Novosibirsk, Russia)*

# PLENARY AND KEYNOTE LECTURES

# Fine tuning magnetic nanoparticles catalysts properties for selective transformation of cellulose to value-added chemicals

Natalia Candu, Alina Negoi, Iunia Podolean, Madalina Tudorache, Simona M. Coman, Vasile I. Parvulescu

*University of Bucharest, Faculty of Chemistry, Department of Organic Chemistry, Biochemistry and Catalysis, Bdul Regina Elisabeta, 4–12, Bucharest 030016, Romania;*
*e-mail: vasile.parvulescu@g.unibuc.ro*

*Keywords:* *Ru silica coated magnetic nanoparticles, Mossbauer, EXAFS*

## 1. Introduction

In the last decades catalysis became a strategic field of science representing the new way to meet the challenges of sustainability. In this context, one of the big challenges is the development of the cleaner catalytic processes to convert biomass to multiple platform molecules (e.g., levulinic acid (LA)) as strategic precursors for valuable products [1]. The development of the cleaner catalytic processes to convert lignocellulosic biomass directly to value-added chemicals is even a bigger challenge. Therefore, an emerging technique is to combine cellulose hydrolysis with other chemical transformation over multifunctional solid catalysts.

Creating nanocatalysts became the most important goals in the last years [2]. However, isolation and recovery of these tiny materials is not easy, this limitation hampering the economics and sustainability of these protocols. To overcome this limits, the use of magnetic nanoparticles has emerged as a viable solution; their insoluble and paramagnetic nature enables easy and efficient separation of the catalysts from the reaction mixture with an external magnet. Furthermore, magnetic separation is a "green" process since it avoids the complications of filtration, the waste and costs being greatly reduced [3].

Here, we report a highly selective transformation of cellulose to LA using magnetic nanoparticles (MNPs) catalysts with acid properties. In turn, LA can be selectively transformed into added-value chemicals by using Ru(III)- or Ru(0)-based magnetically nanoparticles (MNP). A fine tuning of the catalysts properties led to a highly efficient aqueous phase hydrolytic protocol for the selective transformation of cellulose to value-added chemicals. Moreover, the catalyst/product(s) separation was easily achieved with a permanent magnet while the catalyst recovered after the reaction was reused without a significant loss of the catalytic performances.

## 2. Experimental

The preparation of the catalysts comprised three steps: (i) the synthesis of the silica-coated $Fe_3O_4$ nanoparticles [4]; (ii) the functionalization of the silica shell with aminopropyl groups; (iii) the impregnation of the MNPs carrier with triflic acid (HOTf), $RuCl_3$ or both species. Moreover, reduction of the Ru(OH)x species with $NaBH_4$ lead to Ru(0) species. The catalysts have been characterized using nitrogen adsorption-desorption isotherms, XRD, FTIR, UV-VIS, DLS, TEM, XPS, Mossbauer and EXAFS. Activity tests in batch mode were carried out in the following procedure: to a slurry of 0.14 g α-cellulose in 8 mL of water, 0.06 g of catalyst were added and heated up to 423-453 K, under stirring, for 1-6 h. The oxidation tests were conducted in similar conditions with 1 atm of molecular oxigen. For reduction test the same procedure was suitable but by replacing oxigen atmosphere with molecular hydrogen one (1-12 atm). After reaction the catalyst was magnetically recovered by placing a permanent magnet on the reactor wall, the untransformed cellulose was filtered out from the slurry of products and the water soluble products were separated by distillation under vacuum.

## 3. Results and discussions

The created catalytic samples provides access to a series of bi-acidic (e.g., Lewis/Brønsted) water tolerant solid acids suitable for the degradation of cellulose to LA. Moreover, the presence of Ru(OH)x species made the catalysts suitable for the consecutive aerobic oxidation of levulinic

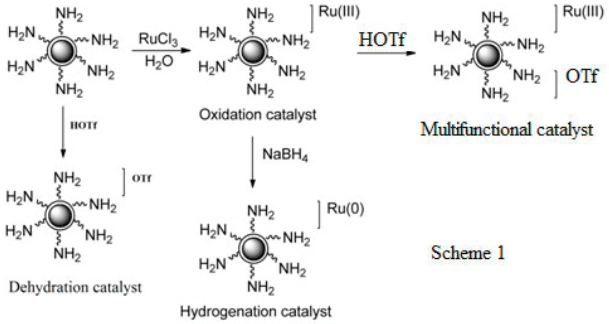


Scheme 1

acid to succinic acid. Reduction of the Ru(OH)x species to Ru(0) species was suitable for the selective reduction of levulinic acid to MTHF. Finally, the consecutive treatment of Ru-based catalysts with triflic acid led to multifunctional catalysts for the selective transformation of cellulose to value-added chemicals (Scheme 1). Therefore, NMPs materials modified with HOTf provided selectivities higher than 50% to LA. The hydrolysis of cellulose is also promoted under hot compressed water by Ru(III) species on MNP, in agree with previous model experiments [5]. In the presence of water Ru species may generate $H^+$ and $[Ru(H_2O)_5OH]^{2+}$ ($pK_a$ = 2.9 at 298 K) as Brønsted acids via a similar mechanism with $[Ru(H_2O)_6]^{3+}$ [6]. In this way it is explained the high selectivities of these catalysts to levulinic acid. Further, in the presence of 1 atm of molecular oxygen, Ru(III) was proved as active specie for the levulinic acid conversion into succinic acid. In the presence of molecular hydrogen, Ru(0) was proved as active species for the levulinic acid conversion into methyl-tetrahydrofuran (MTHF) with high selectivities. Combining Ru(III) species with triflic acid ones, the obtained multifunctional catalysts made possible the selective transformation of cellulose to value-added chemicals. As a function of the active species ratio and reaction conditions, selectivities into different value-added compounds may be varied. It will be taken into discussion the catalytic performances - catalysts properties and a series of economical criteria as: the economy of the catalyst, the stability and handling of the catalysts, recycling issues, and catalyst loading. The characterization of the catalysts using XRD, FTIR, UV-VIS, DLS, TEM, XPS, Mossbauer and EXAFS provided an insight in the properties generating the activity and selectivity of the investigated nanoparticles.

**Acknowledgements:** The authors kindly acknowledge to UEFISCDI for the financial support through the project PN-II-PCCA-2011-3.2-1367.

## 4. References

[1] R. H. Leonard, *Industrial and Engineering Chemistry* **48** (1956) 1331.
[2] G. A. Somorjai, H. Frei, J. Y. J. Park, *Am. Chem. Soc.* **131** (2009) 16589.
[3] D.-m. Lai, L. Deng, J. Li, B. Liao, Q.-x. Guo, Y. Fu, *ChemSusChem* **4** (2011) 55.
[4] J. Lee, Y. Lee, J. K. Youn, H. B. Na, T. Yu, H. Kim, S.-M. Lee, Y. -M. Koo, J. H. Kwak, H. G. Park, H. N. Chang, M. Hwang, J.-G. Park, J. Kim, T. Hyeon, *Small* **4** (2008) 143.
[5] T. Komanoya, H. Kobayashi, K. Hara, W.-J. Chun, A. Fukuoka, *Appl. Catal. A: General* **407** (2011) 188.
[6] W. Böttcher, G.M. Brown, N. Sutin, *Inorg. Chem.* **18** (1979) 1447

# Interactions of Nanoparticles with Pulmonary Immune Cells – from Principles to Consequences

Anna A. Shvedova, PhD, DSc, FATS[*,1]

[1] *Pathology & Physiology Research Branch/NIOSH/CDC, & Department of Physiology and Pharmacology, School of Medicine, WVU, Morgantown, WV, USA*

(*) corresponding author: ats1@cdc.gov

*Keywords: nanomaterials, immune toxicity, inflammation, pulmonary injury, occupational settings, biodiesel*

Engineered nanomaterials (EN) have unique physico-chemical properties that make them promising for many biomedical applications, including tissue regeneration, drug and gene delivery, and monitoring of disease processes. The potential toxicological hazard posed by ENs is a major concern since several industrial sectors (e.g. electronics, biomedicine, bioengineering and cosmetics) are exploiting the innovative features of nanostructures resulting in large-scale manufacturing. A number of consumer products contain nanomaterials and, given their multifaceted life-cycle, it is essential to foresee their adverse effects on human health and the environment. Application of quantitative or qualitative structure-toxicity paradigm to nanomaterials represents a promising approach in predicting toxic effects directly from the physicochemical properties of the EN entities. This could be beneficial for prioritizing resources in toxicological investigations while reducing the ethical and monetary costs that are related to animal testing.

Encounter of EN by cells of the innate immune system, our primary defense outpost against foreign invasion, is a critical point. The presence of specific recognition patterns primarily defined by the nanoparticles' size and charges are essential for their recognition and uptake by macrophages. Interactions of EN with respiratory and immune cells are affected by many factors, including direct interface of NP with cellular constituencies - particularly lipids and proteins - thus determining their fate and toxic potential in the body. There are complex relationships between the infection process and inflammatory responses to nanoparticles resulting in potent effects of nanoparticles on pulmonary clearance of bacteria. Our studies with Listeria monocytogenes demonstrated that enhanced acute inflammation and pulmonary injury with delayed bacterial clearance after SWCNT exposure may lead to increased susceptibility to lung infection in exposed populations.

This talk will address important issues of respiratory immune toxicity of carbonaceous nanomaterials causing substantial pulmonary injury; including fibrosis, allergic response and cancer providing clues toward underlying mechanisms of toxicity with respect to current regulations in occupational settings. In addition, the issues relevant to combustion-derived NPs (CDNPs), (including those generated from the utilization of diesel and biodiesel) - which represent a significant component in urban and occipational air pollution - will be considered.

**ACKNOWLEDGMENTS**

This work was supported by NTRC3927ZJHF and NIOSH 2927ZKCY.

**DISCLAIMER**

The findings and conclusions in this report are those of the authors and do not necessarily represent the views of the National Institute for Occupational Safety and Health.

# Field-Flow Fractionation for nanoparticles separation, characterization and fractionation: history, instruments and examples of separations in nanotechnology and environmental studies

Dr. Anatoly S. Lermontov[1], Michel Palu[2]

[1] *Head of Development Department, Soctrade, Moscow*
[2] *Sales Director, Postnova North Europe, Vantaa, Finland*

Particles in a range of a few nanometers up to several microns are more and more frequently used in numerous products. Many applications are based on the specific properties of these nanomaterials. Therefore, an accurate characterization of nanoparticles is essential to understand their impact on technological processes, occupational health, environment, and food safety. This can be a relatively easy task for nanoparticle populations with uniform size distribution, using established methods such as DLS, XRD, TEM/SEM, and ICP. However, samples are often very heterogeneous and complex systems, mixtures, colloids, sediments, etc, which contain various species which differ in concentration, size, shape and composition. For this reason, techniques which are not involving a fractionation step prior to the measurement might deliver partially erroneous or even wrong results. Despite of an evident necessity, there are few methods, such as ultracentrifugation and solubility fractionation, used for the separation of nanoparticles. These techniques can give good results but have some limitations, such as being not universally applicable, low-resolution, expensive, time consuming or complex.

Invented in 1966 by Prof. Calvin Giddings, Field-Flow Fractionation (FFF) was first commercialized in 1986. During the last decade dramatic improvements have been made and FFF is now definitively a robust analytical technique. FFF methods for particles separation are available as complete solutions, which are gaining in popularity in both research and QC laboratories. FFF is a family of separation techniques that was developed specifically for the separation and characterization of materials ranging in size from macromolecules to particulates. Unlike chromatography, FFF separations are carried out in a single phase. A solution or suspension is pumped through a long and narrow channel, under parabolic laminar flow conditions. A field, perpendicular to the direction of flow, is applied. Under the influence of the forces of the field and the counteracting forces of diffusion, an equilibrium layer is established for each sample component at unique position across the parabolic flow profile. Sample components that on average spend more time further away from the channel wall will be transported out of the channel faster than their counterparts near the wall.

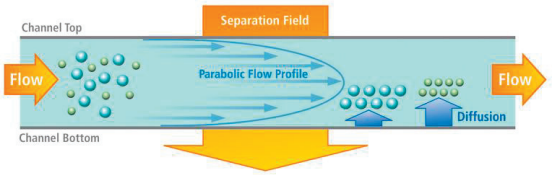


Figure 1. The common principle of FFF methods

In commercially available FFF systems the field can be asymmetrical flow (crossflow) through a membrane (giving rise to Asymmetrical Flow FFF), centrifugal (Centrifugal or Sedimentation FFF), temperature gradient (Thermal FFF), or gravitational (Split Flow Thin Cell Fractionation).

The main advantage of FFF is its ability to provide fast, gentle and high resolution separations of any particles, both soluble and colloidal components, over a wide size range, from 1 nm up to 100 µm.

In the lecture a short history of the method from the invention to the last decade of successful commercialization will be presented along with a brief description of the existing types of instruments and detectors. Examples of separations will cover different fields of nanotechnology studies with focus on the online coupling of FFF with Inductively Coupled Plasma Mass Spectrometry (ICP-MS), a state-of-the-art method for high sensitive nanoparticle analysis.

# Design of Catalytic Materials in the Subnanometer and Nanometer Size Range: From the Understanding of Size, Composition an Support Effects via in Situ and ex Situ Studies, to Optimizing Performance

S. Vajda[1,2,3*]

[1] *Materials Science Division, Argonne National Laboratory, 9600 South Cass Avenue, Argonne, IL 60439, USA*
[2]*Nanoscience and Technology Center, 9600 South Cass Avenue, Argonne, IL 60439, USA*
[3]*Depatment of Chemical and Environmental Engineering, School of Applied Sciences, Yale University, 9 Hillhouse Avenue, New Haven, CT 06520, USA*

* vajda@anl.gov

*Keywords: model catalysts, size-selected clusters, X-ray scattering, X-ray absorption, dehydrogenation, partial oxidation*

## 1. Introduction

The elucidation of the size, composition, shape,structure and function correlation, the effect of support along with the determination and control of the nature of the catalytic particles under reaction conditions are instrumental for addressing fundamental aspects of catalysis on the way to the design of new classes of catalytic materials. Highly uniform particles on technologically relevant supports are prerequisites for such studies.

## 2. Experimental

### *2.1. Support Material*

As support material, carbon based (e.g. ultrananocrystalline diamond - UNCD) and by atomic layer deposition prepared thin oxide films on the top of naturally oxidized silicon wafers are used.

### *2.2. Catalyst Synthesis.*

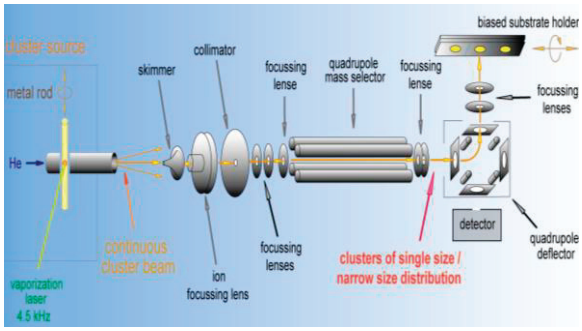


Figure 1. Schematics of the cluster deposition apparatus used for the atomic precision synthesis of model size-selected subnanometer catalysts.

Size-selected cluster deposition method is used to prepare model catalysts with well-defined size and surface coverage. Wet chemical methods were applied to prepare practical ("real") catalysts.

### *2.3. Catalyst Characterization and Test of Performance.*

Our experimental studies are based characterization of the catalysts under realistic working conditions *In situ* X-ray scattering and absorption are used to characterize the size, shape and oxidation state of the working catalysts, complemented by e*x situ* and *in situ* microscopies. The *in situ* experiments are coupled with mass spectroscopy analysis of the reaction products. The experimental studies are complemented with DFT calculations.

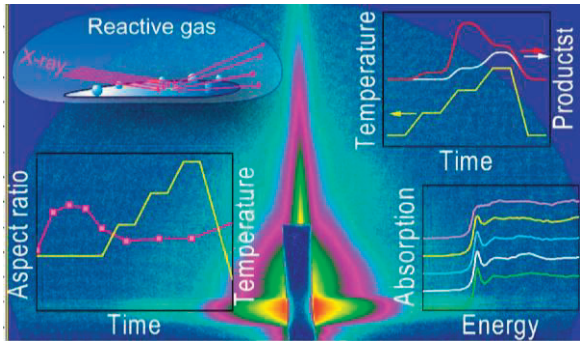


Figure 2. Schematics of the information gained form *in situ* characterization of catalysts: Grazing incidence X-ray scattering and absorption, temperature programmed reaction allows for correlating particle size/shape, with its oxidation state and reactivity under realistic conditions of temperature and pressure.

## 3. Results

Select examples will be presented on studies of model and practical catalysts.

*3.1. Oxidative and non-oxidative dehydrogenation of cyclohexane on subnanometer Co clusters*

In the absence of oxygen, the cobalt clusters become active around 300 ºC, with the larger clusters ($Co_{27}$) being about two times as active as the smaller ($Co_4$) ones and about an order of magnitude more active as nanometer size cobalt oxide particles prepared by wet chemical methods. In the presence of oxygen, the clusters are found active at considerably lower temperatures, though with somewhat different selectivities for the two cluster sizes. Notably, the high activity of cobalt clusters under oxidative conditions makes them as potential candidates to replace platinum based dehydrogenation catalysts.

*3.2. Dehydrogenation of cyclohexene on $Co_{27}$ clusters: Increased activity through structural fluxionality and role of the support.*

The 27-atom cobalt clusters were deposited on $TiO_2$, ZnO, $Al_2O_3$, MgO and UNCD. While the activity and selectivity of $TiO_2$, ZnO and $Al_2O_3$ supported clusters are comparable, MgO-supported clusters are 2 to 3 times more active under oxygen rich conditions. *In situ* data reveal that a formation of a fluxional ~2-3 nm structure of a $Co_xMg_yO_z$ composition is responsible for the dramatic increase in activity. Under oxygen lean conditions, UNCD-supported clusters UNCD-supported clusters possess the highest activity as well as highest toward selectivity towards dehydrogetanted C6 products. Along with the dehydrogenation of cyclohexane, these results indicate extraordinary propensities of sub-nm Co clusters in low-temperature activation of $O_2$.

*3.3. Selective oxidation of propene to propylene oxide using molecular oxygen.* The efficacy of propylene oxide *vs.* acrolein production as function of the size and shape of alumina-supported subnanometer to nanometer size silver clusters will be discussed and compared to the performance of alumina supported subnanometer size gold clusters.

## 4. References

[1] S. Vajda, S. Lee, K. Sell, I. Barke, A. Kleibert, V. von Oeynhausen, K.-H. Meiwes-Broer, A. Fraile-Rodriguez, J. W. Elam, M. J. Pellin, B. Lee, S. Seifert, R. E. Winans, Combined Temperature Programmed Reaction and *in-Situ* X-ray Scattering Studies of Size Selected Silver Clusters under Realistic Reaction Conditions in the Epoxidation of Propene, *J. Chem. Phys.*, 131, 121104-1-4 (2009), Communication.

[2] S. Lee, L. M. Molina, M. L, María J. López, J. A. Alonso, B. Hammer, B. Lee, S. Seifert, R. E. Winans, J. W. Elam, M. J. Pellin, and S. Vajda, Selective Propene Epoxidation on Immobilized $Au_{6-10}$ Clusters: The Effect of Hydrogen and Water on Selectivity and Activity, *Angew. Chem. Int. Ed.* **48**, 1467-1471 (2009).

[3] S. Vajda, M. J. Pellin, J. P. Greeley, C. L. Marshall, L. A. Curtiss, G. A. Ballentine, J. W. Elam, S. Catillon-Mucherie, P. C. Redfern, F. Mehmood and P. Zapol, Subnanometre Platinum Clusters as Highly Active and Selective Catalysts for the Oxidative Dehydrogenation of Propane, *Nat. Mater.* **8**, 213-216 (2009).

[4] Y. Lei, F. Mehmood, S. Lee, J. P. Greeley, B. Lee, S. Seifert, R. E. Winans, J. W. Elam, R. J. Meyer, P. C. Redfern, D. Teschner, R. Schlögl, M. J. Pellin, L. C. Curtiss, and S. Vajda, Increased Silver Activity for Direct Propylene Epoxidation via Subnanometer Size Effects, *Science* **328**, 224-228 (2010)

[5] L. M. Molina, S. Lee, K. Sell, G. Barcaro, A. Fortunelli, B. Lee, S. Seifert, R. E. Winans, J. W. Elam, M. J. Pellin, I. Barke, A. Kleibert, V. von Oeynhausen, Y. Lei, R. J. Meyer, J. A. Alonso, A. Fraile-Rodríguez, S. Giorgio, C. R. Henry, K.-H. Meiwes-Broer and S. Vajda, Size-Dependent Selectivity and Activity of Silver Nanoclusters in the Partial Oxidation of Propylene to Propylene Oxide and Acrolein: A Joint Experimental and Theoretical Study, *Catal. Today* **160**, 116-130 (2011

[6] S. Lee, M. Di Vece, B. Lee, S. Seifert, R. E. Winans and S. Vajda, Oxidative Dehydrogenation of Cyclohexene on Size Selected Subnanometer Cobalt Clusters: Improved Catalytic Performance via Evolution of Cluster-Assembled Nanostructures, *Phys. Chem. Chem. Phys.,* **14**, p. 9336 - 9342 (2012)

[7] E. C. Tyo, C. Yin, M. Di Vece, Q. Qian, S. Lee, B. Lee, S. Seifert, R. E. Winans, R. Si, B. Ricks, S. Goergen, M. Rutter, B. Zugic, M. Flytzani-Stephanopoulos, Z. Wang, R. E. Palmer, M. Neurock, and S. Vajda, Oxidative Dehydrogenation of Cyclohexane on Cobalt Oxide ($Co_3O_4$) Nanoparticles: The Effect of Particle Size on Activity and Selectivity,*ACS Catal.* **2**, p. 2409−2423 (2012).

# Rigid rod-like carbon nanotubes induce signs of allergic asthma

Marit Ilves[1], Elina Rydman[1], K.Savolainen[2] and Harri Alenius[1]

*[1]Unit of Systems Toxicology and [2(*)] Nanosafety Research Centre, Finnish Institute of Occupational Health, Topeliuksenkatu 41 aA, 00250 Helsinki, Finland)*

Corresponding author (*): Kai-Savolainen@ttl.fi

*Keywords: NanoSafety Cluster, Research Priorities, Research Roadmap, Future Nanosafety Research*

## 1. Introduction

The rapid growth of the use of engineered nanomaterials (ENM) and their applications in nanotechnology has been astonishing during last decade. Engineered nanomaterials, due to their small size, surface to mass and volume ratios, surface reactivity, morphology, especially in fibrous carbon containing carbon nanotubes, have found numerous applications in industrial processes and products as well as in a huge number of consumer products. These materials allow one to produce light and strong materials e.g. by using light and strong carbon nanotubes in electronic devices or different consumer applications. Metal oxides such as titanium dioxide are used in self-cleaning surfaces in outside windows and in bath rooms. These materials are also used in the production of energy and clean water. The special characteristics of these materials have also the other side of the coin. Due to their small size these materials have an easy access to the mammalian organisms, and due to the reactivity of many ENM they have a strong ability to react with biological molecules in living organisms.

The current situation is a marked challenge for the assessment of potential hazards, exposure and risks of ENM because very little systematic knowledge is available on their possible harmful effects, or their mechanisms in different disease models or effects in different target tissues.

One of the most important groups of ENM are the different types of carbon nanotubes used in a large number of light and strong consumer products and electronic industrial applications.

The prevalence of allergic diseases has greatly increased for example in Finland and several other countries during last fifty years. This prompted us to explore whether exposure to different types of carbon nanotubes could have an effects on the cellular pathways responsible for allergic asthma. We used mice to test the hypotheses that these materials could have such an effect on allergic asthma in mice. The typical features of allergic asthma include increased airway reactivity to inhaled metacholine, lung inflammation with eosinophilia and increased influx of Th2 lymphocytes, increased bronchial mucus secretion, and increased expression of Th2 cytokines.

## 2. Experimental

Male mice were exposed via inhalation either to long rod-like multiwalled carbon nanotubes (MWCNT) or tangled carbon nanotubes. Control mice were sham- exposed. The mice were exposed four hours a day for four days to either the rod-like CNT or the tangled CNT at low doses, and samples were collected on the fifth day.

To explore early events of the carbon nanotubes, some of the mice were exposed only once for four hours, and samples were collected immediately after the exposures.

Lungs were studied for morphology, airway sensitivity and bronchial mucus secretion as well as expression of chemokines and cytokines in the lung tissue. Also the role of pulmonary mast cells in evens evoked by the carbon nanotubes were explored.

## 3. Results

Four day exposure to MWCNT induced at low doses a strong pulmonary eosinophilia characterized by the formation of giant cells attached to each other by means of rod-like MWCNT. Rod-like MWCNT also induced a strong airway reactivity toward inhaled metacholine and an active bronchial mucus secretion. In addition to these observations, there was also a drastic expression of Th2 cytokines and chemokines in the lung tissues. Mast cells seemed to be closely associated, and to regulate, the pulmonary eosinophilia induced by rod-like MWCNT. None of these observations were found in the control mice or in mice exposed via inhalation to the tangled CNT. Transcriptomics analysis also revealed that there were dramatic up-regulation of genes controlling pro-inflammatory and Th2 associated genes whereas no such events were found in control mice or in mice exposed to MWCNT.

When mice were exposed only for four hours to rod-like MWCNT, tangled CNT, or when they were sham exposed (controls) MWCNT induced early expression of pro-inflammatory and pro-allergenic cytokines and chemokines derived from alveolar macrophages. It was also apparent that at this early stage, mast cells regulated this rod-like MWCNT induced eosinophilia. Such effects were not seen in control mice or in mice exposed to tangled CNT.

## 4. Conclusions

These observations demonstrate that exposure of mice via inhalation to low doses of rod-like MWCNT induce rapidly strong sings of typical allergic asthma during four days of exposure without any preceding contact to any allergen that could explain the observed effects. It was strongly evident that sole exposure to rod-like MWCNT induced a strong pulmonary eosinophilia in these mice associated with increased airway hyper-reactivity, mucus formation, and a dramatic expression of Th2 cytokines and chemokines in the lung tissue. These effects were clearly due to the effects of the rod-like CNT as such effects were not seen in control mice or mice exposed to tangled CNT. This strong allergic asthmatic reaction was hence evoked by some features of the rod-like CNT, but the exact mechanisms still need to be worked out. The studies at an early time point (4 hours) indicated that the rod-like MWCNT-induced allergic reaction was a rapid one and was initiated only a few hours after the beginning of the exposure.

## 5. Acknowledgements.

Supported by EU Commission Grant CP-IP 211464-2 (NANODEVICE).

# The design of nanomagnets for medical applications

M. Forrester[1*], F. Kusmartsev[1], E. Kovács[2]

[1] *Department of Physics, School of Science, Loughborough University, Leicestershire, LE11 3TU (United Kingdom)*
[2] *Department of Physics, University of Miskolc, H-3515 Miskolc, Hungary*

(*) d.m.forrester @lboro.ac.uk

*Keywords: nanomagnetism, magnetic forces, anisotropy, energy relaxation*

## 1. Introduction

We present the magnetic phase diagrams, analytical formalisms and numerical results that are used to design high moment synthetic antiferromagnetic (SAF) nanomagnets for biomedical applications [1]. These SAF structures contain layers of nanomagnets with elliptical cross-sections and are separated from one another by non-magnetic materials. With nanomagnets increasingly being used and proposed as functional units for in-vivo applications, it is vital to understand how to optimize their structure, geometry and size, the effects of temperature on them, and their responses to electromagnetic stimulation. This has to be established first, before bio-functionalization, so as to find the highest likelihood to survive the biophysical barriers that protect the body, whilst maintaining the required magnetic responses to external radiation. As the SAF are on the scale of biological entities, interactions with cells and molecular constituents can be extreme.

## 2. Magnetic response of SAF devices

The energy dissipated by Brownian relaxation greatly depends on the local environment. However, the use of magnetic particles that dissipate energy primarily through heat by magnetic hysteresis losses or Néel relaxation is of preference for understanding the magnetic properties themselves. The magnetic properties of the SAF depend on the saturation magnetization ($M_S$), elongation, size, magnetic anisotropy ($a$), the applied field amplitude ($h$), frequency ($\omega$) and the effective permeability ($\mu_r$). Increasing the magnetic permeability of the structure allows one to

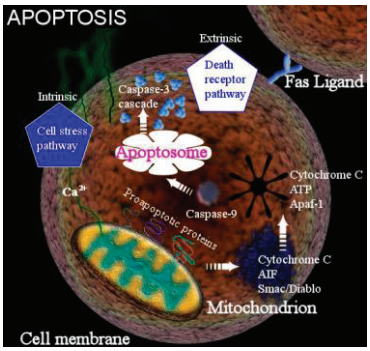


Figure1. Apoptosis mechanically induced by the torque of a SAF structure or a micro-disk.

apply a smaller magnetic field to the structure whilst maintaining a strong magnetic response. Also, increasing the thickness of the magnetic layers, up to about 20 nanometers in SAF structures, can also keep levels of magnetic torque sufficient for many purposes. It has been shown that micron sized disks open ion channels and can induce apoptosis (Fig.1) in cancer cells by mechanical force [2]. The level of force required was on the order of a few pico-newtons. This force/torque on the disks was created by a controlling applied magnetic field ($H_{app} \approx 100Oe$).

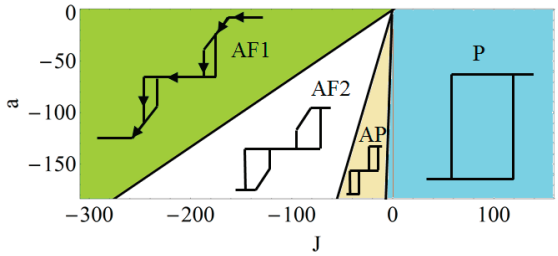


Figure2. A magnetic phase diagram for two nanomagnets with anisotropy a and interaction strength J. There are four phases "AF1", "AF2", "AP" and "P" related to the shape of the magnetization hysteresis loops as shown.

By predetermined design, nano-magnetic structures can also be created that have the capability to influence biological processes.

For example, SAF of high permeability ($\mu_r \approx 1000$ at $\omega \approx 1GHz$) with various thicknesses and magnetic coupling strengths can produce mechanical forces ranging from femtonewtons to piconewtons.

There is a fundamental connection of mechanical strain on cellular activity and even on gene expression [3]. It is well known that mechanical forces can regulate biological processes and as we enter an era of exploration of cell manipulation using nanoparticles we must understand the intricacies of perturbing the biological processes at the intracellular level and below. The aforementioned mechano-sensitive ion channels are one such example of mechano-sensitive signaling to levels deep within a cell. As we create more nanomagnetic devices for in-vivo operations and drug deliveries it is essential to develop complete understanding of our magnetic devices.

## 3. Results

It is an area of intense research in itself to understand the mechanisms of magnetic interactions between magnetic devices alone, never-mind with the inclusion of biological materials. Thus, we develop a complete picture of magnet interactions between single domain ferromagnetic elements on the nano-scale. Figure 2 demonstrates a phase diagram of the magnetic interaction of two nanomagnets with varying anisotropy and coupling strengths.

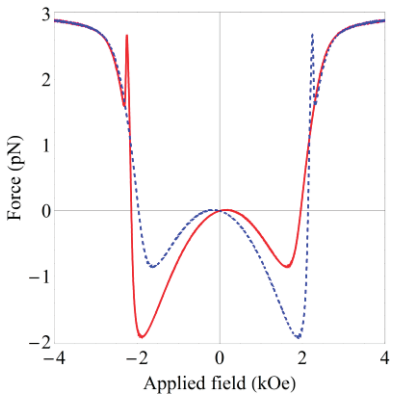


Figure3. The magnetic force stimulated by an alternating magnetic field for a SAF structure comprising two nanomagnets made from permalloy. The red (blue dashed) line is the force upon going from a positive (negative) applied field to a negative (positive) one.

The phases are characterized by the shape of the magnetization against applied field strength plots that are shown schematically in Fig. 2. Figure 3 illustrates the mechanical force that is produced by the interaction of a typical SAF structure with an applied magnetic field. The peaks and troughs in the force occur when the magnetic moments in the nanomagnets undergo a radical change in orientation as the energy balances of the system change in response to the applied field. By tuning the magnetic field to these points, where a maximum force occurs, one can produce the greatest stresses on a cellular membrane. Figure 4 gives some examples of hysteresis curves that can emerge for arrangements of nanomagnets.

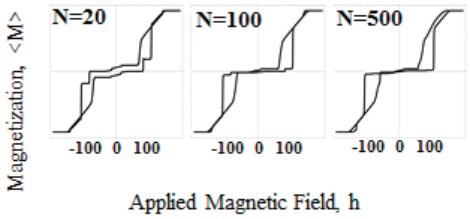


Figure4. Magnetization hysteresis loops for N interacting nanomagnets of elliptical cross sections.

The interactions to eliminate or enhance magnetic remanence can be exploited so as to control the magnetic aggregation of the SAF in the absence of an applied magnetic field.

## Discussion

Little is known about the physics behind gene expression and cellular processes. Nanomagnets can be used to explore cell regulation by using tailored SAF that exert very small forces on them. Our phase diagrams and understanding of magnetism at the nanoscale will allow us to begin to do this as we control the magnetization of the structures. This is only possible through interdisciplinary efforts.

## References

[1] M. Forrester, E. Kovacs, F. Kusmartsev. Phys. Rev. B **87**, 174416 (2013) .

[2] D-H Kim *et al*. Nature Materials **9**, 165–171 (2010).

[3] Y-F Chen, J.N. Milstein, J-C. Meiners. Phys. Rev. Lett. **104**, 048301 (2010).

# "Nanoimmigration" into a cell: through customs, or ...

E. Ryabchikova

*Institute of Chemical Biology and Fundamental Medicine SB RAS, Russia, Novosibirsk, Lavrentiev Ave. 8*
*Novosibirsk State University, Russia, Novosibirsk, ul. Pirogova, 2*

corresponding author: lenryab@yandex.ru

*Keywords: metallic nanoparticles, prokaryotic and eukaryotic cells, penetration*

## 1. Introduction

Increase of metal nanoparticles (NPs) usage in various fields of science, industry and daily life give rise to direct contact of the NPs with living organisms. There is a big gap between avalanche application of NPs and the knowledge about their influence on living organisms. Classic methods are used for evaluation of NPs toxicity currently, while sizes of NPs call for particular attention to the responses at cellular and subcellular level.

Eukaryotic cells during the evolution developed special mechanisms for internalization of molecules, molecular aggregates and solid particles. The mechanisms possess strong specificity, and to bar out "undesirable persons", as customs monitor the penetration of drugs and weapons. We tried to understand what mechanisms operate when a cell is attacked by metallic NPs, and our studies were aimed at examination of fine mechanisms of NPs interaction with a cell.

## 2. Experimental

We used titanium dioxide ($TiO_2$) NPs (4-5 nm) synthesized by Dr. N. Shikina (Institute of Catalysis, SB RAS); spherical gold NPs (12-14 nm) synthesized by Dr. I. Pyshnaya (Institute of Chemical Biolofy and Fundamental Medicine, SB RAS); and palladium NPs (4-6 nm) synthesized by Dr. S. Troitsky (Institute of Catalysis, SB RAS). All preparations of NPs had pH 7.2-7.4 and could be dissolved in cell culture mediums.

Cultures of HeLa and MDCK cells were used for *in vitro* studies. Mice peritoneal macrophages and tumors hepatoma A-1 and lymphosarcoma RLS were used in experiments *in vitro* and *in vivo*.

Examination of fine mechanisms of metallic NPs interaction with a cell was performed by JEM 1400 (Jeol, Japan) transmission electron microscope supplied with digital by side-mounted camera Veleta (SIS, Germany). Ultrathin sections were prepared on Leica Ultracut-6 (Reichert-Young, Austria) and routinely contrasted with uranyl acetate and lead citrate.

## 3. Results

$TiO_2$ NPs are among most widely used NPs, including cosmetics and pharmacy. We examined interaction of different crystalline forms of $TiO_2$ NPs with MDCK cells. Cell responses to amorphous, anatase and brookite modifications of $TiO_2$ NPs clearly differed despite of identical sizes of the NPs. Amorphous modification induced formation of deep invaginations of cell surface. Some NPs passively entered cell cytoplasm by microendocytosis. Anatase caused similar changes in the cells, and additionally activated clathrin-dependent endocytosis. Both modifications had low cytotoxicity. In contrast, brookite, which is identical in shape and size with anatase, induced smoothing of cell surface, and subsequent swelling. No signs of brookite entry into MDCK cells were found. Thus, $TiO_2$ NPs, having identical chemical composition, could induce opposite responses of the same cells. This is an evidence of direct interaction of $TiO_2$ NPs with cell membrane macromolecules.

We examined palladium NPs effect on two kinds of cells: peritoneal macrophages isolated from mice and seeded on glass coverslips, and epithelioid MDCK cell culture. These NPs were synthesized to reproduce interaction of different cells with palladium NPs released by car motors in atmosphere. Palladium NPs showed high

cytotoxicity. The NPs crossed plasma membrane of MDCK cells, freely traveled in cytoplasm, "visited" various cell structures and accumulated in nucleus. Macrophages demonstrated resistance of cell membrane to palladium NPs, and trapped NPs by phagocytosis and microendocytosis. These data demonstrate different abilities of different cells to resist palladium NPs. Indeed, macrophages are specialized at defensive functions, and probably have more resistant cell membrane.

Spherical gold NPs were non-toxic for cells, and were used for study of internalization mechanisms in different cells. HeLa cell culture showed "classical" ways of the entry of gold NPs by microendocytosis. The process included both clathrin- and raft-dependent pathways, signs of phagocytosis also were observed. Gold NPs, internalized by HeLa cells, remained enclosed in cell membranes, no entry into cytosole and nucleus was found during 72 h of the incubation. The NPs accumulated in endosomes, which "matured" to lysosomes during the incubation.

Cells of hepatoma A-1 inside peritoneal cavity of mice showed fast and active internalization of gold NPs. The cells ingested huge mass of the NPs during first 10-15 min after their injection. Main mechanisms of the internalization were macropinocytosis and raft-dependent endocytosis, accompanied by phagocytosis. The cells accumulated many NPs, which were observed in early and sorting endosomes. It is interesting, that very few of them converted to lysosomes during 72 h after gold NPs injection. It seemed like cells, "swallowing" nanoparticles do not know what to do with them. Hepatoma A-1 cells cultivated on glass coverslips showed identical to *in vivo* pathways of gold NPs internalization.

Mouse peritoneal macrophages *in vivo* ingested gold NPs mainly by phagocytosis, in accordance with their "defensive" specialization. Some NPs entered the cells by clathrin-dependent endocytosis and accumulated in endosomes. Macrophages cultivated *in vitro* used the same pathways of gold NPs internalization.

Cells of lymphosarcoma RLS did not internalize gold NPs during 72 h after injection into peritoneal cavity. The NPs adsorbed on cell surface, and formed solid aggregations.

Thus, different kinds of cells differently interact with the same gold nanoparticles.

## 4. Discussion

Cells are weaponless in front of metallic NPs which are a new agent for living organisms. The evolution did not develop mechanisms of cell adaptation to metallic NPs. Obviously, the NPs can not be indifferent for the cells. However, real impact of NPs is still unknown. Most studies of the interaction of metallic NPs with a cell describe location of the particles in endosomes, phagosomes or lysosomes after 24 h of incubation, or later. We paid particular attention to early events, and found different pathways of NPs internalization which depend on various factors. This information is important for usage of metallic NPs for drug delivery, because different pathways of NPs entry mean different mechanisms of processing in a cell and different interaction with cell structures.

The obtained data clearly show that metallic NPs are active players which interact with cell macromolecular structures. Probably, in some cases NPs affect a cell by chemical way, or have "behavior" of large macromolecules. A "game" is two-way – both cell mechanisms and nature of NPs are important. Undoubtedly, small metallic NPs could be more harmful, because they do not follow cell "rules" and enter the cells without endocytosis "customs". Bigger NPs (more that 10 nm) could be recognized by a cell and be trapped in membrane-bound structures, and theoretically - pushed out from a cell over the time. In any case, it is necessary carefully examine cell response to metallic NPs before their application.

Studies were performed in frames of Interdisciplinary Integration Project of SB RAS № 57, and State Task of Ministry of Education, Project #4.3924.2011.

# Interactions of Nanoparticles with Biological Matter

E. Rühl*

[1] *Physikalische Chemie, Freie Universität Berlin, Takustr. 3, 14195 Berlin, Germany*

(*) corresponding author: ruehl@zedat.fu-berlin.de

*Keywords: Colloidal chemistry, functionalization, colloidal stability, cell uptake, spectromicroscopy*

## 1. Introduction

Recent progress on the interactions of nanoparticles with biological matter is reviewed [1-15]. The size, shape, and functionalization of the particles is of crucial importance for the uptake into cells and organisms. Therefore, strategies on nanoparticle synthesis [1-3, 5], surface functionalization [6, 8, 12], and characterization are discussed, where the emphasis is put on colloidal chemistry approaches. Most important for interactions of nanoparticles with their chemical or biological environment is the surface functionalization. The stability of various ligands, including mono-, di-, and multivalent ones, in different solvents and biological media is reviewed. Aggregation of nanoparticles is of crucial importance, which is monitored by electron microscopy and dynamical light scattering [12].

## 2. Experimental

Details on the experimental approaches to be presented have been published before. Please find details in the following references [1-15].

## 3. Results

Details on the presented experimental results which are presented have been published before. Please find details in the following references [1-15].

## 4. Discussion

Uptake studies of nanoparticles into cells and skin are discussed, which also includes diagnostics using advanced methods in X-ray microscopy and tomography, optical near field microscopy [15], and MRT imaging [7]. Perspectives of this research covering the fields of nanodiagnostics and therapy using nanoparticles and drug nanocarriers are discussed, as well.

## 5. References

[1]. C. Graf, S. Dembski, A. Hofmann, and E. Rühl, Langmuir **22** (2006) 5604-5610.

[2]. A. Hofmann, C. Graf, C. Boeglin, and E. Rühl, ChemPhysChem **8** (2007) 2008-2012.

[3]. S. Dembski, C. Graf, T. Krüger, U. Gbureck, A. Ewald, A. Bock, and E. Rühl, Small **4** (2008) 1516-1526.

[4]. C. Graf, M. Meinke, Q. Gao, S. Hadam, J. Raabe, W. Sterry, U. Blume-Peytavi, J. Lademann, E. Rühl, and A. Vogt, J. Biomed. Opt. **14** (2009) 021015.

[5]. C. Graf, A. Hofmann, T. Ackermann, C. Boeglin, R. Viswanatha, X. Peng, A. Fraile Rodríguez, F. Nolting, and E. Rühl, Adv. Functional Mat. **19** (2009) 2501-2510.

[6]. A. Hofmann, C. Graf, S.-H. Kung, M. Kim, X. Peng, R. El-Aama, and E. Rühl, Synthesis **42** (2010) 1150-1158.

[7]. A. Hofmann, S. Thierbach, A. Semisch, A. Hartwig, M. Taupitz, E. Rühl, and C. Graf, J. Mat. Chem. **20** (2010) 7842-7853.

[8]. S. Perumal, A. Hofmann, N. Scholz, E. Rühl, and C. Graf, Langmuir **27** (2011) 4456-4464.

[9]. O. Lademann, H. Richter, A. Kramer, A. Patzelt, M.C. Meinke, C. Graf, Q. Gao, E. Korotianksiy, E. Rühl, K.-D. Weltmann, J. Lademann , and S. Koch, Laser Phys. Lett. **8** (2011) 758-764.

[10]. F. Rancan, A. Todorova, S. Hadam, D. Papakostas, E. Luciani, C. Graf, U. Gernert, E. Rühl, B. Verrier, W. Sterry, U. Blume-Peytavi, and A. Vogt, Eur. J. Pharma. Biopharma. **80** (2012) 76-84 .

[11]. M. Jansch, P. Stumpf, C. M. Graf, E. Rühl, and R. H. Müller, Int. J. Pharmaceutics, **428** (2012) 125-133.

[12]. C. Graf, Q. Gao, I. Schütz, C. Niki Noufele, W. Ruan, U. Posselt, E. Korotianskiy, D. Nordmeyer, F. Rancan, S. Hadam, A. Vogt, J. Lademann, V. Haucke, and E. Rühl, Langmuir **18** (2012) 7598-7613.

[13]. W.C. Mak, A. Patzelt, H. Richter, R. Renneberg, K.K. Lai, E. Rühl, W. Sterry, and J. Lademann, J. Controlled Release **160** (2012) 509-516.

[14]. F. Rancan, Q. Gao, C. Graf, S. Troppens, S. Hadam, S. Hackbarth, C. Kembuan, U. Blume-Peytavi, E. Rühl, J. Lademann, and A. Vogt, ACS NANO **6** (2012) 6829-6842.

[15]. P. Hermann, A. Hoehl, P. Patoka, F. Huth, E. Rühl, and G. Ulm, Opt. Express, **21** (2013) 2913-2919.

# Brain as a target for nanoaerosols

M.P. Moshkin*[1], A.V. Romashchenko[1,5], S.Yu. Troitsky[2], D.V. Petrovski[1], A.E. Akulov[1], L.A. Gerlinskaya[1], V.I. Bukhtiyarov[2], I.V. Koptyug[3], A.A. Savelov[3], V.L. Ganimedov[4], M.I. Muchnaya[4], A.S. Sadovsky[4], N.A. Kolchanov[1], R.Z. Sagdeev[3], V.M. Fomin[4]

[1]*Institute of Cytology and Genetics, Siberian Branch of RAS, Novosibirsk 630090, Russia*
[2]*Boreskov Institute of Catalysis, Siberian Branch of RAS, Novosibirsk 630090, Russia*
[3]*International Tomographic Center, Siberian Branch of RAS, Novosibirsk 630090, Russia*
[4]*Khristianovich Institute of Theoretical and Applied Mechanics, Siberian Branch of RAS, Novosibirsk 630090, Russia*
[5]*Design Technological Institute of Digital Techniques Siberian Branch of RAS, Novosibirsk 630090, Russia*

(*) corresponding author: mmp@bionet nsc.ru

*Keywords: nanoparticles, brain, behaviour, MRI, natural adaptation*

## 1. Introduction

The main negative impact of the inhaled aerosols is addressed traditionally to upper airways [1]. At the same time the nanoparticles deposited in the area of the olfactory epithelium can be transported into the olfactory bulbs and further to the brain [2]. Moreover nanotraffic from nose to brain might be more appreciable that transportation from the lung surface to blood and to the peripheral organs. In our study on the laboratory mouse we have found that 30 h exposition (10 times for 3 h) in the atmosphere with nanosized $SiO_2$ led to the 3.5-fold increase of the Si content in olfactory bulbs and only the 1.4-fold in the kidney and liver.

## 2. Nanoparticles and neurodamage

Neuronal effects of nanoparticles are varied from the minor behavioral deviations up to severe neurodegenerative diseases [2, 3]. Neurotoxicity of the nanoaccumulation depends on the duration of the exposition, chemical structure, size, hydrophobicity and other pequarilities of the nanoparticles [2-4]. Most common explanation of the pathogenic effects of the nanoparticles based on evidences of activation of the free radical oxidation and expression of the pro-inflammatory cytokines. These effects are induced in the brain tissue by different kinds of nanoparticles including relatively neutral compounds such as silicon and titanium oxide [2-4].

## 3. Nose to brain nanotraffic

### *3.1. Nanoparticle roadmap*

Although transportation of nanoparticles from nose to brain supported by multiple experiments, we don't know precisely time, which nanorparticles entrapping on the olfactory epithelium spend for reaching a certain space in brain. Using the thread-like nanoparticles of manganese hydroxides (TNM), which are visible in magnetic resonance imaging (MRI), we described roadmap of TNM instilled into nasal cavity. According this study, TNM reach olfactory bulbs for the 3 h, hippocampus and pituitary gland for the 96 h after administration. Since, during 2 weeks after administration TNM detected in the brain presumably according to hodology of the olfactory tract, we can conclude that nanoparticles are moving inside axons and successfully overcome between neuron synaptic junctions.

### *3.2. External modulation*

The nose to brain transport of TNM was suppressed by the simultaneous administration of the inhibitors of $Ca^2$+channels, endocytosis, and active axonal transport. At the same time, different kinds of odorant stimulate the transportation rate of TNM. Using sexual pheromones, which addressed to receptors of the vomeronasal organ, we can modulate TNM roadmap.

### *3.2. Behavioral an physiological effects of TNM*

Long term (3 weeks) intranasal treatment by TNM led to decline of the body mass and reduction of the motoric skill. . Also treated mouse revealed MRI detected brain damages. Asymmetry in brain lesion was accompanied of the body rotation in mouse lifted for tail. In some cases TNM induce breath arrest. This effects is coincided with accumulation of nanolarticles in the 4-th ventricular.

## 4. Natural adaptation to nanoaerosols

The subterranean rodents need protection against the dust inhaled while digging tunnels with their incisors. One of the protective mechanisms could be nasal aerodynamics. To check this hypothesis, the airflow and dust sedimentation in the nasal cavities were studied in the mole vole *Ellobius talpinus*, as a subterranean rodent, and in the mouse *Mus musculus*, as a terrestrial rodent. Quantitative simulation of the deposition of micro and nano-sized aerosols indicated that sedimentation of particles on the total surface of the nasal cavity is higher in the mole vole than in the mouse, but vice versa on the olfactory epithelium, which surface plays key role in transference of nanoparticle from nose to brain. Last theoretical prediction was confirmed experimentally through inhalation of nano-sized $MnCl_2$ aerosols. There was found the reduced manganese accumulation in the olfactory bulbs of mole voles in comparison with the mice. However, intranasal instillations of $MnCl_2$ solution and TNM revealed a similar transportation rate from nose to brain in the both species. There is the first evidence that specificity of nasal aerodynamics in underground rodent guarantees a more effective dust protection of the brain in comparison with terrestrial species.

## 5. Summary

Thus transportation of nanoparticle from nose to brain let us to consider the nano aerosols as an appreciable risk factor for the neurobehavioral diseases. The significance of air pollution by nano-sized dust, which “well understanding” by natural selection, is underestimated, yet, by health control services.

## 6. Acknowledgements:

Study was supported by the Interdisciplinary integration research grants from the Siberian Branch of the Russian Academy of Sciences (grants no. 57, 60, 61, 108 and 122) and by grant of Russian Foundation for Basic Research (grant no. 11-04-00414-a).

## 7. References

[1]. M. Kendall, S. Holage Health impact and toxicological effects of nanomaterials in the lung, *Respirology* **17** (2012), 743–758.

[2]. T.-T. Win-Shwe, H. Fujimaki Nanoparticles and Neurotoxicity. *Int. J. Mol. Sci*. **12** (2011), 6267-6280.

[3]. R.G. Lucchini, D.C. Dorman, A. Elder, B. Veronesi. Neurological impacts from inhalation of pollutants and the nose–brain connection. *NeuroToxicology* **33** (2012), 838–841.

[4]. H. S. Sharma, A. Sharma Neurotoxicity of Engineered Nanoparticles from Metals. *CNS & Neurological Disorders - Drug Targets* **11 (**2012), 65-80.

# Evaluation of genotoxicity of nanomaterials

L.P. Sycheva, V.S. Zhurkov, F.I. Ingel, V.V. Iurchenko, L.V. Akhal'tseva, E.K. Krivtsova, M.A. Kovalenko, S.M. Sheremet`eva, N.A. Iurtseva, L.V. Andreeva

[1] *A.N.Sysin Research Institute of Human Ecology and Environmental Health, Moscow, Russian Federation*

*Keywords: genotoxicity, cytotoxicity, oxide and hydroxide nanoparticles, carbon nanotubes*

The system of assessment of mutagenicity of chemicals - pollutants of air, water, soil, pesticides, drugs - in Russia is the same as in other countries. It is based on OECD guidelines. The most perfect scheme of mutagenicity testing is designed for drugs. The latest Guideline was published in 2012. The minimal optimal set of tests consists of Ames test on Salmonella typhimurium for detection of gene mutations (OECD guideline 471) and micronucleus test or chromosome aberration test for detection of chromosome mutations (OECD guidedelines 474, 475). As new approach polyorgan micronucleus test or Comet-assay are used in some laboratories.

Biological effects of chemicals in the particle form are poorly understand, especially effects of nanomaterials (NM). At the same time the NM are characterized by a number of features, which point out on their potential toxicity and genotoxicity. So, the NM are characterized by high permeability in bodies, organs, tissues and cells; an induction of free radicals, including active forms of oxygen and nitrogen (Gurr J.R. et al., 2005; Wang L. et al., 2007; Papageorgiou I. et al., 2007); damage of cell structure (Jin S. et al., 2007); ability of some NM to penetrate through karyolemma to nucleus (Lovric J. et al., 2005); conjugation with DNA (Dubertret et al., 2002); structure of some NM including atoms of chemicals, possessing carcinogenic action, for example, cadmium or arsenic (Hardman, 2005); similarity in a structure of some NM with asbestos fibers (Oberdoster G. et al., 2005) which are genotoxic and carcinogenic (IARC Monographs, 1977).

We studied the geno- and cytotoxicity of some NM: aluminum hydroxide, titanium dioxide, magnetite nanoparticles in a coating of silicon, silver nanoparticles and carbon nanotubes of three different types. Experimental studies were carried out in the laboratory of genetic monitoring of Institute in 2008-2012 in cooperation with the laboratories of histology, hygiene, drinking water studying, as well as with laboratories of Institutes of Pharmacology, Toxicology Research, CDC/NIOSH (USA). The studies were carried out with polyorgan karyological test. End points of mutagenicity, proliferation and apoptosis were evaluated. The data indicate the following:

- Genotoxic effect of studied NM was identified in vitro- and in vivo;
- Mutagenicity of all studied NM was not revealed in the Salmonella /microsome test (Ames test);
-Mutagenic effect of the studied NM was detected in the test of somatic mosaicism and was not revealed in the test of dominant lethal mutations in Drosophila. The cytogenetic effect of NM was not detected in mice testes. It apparently indicates that germinal tissue is more protected compared with somatic tissues.
- Bone marrow and lungs of mice are the main target organs of genotoxic effect of NM at the different routes of exposure in vivo.
- The colon and bladder are main target organs cytotoxic effects of MN in terms of proliferation and apoptosis. It was determined the difference between the nano- and ionic form of silver in terms of proliferation.
- In the model of silver study the differences of nano- and ionic forms were defined by the next criteria: presence or absence of effect in vitro, target organs and doses of their genotoxic and toxic effects.

- The comparison of nanoparticles of different sizes of titanium dioxide shows differences in target organs of genotoxic effect and types of genetic damages.

- Single-walled carbon nanotubes increased of the frequency of micronucleated lung cells in mice (inhalation) in 3 times and reduced pyknosis (destruction of nuclei) in a year after the end of exposure.

- On the model of short carbon nanotubes with intranasal exposure the gender differences were revealed in mice: males were more sensitive to nanotubes compared with females; the dose curve was the same.

- Comet assay (detected premutational events) was more sensitive compared to the micronucleus test (detected mutations) in the same experiment with titanium dioxide.

- In studies of the safety of NM there is the problem of their detailed physic-chemical characteristics: structure, particle size, surface coating with other materials, and others. Creation of NM must be accompanied by the development of devices to determine their content in the air, water, soil, biological fluids. It is necessary to unite physicists, chemists and toxicologists with their equipment, knowledge and experience in working groups to assess the safety of NM.

Now understanding of the necessity of in-depth toxicological studies of NM introduced into the human environment enhanced.

# Biological markers relevant to realistic occupational exposures to multiwalled carbon nanotubes

L.M. Fatkhutdinova[1*], T.O. Khaliullin[1], R.R. Zalyalov[1], I.G. Mustafin[1], E.M. Birch[2], E.R. Kisin[2], A.A. Shvedova[2]

[1]*Kazan State Medical University (Kazan, Russia)*

[2]*National Institute for Occupational Safety and Health (NIOSH, USA)*

(*) corresponding author: liliya.fatkhutdinova@gmail.com

*Keywords: MWCNT, fibrosis, biomarkers, in vivo, pilot human study*

## 1. Introduction

The number of enterprises, which synthesize and use carbon nanotubes (CNTs), is growing from year to year. The world market of CNTs reached $192 million in 2011. Market dynamics suggests growth to $527 million in 2016 with average annual rate of 22.4% [1]. In Russia there are a few businesses: in Tambov, Vladimir, Novosibirsk, Kaliningrad, and their number is increasing due to rising demand for the product. These workplaces are mainly small businesses established on the basis of universities and research institutions. However, several large manufactures are in the project stage. Carbon nanotubes are composed of one or more folded sheets of graphene and have a dual nature. According to the EU definition [2], they refer to nanomaterials. On the other hand, the morphology of the carbon nanotubes allows considering them as the fibers [3]. At present, there is a considerable amount of information on respiratory diseases linked to fibers. Furthermore, nanomaterials have high penetration rate and reactivity. All this makes it necessary to study biomedical effects of CNTs, including the assessment of potential risks to workers and the public.

## 2. Experimental

### *2.1. Exposure assessment*

The study was conducted at 2 multi-walled carbon nanotubes (MWCNTs) producing enterprises with the same reactor. Air sampling was carried out in breathing zone with and without cyclone for respirable fraction. The air samples were collected on a high-purity quartz filter, the content of elemental carbon (EC) being determined using a thermo-analyzer (a modified NIOSH method 5040). TEM coupled with energy dispersive x-ray spectroscopy was performed after sampling on mixed cellulose esters (MCE) filters (a modified method NMAM 7402). The presence of MWCNTs in workplace air was accepted when both elemental carbon content, and individual nanotubes or their agglomerates by TEM were found out.

### *2.2. In vivo study*

The local inflammatory response in lungs and fibrogenic potential of multi-walled carbon nanotubes was studied during the acute pharyngeal aspiration experiment in mice. Animals were divided into control and three experimental groups of 40 mice each. The dosage had been chosen based on the MWCNTs aerosol concentration at the company-producer's workplaces. Exposure groups were given 20, 40 and 80 mg of the non-purified MWCNTs. Mice were euthanized on 1, 7, 28 and 56 days. ELISA (cytokines in BALF, TGF-β1 and osteopontin in serum), microscopy, and histological examination were implemented.

### *2.3. Pilot human study*

11 workers who had more than 1 year contact with MWCNT aerosol composed the exposure group, the control group consisted of 14 people. Elemental carbon was evaluated in air samples and the CNT presence was confirmed by TEM-analysis. Blood and induced sputum samples were obtained from workers, TGF-β1, KL-6 and osteopontin levels evaluated. To assess the relationship between MWCNT exposure and biomarker levels (age, gender, smoking have been chosen as cofounders)

generalized linear models including main effects and interactions in-pairs were created. The regression coefficients confidence intervals were refined by bootstrap analysis.

## 3. Results

### *3.1. Exposure assessment*

Time-weighted average respirable MWCNT fraction was up to 6.11 mg/m3 (elemental carbon), exceeding the NIOSH recommended exposure level (1 mg/m3). TEM has shown the presence of MWCNT agglomerates sized 0,5-10 μm in all air samples.

Table 1. MWCNTs at workplaces

| | Cyclon | EC, Cmax, мкг/м$^3$ | EC, Ctwa мкг/м$^3$ |
|---|---|---|---|
| Gathering | + | 32,59 | 6,11 |
| | - | 157,77 | 29,60 |
| Desintegration | + | 10,83 | 2,03 |
| | - | 10,92 | 2,05 |
| Packing | + | 14,15 | 2,65 |
| | - | 134,85 | 25,30 |
| Laboratory | + | 2,87 | 0,54 |
| | - | 3,78 | 0,71 |

Fig. 1. MWCNTs on MCE filter (TEM)

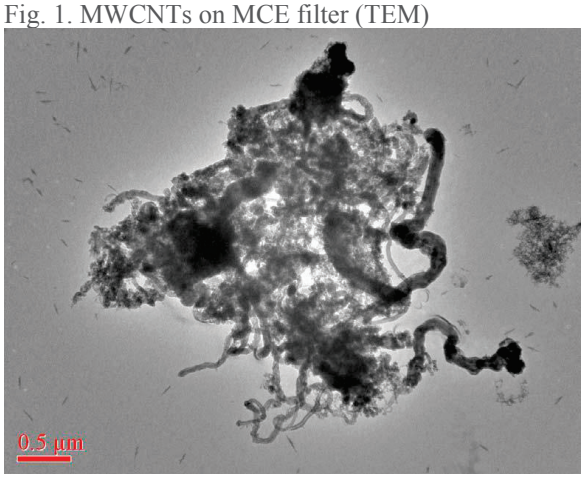


### *3.2. In vivo study*

ELISA, microscopy, and histological examination showed that MWCNTs were able to cause a dose-and time-based changes and damage in mice lungs as well as local inflammatory process, oxidative stress induction and connective tissue development (fibrosis). It was shown that TGF-β1 and osteopontin in blood serum may serve as potential exposure biomarkers.

### *3.3. Pilot human study*

It was found that exposure to MWCNT aerosol at workplaces may alter the fibrosis biomarkers in blood serum and induced sputum. The levels of TGF-β1 in serum were significantly dependent on exposure to MWCNTs (β=10.47, 95%BCa=1.18-51.75), the KL-6 levels in induced sputum was significantly higher in exposure group (β=235.9, 95%BCa=21.2-482). Osteopontin proved itself as an uninformative indicator.

## 4. Discussion

Real exposure to MWCNTs for workers has been shown. Our data suggest that exposure to MWCNTs at the workplace can change the content of some markers of fibrosis in serum and induced sputum samples. In particular, the levels of TGF- β1 in serum and KL-6 in induced sputum were significantly dependent on exposure to MWCNTs. Osteopontin in this study did not show itself as informative index, but it is still recommended to be included in the test battery for future research. Based on the principle of reasonable precautions, plants producing and applying MWCNTs should implement measures to control MWCNT exposure in the working area and perform medical surveillance of workers.

## 5. References

[1] Global Markets and Technologies for Carbon Nanotubes // BCC Research. Market forecasting. http://www.bccresearch.com/report/carbon-nanotubes-markets-technologies-nan024e.html

[2] http://eur-lex.europa.eu/LexUriServ/LexUriServ.do?uri=CELEX:32011H0696:EN:NOT

[3] Reference Methods for Measuring Airborne Man-Made Mineral Fibers. Environmental Health Series 4. Copenhagen:World Health Organization. – 1985

# The dynamics and control of nanomagnet cluster formation in a flow for medical applications

M. Forrester[1*], F. Kusmartsev[1]

[1] *Department of Physics, School of Science, Loughborough University, Leicestershire, LE11 3TU (United Kingdom)*

(*) d.m.forrester @lboro.ac.uk

*Keywords: nanomagnetism, magnetic forces, anisotropy, energy relaxation*

## 1. Introduction

The modern science has recognized the importance of nano-particles in studies of life processes, cancer and curing it. However, the dynamics of such particles is complex and includes the interplay of different degrees of freedom that consist of both magnetic and non-magnetic elements. We discuss here the dynamical behavior and stationary states of a flow consisting of many interacting high-moment synthetic antiferromagnetic (SAF) nanomagnets [1].

Each of these particles has near spherical or a disk-like shape and strong magnetic moment. Because of these moments all particles are strongly interacting via magnetic dipole-dipole interaction. Note that the lowest energy occurs for particles in which magnetic moments are ordered anti-parallel. That is, they have anti-ferro-magnetic orientation with respect to each other. So these forces effectively create an attraction between anti-ferro-magnetically ordered particles with the potential:

$$V(R) = -\frac{\mu_0 M^2}{4\pi R^3} \qquad (1),$$

where *R* is the separation radius of the SAF particles and M is the value of their magnetic moment. On the other hand the relative kinetic energy of the two interacting particles is described by the equation:

$$K(R) = \frac{\hbar^2}{mR^2} \qquad (2),$$

where *m* is the reduced mass of the two SAF particles. The total energy of the particles is the sum of *E(R)=K(R)+V(R).* It has a maximum when the distance between particles is equal to

$$R_{barrier} = \frac{3\mu_0 m M^2}{2\hbar^2} \qquad (3)$$

When the distance between particles is smaller than then critical one that is equal to $R_{barrier}$, the energy between these attracting particles decreases if their separation distance decreases. The minimal energy corresponds to the situation when these two particles are in contact with each other, that is, they form a new double particle.

In principle in the flow of such magnetic nano-particles there may not only be created double particles but trimers, four-mers and in general big clusters of magnetic particles, where the magnetic energy dominates over their individual kinetic energy. Such SAF clusters may contain many layers of anti-ferro-magnetically ordered nano-magnets with elliptical cross-sections and which may be separated from one another by non-magnetic materials. With nanomagnets increasingly being used and proposed as functional units for in-vivo applications, it is vital to understand how these clusters form and the effects of temperature on them, as well as their responses to electromagnetic radiation. The formation of the magnetic clusters can be controlled by magnetic field. For example by applying magnetic field the magnetic moments of the particles will be polarized and they will be all ordered in parallel. At such ordering the attraction between particles described by the eq. (1) is transferred into their repulsion and the particles in the clusters will be decomposed and become free. Thus the application of magnetic field may prevent to the clusterisation of magnetic particles and protect the living body from their intoxication. Thus we propose the

mechanism of the SAF clusters control which is based on an application of magnetic field.

## 2. Magnetic clustering of synthetic antiferromagnetic/ferromagnetic particles

The controlled agglomeration and dispersal of nanomagnets is of high importance for medical applications and for the understanding of biological interactions. Below we present, in Fig.1, the control of clusters of nanomagnets using applied magnetic fields. These systems of interacting nanoparticles, in which the shape of the particles and their size heavily influence the competition between magnetic properties and random thermal fluctuations, have a mean diameter of 30nm.

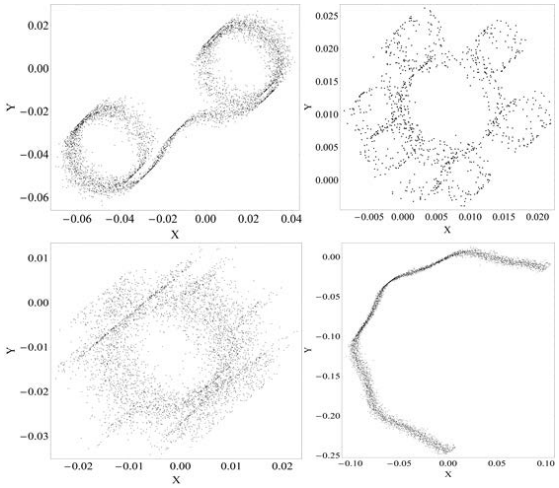

Figure1. An alternating applied magnetic field of sufficient strength and frequency forms clusters or strings of nanoparticles in competition with thermal fluctuations.

Alignment of the nanomagnets occurs in the magnetic field and rotating the field causes the chains to form loop structures. Upon turning the field off, the chains form into three dimensional coils. When a cluster forms, individual moments vector in a manner than minimizes the total magnetic moment of the group, i.e. a synthetic anti-ferro-magnetic state occurs. The exposure of nanomagnets to a switching magnetic field increases the ordering of the cluster. Figure 2 schematically shows the break-up of agglomerated nanomagnets under the action of an applied magnetic field.

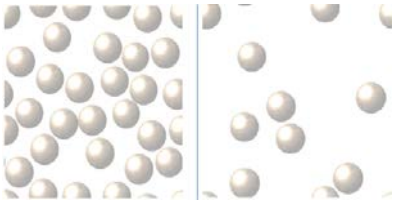

Figure2. The nanomagnets will predominately cluster as on the left. On the right, a microwave frequency field is applied to disperse the nanoparticles. Intricate chains of closed loops or long strings, or interspersed clusters can emerge ( as shown in Fig. 1).

It is interesting that the geometry of the nanoparticles can also dictate the magnetic response by introducing varying degrees of anisotropy. Phase diagrams such as that in Fig.3 characterize the repulsion and attraction of the nanomagnets.

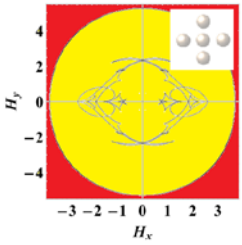

Figure3. In a rotating magnetic field (field angle from zero to $2\pi$ going around the quadrants of the $H_x - H_y$ plot above) the field strengths required to separate the nanomagnets are shown in red (measured in $kOe$). In the yellow region there is a stronger propensity for the nanomagnets to cluster. In this case five magnets are considered (top inset).

The interactions to eliminate or enhance magnetic remanence and coercivity can be manipulated under the control of the magnetic fields to create large synthetic antiferromagnetic or ferromagnetic structures.

## 3. Discussion

We have briefly outlined the magnetic manipulation of clusters of nanomagnets. Nanoparticles can enter the body by various routes, including inhalation, and can be distributed by systemic circulation throughout the body. Thus, the importance of controlling nano-clusters is very high.

## 4. References

[1] M. Forrester, E. Kovacs, F. Kusmartsev. Phys. Rev. B **87**, 174416 (2013).

# Aerogel Technology for Preparation of Nanoscale Oxides

A. Vedyagin[*,1,2], A. Bedilo[1], E. Ilyina[1], I. Mishakov[1,2]

[1] *Boreskov Institute of Catalysis, Novosibirsk, Prospekt Lavrentieva 5, 630090, Russia*
[2] *Novosibirsk State Technical University, Novosibirsk, Prospekt K.Marksa 20, 630092, Russia*

(*) corresponding author: vedyagin@catalysis.ru

*Keywords: aerogel synthesis, nanocrystalline oxides, catalysts, destructive sorbents*

## 1. Introduction

Nanoscale oxides can be synthesized by drying of gels in supercritical conditions, so that the collapse of the pore structure can be avoided. This technology yields materials with small particles size, very high surface area, along with a considerable quantity of superficial defects and low density. This makes them very promising for application as adsorbents and catalysts. It is well known that physicochemical properties of very small oxide crystals substantially depend on their size. Various nanocrystalline oxides synthesized by aerogel technique have been widely investigated as destructive sorbents for decomposition of harmful organic substances [1], neutralizations of bacteria [2], as well as in various catalytic processes [3].

## 2. Experimental

As a rule, nanoscale oxides are synthesized by a widely spread technique based on the use of such organometallic reagents as alkoxides, β-biketonates and carboxylates of metals. Alkoxides are applied most often to synthesize nanocrystalline oxides (MgO, $Al_2O_3$, $ZrO_2$, $TiO_2$) as well as binary oxide systems ($VO_x$/MgO, $CoO_x$/MgO etc.) [3-4]. In this case it is possible to avoid using water as the solvent leaving the whole set of parameters free to be controlled. These parameters can be varied to tune the desired properties of resulting gels.

Sulfated alumina aerogels were synthesized by a similar procedure with sulfuric acid used as a modifying agent. The introduction of sulfuric acid to the solution before gelation results in a substantial decrease of the pore volume, whereas the high surface area of the $Al_2O_3$ aerogels is preserved.

## 3. Results and Discussions

It was shown that applied aerogel technique allowed us to prepare $VO_x$/MgO materials possessing exceptionally uniform distribution of vanadium in the MgO structure at a wide range of V/Mg ratios [5]. Dehydration of aerogel $VMg(OH)_x$ hydroxides in mild conditions results in the formation of $VO_x$/MgO samples with high surface area (~ 450 $m^2$/g) consisting of cubic crystals with the size below 5 nm. The synthesized mixed aerogels showed superior performance in oxidative dehydrogenation of propane substantially exceeding that of similar materials prepared by impregnation.

The surface areas of the sulfated alumina aerogels after calcination at 600°C usually required to make active acid catalysts was about 600 $m^2$/g. These samples showed excellent catalytic activity in dehydrochlorination of 1-chlorobutane, substantially exceeding those of conventionally prepared materials. Also they showed outstanding performance in the destructive sorption in destructive adsorption of (2-chloroethyl)ethyl sulfide that is a mustard gas mimic.

## 4. Acknowledgement

Financial support by Russian Foundation for Basic Research (projects 12-03-00905-a and 12-08-31426 mol_a) is acknowledged with gratitude.

## 5. References

[1]. A. F. Bedilo, M. J. Sigel, O. B. Koper, M. S. Melgunov, K. J. Klabunde, J. Mater. Chem., 12, 3599, 2002.
[2]. P. K. Stoimenov, R. L. Klinger, G. L. Marchin, K. J. Klabunde, Langmuir, 18, 6679, 2002.
[3]. I. V. Mishakov, A. A. Vedyagin, A. F. Bedilo, V. I. Zailovskii, K. J. Klabunde, Catal. Today, 144, 278, 2009.
[4]. E. V. Ilyina, I. V. Mishakov, A. A. Vedyagin, Inorg. Mater., 45, 1267, 2009.

# Application of inorganic nano-scaled particles in experimental oncology

Bgatova N.P.

*Federal State Budgetary Institution «Scientific Institution of Clinical and Experimental Lymphology» of the Siberian Branch under the Russian Academy of Medical Sciences*

(*) corresponding author: n_bgatova@ngs.ru

*Keywords: lithium carbonate nanosized particles, hepatocarcinoma 29, lipid peroxidation, necrosis, proliferation*

## 1. Introduction

Cancer is one of the major causes of mortality and the worldwide incidence of cancer continues to increase. The most common cancer treatments are limited to chemotherapy, radiation, and surgery. Frequent challenges encountered by current cancer therapies include nonspecific systemic distribution of antitumor agents, inadequate drug concentrations reaching the tumor, and the limited ability to monitor therapeutic responses. Poor drug delivery to the target site leads to significant complications, such as multidrug resistance [1]. By applying a vast and diverse array of nanoparticles, whose design is based on techniques developed in the fields of engineering, chemistry, and medicine, to molecular imaging and targeted therapy, cancer nanotechnology promises to overcome several of the current obstacles faced by cancer therapies.

In recent years, the importance of nanoparticles for experimental medicine became apparent, leading to their wide use. These nanosized objects take on novel properties and functions that differ markedly from those seen in macro-scale objects made of the same materials. The small size, customized surface, improved solubility, and multi-functionality of nanoparticles will continue to open many doors and create new biomedical applications. Indeed, the novel properties of nanoparticles offer the ability to interact with complex cellular functions in new ways [2]. For practical applications of nanoparticles to the therapy in vivo, the highly specific, efficient, and rapid internalization of nanoparticles into specific target cells is necessary, meaning that biodistribution, “cellular uptake” and “intracellular behavior” are important. In the present work, the effects of lithium carbonate nanosized particles on several structural and biochemical parameters were studied in male CBA mice.

## 2. Experimental methods

Biological effects of lithium carbonate nanosized particles on intact CBA line mice and in condition of tumor growth were evaluated by methods of light, electron microscopy and biochemistry. Lithium carbonate nanosized particles (2 mg/kg body weight) were administered by intramuscular injections daily for 10 days to intact mice and mice with hepatocarcinoma-29 (on periphery of tumor growth in a leg of CBA mice).The effects of lithium carbonate nanosized particles on hepatocarcinoma 29 (HCC-29) cells proliferation were examined using Cell-IQ analyzer (Chip-Man Technologies Ltd, Tampere, Finland), having a visualization system integrated with a camera, microscope, and an incubator for culturing cells.

## 3. Results

It was shown that intramuscular injection of lithium carbonate nanosized particles increased the lipid peroxidation activity in muscle tissue. Structural changes in leg muscle tissue and liver at intact mice of line CBA were revealed. Processes of destruction of muscle fiber, increase in vessels density and in quantities of macrophages and neutrophil, increase of the sizes of lymph sinus regional iliac lymph node and the maintenance of macrophages there are shown. Accumulation of lithium nanosized particles in phagosome of fibroblast, macrophages of a muscular tissue of a leg and lymph sinus regional iliac a lymph node is noted. In the liver, parenchyma marked the focus of hepatocyte necrosis mainly in the field of portal tract and a hemorrhage in parenchyma was revealed. Intramuscular injection of lithium

carbonate nanosized particles has caused considerable growth in peritoneal macrophages activity. It was shown that addition of lithium carbonate nanosized particles in culture of macrophages, depending on the dose, can reduce potential macrophages activity, estimated from production of reactive metabolite of nitrogen. After one and five-fold injection of lithium carbonate nanosized particles in the thigh muscle anaerobic glycolysis is activated, as it is evidenced by the accumulation of lactic acid. Hydrolysis of triglycerides was registered after single injection of nanosized of lithium carbonate particles. The levels of these lipids in muscular tissue decreased four times and accumulation of these lipids was noted after the 4 and 5-fold injection. Injection of nanosized lithium carbonate particles caused system to undergo metabolic changes: increased utilization of lactic acid in the liver into glucose and then use of the glucose in the synthesis of glycogen and triglycerides. Intramuscular injection of lithium carbonate nanosized particles did not cause significant damage of the liver.

After injection of lithium carbonate nanosized particles on periphery of tumor growth (hepatocarcinoma-29 in a leg of CBA mice) increase of the maintenance of macrophages and neutrophil in tumor, growth volume of cancer cells necrosis and destructive changes in cytoplasm and nucleus of cancer cells were observed. Also seen is dissemination of cancer cells in regional iliac lymph node, increase maintenance of neutrophils and macrophages in lymph sinus and parenchyma in iliac lymph node.

Our results indicate that injection of lithium carbonate nanosized particles on periphery of tumor growth induces triglycerides accumulation in muscular tissue and liver. Lithium carbonate nanosized particles stimulate production of NO by peritoneal macrophages in condition of tumor growth. A significant decrease of volume density of blood vessels in tumor area was observed in treated rats. After injection of lithium carbonate nanosized particles on periphery of tumor growth, we observed a decrease in the quantity of the most abundant cancer cells at the 3rd stage of a differentiation. Additionally, mice treated by lithium carbonate nanosized particles demonstrated the increase of 30 % in the life expectancy compared with control mice. We also studied the effects of different concentration of lithium carbonate nanosized particles on hepatocarcinoma 29 cells proliferation in vitro. Our results show that lithium carbonate nanosized particles exhibited cytotoxic effect on hepatocarcinoma cells in dose-dependent manner.

## 4. Discussion

Lithium has a number of effects on various biological processes, including embryonic development, glycogen synthesis, hematopoiesis, neuronal communication. Lithium exerts its cellular effects by targeting a variety of enzymes that require metal ions for catalysis or enzymes that transport metal ions between cellular compartments. It is shown that lithium at doses commonly used to inhibit GSK3β and activate the Wnt/β-catenin signaling pathway in transformed cell lines and tumor cells, induces a G2/M cell cycle arrest instead. Lithium salts can considerably increase the direct cytotoxic effect of tumor necrosis factor on various tumor cells in vitro and in vivo and can suppress tumor growth. The data indicate that lithium administration may represent a target therapy for cancer [3].

Because the novel properties of nanoparticles offer the ability to interact with complex cellular functions in new ways, biological effects of lithium carbonate nanosized particles administration were studied in this investigation. We found that lithium carbonate nanosized particles can block cancer cell proliferation, tumor angiogenesis, possess cytotoxic effect on hepatocarcinoma cells and can be used for cancer treatment.

## 5. References

[1]. X. Wang, L. Yang, Z. Chen, D.M. Shin, Cancer J Clin. 58 (2008) 97-110.

[2] R. Singh, J.W.Jr. Lillard, Exp Mol Pathol. 86(3) (2009) 215-223.

[3] Q. Zhu, J. Yang, S Han et al. Prostate. 8 (2011) 835-845.

# Features of Microorganisms and Nano- and Microparticles of Minerals Interaction

Buzoleva L.S., Chayka V.V., Bogatyrenko E.A., Golokhvast K.S.

*Keywords: zeolites, bacterial cell*

## 1. Introduction

Zeolites are eaten by many animals under natural conditions [3] and, undoubtedly, influence the microbiological status of a macroorganism. In modern literature there are a number of the publications concerning influence of zeolites on bacteria [4; 5; 13]. In particular, in G.I. Chubenko's (2000) work, it is noted that «zeovite» (the sorbent made of zeolites of Sakhalin) possesses expressed antimicrobic, adsorptive, eliminative and anti-toxic activities in vitro and in vivo concerning Salmonella Kottbus 5753, Staphylococcus aureus 6538-209 p and Escherichia coli O 86 E 990. In Vesna L. and coauthors work (2004) probiotic effects of the biologically active supplement "Megamin" on growth of probiotic microorganisms (Lactobacillus acidophilus and Bifidobacterium bifidum) were investigated. Data accurately show probiotic effect of "Megamin" on both species of microorganisms. There are messages on removal of bacteria by means of zeolites from an organism and from water [2; 7; 12]. In literature there are data that zeolites suppress growth of aerobic bacteria, and promotes growth of anaerobes. At first it was explained only by adsorption of microbes on surface of zeolite and mechanical elimination. Recently researchers [11] agree in opinion that zeolites suppress growth of some microorganisms by formation of powerful double electric layer owing to hydrophobic interactions on a zeolite surface. For increase of antimicrobic properties of zeolite researches on saturation of these minerals by silver and zinc cations are also conducted [6; 8]. It should be noted also there is data about zeolites properties allowing them to influence some metabolic ways of bacteria, in particular protein [10] synthesis. There are messages on anti-virus properties of zeolite [9].

## 2. Materials and methods

Zeolitic minerals were applied both sterile (processing in autoclave case at a temperature of 1800C within 3 hours) and unsterile. Before all actions zeolite was crushed (VKMD6 crusher) (Vibrotechnician, USSR) and an ultrasonic homogenizer Bandelin Sonopulse 3400 (Italy). As a result the size of particles of a zeolitic tufa was about 1-5 microns. For determination of microbiological activity of zeolitic tufa of Vanginsky, Kulikovsky and Lyutogsky fields cultures of opportunistic bacteria of E. coli 25922, St. aureus 209-P and 906 received from SISC of L.A. Tarasevich were taken. Cultures parted from 109 cages in 1 ml (received according to the turbidity standard) to 102 cages in 1 ml with a cultivation step multiple 10. Researches were conducted on the basis of microbiology laboratory of Epidemiology and Hygiene Center in Primorsky region, Vladivostok. To culture in a certain dilution added zeolite and held during the min. Then 1 ml of a zeolitic and cultural mix sowed on mediums: yolk-salt agar, meat-peptone agar (MPA) and Endo. Calculation of colony forming units (CFU) carried out visually. Concentration of zeolite in tuffs of all three fields was about 60-70%. Statistical data processing was carried out by means of the Statistica 6.0 and Microsoft Excel program. Assessment of reliability of distinctions determined by Student's t-test.

## 3. Results and discussion

As a result of the conducted researches it is established that zeolite of the Vanginsky field actively adsorbed bacteria of E. coli 25922 in dilution 10-7 and St.

aureus 209-P in dilution from 10-7 to 10-5. According to table 1 it is visible that with increase in concentration of zeolite the number of cells in cultural liquid considerably decreases. With increase in number of bacterial cells in solution efficiency of their sorption by zeolite also decreases.

Table 1. Influence of particles concentration of Vanginsky zeolite on St. aureus 209-P sorption (CFU/ml)

| **Zeolite concentration / Dilution of culture (CFU/ml )** | $10^2$ | $10^3$ | $10^4$ |
|---|---|---|---|
| Control (no zeolite) | 120±15 | (1,53±0,8) x$10^2$ | (1,1±0,1)x$10^3$ |
| 10 mg/ml | No growth | (1,4±0,2) x $10^2$ | (2±0,2) x$10^2$ |
| 20 mg/ml | No growth | (0,5±0,0)x$10^2$ | (0,22±0,0)x$10^2$ |
| 50 mg/ml | No growth | No growth | (0,7±0,1)x$10^2$ |

Results of zeolite use from Kulikovsky field also showed that efficiency of bacteria sorption depends on concentration of zeolite and concentration of bacteria in the environment. Besides, it was shown that unsterile zeolite occludes more bacterial cells in comparison with sterile (table 2).

Table 2. Influence of particles concentration and sterilization of zeolite from Kulikovsky field on St. aureus 906 sorption (CFU/ml)

| **Zeolite concentration** | sterile | | unsterile | |
|---|---|---|---|---|
| **Control (no zeolite)** | (4,2±0,5) x$10^5$ | (2,8±0,2)x$10^6$ | (8,2±0,5) x$10^5$ | (5,5±0,2)x$10^6$ |
| 10 mg/ml | (0,5±0,0) x$10^3$ | (5±0,2) x$10^3$ | (1,5±0,0)x$10^2$ | (1,9±0,0)x$10^3$ |
| 20 mg/ml | (0,58±0,1)x$10^2$ | (8,4±1,2)x$10^2$ | (0,06±0,0)x$10^2$ | (5,4±0,3)x$10^2$ |
| 50 mg/ml | (1,26±0,2)x$10^3$ | (2,2±0,2)x$10^3$ | No growth | (2,2±0,1)x10 |

a) b)

Fig. 1 a) St. aureus colonies in dilution $10^{-3}$ in presence of unsterile zeolite from Kulikovsky field in concentration of 50 mg/ml. b) lack of growth of St. aureus in dilution 10-3 in presence of unsterile zeolite from Lyutogsky field in concentration of 10 mg/ml

While researching of influence both sterile and unsterile zeolite from Kulikovsky field on sorption of E. coli 25922 in all concentration (from 102 to 106) we found the drain growth of colonies – number of CFU couldn't be estimated. Therefore, gram negative bacteria of an intestinal rod weren't occluded by this zeolite.

Zeolite from Lyutogsky field (both sterile and unsterile) in case of use of all its studied concentrations completely occluded bacteria St. aureus 209-P in concentration from 103 to 106 CFU/ml. Concerning E. coli 25922 it is possible to note that unsterile zeolite also almost completely occluded cells of an intestinal rod in quite high their concentration in the environment.

Table 3. Influence of particles concentration of Lyutogsky zeolite on sorption of E. coli 25922 (CFU/ml)

| **Concentration** | sterile | | unsterile | |
|---|---|---|---|---|
| Control (no zeolite) | (2,2±0,5) x$10^5$ | (2,8±0,2) x$10^6$ | (8,2±0,5) x$10^5$ | (5,5±0,2) x$10^6$ |
| 10 mg/ml | 9,7x10$^2$ | 1,8x$10^3$ | No growth | 0,57x$10^2$ |
| 20 mg/ml | 1,4x10$^2$ | 9,2x$10^2$ | No growth | 0,3x$10^2$ |
| 50 mg/ml | 1,2x10$^2$ | 1,7x$10^2$ | No growth | No growth |

Earlier we have shown [1] that crushing of zeolite particles to the sizes from

100 to 500 nanometers leads to almost full loss of sorption properties of zeolites of those fields which with more coarse grinding (1-5 microns) possess such properties. It is obvious smaller particles completely cover a surface of a bacterial cell (fig. 1). There is an assumption that intensity of interaction of zeolite with a bacterial cell depends on an ionogenic surface of a bacterial cell (pure – carboxyl, complex – carboxyl-amine) and has noticeable impact on its interaction with zeolite particles. The complex surface of a cell promotes mosaic distribution of zeolitic particles on it that gives the chance to carry out an active gas exchange with environment for cell [14.]. On large particles bacterial cells are adsorbed and get into pores of mineral (fig. 2).

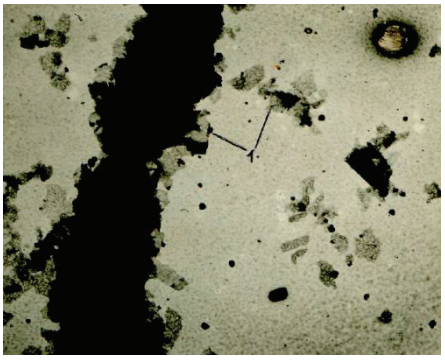

Fig. 2. Bacterial cells are adsorbed on minerals (pointed by number 1).

Thus, particles of zeolites of different fields possess ability to occlude cells of gram negative and gram positive bacteria. Thus, efficiency of sorption depends on concentration of particles and the zeolite nature, and also on concentration of bacteria in solution. Zeolites of Vanginsky and Kulikovsky fields are similar on the adsorptive properties, unlike zeolite of the Lyutogsky field possessing high sorption rates concerning studied bacteria. Such difference in results can be explained with existence of crystal lattice on a surface of zeolites with specific electric charge [11] which differs depending on a zeolite field. The nature of zeolite is also important since unsterile zeolites more occlude bacteria in comparison with the sterile.

The project was supported by the Scientific Fund of Far Eastern Federal University.

## 4. References

[1]. K.S. Golokhvast, A.M. Panichev, A.N. Gulkov, P.A. Nikiforov, I.G. Fedotova, A.A. Anisimova, I.E. Pamirsky, E.G. Avtomonov // News of Samara scientific center of Russian Academy of Sciences, 2009. – Vol.11, No. 5 (2). – P. 448-451.

[2]. Dashibalova L.T. Intensification of biological purification of economic and household sewage with application of biosorption filtering on natural zeolites: Abstract for PhD in tech. sciences. - Irkutsk, 2000. - 25 p.

[3]. Panichev A.M. Lithophagy in the world of fauna and human. - M: Science, 1990. - 224 p.

[4]. Chubenko G. I. Microbiological, immunological and allergic aspects of enteric infections of children and a way of their correction: Thesis of Doctor of medical sciences. - Vladivostok, 2000. - 391 p.

[5]. Shurubikova A. A. Influence of natural zeolites on Saccharomyces cerevisiae: Abstract for PhD in biol. sciences. - Ulan-Ude, 2004. - 19 p.

[6]. B. Concepción-Rosabal, N. Bogdanchikova, I. De la Rosa, M.T. Olguín, D. Alcántara, and G. Rodríguez-Fuentes // Book of abstracts 7th International Conference on the Occurrence, Properties, and Utilization of Natural Zeolites «Zeolite'06», 16–21 July 2006, Socorro, New Mexico, USA. – Socorro, 2006. - P. 88-90.

[7]. Foglar L, Sipos L, Bolf N. // World Journal of Microbiology & Biotechnology. - 2007. - №23. - P. 1595-1603.

[8]. Galeano B., Korff E., Nicholson W.L. // Applied and Environmental Microbiology. - 2003. - №69. - P. 4329-4231.

[9]. Grce M., Pavelic K. // Microporous and Mesoporous Materials. - 2005. - Vol. 79, Issues 1-3, №1. - P. 165-169.

[10]. Kim D.M., Kim Y.E., Choi C.Y. // Biotechnology Letters. - 1995. - №17. - P. 1043-1046.

[11]. Kubota M, Nakabayashi T, Matsumoto Y, Shiomi T, Yamada Y, Ino K et al. // Colloids and Surfaces B-Biointerfaces. - 2008. - №64. - P. 88-97.

[12]. Milan Z., de Las Pozas C., Cruz M. et al. // J. Environ. Sci. Health. – 2001. - Vol. 36, №6. - P. 1073-1087.

[13]. Vesna L., Ivkovic S., Vesna T. // 5-th International Conference and Exhibition on Nutraceuticals and Functional Foods, San Francisco, SAD, 2004. – San Francisco, 2004. - P. 18-19.

[14]. Marshall K.C. // Biochimica et biophysica acta. - 1968. - Vol.156. - №1. - P. 179-186.

# On-board Catalytic Nanoplant for Abatement of Vehicle Exhausts

I. Mishakov[*,1,2], A. Vedyagin[1,2], V. Stoyanovskii[1], Yu. Shubin[3]

[1] *Boreskov Institute of Catalysis, Novosibirsk, Prospekt Lavrentieva 5, 630090, Russia*
[2] *Novosibirsk State Technical University, Novosibirsk, Prospekt K.Marxa 20, 630092, Russia*
[3] *Nikolaev Institute of Inorganic Chemistry, Novosibirsk, Prospekt Lavrentieva 3, 630090, Russia*

(*) corresponding author: mishakov@catalysis.ru

*Keywords: three-way catalysts, diesel oxidation catalysts, Pt-Pd and Pd-Rh alloyed systems*

## 1. Introduction

Increasing number of vehicles equipped with gasoline and diesel engines may now be responsible for more than 60% of total atmosphere pollution in large cities. An effective abatement of main constituents of automobile exhaust gases, such as $NO_x$, CO, hydrocarbons (HCs) and soot, today is considered to be one of the most important ecologic issues.

Catalytic on-board convertor is already used widely in many countries to reduce the level of toxic compounds released with exhaust gases. It consists of metal or ceramic substrate with supported layered active component - washcoat (Fig.1). Typically washcoat comprises metal oxides serving as support for nanoparticles of noble metals (Pd, Pt, Rh).

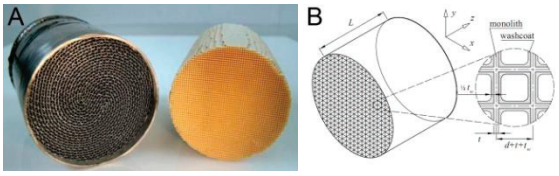


Figure 1. Metal (A, left) and ceramic (A, right) catalyst substrate and ceramic catalyst substrate nomenclature (B).

During the working cycle automotive convertors are exposed to rather high temperatures and sudden temperature oscillations which may lead to quick deactivation of catalyst. At temperature of 900°C and above the alumina surface area drops down, and the sintering of noble metal particles occurs, too. Dispersed Pd particles readily undergo sintering into agglomerates; rhodium gets oxidized from $Rh^0$ to $Rh^{3+}$ state followed by diffusion of the $Rh^{3+}$ ions into the support bulk [1].

## 2. Experimental

Both three-way (TWC) and diesel oxidation (DOC) Pd-Rh and Pt-Pd alloyed catalysts were synthesized and studied. Catalytic activity was tested in oxidation of CO, HCs, and in $NO_x$ reduction. Ethane hydrogenolysis testing reaction was used to determine the surface concentration of Pd and Rh, and to confirm the alloy formation. Stability of samples was estimated by prompt thermal aging *in situ* technique. Photoluminescence method was applied to elucidate the mechanism of stabilization.

## 3. Results and Discussion

It was shown that Pd-Rh alloyed catalyst is characterized by comparable activity and enhanced stability as compared to reference sample. While the Pd and Rh particles of monometallic samples were found to interact with support at high T resulting in sintering and bulk diffusion, the particles of alloy type kept their initial state of dispersion and catalytic activity.

In case of DOC, stabilized Pt-Pd catalytic system has been prepared. Use of double complex Pt and Pd salts as precursors allowed us to synthesized rather active and stable alloyed catalyst which was confirmed by means of XRD, TEM and XPS methods. It was found that the atmosphere of salt decomposition has strong effect on resulting performance of catalyst.

## 4. Acknowledgement

Financial support from Russian Foundation for Basic Research (Grant #13-03-00988) is gratefully acknowledged.

## 5. References

[1]. V.O. Stoyanovskii, A.A. Vedyagin, et al, Applied Catalysis B: Environmental, 90, 141 (2009).

# Synthesis of Nanostructured Mixed Oxides M(II)M(III)Ox as Supports for Platinum Catalysts.

O.B. Belskaya

*Institute of Hydrocarbons Processings SB RAS, Omsk, Neftezavodskaya, 54*

obelska@ihcp.ru

*Keywords: : mixed oxides, layered double hydroxides, anionic platinum complexes*

## 1. Introduction

Catalysts $Pt/M^{2+}M^{3+}O_x$ are the object of intensive studies, since they are important not only for the base catalysis, but also for conversion of hydrocarbons. The advantages of the mixed oxides as supports consist in moderate and easily controllable basicity, high stability in oxidative regeneration, and provide high dispersity of supported platinum. Mixed oxides may be synthesized by calcination of hydrotalcite-like layered double hydroxides (LDH). LDH have the composition $(M^{2+}_{1-x}M^{3+}_x(OH)_2)^{x+}(A^{n-})_{x/n}$ $nH_2O$, where $M^{2+}$ and $M^{3+}$ are bi- and trivalent metal cations, and comprise positively charged hydroxide layers and anions $A^{n-}$ located in the interlayer space. The properties of LDH and mixed oxides depend on the temperature of thermal treatment , the nature of metals, the $M^{2+}/M^{3+}$ ratio, and the properties of the interlayer anion. Besides the unique property of the mixed oxides to the restoration of a layered structure as a result of contact with water (memory effect) should be noted. The layered structure formed by oxide reconstruction in water (activated hydrotalcite) exhibits catalytic activity because Brønsted $OH^-$ groups appear as the compensating anions and improved anion-exchange parameters.

The use of this type supports with spatially ordered structure is a promising way to control deliberately the characteristics of supported metal and obtain nanoparticles with uniform properties. The interaction of Pt(IV), Pt(II) and Pt(0) anionic complexes with the layered hydroxides that comprise $Mg^{2+}$, $Zn^{2+}$, $Ni^{2+}$, $Al^{3+}$ and $Ga^{3+}$ cations and differ in the nature of interlayer anions ($CO_3^{2-}$ or $OH^-$) and $M^{2+}/M^{3+}$ ratio was studied. These parameters were found to affect both the support properties (structure, texture, acid-base and ion-exchange properties) and the dispersion, morphology and electronic state of supported platinum. Propane dehydrogenation was used as a model reaction for testing the platinum sites.

## 2. Experimental

### *2.1. Synthesis of the supports and catalysts*

LDH with carbonate counter ions ($M^{2+}M^{3+}$-$CO_3$) were synthesized by coprecipitation of appropriate Mg and Al, Zn and Al, Ni and Al, Mg and Ga hydroxides from diluted solutions of nitrates at their interaction with solutions containing carbonate and hydroxide ions. LDH with different $M^{2+}/M^{3+}$ ratios were obtained by varying the concentration of metals. To obtain a sample containing mainly the interlayer $OH^-$ anions ($M^{2+}M^{3+}$-OH), the initial support ($M^{2+}M^{3+}$-$CO_3$) was calcined at 600 °C and hydrated again. Anionic platinum complexes $[PtCl_6]^{2-}$, $[PtCl_4]^{2-}$ and $[Pt_3(CO)_6]_n^{2-}$ were sorbed on LDH from an excess of solutions at room temperature.

### *2.2. Supports and catalysts characterization*

Diffraction patterns were obtained using the D8 Advance diffractometer (Bruker, Germany) with monochromatized Cu-Kα radiation in the range 2θ = 5°-80°. The isotherms of nitrogen adsorption–desorption were measured at 77.4 K on an ASAP-2020 Micromeritics volumetric vacuum system. The TG-DTA method with mass spectrometry was used to study the thermal decomposition of LDH samples

(STA-449C Jupiter instrument, Netzsch). Diffuse reflectance UV-Vis spectra of supported platinum complexes were recorded in the 11000-54000 $cm^{-1}$ range on a UV-2501 PC spectrophotometer (Shimadzu). The reduction dynamics of adsorbed complexes was studied by TPR using an AutoChem-2920 (Micromeritics) instrument. Platinum dispersion was measured by pulse chemisorption of $H_2$ molecules. The high-resolution transmission electron microscopy (HRTEM) images were taken on a JEM-2010 (JEOL) electron microscope. The $^{195}Pt$ MAS NMR spectra of solid samples were recorded on an Avance-400 NMR spectrometer (Bruker).

Propane dehydrogenation was carried out in a flow reactor with a fixed bed catalyst at a temperature of 550 °C, atmospheric pressure, molar ratio $H_2/C_3H_8$ = 0.25. Prior to reaction, the catalyst was calcined for 3 h at 550 °C and reduced in a flow of $H_2$ for 1 h at 550 °C.

## 3. Results

### *3.1. The influence of the interlayer anion nature on the properties of the mixed oxides and the process of platinum anchoring*

The nature of an interlayer anion in the LDH is an important factor affecting the formation of the oxide support, its structural parameters and texture characteristics. It was demonstrated the possibility of preparing both a predominantly coarsely porous oxide support (precursor MgAl-$CO_3$) and a support with a predominant pore size smaller than 20 nm (precursor MgAl-OH) at close specific surface areas and the same chemical composition. The nature of interlayer anion is also an essential parameter affecting the amount of anchored platinum, the composition of surface species, and their location in the structure of layered material. The exchange of interlayer $CO_3^{2-}$ anions for $OH^-$ anions makes it possible to pass from coordinative anchoring of platinum complexes with participation of OH groups of the hydroxide layers to electrostatic interaction of platinum(IV) chloride complexes in the interlayer space of LDH.

### *3.2. Influence of the cation composition of LDH on the properties of the mixed oxides and the process of platinum anchoring*

An increase in the fraction of triple-charged cation led to changes in the structural characteristics and adsorption properties of LDH and to the formation of oxide phase with a more developed surface area and a larger pore volume. The growing density of the positive charge of hydroxide layers and the increasing electrostatic interaction facilitated the adsorption of a greater amount of anionic platinum complexes in the interlayer space and their stronger interaction with the hydroxide layers. As a result, when Mg/Al and Zn/Al ratios decreased from 4 to 2, the dispersion of supported platinum particles increased, which was accompanied by increasing activity of Pt/Mg(Zn)AlOx catalysts toward propane dehydrogenation. The introduction of zinc, nickel and gallium, which are used to modify the state of supported platinum, into hydroxide layers provides a uniform distribution of the modifying element in the support structure; the extent of modification can be adjusted continuously by varying the content of these cations.

### *3.3. The influence of the platinum complex nature on the formation and properties of platinum centers of $Pt/M^{2+}M^{3+}O_x$ catalysts*

The role of the platinum complexes geometry for mechanism of their fixing and the platinum centers formation was established. It was shown that anionic chloride complexes of Pt(II) and Pt(IV) are different in the mechanism and strength of interaction with a layered support. The use of carbonyl complexes of various nuclearity $[Pt_3(CO)_6]_n^{2-}$ allows obtaining the uniform platinum particles with a required size.

Thus, the choice of interlayer anion with desired exchange properties, ratio and nature of bi- and trivalent cations of the hydroxide layers as well as the choice of the nature and geometry of the platinum complex could be used as efficient tool for the formation of supported platinum particles with specified dispersion, morphology and electronic state.

# Toxicity of Nanoparticles and Nanostructures: Arising Problems, Potential Risks, Means and Ways to Safety

T. Sukhanova[*,1], S. Valueva[1], M. Vylegzhanina[1], M. Sokolova[1], M. Gelfond[2]

[1] *Institute of Macromolecular Compounds RAS, Bolshoj pr. V.O. 31, 199004 St.-Petersburg, Russia*
[2] *N.N. Petrov Research Institute of Oncology, The Health Ministry of RF*

(*) corresponding author: T. Sukhanova @E-mail address: tat_sukhanova@mail.ru

*Keywords: nanoparticles, selenium-containing polymer nanostructures, toxicity*

## 1. Introduction

For decades the use of nanoparticles (NPs), quantum dots (QDs) and nanostructures (NS) in medicine and pharmacology is spreading rapidly. Several drastically novel approaches based on nanobiotechnological platform have appeared. New generation of nanomaterials - multifunctional nanosystems containing NPs, QDs, or NS has developed and some of them have already found its first commercial applications in consumer and industrial products (food and cosmetic), and in medicine – as fluorescent cellular labels, deep-tissue and tumor imaging agents, NP-mediated drug delivery systems, and more recently - as sensitizers for photodynamic therapy (PDT) [1].

While benefits of NPs/NS application in reducing toxicity and side effects of conventional drugs are widely publicized, the discussion of the potential effects of their widespread use and health risks to humans are just beginning to arise [2]. Humans can be exposed to NPs through inhalation, ingestion, dermal contact, and injection or implantation.

The analysis of literature data showed that NPs have a higher toxicity as compared to micro-particles. They are capable to penetrate through cellular membranes and blood-brain barrier as well into the central nervous system, to circulate and accumulate in various organs (lungs, liver, kidneys, brain) and tissues. Toxicity of nanoparticles is determined by their size and shape. The smallest spindle-shaped nanoparticles, for example, carbon nanotubes, producing more destructive effects on the organism than the similar ones of spherical form. Exposure of the organism distinctly shows «dose-effect» dependence. Exposure dose should not only be measured in terms of mass, but also in terms of total surface area, number of NPs, or their combination [3].

This paper presents an overview of the recent advances related to investigations on health effects of nanomaterials, especially, NPs and polymer/NPs-based nanosystems, and characteristics which are relevant for their toxicity.

Novel hybrid nanosystems based on zero-valence selenium ($Se^0$) and zinc selenide (ZnSe), stabilized by water-soluble polymers [4-6] possessing high photosensitivity and biological activity, will be consider as well.

## 2. Experimental

### *2.1. Materials and Preparation*

The paper briefly covers the basic synthetic approaches to preparation, mechanisms of formation, and the recent developments in fabrication of NPs and NS with the reduced toxicity, makes an emphasis on ZnSe and selenium-containing NS in combination with a new generation photosensitizer "Photoditazin" (PD) (http://fotoditazin.ru/), which can be used as drugs for cancer treatment in PDT.

### *2.2. Characterization*

The structure, morphology, optical and thermal properties of the prepared NS, under changes of molar ratio between the components and time of the reaction, are investigated using the combination of WAXD/HREM/AFM/DSC/IR/UV, static

(SLS) and dynamic light scattering (DLS) methods. Cytotoxicity evaluation is performed on the promyelocytic leukemia cells HL-60 and "FLECH" cells.

## 3. Results

### *3.1. Size and Shape of Nanostructures*

The relations between the components in the reaction mixture in a wide range of variation of mass ratio are defined, under which the ZnSe/polymer+PD and $Se^0$/polymer+PD nanostructures of spherical form with the sizes from 5 up to 200 nm are formed as evidenced by AFM (Fig. 1), TEM and SLS.

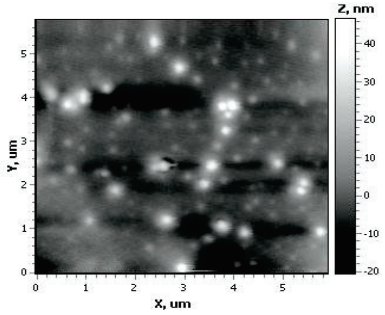


Figure 1. AFM image of thin film, prepared from solution of selenium-containing nanosystem.

### *3.2. Complex Formation between the Component*

It is known, that for low-toxic NS preparation, it is necessary to form stable complexes between NPs and polymers. Therefore, in our work we used water-soluble polymers containing the hydrophobic fragments in macromolecules and PD, which exhibit a high ability to complex formation [7].

## 4. Discussion

### *4.1. Toxicity of NPs and NS*

Selenium is an essential element and a constituent of proteins which act as antioxidants, playing an important role in the protection of cellular damages from oxygen radicals and preventing the development of chronic ailments like cancer and heart diseases [5,6]. Inspite of health benefits at low concentrations, selenium compounds are highly toxic that depends on Se chemical form.

Evaluation of the acute and chronic toxicity of synthesized $Se^0$/polymer+PD and ZnSe/polymer+PD nanostructures on cells cultures has shown that cytotoxic action on tumor cells is absent. The anticancer activity of $Se^0$/polyvinilpyrrolidone (PVP) and Se/bovine serum albumin (BSA) nanosystems is detected on cells of promyelocytic leukemia HL-60. It is found that synthesized ternary systems ZnSe/PVP+PD and ZnSe/BSA+PD inhibit a cellular growth of the Ehrlich tumor inoculated to experimental mice.

### *4.2. Related Issues*

Several important related issues concerning safety of NS such as surface coatings of NPs, possible deterioration of their surface coating and aggregation of NPs in capillaries, poor clearance of NPs with diameter > 5 nm from the body, are also considered.

Finally, it can be concluded that a conceptual understanding of biological responses to NPs and NS is needed to develop and apply safe nanomaterials in medicine in the future.

## References

[1]. M.L. Gelfond, *Practicheskaya onkologiya.* ***8*** (2007) 4, 204. [2]. P. Hoet, I. Bruske-Hohlfeld, O. Salata, *Journal of Nanobiotechnology.* **2** (2004) 12. [3]. W.H.De Jong, P. Borm, *Int. J. Nanomedicine*. 3 (2008) 2, 133. [4]. T.E. Sukhanova, S.V. Valueva, A.Y. Volkov, L.N. Borovikova, M.L. Gelfond, V.A. Bershtein *Ist Int. Theor. Pract. Conf. "Vysokie technologii. Fund. i prikl. issledovanija v fiziologii i medicine", Nov.23-26. St.-Petersburg. Russia.* (2010) 174. [5] T.E. Sukhanova, M.E. Vylegzhanina, S.V. Valueva, L.N. Borovikova, A.Y. Volkov, N.A. Matveeva, M.L. Gelfond. *IX Int. conf. "Metodolog. aspecty scanirujuschei zondovoj microscopii". Oct.12-15. Minsk.* Belarus'. (2010) 35. [6]. Valueva S.V., Borovikova L.N., Vylegzhanina M.E., Sukhanova T.E. *Rus. J. Phys. Chem. A.* ***84,*** (2010) 9, 1473. [7]. T. Sukhanova, V. Bershtein, S. Valueva, A. Volkov, L. Borovikova, G. Matveeva, M. Vylegzhanina, N. Matveeva, L. Egorova, V. Ryzov, M. Gelfond. *14th IUPAC Int. Symp. MacroMolecular Complexes MMC-14*. Helsinki, Finland. (2011). P.64.

# Multi-layered Nanotechnology for Nanomedicine: overview

Adriele Prina-Mello[1,2]

[1] *Institute of Molecular Medicine, School of Medicine,*
[2] *Centre for Research on Adaptive Nanostructures & Nanodevices, Trinity College Dublin, Ireland.*

*Keywords: engineered nanoparticles, nanomedicine, risk assessment,*

## 1. Introduction

The use of engineered nanoparticles (ENP) in the medical/clinical field is well-established, through the use, for example, of superparamagnetic iron oxide nanoparticles (SPIONs) as magnetic resonance imaging (MRI) contrast agents [1].

Current development in this field are leading to believe that modified nanoparticles will improve disease treatment through a more adaptive and personalized approach to medicine. Possible route of delivery will be the selective accumulation of nanoparticles around the targeted cell/tissue allowing for the diagnosis of diseases and either imaging or monitoring of treatment efficacy. Proteomics or genomics personalised to patient will then allow for personalised treatment.

Surface modifications of ENPs can be designed in layers in order to achieve multilayered theranostic ENP for personalized medicine applications. One example is the making of functional SPIONs formed by three main components: (1) an iron oxide core functioning as MRI contrast agent, (2) a biocompatible coating and (3) a therapeutic coating targeted with a pharmacogenomics biomarker.

Compared to conventional pharmaceutical products, nanometric drug delivery systems can often lead to higher drug bioavailability with lower adverse side effects. In addition, targeting moieties decorating the ENP surface can direct efficiently the clinical treatment to the affected tissue/cell with optimal selectivity.

For accelerating the translation of these materials into clinical markets, the impact of multilayered ENP on human health should be also assessed and modelled systematically on the relationship between surface properties and ENP toxicity behaviour. It emerges the need for assessment strategy and decision making tools on the efficacy of this complex ENPs [3]. This becomes a priority in order to deliver a commercially viable tool with direct potential on the categorization and labelling of potential ENP-based nanomedical products for medicine.

## 2. Acknowledgement

This work was partially supported by the EU FP7 NAMDIATREAM project (NMP-2009-LARGE-3-246479), MULTIFUN project (NMP-2010-LARGE-4-262943) and Science Foundation Ireland CRANN-CSET (Pathfinder project).

## 3. References

[1] A. Prina-Mello, K. Crosbie-Staunton, G. Salas, M. del Puerto Morales, Y. Volkov. Multiparametric Toxicity Evaluation of SPIONs by High Content Screening Technique: Identification of Biocompatible Multifunctional Nanoparticles for Nanomedicine. IEEE Transactions on Magnetics 01/2013; 49:377-382. DOI:10.1109/TMAG.2012.2225024 pp.377-382.

[2] Movia D., Tran L., Volkov Y., A. Prina-Mello. Chapter titled “Multilayered Nanoparticles for Personalized Medicine: Translation into Clinical Markets.” Editors: R. Bawa, G.F. Audette and I. Rubinstein,. Handbook of Clinical Nanomedicine: From Bench to Bedside. Singapore: Pan Stanford Publishing Pte Ltd; 2013.

[3] A Prina-Mello, B M Mohamed, NK. Verma, N Jain, Yuri Volkov, Chapter titled “Nanotoxicology: Progress towards Nanomedicine”. Editors: N.A. Monteiro-Riviere and C.L. Tran. Nanotoxicology Second Edition, Taylor & Francis, Informa Healthcare Books.

# Application of nanoparticles in oncology: laser thermal destruction of cells in the presence of metallic nanoparticles

Yu.P. Meshalkin

[1] *Institute of Laser Physics SB RAS, 630090 Novosibirsk,Lavrentyeva pr. 13/3,*
[2] *Novosibirsk State Technical University, 630092 Novosibirsk, 20 pr. K. Marksa,*

yurimesh@ngs.ru

*Keywords: oncology, gold nanoparticles, plasmon resonance, thermal degradation*

According to the American bibliographic database «Photochemical Database» The number of publications devoted to the synthesis, properties and applications of gold nanoparticles (NPs) is steadily growing. If in the year of establishment of this database there were only 3 publications on this topic, then in 2008 this number increased to 50 times:

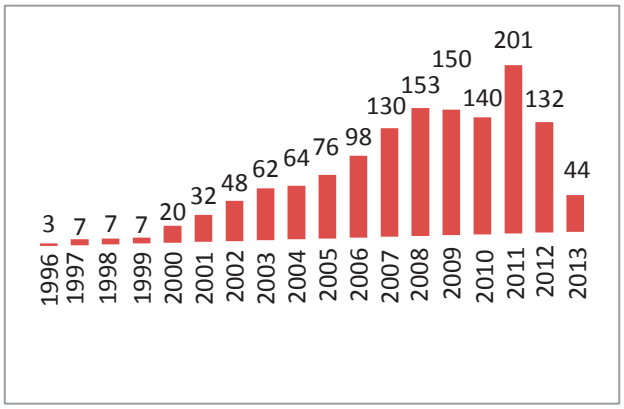


First paper on gold NP application in oncology was published in 2002 [1]. In this paper NPs were studied as delivery system of photosensitizers to pathological cells. In 2003 Pitsillides et al. [2] developed approach of NP laser heating on the plasmon resonance length. In the same year, it was proposed to use bioconjugated gold NPs as a contrast agent for cancer detection [3].

**Thus, one can distinguish two main ways of NP application in oncology - diagnosis and therapy.**

Both directions are based on ability of NPs to relatively easy pass through plasma membrane of cells and to accumulate in multivesicular bodies. Advantages of nanoparticles over traditional photo-sensitizers (PS) were considered to: low cytotoxicity, biological inactivity, relatively simple functionalization in order to tune delivery to the pathological target, high capacity by means of delivery systems, ability to be affected by physical methods, such as laser heating at the plasmon resonance wavelength.

However, such questions as “how nanoparticles affect biochemical processes in the human body?”, “what is their path after delivery, the residence time in body, sites of accumulation?”, “How do they affect cellular and tissue function?”, “Do they have any access to the blood circulation?”, “Is there any possibility of unexpected reactions *in vivo*?” are still challenging [4].

About ten years ago, metal NP were promising in oncology due to their possibility to be heated causing thermal destruction of cells

It is well-known that with local hyperthermia cells which are under division, die first of all. Such cells include the tumor cells. Functionalization of nanoparticles by anchoring on the surface of specific proteins and antibodies in principle allowed obtaining target delivery of NPs to abnormal cells.

Irradiation of gold nanoparticles by pulsed Nd: YAG laser (wavelength of 532 nm) actually causes heating of NPs and denaturation of neighbor proteins [5]. Laser wavelength were selected from the condition of wavelength of the plasmon resonance for specific nanoparticles. For spherical gold NPs plasmon resonance wavelength is about 530 nm for silver NPs - 390 nm.

Possibility photothermal cell damage was also demonstrated in *in vitro* experiments [6]. However in practice radiation with wavelength less than 600 nm

does not pass to a considerable depth in the biological tissue, i.e. it can't really heat NPs.

Attempts were made to shift the plasmon resonance wavelength to infrared band, i.e. to the "transparent window" of biological tissue, by modifying NP shape. There is the longitudinal component of the nanorods, which have plasmon resonance wavelength in the infrared region. This wavelength can be modified by tuning of nanorod aspect ratio (length to diameter ratio).

Nanorod synthesis turned to be much more complex issue than spherical NP synthesis. It was carried out with using agents with high cytotoxicity. Furthermore, nanorods much harder pass though cell membrane, and are more toxic than spherical NP s.

At present, one can confidently say that the significant breakthrough in the application of nanoparticles in oncology has not happened. Undoubtedly, possibility of medical applications allowed to involve a certain facilities and funding in order to develop methods of synthesis of NPs with different shapes. It stimulated research on the physicochemical properties of the nanoparticles, their interaction with biological molecules, cells and tissues, but not more than this. Among new properties of NPs their photo-protective properties, which prevent photobleaching of dyes and photosensitizers [7], as well as thermal protective properties which protect the dye molecules from the thermal decomposition [8] should be stressed.

Analysis of papers published in 2011-2013 shows that interest on application of NPs in oncology significantly reduced. Only a few works are devoted to the further development of photothermal therapy.

The main direction of research is related to the study of traditional transport photosensitizers and drugs for chemotherapy by nanoparticles.

## References

[1] D.C.Hone, P.I.Walker, R.Evans-Gowing, e.a. *Langmuir,* **18** (2002) 2985

[2] C.M. Pitsillides, Joe E.K., Wei X., e.a., *Biophys. J.*. **84** (2003) 4023

[3] M.A.Eghtedari, J.A.Copland, V.L.Popov e.a. *Proc.SPIE,* **4960** (2003) 76

[4] Yu.P.Meshalkin, N.P.Bgatova *J.Sib.Fed.Univ. Biology,* **3** (2008) 248

[5] Yu.P.Meshalkin, I.N. Lapin, V.A.Svetlichniy K*vant. Electronica (RUS),* **41** (2011) 754

[6] I.H.El-Sayed., X.H.Huang., M.A.El-Sayed *Cancer Lett*, **239** (2006) 129

[7] L.Bekale, S.Barazzouk, S.Hotchandani *J. Mater. Chem*., **22** (2012) 2943

[8] Yu.P.Meshalkin, I.N. Lapin, A.A.Tomshina, V.A.Svetlichniy *Med. Physika (RUS),* **55** (2012) 70

# Electron microscopy investigation of carbon nanomaterials under the influence of high energy beams

M.V. Trenikhin

*Institute of Hydrocarbons Processing, Siberian Branch, Russian Academy of Sciences, ul. Neftezavodskay 54, Omsk, 644040 Russia*

tremv@ihcp.ru, tremv@yandex.ru

*Keywords: carbon black, irradiation, transmission electron microscopy*

## 1. Introduction

In recent years, significant attention is given to the structural changes in carbon nanomaterials (CNM) when exposed to the powerful energy beams. Considerable changes are observed in morphology and crystal lattice of primary particles, frequently leading to allotropic transformation of substances in the irradiated CNM. Fast heating of the primary particles to temperatures characteristic of vaporization and partial evaporation of the carbon material occurs under electronic, ionic or laser irradiation.

Subsequent process of rapid cooling is accompanied by crystallization in graphite-like nanostructures. For example, the impact of millisecond laser pulses on soot and carbon black may lead to the formation of onion-like, rose-like particles or nanodiamonds and nanocages this depends on the experimental conditions and the power of the laser pulse. An increase in the energy density of laser radiation up to 5-$10^6$ $Wcm^{-2}$ reduces the distance between the graphene layers to the values characteristic of graphite-like structures [1].

Transmission electron microscopy is seen as an informative tool in CNM research. It is important to receive information about the morphology of the primary particles and the structural changes that occur at the atomic level.

Electron microscopy allows to obtain statistical data on the extent and thickness of graphene clusters, the degree of curvature of individual graphene layers and other morphological features.

Results of the investigation of structural transformations in carbon black (CB) under the influence high energy beams, that was carried out with direct involvement of the author, are presented in this work.

## 2. Experimental

The experiments were performed with two types of CB: low dispersive (diameter of the primary particles – 100-300 nm) and high dispersive (diameter of primary particles - 10-30 nm). Irradiation of carbon materials was carried out with using Nd:YAG laser operating at 1064 nm (fluence - 1200-6300 $J/cm^2$) and electron beam with an energy density of ~10-50 $J/cm^2$ [2]. High resolution transmission electron microscopy (HRTEM) on a JEM-2100 instrument (JEOL, Japan) was used for the structural investigations.

CNM degree of crystallinity was determined by the analysis of the electron diffraction patterns and the Fast Fourier Transform (FFT) electron microscopic images. Subsequently, image processing FFT data were obtained, characterized by the distance between the graphene layers ($d_{002}$), and in some instances the size of graphene clusters in globules of CB. The average distance ($d_{002}$) for the initial and irradiated samples of carbon were determined by building profiles of FFT radial intensity method [3].

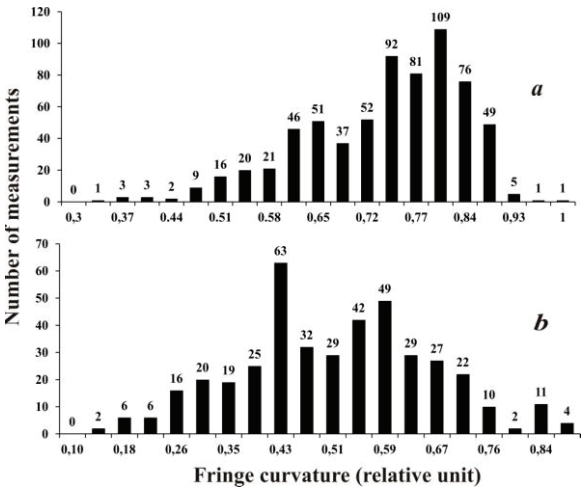


Figure 1. Fringe curvature distribution of the low–dispersive (a) and high–dispersive (b) carbon black.

## 3. Results and discussion

According to HRTEM data, the initial carbon black particles (globules) have a nearly amorphous structure with low ordered graphene layers spaced by 0.37 – 0.40 nm. The curvature of a fringe (graphene layers) is defined as the ratio of the fringe length to the distance between the two its endpoints. Curvature coefficient of the graphene layers in the high dispersive primary particles is more than in a low dispersive carbon black (Fig. 1 a, b). The length of graphene layers in the high dispersive particles prevailed in the range 0.4 – 1.0 nm and 0.4 – 2.0 nm for the low dispersive particles respectively.

Electron microscopy (EM) research of samples of high dispersive CB after laser and electron irradiation, indicate the formation of spheroidal particles with diameters of 10-30 nm with a shell consisting of 5-10 graphene layers. In the literature, such morphology of carbon particles is called hollow spheres or capsules [4]. The average distance between the graphene layers in such particles, measured by electron diffraction, is 0.355 - 0.365 nm.

The experiment on irradiation of low dispersive CB has revealed a deep structural change in the carbon material. HRTEM has shown formation of globular structures with a diameter of 100 to 500 nm, consisting of a series of parallel spatially extended graphene layers [5]. In case where the energy density of radiation were 6300 J/cm$^2$ the average distance between the layers were 0.344 ± 0.002 nm as measured by the electron diffraction. Reducing the energy density to a value of 3500 J/cm$^2$ resulted in an increase $d_{002}$ to 0.355-0.360 nm. The morphology of the particles resembles a cut rosebud as can be seen in Fig. 2 showing the electron micrograph.

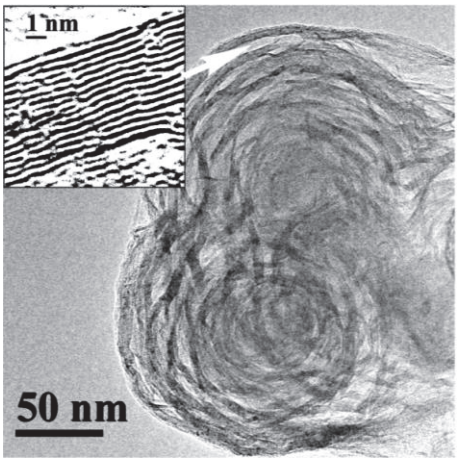


Figure 2. Structure of the low-dispersive carbon black after laser irradiation.

Thus, it was shown the possibility of the pulse laser and electron beam irradiation application for the structure reorganization of CB. During irradiation CB occur globules fast heat processes up to the temperature 4500K, that typically for carbon plasma. This leads to convert sp$^3$-bonded carbon to sp$^2$-bonded species (in the primary CB concentration sp$^3$-bonded may reach 23% [6]) and the formation of graphite-like nanoparticles. Subsequent HRTEM image analysis of the irradiated CB samples shows that the formation of either nanocapsules or rosette particles largely depends on the initial diameter and graphene layers structure of nanoglobular carbon particles.

## 4. References

1. Hu. Shengliang et al. *Materials Science and Engineering B*. **157** (2009) 11–14.
2. Yu.G. Kryazhev, N.N. Koval, V.A. Likholobov, A.D. Teresov, V.A. Drozdov, M.V. Trenikhin. *Technical Physics Letters*. **4** (2012) 301–303.
3. K. Oshida, T. Nakazawa, T. Miyazaki, M. Endo. *Synthetic Metals*. **125** (2002) 223-230.
4. R.L. Vander Wal, A.J. Tomasek. *Nano Lett.* **3** (2003) 223-229.
5. M.V. Trenikhin, O.V. Protasova et al. *Chemistry for Sustainable Development*. **1** (2013) 109-114.
6. J.-O. Muller et al. *Phys. Chem. Chem. Phys*. **9** (2007) 4018–4025.

# Pilling-Bethworth ratio and the Periodic Table

M.S. Mel'gunov*, V.B. Fenelonov

*Boreskov Institute of Catalysis SB RAS, pr.Akad. Lavrentieva, 5, Novosibirsk, 630090*

(*) corresponding author: max@catalysis.ru

*Keywords: Pilling-Bethworth ratio, topochemical reactions, solid phase transformations, nanomaterials, texture*

## 1. Introduction

The lifetime of porous and disperse solid phase materials (catalysts, adsorbents, etc.) is full of topochemical reactions. The result of each such reaction is the formation, transformation, or elimination of a part of, or the whole solid phase of the material. Any topochemical reaction proceeds with the change of the solid phase volume, which can be evaluated by means of Pilling-Bethworth ratio (PBR) that is the relation of the molar volume of product solid to that of the precursor solid. Simplicity of PBR evaluation should be but unfortunately not always applied in the analysis of materials properties. However, this parameter is very useful when changes of porous structure are considered. It allows prediction of possible changes in porous space and solid phase.

In known literature PBR concept is applied for particular transformations and never have been considered from a general point of view, for example from the view of Periodic Table (PT). This communication is scoped on this topic.

## 2. PBR evaluation and application

### *2.1. PBR evaluation*

PBR can be calculated in two possible ways: either assuming reaction stoichiometry ($a\,A_{(solid)} \rightarrow b\,B_{(solid)} \pm c\,C_{(gas)}$), molar masses ($M_A, M_B$), and reference or measured true density values ($\rho_A, \rho_B$) for precursor solid $A$ and product solid $B$, correspondingly:

$$f_{PBR} = \left(b \cdot M_B / \rho_B\right) / \left(a \cdot M_A / \rho_A\right),$$

or using the values of unit cell volumes from reference or measured diffraction data. The second way is possible for crystalline materials. It comprises evaluation of crystallographic unit cell volumes $u_B$ and $u_A$ accounting the number of atoms in product unit cell and precursor unit cell. Namely, if an element $A$ transforms to it's oxide $B$, $f_{PBR} = \left(a^* \cdot u_B\right) / \left(b^* \cdot u_A\right)$, where $a^*$ and $b^*$ are the numbers of element $A$ atoms in the unit cells of precursor and product, correspondingly. For example, the reference data on true density are summarized, in CRC Handbook of Chemistry and Physics [1], and data on unit cell volumes are stored in Inorganic Crystal Structure Database [2]. To measure true density values helium pycnometry, and to measure unit cell volumes X-ray or electron diffraction can be applied. Temperature has minor effect on evaluation of PBR, because temperature expansion of solids is low and works for both precursor and product solids. One also can observe the effect of unit cell expansion with the decrease of particles size, which as well is not significant for known nanomaterials.

### *2.2. Application of PBR values*

PBR is very useful for the prediction of porosity or density (true, apparent, or bulk) changes during supported and self-supported catalysts preparation, topochemical transformations during burning out or dissolving of solid phase components under pseudomorphic conditions. If a transformation proceeds with the change of a material external volume and/or shape (non-pseudomorphous conditions), together with porosity data (usually, mercury and/or adsorption porosimetry) it allows estimation of material shrinkage or volumertic extension

depending on the direction of transformation.

## 3. PBR and the Periodic Table

A certain number of correlations can be found for PBR and Periodic Table.

Oxidation reaction has the most representative data for both precursor and product in reference tables, which can be used to elaborate PBR concept. Fig. 1 shows an example of correlation between PBR values and position in PT for the transformation of elements to their normal oxidation state oxides (oxidation state of element in the product oxide is equal to the group number). For convenience sub-groups A and B are considered separately.

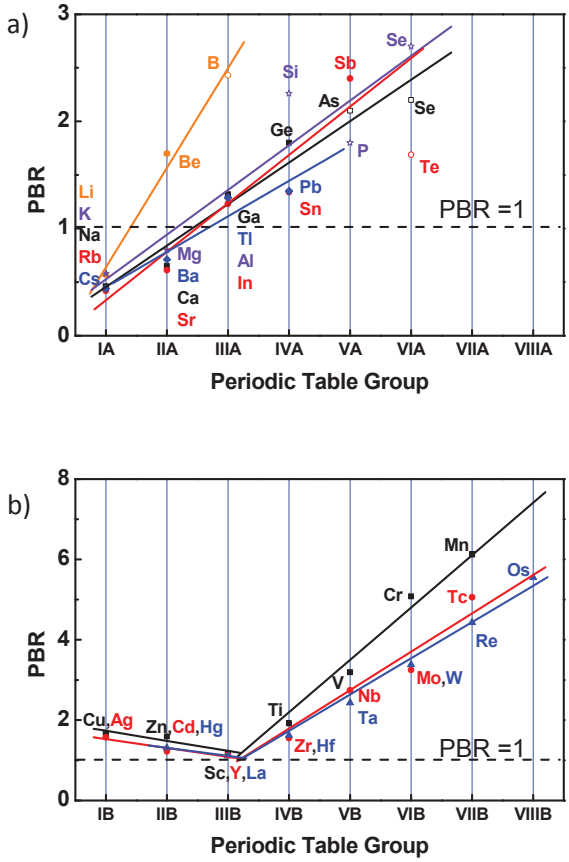


Fig. 1. PBR values for the transformation of elements to corresponding normal oxidation state oxides (oxidation state of metal equal to the group number): a) sub-groups A (metals are marked as filled, and non-metals as hollow symbols) and b) sub-groups B. For each row in PT a corresponding linear interpolation is provided.

We consider here only transformations of elements to oxides, which both solid under normal conditions, as well as for mercury. One can observe the almost linear changes of PBRs for different rows of PT. The deviation can be found only for few elements, mostly non-metals. All deviations are not the results of experimental errors and can be explained with different reasons. For example, Si falls out from linear dependence due to the short Si-O length and predominantly tetrahedral coordination, which restricts dense packing in the oxide framework. Alkaline, alkaline-earth metals, and Eu and Yb (both not shown) have PBR values below 1. This means the shrinkage of the material with the increase of atoms in the solid. This is an interesting feature that is observed not only for oxidation, but, for example, for the formation of hydrides.

All lanthanides have PBRs close to 1. Absence of or low shrinkage or expansion of solid in topochemical reaction can provide additional strength to the constructions made of such elements. For example, rare earth elements are widely used in catalytic combustion not only due to their redox properties, but also due to absence of solid volume changes under reaction conditions.

Reference data are absent for hypothetic $Au_2O$ phase; as well only for Os (VIII) from VIIIB group corresponding $OsO_4$ oxide has reference data to calculate PBR. The observed linear correlations can be utilized to predict PBRs, and thus density values for corresponding phases, which are absent.

## 4. Conclusion

Pilling-Bethworth ratio (PBR) is an important and useful instrument for the analysis of materials formation, evolution, and degradation. Proper use of PBR can allow the non-random, but the direct search of the most appropriate compositions for various applications.

The work was fulfilled in the framework of base budget financing (program V.44.1.16).

## 5. References

[1] CRC Handbook of Chemistry and Physics / D. R. Lide (Ed.). — 90th edition. — CRC Press; Taylor and Francis, 2009.
[2] http://icsd.fiz-karlsruhe.de

# Strategic Priorities of Research on Nanosafety during 2015-2025

K.Savolainen[1]

[1(*)] *Nanosafety Research Centre, Finnish Institute of Occupational Health, Topeliuksenkatu 41 aA, 00250 Helsinki, Finland)*

Corresponding author (*): Kai-Savolainen@ttl.fi

*Keywords: NanoSafety Cluster, Research Priorities, Research Roadmap, Future Nanosafety Research*

## 1. Introduction

The growth of the use of engineered nanomaterials (ENM) has been rapid during the recent years. These unique materials, due to their small size, surface to mass and volume ratios, and surface reactivity, have found numerous applications in industrial processes and products as well as in a huge number of consumer products. These materials allow one to produce light and strong materials for e.g. construction, and cars, active surfaces for spaces where hygienic requirements are high (such as bath rooms, hospital facilities, or self-cleaning windows). These materials are also used in the production of energy and clean water. The special characteristics of these materials have also the other side of the coin. Due to their small size these materials have an easy access to mammalian and environmental organisms, and due to the reactivity of many ENM they have a strong ability to react with biological molecules in living organisms.

The current situation is a marked challenge for the assessment of potential hazards, exposure and risks of ENM because very little systematic knowledge is available on their possible harmful effects, and the quality of many of the available methods is questionable. This causes major challenges to regulatory activities, and due to the shortage of knowledge, the European Commission requested the European Nanosafety Community consisting of a large number of EU funded nanosafety research projects to prepare a vision for research required on nanosafety in the future. The Community, the NanoSafety Cluster (NSC) decided to prepare on the EU Commission's request a strategic research agenda for 2015-2025 to provide insights on the required strategic nanosafety research in the future.

## 2. Experimental

The NSC established fourteen working groups to tackle with different aspects of nanosafety research in 2011 with the aim of producing a bottom-up strategic document providing insights on the nanosafety research with a time-horizon between 2015-2025. This horizon tallied well with the timing of the novel EU Framework Programme on Research and Innovation called "Horizon 2020" with an overall 7-year budget between 70 and 80 billion euros. The share of nanosafety research of this amount during seven years might be in the range of 200-300 million euros.

After the fourteen working groups had finalized their work, there was a need to merge the outcome of the work of several working groups into four larger entities which were: 1) Material characterization and classification; 2) Exposure, release and transport through the entire life-cycle; 3) Hazard mechanisms; and 4) Risk assessment tools. An Editorial Group was established in 2012 consisting of 7 scientists to finalize the work and to produce a strategic and coherent document which could provide useful guidance to the EU Commission in defining topic for the "Horizon 2020" Programme on nanosafety research. This document, still in a draft stage, will be handed over to the EU Commission on June 20th in Dublin. The Finnish Institute of Occupational Health, the Coordinator of the NSC activities, will finalize the document to be handed over to the EU Commission.

The document introduces the importance of the ENM and

nanotechnologies for technological and economic development in general, describes the research landscape in Europe and globally, and carefully considers the cross-cutting issues that are crucial for the success of nanosafety research such as regulatory framework of ENM and nanotechnologies, available infrastructures, the importance of environmental and health and safety research for the industry value chain, and communication and international collaboration. One of the proposals of this part of the document is the establishment of a Virtual Network Based Nanosafety Research Centre in the European Union.

### *2.1. Thematic Priorities of Nanosafety Research*

The four thematic chapters on the priority topics introduce most burning challenges in the nanosafety research area in that given topic. Material characterization emphasizes the importance of grouping ENM based on their bio-identity, i.e. the association between material characteristics with ensuing toxic effects to support identifying harmful ENM from harmless ones. The chapter on exposure, release, and life-cycle emphasizes the importance to understand the mechanisms of the behavior of different ENM in different matrices, their identification and measurement against the ubiquitous background nano-sized materials, mechanisms of release from various matrices, transport through different avenues to human as well the environmental species. The chapter on hazard mechanisms focuses on the translocation of ENM, their penetration of biological barriers, toxicity mechanisms which also could be used to group the ENM into different classes, and the use of these data in hazard evaluation of ENM. The chapter on risk assessment tools assesses the data requirements for reliable risk assessment, the importance of databases of companies and exposed workers to provide a reliable understanding of the numbers of exposed workers and consumer. The chapter also deals with the need of ENM ontologies in the risk assessment context, and emphasizes the importance to carry out epidemiological studies on workers exposed to ENM.

## 3. Research Priorities, Roadmap and the Implementation of the Roadmap

The roadmap presented in the "Strategic Research Agenda for the Nanosafety Research" introduces the state-of-the-art where European nanosafety Research should be at 2015, 2020, and 2025 with the main aim of providing scientific foundation of risk assessment and management of ENM. The goal is to provide means through research to replace the current risk assessment paradigm with a new one which is reliable, affordable and much quicker that the current paradigm used world-wide. In the document, the research priorities have been grouped under larger entities, topics, for each thematic area separately, and then then under the topics the specific research priorities are given in a tabular form useful for e.g. the EU Commission when making decisions on areas to be funded within the frame of the "Horizon 2020".

In the implementation of the document, important is European wide and global dissemination of the strategic research vision developed in the document until 2025. European Commission, key stakeholders such as the academic community, national European funding organizations, industry and social partners need to be involved in the circulation. An important element of the document is international collaboration, and hence stakeholder interested in nanosafety research globally will be informed.

An essential part of the document is a continuous feedback and updating of the proposed research priorities so that the document is updated every two-to-three years to assure that new discoveries of nanosafety research can be considered.

Supported by EU Commission Grant CP-IP 211464-2 (NANODEVICE).

# ORAL AND POSTER PRESENTATIONS

# Some inferences from toxicological experiments with metal nanoparticles: the pulmonary phagocytosis response to their deposition, subchronic systemic toxicity and genotoxicity, the attenuation of the latter with bioprotectors

B. Katsnelson*[1], L. Privalova[1], B.Gurvich[1], S. Kuzmin[1], M. Sutunkova[1], V. Shur[2], E. Shishkina[2] , M. Khodos[3], Ya. Beikin[4], O. Makeyev[5], I. Valamina[5], N. Loginova[1]

[1]*The Medical Research Center for Prophylaxis and Health Protection in Industrial Workers; 30 Popov Str., Ekaterinburg, 620014, Russia*

.[2] *The Institute of Natural Sciences, the Ural Federal University, Ekaterinburg 620000, Russia*

[3]*Ural State Universityof Economics, 62 8th March Str, Ekaterinburg, 620019,.Russia*

[4]*The City Clinical Diagnostics Centre, 38 Dekabristov Str., Ekaterinburg 620142, Russia*

[5] *The Ural State Medical Academy; 17 Klyuchevskaya Str., Ekaterinburg 620109, Russia*

(*) corresponding author: @E-mail address bkaznelson@etel.ru

*Keywords: nanometals, phagocytosis, cytotoxicity, systemic toxicity, genotoxicity, bioprotectors*

## 1. Introduction

Nanoparticles (NPs) of metals and of their oxides are of special interest in the light of health risks assessment because, in parallel with engineered NPs, there exists a substantial fraction of nanoscale ("ultrafine") particles of the same substances within the particle size distribution of condensation aerosols generated by arc-welding and metallurgical technologies, other fractions being presented by chemically similar micrometer particles (MPs).

Thus, for metal NPs more urgently than for many others, the everyday practice needs solving some theoretical problems of nanotoxicology: (1) are NPs recognized by organism's main defenses worse or just as well as respective MPs are? (2) are they much more toxic as compared with MPs on both cellular and systemic levels? (3) is there a definite dependence of defense and adverse responses to NPs on their dimensions *within* the conventional nanometer range and/or on their chemical nature, and last but not the least, (4) is it possible to protect health of humans dealing with either engineered or "spontaneous" NPs by establishing low but still practicable permissible exposure levels (PELs) and by enhancing organism's resistance to NPs toxicity (genotoxicity included).

During last 4-5 years our experimental work was focused on trying to find answers to these important questions.

## 2. Experimental

We experimented with NPs of $Fe_3O_4$ having mean diameters 10 or 50 nm, gold (ca 4 or ca 50 nm), silver (the same) and copper (ca 30 nm) and, in parallel, with fine MPs of the same metals (ca 1 μm).

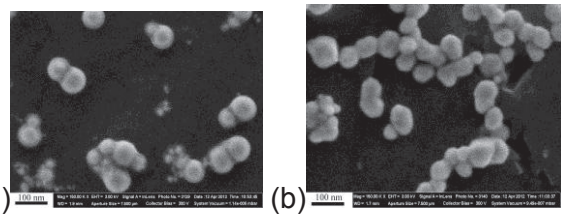


Figure 1. Images of gold (a) and silver (b) NPs in suspensions prepared for comparative toxicological experiments. Scanning electron microscopy at *150 000.

Keeping in mind the above mentioned theoretical premises of our research, we used as a rule not available commercial nanomaterials but purposefully prepared and accurately characterized NPs of pure metals suspended in de-ionized water without any chemical admixtures. An example is given in Figure 1.

Cell population of bronchoalveolar lavage fluid (BALF) obtained 24 hrs after intratracheal instillation to rats of NPs or MPs was studied with optical (OM), transmission electron (TEM) and semi-contact atomic force microscopy (sc-AFM). Subchronic toxicity was modeled by repeated i.p. injections of the same particles during 5-7 weeks and assessed with a lot of biochemical, functional and morphometrical indices;

the accumulation of particles in organs was estimated too. In the comparative subchronic experiment with nAg and nAu the genomic DNA fragmentation in several tissues was assessed as well, using the RAPD test. Both geno- and systemic toxicity of nAg were assessed also on the background of oral administration of a bio-protective complex (BPC) comprising pectin, multivitamins, some amino acids, calcium, selenium, and omega-3 PUFA.

## 3. Results

In our presentation to the Conference we shall overview and summarize main results of the above experiments published in detail in both Russian [1-6] and international [7-12] Journals.

## 4. Discussion

Given equal mass doses and identical metal composition, NPs induce much more intensive recruitment of phagocytes with a much more significant shift toward neutrophile leukocytes (NL) count in the BALF than MPs do, this shift being an indirect but informative index of particle cytotoxicity for alveolar macrophages (AM). The OM, TEM and sc-AFM data testify to a marked internalization of NPs by both AMs and NLs, the active endocytosis (rather than a mere diffusion) playing an important role. High cytotoxicity of NPs for both AM and NL is confirmed by the TEM images of ultrastructural damage to these cells (first of all, to its mitochondria). Judging by NL/AM ratio, cytotoxicity of NPs diminishes with increasing NPs diameter, while the sc-AFM count of micro-invaginations on the surfaces of these cells shows that their phagocytizing avidity for NPs decreases in the same succession.

The same NPs possess also considerably higher systemic toxicity than their micrometer counterparts do, but *within the nanometric range* the relationship between size and toxicity is intricate and non-unique. This fact was attributed to differences in different NPs' toxicokinetics controlled by both more or less substantial penetration of NPs through biological barriers and their unequal solubility. For equidimensional NPs, intensity of phagocytosis response, cytotoxicity and systemic toxicity (genotoxicity included) strongly depend on just what metal is being considered.

Because of high activity of the key mechanism of pulmonary clearance, safe levels of human exposure to airborne NPs are possible in principle, although there may be no reliable foundations for establishing different PELs for NPs of different size. For metal NPs, such PELs ("OBUV" in the Russian hygienic standards system) can be proposed at this stage, even if tentatively, based on a sufficiently conservative approach of decreasing approximately tenfold the exposure limits established for respective microscale industrial aerosols.

Our experiment with nAg demonstrated also that organism's sensitivity to the adverse health effects of NPs can be significantly attenuated with an adequately composed BPC.

## 5. References

[1]. Кацнельсон Б., Привалова Л., Кузьмин С. и др. *Мед. тр. и пром. экол.* **№2**. (2010), С.12-16.
[2]. Кацнельсон Б., Привалова Л., Кузьмин С и др. *Токсикол. Вест*. **№2** (2010), 18-25.
[3]. Кацнельсон Б., Привалова Л., Сутункова М. и др. *Бюлл. экспер. биол. и медиц*. **№11** (2011), 560-563.
[4]. Кацнельсон, Б., Привалова Л., Дегтярёва Т. и др. *Токсикол. Вест.* **№4** (2012) 26-29.
[5]. Привалова Л., Сутункова М., Пичугова С. и др. *Мед. тр. и пром.экология* **№11** (2012) 42-46.
[6]. Кацнельсон Б., Макеев О., Привалова Л. и др. *Токсикол. Вест.* **№2** (2013).
[7]. Katsnelson B., Privalova L., Kuzmin S., Sutunkova M. et al. *Internat. J. Environm. and Occupat. Health*. **16** (2010) 503-519.
[8]. Katsnelson B., Privalova L., Degtyareva T. et al. *Central European J. Occupat. and Environm. Medic*. **16** (2010) 47-63.
[9]. Katsnelson B., Degtyareva T., Minigalieva I. et al. *Internat. J. Toxicol*.**30** (2011) 59-68.
[10]. Katsnelson B., Privalova L., Kuzmin S. et al. *ISRN Nanotechnology* **2012** (2012) 12 pp.
[11]. Katsnelson B., Privalova L., Sutunkova M. et al. *J Nanomedic. & Nanotechnol*. **3** (2012).1-8.
[12]. Katsnelson B., Privalova L., Gurvich V. et al. *Int. J. Mol. Sci.* **14** (2013) 2449-2483.

# Functionalized Magnetic Nanoparticles for Bioassay

C. Bala*[1,2], L. G. Zamfir[2], Nicole Jaffrezic-Renault[3]

[1] *University of Bucharest, Department of Analytical Chemistry, 4-12 Regina Elisabeta Blvd., 030018 Bucharest, Romania*

[2] *University of Bucharest, R&D Center LaborQ, 4-12 Regina Elisabeta Blvd., 030018 Bucharest, Romania*

[3] *University of Lyon, Institute of Analytical Sciences, UMR CNRS 5280, 5 Rue de la Doua, 69100 Villeurbanne, France*

(*) corresponding author: camelia.bala@g.unibuc.ro

*Keywords: magnetic nanoparticles, mycotoxins, label-free immunosensor*

## 1. Introduction

Mycotoxins are secondary metabolites of the fungi such as: *Aspergillus*, *Fusarium*, *Penicillium*, *Alternaria* and *Claviceps I.* So far, near 300-400 types are known, 20 of them being found to contaminate food products and animal feeds. The most common mycotoxins are aflatoxins, ochratoxin A, fumonisins, deoxynivalenol, T-2 toxin and zearalenone. The contamination of cereals such as wheat, maize, rice or nuts and bean may occur before harvest, during harvesting and drying and in storage producing a wide range of adverse and toxic effects in animals in addition to being foodborne hazards to humans [1]. Ochratoxin A (OTA) is one of the mycotoxin known as the most toxic compound and widespread from the ochratoxins group. Studies have shown that this molecule can have several toxicological effects such as nephrotoxic, hepatotoxic, neurotoxic, teratogenic and immunotoxic and it is believed to cause increased oxidative stress at a cellular level [2]. The maximum levels of OTA allowed by the EU in various food products are 5 ppb for raw cereals, 3 ppb for products derived from cereals, 2 ppb for wines and 0.5 ppb for baby foods (Commission Regulation No. 123/2005). The concerns about OTA contamination lead to the development of high-performance detection techniques for quality assessment. The immunosensor technology has revolutionized modern analysis because they are sensitive, selective, real-time monitoring instruments with technical simplicity and they have speed in response by the direct transduction to electronic equipment [3].

We report the development of a new immunoassay fot OTA detection, combining the magnetic nanoparticles (MNPs) advantages with label free detection.

## 2. Experimental

### *2.1. Antibody immobilization on MNPs*

OTA monoclonal antibody was covalently immobilizate on the surface of carboxyl-modified MNPs via 1-ethyl-3-(3-dimethylaminopropyl) carbodiimide hydrochloride (EDC) / N-hydroxysuccinimide (NHS) method [4].

### *2.2. Preparation of Au immunosensor*

Gold sensors were fabricated using standard silicon technologies. Silicon wafers (1 0 0)-oriented, Ptype (3–5 Ωcm) were thermally oxidized to grow 800-nm thick field oxide. Then, a 30-nm thick titanium layer followed by a 300-nm thick gold top layer was deposited by evaporation under vacuum.The surface of the gold sensors was 0.07 $cm^2$. All the immobilization steps are schematically presented in Fig. 1.

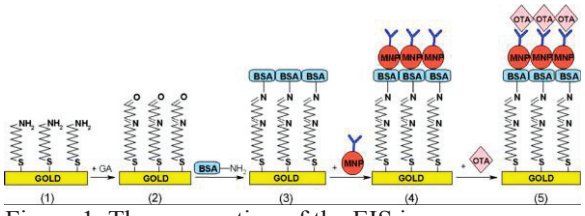


Figure 1. The preparation of the EIS immunosensor.

## 3. Results

### *3.1. Electrochemical impedance spectroscopy study*

Each immobilization step was characterized by EIS and the Nyquist plots are presented in Fig. 2.

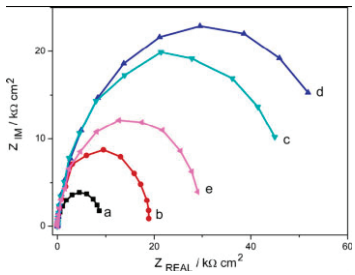


Figure 2. Nyquist diagram for the Faradaic impedance measurements corresponding to the electrodes: (a) Au; (b) Au/TA; (c) Au/TA/GA; (d) Au/TA/GA/BSA; (e) Au/TA/GA/BSA/Ab–MNP (E = −400 mV).

### *3.2. Ochratoxin A detection*

The specific Ab–OTA interaction induces an increase of the resistance shown by larger semi-circular diameter proportional to the different tested concentrations. After Ab–OTA binding, the electrical properties of the nanoparticle layer change and it becomes a more blocking layer. OTA samples with concentrations ranging from 0.01 to 10 ng/mL were incubated with the immunosensor and the impedance measurements were performed after each antigen addition. The calibration curves are presented in Fig. 3.

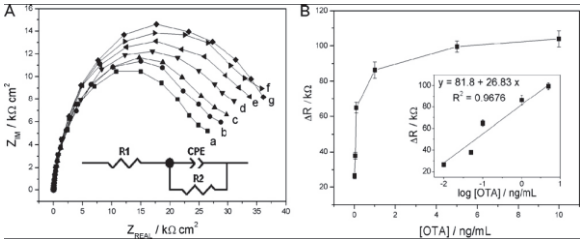


Figure 3. (A) Nyquist plots for different OTA concentrations: (a) 0 ng/mL; (b) 0.01 ng/mL; (c) 0.05 ng/mL; (d) 0.1 ng/mL; (e) 1 ng/mL; (f) 5 ng/mL; (g) 10 ng/mL. (B) Increase of charge transfer resistance with OTA concentration ranging from 0.01 to 10 ng/mL (n = 5); inset: linear calibration plot of the EIS OTA immunosensor.

## 4. Discussion

One can observe in fig. 2 that the immobilization of the thiolamine (TA) and glutaraldehyde (GA) induces an increase in the semi-circular diameter indicating an increase of the electron transfer resistance. The immobilization protocol, designed to reduce the non-specific interactions, led to an increase of the impedance, but the MNPs-Ab layer drastically reduced the impedance of the system at approximately half comparing with the impedance of the Au/TA/GA/BSA electrode (fig. 2). This behavior is expected to have a positive effect on the sensitivity and detection limit for OTA detection. The immunosensor shows a sensibility of 26.83 kΩ per decade of concentration, and a detection limit of 0.01 ng/mL (S/N = 3). This is one of the lowest reported [5]. A relative standard deviation of 4.7% obtained for 5 repeated measurements proves a very good reproducibility of the immunosensor.

The EIS immunosensors was tested on white wine samples spiked with OTA. Results were compared with ELISA test (Ridascreen OTA test kit) as reference method. As shown in Fig. 4, a variation of the analytical signal with no more than 10% was observed for real samples without any interference from the real sample matrix.

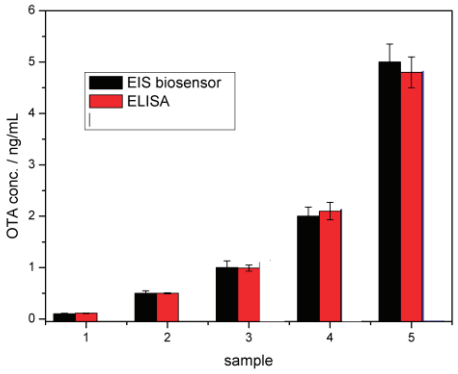


Figure 4. Comparative test on white wine spiked with OTA 0.1, 0.5, 1, 2 and 5 ng/mL for EIS immunosensor and ELISA test (n = 5).

*Acknowledgements*

This work was supported by the grants of the Romanian National Authority for Scientific Research, UEFISCDI, grant no. 107/2012.

## 5. References

[1]. J. L. Richard, *International Journal of Food Microbiology*, **119** (2007) 3.
[2]. P.M. Scott, *Mycotoxins and Food Safety*, **504** (2002) 134.
[3]. D. Samanta, A. Sarkar, *Chemical Society Reviews*, **40** (2011) 2567.
[4]. L.-G. Zamfir, I. Geana, S. Bourigua, L. Rotariu, C. Bala, A. Errachid, N. Jaffrezic-Renault, *Sensors and Actuators B*. **159** (2011) 178.
[5]. R. Khan, M. Dhayal, *Biosensors & Bioelectronics* **24** (2009) 1700.

# Nanostructuring of carbon microfiber surface

Tokareva I.V.[1], Mishakov I.V.[1,2], Vedyagin A.A.[1,2], Solov'eva S.V.[3], Petuhkova E.S.[3]

[1] *Boreskov Institute of Catalysis, pr. Lavrentieva 5, Novosibirsk, Russia, 630090*

[2] *Novosibirsk State Technical University, 20 Prospekt K. Marksa, Novosibirsk, Russia, 630073*

[3] *Institute of Oil and Gas Problems of the Siberian Branch of the RAS, 1, Oktyabrskaya str, Yakutsk, 677891*

(*) corresponding author: tokareva@catalysis.ru

*Keywords: carbon nanofiber, microfiber, catalytic CVD*

## 1. Introduction

Nowadays composite materials based on polymer matrix and carbon microfiber (MF) are of a great importance. Such materials possess high strength and low weight. By adding carbon MF to polymer matrix for construction purposes one can obtain material such strong as steel. This is useful for pipe construction in regions with cold climate.

Strength of composite materials depends on several factors such as type of polymer matrix, type of reinforcement additive and adhesive strength between matrix and agent. The main futures of carbon MFs (low density and high strength) allow us to develop ultra light composites. Adhesive strength is determined by contact area between matrix and reinforcement agent (value of specific surface area) [1]. Carbon MF obtained by pyrolysis of polymer precursor are characterized by smooth surface (0.7 - 1.8 $m^2/g$), which is needed to be modify [2]. For plastic reinforcement partial oxidation of surface is usually used. This approach has some significant disadvantage: since MF's elasticity is provided by using special epoxides, surface acidic or alkaline treatment lead to surface destruction. In this case method of surface modification consisted of MF's surface covering with carbon nanofibers (CNF) was suggested. This technique results in obtaining carbon-carbon composites (CNF/MF) with high surface area.

## 2. Experimental

In terms of research composite samples образцы x%CNF/MF were synthesized (x – mass % CNF, ranged from 1 to 200%).

All samples were prepared by unique technique. Nanostructuring of carbon microfiber surface were carried out by catalytic chemical vapor deposition (CCVD) of hydrocarbons [3].

Catalytic particles of nickel and Ni-Cu alloy were deposited via impregnation technique with the following drying and reduction in hydrogen flow. Ethylene, propane-butane mixture, natural gas and 1,2-dichlorethane were used as a hydrocarbon source. It is worth mention that 1,2-dichlorethane is the component of the wastes from poly-vinyl manufacture.

Production of experimental samples CNF/MF was carried out at special apparatus with rotor-type reactor [4]. Modified MFs (CNF/MF composites) were introduced into pipe-polyethylene PE80B by regranulation using Brabender plasticorder.

Examination of physico-mechanical properties of such composites were carried out in according government standards at universal testing machine UTS-2.

## 3. Results and discussion

In this work effect of different factors on reinforcement ability synthesized composites such as catalyst composition, hydrocarbon type, MF's type and % of MF's covering were investigated. Kinetics of CNF growth on MF surface were investigated in flow gravimetric device with McBain balances. It was shown, that addition of Cu leads to stabilization of catalyst work caused by dispersed Ni-Cu alloy particles formation. It was established that ethylene and 1,2-dichlorethane are decomposed more efficiently than other gases with the CNF yields on MF surface up

to 300 and 80 % correspondingly. CNF/MF composites produced from decomposition of different carbon sources.

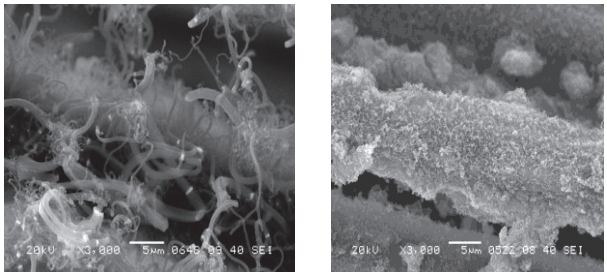

Fig. 1. SEM images of carbon-carbon composites obtained from ethylene (*left*) and propane-butane mixture (*right*) decomposition on Ni catalyst.

It is worth mention that the developed method allow us to obtain composites CNF/MF with different morphology of carbon nanofiber: from feathery structure with thick fiber diameter (300 nm) to thin nanotubes (30 nm). CNF with feathery and 'pale of plates' morphology are shown on figure 2.

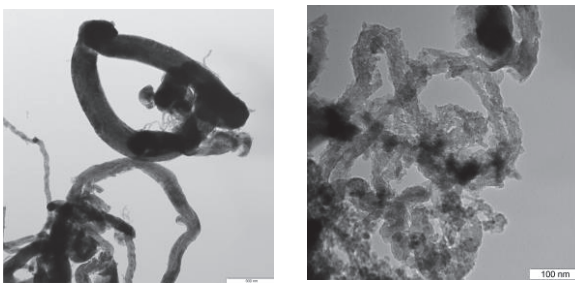

Fig. 2. TEM images of carbon-carbon composites with feathery (*left*) and 'pale of plates' morphology (*right*).

Table 1. Physico-mechanical properties of pure and reinforced polyethylene.

| N | **Sample** | **$\sigma_т$, MPa** | **E, MPa** | **$\varepsilon_р$, %** |
|---|---|---|---|---|
| 1 | Regular polyethylene | 21,2 | 986,0 | 0 |
| N | **Sample** | **$\sigma_т$, MPa** | **E, MPa** | **$\varepsilon_р$, %** |
| 2 | Polyethylene + MF | 23,8 | 1499,3 | +88 |
| 3 | Polyethylene + MF + CNF | 25,8 | 1626,2 | +19 |
| 4 | Polyethylene + CNF/MF composite | 26,3 | 1323,3 | +164 |

Using the BET method it was shown that surface area after modification increased up to ten times. In other words modification results in Increasing of surface area from 1.8 $m^2/g$ to 6-20 $m^2/g$.

It was shown that method suggested provide improvement of physico-mechanical properties of materials reinforced with carbon Nf/Mf composite (table 1).

Results of SEM investigation of reinforced pipe polyethylene are shown of figure 3. It is seen that composites with modified MF are characterized by physical bonding between MF and polyethylene while non-modified MFs have no interaction with polymer matrix.

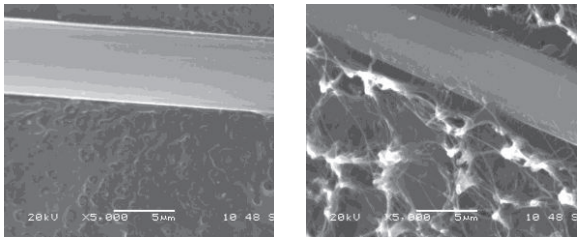

Fig. 3. SEM images of polyethylene composite reinforced with non-modified MF (*left*) and CNF/MF(*right*).

Thus, nanostructuring of carbon microfiber surface with CNF seems to be useful for current applications (cold and wet climate).

## References

[1]. Simamura S. Carbon fibers. M. (rus): Mir, 1987
[2]. David B. Curliss, Jason E. Linkoln, US 2009 0220409 A1.
[3].Buyanov R.A., Chesnokov V.V. // Catalysis in Industry. – 2006. – № 2. – C. – 3-15.
[4]. MishakovI.V., Buyanov R.A., Chesnokov V.V., Strel'cov I.A., Vedyagin A.A. // Catalysis in Industry – 2008. – № 2. – C. 26-30.
[5]. Gul V.E. Structure and strength of polymers (rus). M.: Chemistry, 1971

# New catalyst for synthesis of carbon nanofibers from chlorinated hydrocarbons

Yu. Bauman[*,1], A. Lysakova[2], I. Mishakov[1,2], A. Vedyagin[1,2], R. Buyanov[1]

[1] *Institute of Catalysis SB RAS, pr. Lavrentieva 5, Novosibirsk, Russia, 630090*
[2] *Novosibirsk State Technical University, pr. K. Marksa 20, Novosibirsk, Russia, 630073*

(*) corresponding author: bauman@catalysis.ru

*Keywords: carbon nanofibers (CNF), 1.2-dichlorethane (DCE), metal dusting, nickel alloys*

## 1. Introduction

Recycling of hazardous organochlorine wastes is very painful problem for the modern chemical industry. There is a high demand on development of the alternative ecologically harmless technologies excluding usage of dangerous reagents and formation of secondary toxic substances. Catalytic gas-phase dissociation of chlorinated hydrocarbons into valuable chemical products (for example, carbon nanofibers, CNFs [1]) is now considered to be a prospective way for abatement of such dangerous organochlorine wastes [2].

Decomposition of regular hydrocarbons with deposition of CNFs occurs in accordance with so-called carbide cycle mechanism [3] and is known as catalytic vapor deposition (CVD). Different aspects of synthesis of carbon nanomaterials (such as catalyst composition, temperature, nature of hydrocarbon source etc.) and growth mechanism have an effect on morphology and texture of the resulting product [4-6]. Catalytic dissociation of the chlorinated hydrocarbons via carbide cycle mechanism results in formation of very specific morphology of CNF known as “feathery” [1] or “segmented” [6] fibers.

There are some general shortcomings concerning supported catalysts used for processing of chlorinated hydrocarbons (multi-stage synthetic procedure, formation of harmful gases during calcination, and susceptibility to deactivation under action of HCl vapors). Another problem of synthesis is related to impossibility of obtaining the controllable size distribution of active metal particles – an important factor defining efficiency of process.

As it was earlier reported, the action of aggressive gas media containing chlorinated hydrocarbons might cause quite rapid corrosion of bulk metallic materials and alloys in certain conditions [1, 2]. In that case the spontaneous disintegration of alloys that leads to formation of the active sites of CNF growth can proceed. Formed active centers (disperse metallic or alloyed particles) appear to be fixed within the structure of carbon nanofibers which prevents particles from sintering and determines their absolute availability to reagents. The observed process of carbon corrosion is not novel phenomenon; it represents a particular case of metal dusting.

The report will present the results of the decomposition 1,2-dichloroethane (DCE), the major component of the waste production of vinyl chloride, over self-organizing Ni-based catalysts with formation of carbon nanofibres which are characterized by highly disordered and fragmented (mosaic) structure.

## 2. Experimental

A nickel foil (99.9%) and nickel-chrome alloy (80% Ni, 20% Cr, 0.01 mm wire of nichrome) were used as bulk Ni-based precursors for preparation of self-organizing catalysts. Experiments on metal dusting were carried out at 550-700°C in the quartz flow reactor equipped with in situ gravimetric McBain microbalance. The reaction gas feed containing argon and hydrogen was saturated with vapors of DCE via bubbling through a vessel with liquid 1,2-dichloroethane at room temperature. The excess of hydrogen (37.5 vol.%) was necessarily used to promote the chemical

corrosion of metallic surface and prevent it from complete chlorination. After each experiment samples were cooled in an argon stream down to room temperature.

Evolution of growth of CNFs and their structure and morphology were studied by various microscopic techniques (AFM, SEM and TEM). The obtained CNF material (without catalytic particles washed out by acidic treatment) was tested as an enhancing additive to motor oils.

## 3. Results and discussion

In first minutes of interaction with reaction mixture the surface bulk Ni-based alloys undergo tremendous topographic changes as shown on Fig.1. Observed fact can be explained by appearance of dramatic mechanical strains due to transfer of carbon into metal up to oversaturation. This ends up with disintegration of bulk alloy and formation of dispersed metal particles.


Fig.1. Evolution of surface of Ni-Cr bulk alloy during its interaction with DCE at 600°C.

The size of resulted particles varies from 200 to 300 nm. They behave as active centers for the growth of carbon nanostructures. According to EDX data, the redistribution of Cr takes place during metal wastage process. It leads to formation of 2 types of particles: 1 - *active ones* (containing ~ 0.5 at.% of Cr) and 2 – *inactive alloy* containing ballast chromium (~80%).

It was established that Ni-based catalysts prepared via metal dusting of corresponding bulk precursors exhibit very high activity in DCE decomposition and appropriate resistance to deactivation in aggressive medium. The presence of residual chromium in the original alloy was found to have a crucial effect on stability of catalyst, allowing us to achieve much higher yields of carbon product per 1 g of metal (Table 1).

Best carbon yield obtained for Ni-Cr catalyst was as high as 600 g(CNF)/g(Ni) which is about 2 orders superior to that known for supported $Ni/Al_2O_3$ catalysts.

Table 1. Dependence of the carbon product yield upon the decomposition of DCE on the concentration of chromium in its alloy with nickel (550°C; 7 h)

| Sample | Chromium content, wt. % | Induction period, min | Yield, g(CNF)/g(Ni) |
|---|---|---|---|
| Ni foil | 0 | 20 | 2.3 |
| Ni-Cr wire | 20 | 40 | 39 |

The catalytic decomposition of 1,2-DCE results in formation of carbon nanofibers with unique morphology (illustrated by Fig. 2) and textural features (surface area can reach 400 $m^2/g$).

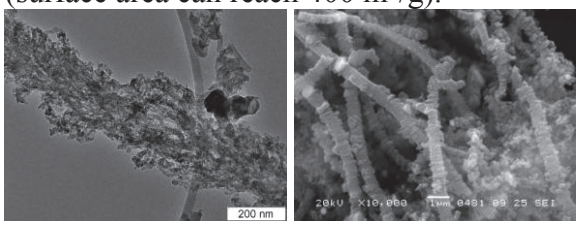


Fig.2. Morphology of CNF obtained via decomposition of DCE over self-organized catalyst: mosaic fiber (left), segmented fibers (right).

The combination of certain characteristics of feathery CNFs makes them very effective and prospective agent (enhancing additive) to lubricants and motor oils, which has been recently confirmed by the set of tribological tests.

This study was financially supported by Department of Chemistry and Materials Sciences RAS (project #5.2.2).

## 4. References

[1]. Yu. Bauman, I. Mishakov, R. Buyanov, A. Vedyagin, A. Volodin, *Kinetics and Catalysis*. **52** (2011) 547.

[2]. Yu.I. Bauman, I.V. Mishakov, A.A. Vedyagin, S.V. Dmitriev, M.S. Mel'gunov, R.A. Buyanov, *Catalysis in industry*. **4** (2012) 261.

[3]. V.V. Chesnokov, R.A. Buyanov, *Uspekhi Khimii*. **7** (2000) 675.

[4]. K. Mukul, A. Yoshinori, *Journal of Nanoscience and Nanotechnology*. **10** (2010) 3739.

[5]. A. Shaikjee, N.J. Coville, *Carbon*. **50** (2012) 3376.

[6]. A. Nieto-Marques, J.L. Valverde, M.A. Keane, *Applied Catalysis A: General*. **332** (2007) 237.

# Polyethylenimine-coated gold nanorods: biocompatibility and photothermal effect

K. Razum*, D. Pyshnyi, I. Pyshnaya, E. Goncharova, E. Ryabchikova

*Institute of Chemical Biology and Fundamental Medicine SB RAS, Russia, Novosibirsk, Lavrentiev Ave. 8*

(*) corresponding author: kk-kristina@mail.ru

*Keywords: gold nanorods, laser photothermal therapy, melanoma*

## 1. Introduction

Gold nanorods (GNRs) attract enormous scientific and technological interest due to their ease of synthesis, chemical stability and unique optical properties. These features make GNRs particularly attractive for disease detection and therapy [1]. Irradiation of GNRs with a continuous wave laser served as a basis of photothermal treatment. The nanorods convert the absorbed light into localized heat within a short period of time due to the surface plasmon resonance effect. However, application of GNRs is limited by the toxicity of cetyl trimethylammonium bromide (CTAB) which is used for synthesis of GNRs [3]. In this study we examined the biocompatibility of polyethylenimine-coated GNRs and possibility of their application in photothermal cancer therapy.

## 2. Experimental

### *2.1. Synthesis and features of PEI-GNRs*

GNRs were synthesized according to standard method envisaging a washing step to remove toxic CTAB [3]. We used linear polyethylenimine (PEI) for coating of GNRs layer by layer. Linear PEI was synthesized from poly(2-ethyl-2-oxozoline) (200 kDa, Alfa Aesar). PEI-coating GNRs were stored in aqueous solution (1 mg/mL).

The morphology and size of PEI-GNRs were examined by transmission electron microscope (TEM) JEM 1400 (JEOL, Japan) with a digital camera Veleta (SIS, Germany). The average size of PEI-GNRs was determined by measurement of 100 particles, using image analysis (iTEM, Version 5.2). PEI-GNRs were studied by dynamic light scattering (DLS) on Zetasizer NanoZS (Malvern, England). Measurements were made according to standard protocols.

### *2.2. Cell culture*

Cultures of melanoma cells (B16) and Baby Hamster Kidney cells (BHK-21) were propagated at 37°C in Dulbecco's Modified Eagle Media (DMEM, Gibco) with 10% heat-inactivated fetal bovine serum (FBS, Gibco) and 1% penicillin/streptomycin in humid atmosphere containing 5% $CO_2$.

### *2.3. Electron microscopic studies*

B16 and BHK-21 cells ($1\times10^5$ in 1 mL per well) were spread into 6-wells tissue culture plate (TTP, LabTech) and allowed to grow for 24h. After this both B16 and BHK-21 cells were incubated with PEI-GNRs (0.15 mg/mL) for 10, 30 min, 1, 3, 5 and 24 h, and prepared according to standard protocols for TEM.

### 2.4. *Laser irradiation of cell cultures*

B16 and BHK-21 cells ($5\times10^4$ in 0.5 mL per well) were spread into each of 12-wells tissue culture plate (TTP, LabTech) on glass coverslips and allowed to grow for 24h. PEI-GNRs suspended in DMEM were added to cells to a concentration 0.1 mg/mL per well, and cells were incubated for 24h. Then cells were irradiated for 15 min with 808-nm (1.1 W/cm$^2$) or 650-nm (0.79 W/cm$^2$) by laser, either in the presence or absence (control) of GNRs. Irradiated cells were stained with trypan blue or immediately fixed for hematoxylin-eosin staining. The samples were studied by light microscope Leica DM 2500 with digital camera Leica DFC420 C (Leica, Germany).

*2.5. Toxicity studies*

Both B16 and BHK-21 cells were incubated in 100 μL DMEM in 96-well plates with PEI-GNRs concentration of $1x10^{-2}$ to $1x10^{-6}$ mg/mL (serial 10-fold dilutions) for 24, 48 and 72h. Untreated cells were used as a control. Cell viability was assessed by the optical density in comparison with the control by MTT assay.

*2.6. Experimental model in vivo*

Tumor-bearing mice were obtained by subcutaneous inoculation of $1.5x10^5$ cells of melanoma B16 per mice C57Bl/6. Female mice (18-20 g) were kept under natural light in cages (5 animals in each) and had free access to commercial chow and water. Mice were randomly divided into 5 groups: with or without laser irradiation (a wavelength of 650 or 808 nm); with or without injection of PEI-GNRs, and control animals with grafted tumors. The PEI-GNRs (100 μL of sterile saline, 2 mg per mouse) were injected into tumor which reached 0.5 cm in size. Irradiation was applied onto tumor for 5 min after 1-2 days post injection of PEI-GNRs. Laser excitation was 650 nm (15.6 $mW/cm^2$) or 808 nm (16.2 $mW/cm^2$). Thermal imager was used to assess the heating area in the tumor, which was heated to 40-42$^0$C. After 2 days the tumor was excised, fixed in 4% paraformaldehyde and routinely processed for light microscopy.

## 3. Results

The PEI-GNRs in TEM had sizes 15 x 50 nm (±10%). The PEI coating was seen as a faint halo around the metal cores. The wavelength of maximum optical absorption of the PEI-GNRs was 760 nm, zeta potential in distilled water was 54.9 mV.

Irradiation laser (diameter of emission 5 mm) of BHK-21 cells treated with PEI-GNRs led to a complete destruction of the cells on coverslips. Decrease the laser beam to 2 mm resulted in decrease of damaged area, and the cells literally "welded together". Photothermal effect on B16 cells was somewhat weaker than in BHK-21 culture. MTT assay revealed that BHK-21 cells have higher viability (85-105%) than B16 cells (50-90%, the control was taken as 100%) at the same conditions.

TEM showed adsorption of PEI-GNRs on plasma membrane of B16 and BHK-21 cells and penetration into these cells through caveolin- and raft-dependent endocytosis. During the incubation PEI-GNRs moved to endosomes, and then to multivesicular bodies (MVB). Sometimes MVB fused with cell plasma membrane, and PEI-GNRs were released into the extracellular space.

Study of plasmon resonance effect of PEI-GNRs in vivo showed following results: 1) warming of the tumors treated with PEI-GNRs was higher than in untreated mice; 2) visual tumor damage was more extensive than in untreated animals. Histologic study found necroses, areas of destroyed cells with homogenized cytoplasm and nucleus, edema and disintegration of the tumor tissue after photothermal therapy. In untreated with PEI-GNRs tumors, laser irradiation caused evidently less damage.

## 4. Discussion

Melanoma is the most aggressive of skin cancers. Primary treatment of many malignancies includes a combination of surgery, chemotherapy, and/or radiation therapy. Despite advances in these treatment modalities, outcomes for melanoma are generally poor, so development of innovative therapies is necessary [2]. Gold nanorods are expected to be useful as photosensitizers for photothermal therapy of tumors.

We found that PEI-coated GNRs are biocompatible: they do not agglomerate in cell culture medium, penetrate into the cells and are not cytotoxic. Laser irradiation in the presence of PEI-GNRs caused damage of cells and tumor, whereas untreated cells and melanoma tumor remained visually unchanged under same laser power and exposure time. Our study showed that PEI-GNRs-mediated heating lead to damage of melanoma tumor without displaying significant systemic toxicity.

## 5. References

[1]. Cabada et al. *Int J Nanomedicine.* **7**(2012) 1511

[2]. James et al. *Cancers.* **2**(2010), 1155

[3]. Wang et al. *Dalton Trans.* **41**(2012) 11134

# Assess the toxicity of carbon nanomaterial by biotesting

I.A. Mansurova*[1], I.P. Pogorelsky[1], K.E. Gavrilov[1], A.S. Gorshkov[2]

[1]FGBOU VPO "Vyatka State University", Kirov, Moskovskaya, 36
[2]FGKU "33 TSNIII Russian Defense Ministry", Kirov, Oktyabr'skiy ave., 119

(*) corresponding author: irinamansurova@mail.ru

*Keywords: carbon nanofibers, toxicity, biotesting*

## 1. Introduction

Expanding the use of carbon nanostructures (fullerenes, nanotubes, nanofibers), including in the field of polymeric composites for industrial, medical and household needs assessment as an integral source of toxicity of nanomaterials and polymer systems containing them.

In this paper, the object of the study were samples of carbon nanomaterials (CNM), which differ in structure, specific surface area and, in some cases, the conditions for the subsequent step of the synthesis process. According to industry CNM are nanofibers with different stacking graphene planes relative to the fiber body: type "fish spine" (fig. 1), "coaxial-conical", etc.

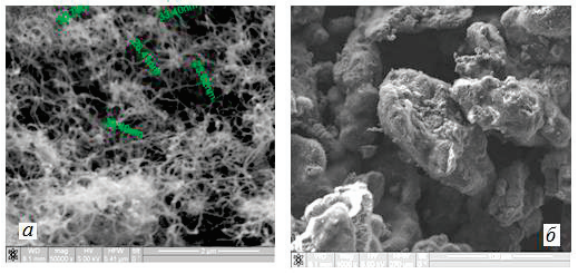


Figure 1. CNM photomicrographs (scanning microscope Quanta 200 3D) at magnifications × 50000 (a) and × 1000 (b).

## 2. Experimental

At the core of the development of ways bioassay samples CNM based on the following provisions.

1. Evaluation of the toxic properties of any substance or advisable to carry out using a variety of test objects [1] as a universal test system that can detect all possible toxicants equally well and able to give an adequate assessment of the overall toxicity does not exist. In this regard the work as test objects used bacteria (growth tests, bioluminescent test "Ekolyum"), ciliates, eukaryotic cells Hep-2 in the MTT assay, white mice.

2. Toxicological evaluation of the properties of nanomaterials should be carried out not only in makrodispersnoy, but also micro-, submicro- and nanodispersed form [2], as the high reactivity of the CNM and the possible toxic effects on living organisms is manifested as time in a dimensional state. Therefore, in this study examined the toxicity CNM in the traditional toxicological methods, i.e. relative to its mass concentrations makrodispersnoy form and dispersed by ultrasound in an aqueous medium samples CNM.

When using bacteria surface dense medium in Petri dishes seeded many test culture (10 ppm ∗ ml-1 bacteria). Then, on the dried surface were coated samples CNM (in makrodispersed form) in an amount of from 1 mg to 100 mg. Petri dishes with crops microbial cultures and CNM were incubated for 48 hours at 35 °C.

Bioassay procedure using fluorescent bacterial bioassay "ekolyum" made in accordance with MR 01.018-07 "Method for determining the toxicity of chemicals, polymers, materials and products through bioassay" ekolyum". The procedure for determining the toxicity of CNM with ciliates - shoes (Paramecium Caudatum) corresponded FR.1.31.2005.01883.

Acute toxicity CNM study performed on white mice weighing 18 - 20 grams, followed by observation for 14 days. Followed the general condition of the animals, the nature of physical activity, the

state of the hair and skin, reactions to various stimuli. Recorded the death of the animals, with all the dead animals were mortem examination of internal organs. Introduction CNM performed orally or by inhalation, placing the animals into the chamber where the samples held CNM dispersion in distilled water using UZDN (22 kHz).

## 3. Results

Research has shown that samples with CNM morphology of the "fish backbone" subjected to additional acid (30 % aqueous solution of $HNO_3$, 90 - 95 °C, 1,5 hours) treatment and heat (200 ° C until drying) have no antibacterial effect on Escherichia coli culture of E.coli, Bacillus B.cereus, B.subtilis, S.aureus and Staphylococci in the concentration range 1 mg to 100 mg. At the same time, suspended in an aqueous medium the fibers have strong toxic effect on bacteria bioassay "Ekolyum". The lowest toxicity index CNM samples is 0.47 ± 0.29. In these conditions, carbon black N220, which is the traditional rubber filler has an acceptable level of toxicity (toxicity index is 0,35 ± 0,10).

In the study of the toxicity of CNM with the MTT assay, which allows you to specify the path of the toxic effect (necrosis, apoptosis, cytoprotection / suppression) found that the dispersed forms of nanofibers acid and subjected to additional heat treatment is no dependence "dose-effect". This means that they exhibit toxic properties in maximum dilutions unlike silver nanoparticle (positive control), in which with increasing degree of dilution is reduced toxicity.

Investigation of the influence of the dispersed forms of nanofibers on white mice showed that the nanofibers subjected to more acid and heat treatment of acutely toxic, causing death in 50% of test-objects. Autopsy studies of test objects revealed the presence of cardiac, pulmonary pathology, and pathology of the abdominal cavity (table 1). It is noted that a day before the death of the animals became lethargic, unkempt, refused to eat, breathing becomes rapid.

Table 1. Pathological changes of the internal organs of white mice, victims of inhalation into the lungs nanofibers subjected to additional acid and heat treatment.

| № animal | Term death, day | The nature of the changes in internal organs |
|---|---|---|
| 1 | 2 | Increasing the size of the heart. Focal hemorrhage in the lung tissue |
| 2 | 2 | Hemorrhage in the right lung with a loss of airiness |
| 3 | 4 | Hemorrhage in the right lung and the upper lobe of the left lung with a loss of airiness. |
| 4 | 5 | Bleeding in the lungs with the loss of airiness. Venous stasis in the abdominal cavity. Enlargement of the spleen. Small intestine black. |
| 5 | 12 | Bleeding in the lungs with the loss of airiness. Enlargement of the spleen. |

## 4. References

1. Methods for determining the toxicity and hazards of chemicals. Ed. Prof. I.V. Sanok. M., "Medicine", 1970. 350.

2. Resolution of Chief State Sanitary Doctor of the Russian Federation dated October 31, 2007 № 79 "On approval of the concept issleldovany toxicology, risk assessment methodology, methods of identification and quantification of nanomaterials".

# In vivo study of hemocytes proliferative activity in *Modiolus modiolus (Bivalvia)* exposed to multi-walled carbon nanotubes

Anisimova A.A.*, Golokhvast K.S.

[1] *Far-Eastern Federal University, Vladivostok, Russia*

(*) corresponding author: anisan77@mail.ru

*Keywords: multi-walled carbon nanotubes, hemocytes proliferative activity, in vivo study*

Bivalve mollusks as suspension-feeders present a suitable target group of organisms in the coastal environmental researches to evaluate the influences of different pollutants including anthropogenic nanoparticles (NPs). The biological effects of different types of NPs on aquatic biota are discussed in some recent papers but the results are often contradictory and there is no clarity about the potential toxicity of NPs to Bivalvia. This discordance seems to be explained by absence in the most *in vivo* studies of the data on physical-chemical characterization of primary NPs, their behavior (dynamics of aggregation/agglomeration) in fresh or sea water and their future fate inside the organism (in review: Canesi et al., 2012).

A major target for NPs in bivalve mollusks is the digestive gland and then the particles can be potentially transferred to hemolymph (in review: Canesi et al., 2012). Hemocytes are involved in phagocytosis of different foreign objects (such as bacteria, microalgae, natural micro- and nanoparticles) as well as in restructuring of the damaged tissues. Correspondingly, the dynamics of the hemolymph cell population (hemocytes count and their proliferative activity) is expected to be changed in mollusks exposed by NPs. In this study the *in vivo* effect of multi-walled carbon nanotubes on proliferative properties of hemocytes was investigated in marine mussel *Modiolus modiolus*.

The adult mollusks were collected in July (water temperature 20 °C) from natural non-impacted water area (Vityaz Bay of Peter the Great Bay, Sea of Japan) and divided into two groups, control and exposed to NPs for 24 h (10 individuals in each group). Nanotubes were added in the experimental tank in concentration 100 mg/l. After 24 h the mollusks of both groups were injected with DNA synthesis precursor, bromodeoxyuridine (BrdU) and then (after 4 h) the hemolymph samples were taken from the muscle and fixed. Total hemocytes count were calculated with the Goryaev`s chamber. The percentage of proliferating cells (labeled with primary mouse monoclonal anti-BrdU and secondary gout polyclonal anti-mouse conjugated with Alexa-488, Invitrogene) was measured by means of laser scanning microscopy (LSM 700, Carl Zeiss). Physical-chemical characterization of primary NPs are presented in Table 1. The synthesis of the NPs was performed in the Boreskov Institute of Catalysis of Siberian Branch of Russian Academy of Sciences (Kuznetsov et al., 2010). The sedimentation rate and dynamics of nanotubes suspended in the sea water from Peter the Great Bay in concentration 100 mg/l were studied by kinetic method with spectrophotometer Shimadzu UV 2550.

Table 1. Physical-chemical characterization of the primary NPs used in the experiment.

| | |
|---|---|
| Type of NPs | MWCNT |
| Diameter, nm | 12-14 |
| Specific surface area ($S_{BET}$), $m^2/g$ | 300 |
| Processing | washed with acid (HCl) |
| Main impurities, mass % | Fe 0.16; Co 0.07; Mg 0.05; Cl 0.01 |

Spectrophotometric evaluation of the sedimentation dynamics of NPs suspended in the sea water in concentration 100 mg/l showed that already during the first hours the light absorption values declined dramatically because the nanotubes

aggregated and settled rapidly to the bottom of the cuvette; after 24 h 100% of NPs were in the bottom and the light absorption level fell to zero (Figure 1).

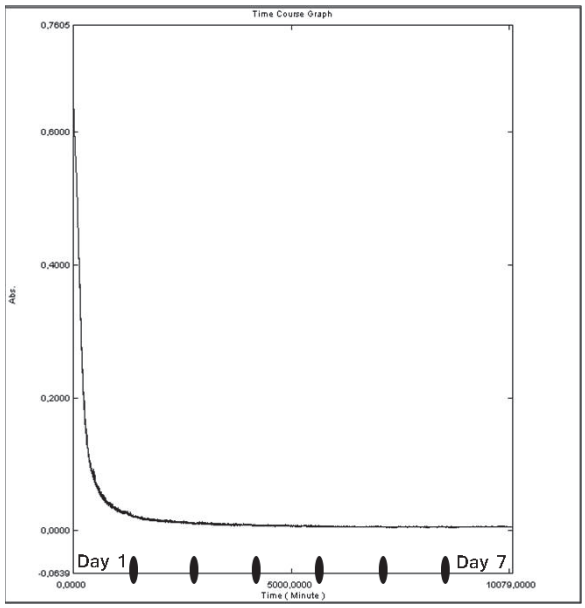


Figure 1. Sedimentation rate and dynamics of NPs suspended in the sea water of Peter the Great Bay in concentration 100 mg/l.

The data on total hemocytes count and their proliferative activity in hemolymph of *Modiolus modiolus* of the control and the exposed groups are presented in Table 2. The great individual variability of the parameters was observed both in control group and exposed one and no significance differences between the means were revealed by *T*-test at a significance level 5%. However, the medians differed strongly: median for total hemocytes count in experimental group was higher twice in comparison with the one in control group although the median for proliferative activity in exposed group on the contrary was lower than in control by 1.7 times. So, total count of hemocytes in hemolymph of the mollusks exposed to NPs increased without elevation (but even with decreasing!) of their renewal rate. Furthermore, a negative correlation was observed between total hemocytes count and their proliferative activity within each group.

All these findings may be explained by the following: 1) in July the mollusks are spawning and during spawning hemocytes migrate from hemolymph into gonads to be involved in resorption and restructuring of the gonad tissues; 2) hemocytes proliferate actively to provide a high concentration of phagocytes but the differentiated cells leave the bloodstream rapidly; 3) getting to an organism, NPs are transferred to the hemolymph and the count of circulating hemocytes increases due to their returning from tissues to eliminate the NPs but not due to elevation of proliferative activity; 4) the formation of NPs aggregates in sea water protects the mollusks from potential toxicological effect of nanomaterials.

The study was supported by Government of the Russian Federation for the state support of researches conducted under the supervision of leading scientists at Russian institutions of higher education, the contract № 11.G34.31.0010 and Scientific Fund of Far Eastern Federal University.

## 1. References

[1]. Canesi L., Ciacci C., Fabbri R., Marcomini A., Pojana G., Gallo G. Bivalve molluscs as a unique target group for nanoparticle toxicity // Marine Environmental Research, 2012. Vol. 76. P. 16–21.

[2]. Kuznetsov V.L., Elumeeva K.V., Ishchenko A.V., Beylina N.Yu., Stepashkin A.A., Moseenkov S.I., Plyasova L.M., Molina I.Yu., Romanenko A.I., Anikeeva O.B., Tkachev E.N. Multi-walled carbon nanotubes with ppm level of impurities // Physica Status Solidi (b), 2010. Vol. 247, Issue 11-12. P. 2695–2699.

Table 2. Total hemocytes count and their proliferative activity in hemolymph of *Modiolus modiolus* in control and with an exposure to NPs.

| Statistical parameters | Control | | Exposure to NPs (24 h) | |
|---|---|---|---|---|
| | Total hemocytes count in 1 mkl of hemolymph | Percentage of proliferating (BrdU-labeled) cells, % | Total hemocytes count in 1 mkl of hemolymph | Percentage of proliferating (BrdU-labeled) cells, % |
| Mean | 1309,1 | 9,9 | 2395,5 | 7,1 |
| Standard error | 182,7 | 1,9 | 557,1 | 1,3 |
| Median | 1400 | 11,3 | 2625 | 6,7 |
| Correlation coefficient of two parameter | -0,7 | | -0,5 | |

# Biological effects and toxicity of multi-walled carbon nanotubes

A.A. Gusev*,[1], I.A. Vasyukova[1], E.S. Ihalainen[1], O.V. Zakharova[1], O.A. Akimova[1], A.G. Tkachev[2]

[1] *Tambov State University after G.R. Derzhavin, Internacionalinaya St., 33, Tambov, 392000, Russia*
[2] *Tambov State Technical University, Sovietskaya St., 106, Tambov, 392000, Russia*

* nanosecurity@mail.ru

*Keywords: multi-walled carbon nanotubes, nanotoxicology, biological effect*

## 1. Introduction

In this paper we analyzed the biological properties and safety of carbon nanostructured material "Taunit" (producer - LLC "NanoTechCenter", Tambov), which is positioned as a representative of a class of multi-walled carbon nanotubes. His large-scale production in the Russian Federation and the little-studied ecotoxicological characteristics make this material a priority subject for research.

## 2. Experimental

As test objects used bacteria, crustaceans, micro-algae, higher plants, and mammals. It was previously the mathematical modeling of the potential hazards of nanomaterials by the procedure recommended by Federal service on customers' rights protection and human well-being surveillance of Russia.

## 3. Results

The simulation showed a high degree of potential danger. At the same time, the bioassay on microscopic objects Esherichia coli, Bacillus cereus, biosensor “Ecolum” (Esherichia coli M-17), Ceriodaphnia affinis Lilljeborg and Scenedesmus quadricauda (Turpin) Brebisson revealed average risk of the nanomaterial (III class, moderately hazardous substances). The bioassay on plants Onobrychis arenaria (Kit.) DC showed the stimulating effect of nanomaterial on the early stages of ontogeny. However, by electron microscopy has been shown to be capable of nanotubes penetrate the roots and accumulate in the leaves of plants, which may have serious environmental consequences. In the experiments in laboratory mice increased lethality was not observed, however test nanomaterial caused dose-inflammatory processes in the liver, lungs and kidneys of animals.

## 4. Discussion

Thus, the toxicity of nanomaterial to bacteria and aquatic organisms can be characterized as middle. Toxic effects on plants are found, but the effect of bioaccumulation of nanomaterial is observed. Acute toxicity to mammals were observed, while there are dose-related histological changes in a number of organs. For a final clarification of the issue of toxicity of multi-walled carbon nanotubes requires further chronic experiments.

# The research of nitrogen compounds effect on the activity of cracking catalysts

T.V. Chernysheva*, V.P. Doronin, O.V. Potapenko, T.P. Sorokina

*Federal State Budget Institution of Science*
*Institute of Hydrocarbon Processing, Siberian Branch of the Russian Academy of Sciences (IHP SB RAS),*
*Laboratory of synthesis of motor fuels,*
*Neftezavodskaya st. 54, Omsk, 644040 Russia*

*E-mail address: tvchern@ihcp.ru

*Keywords: catalytic cracking, catalysts, nitrogen poisoning, deactivation*

## 1. Introduction

The tendency of continuous weighting of feedstock in the world-wide refining has been observed in recent years. In addition to hydrocarbons feed contains metal impurities, oxygen, sulfur and nitrogen. The poisoning effect of nitrogen compounds consists in their adsorption on the acid sites of the cracking catalyst, leading to their neutralization and reducing their activity. This, in turn, results in a decrease of the yield of target products, as well as in an increase of coke formation and emission of nitrogen oxides from the regenerator [1 - 5].

This research is aimed to study the nitrogen compounds effect of different classes on the activity of equilibrium cracking catalyst and to design the approaches of the creation of cracking catalysts, being stable to nitrogen compounds poisoning.

## 2. Experimental

### *2.1. Materials*

Compounds with different hydrogen donor activity – n-undecane, cumene and decalin – were taken as model feeds.

Non-hydrofined vacuum gas oil and unconverted hydrocracking residue were used as real feeds.

There are pyrrole, indole, pyridine, quinoline, and n-butyl amine as model nitrogen compounds in the feed. Nitrogen content ranged from 0 to 3000 ppm.

The study was done by using the industrial equilibrium "LUX-1" cracking catalyst, produced by JSC "Gazprom Neft – Omsk Refinery." The catalyst contained zeolite HREY and the matrix, in which amorphous aluminum silicate, aluminum hydroxide and bentonite clay were presented [6].

### *2.2. Catalytic experiments*

Catalytic tests were performed at the laboratory unit with a fixed bed catalyst in amount of 21.0 g with the temperature range being 450 - 527°C and the weight hourly space velocity 5 $h^{-1}$.

Gas and liquid products of cracking were analyzed by using chromatographs: "Chromos GC-1000", «GC-2010» (Shimadzu), "Crystal Lux – 4000M», equipped with a capillary column (100% dimethylpolysiloxane, 100 m x 0.25 mm), and a module of TID / FID detectors: thermoionic (TID) - to analyze the nitrogen compounds and a flame-ionization (FID) - to analyze hydrocarbon part.

## 3. Results and discussion

### *3.1. Effect of nitrogen compounds concentration on the activity of catalyst*

Analysis of n-undecane catalytic cracking in the presence of nitrogen compound – pyrrole – showed the reduction of the model compound conversion from 42.2 to 20.8 wt.% and the reduction of the yields of desired products with the increase of nitrogen in the feed (Fig. 1).

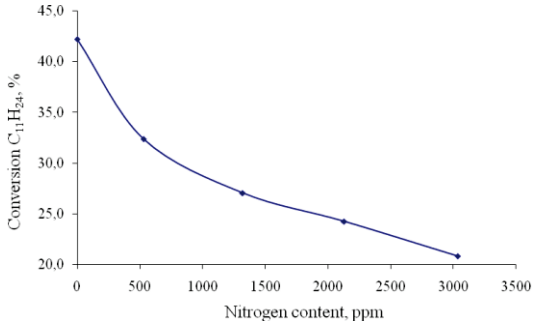


Fig. 1. The dependence of the n-undecane conversion of the nitrogen content (for example, pyrrole) in the feed.

### *3.2. Effect of nitrogen compounds type on the activity of catalyst*

The study of n-undecane catalytic cracking in the presence of nitrogen compounds of different classes showed that indole has the greatest poisoning ability and n-butyl amine has the least one (Fig. 2).

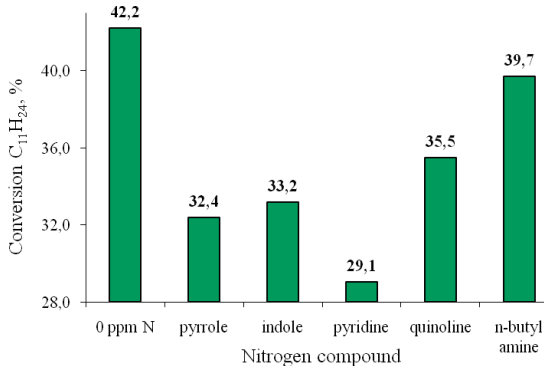


Fig. 2. The dependence of the n-undecane conversion of nitrogen compounds type (500 ppm N).

### *3.3. Conversion of different hydrogen donors in the presence of nitrogen compounds*

The study of cumene and decalin transformations in the presence of nitrogen compounds showed that quinoline has the greatest poisoning power in the case of cracking of cumene (the reduction of conversion from 82.2 to 69.9 wt.%), and indole has one in the case of decalin cracking (the reduction of conversion from 86.8 to 67.7 wt.%). It follows that the neutral nitrogen compounds poison the cracking catalyst to a greater extent in the case of processing paraffin-naphthene hydrocarbons, which are strong hydrogen donors. While the basic nitrogen compounds are more poisonous in the processing of aromatic hydrocarbons.

### *3.4. Nitrogen compounds effect on cracking of real feed*

Quinoline poisons the catalyst more than indole in catalytic cracking of non-hydrofined vacuum gas oil with a high content of aromatic structures. Indole, in its turn, gives the most poison ability in processing hydrocracking residue, which is rich of paraffin-naphthene hydrocarbons. These findings confirm the previously obtained results in analyzing model feedstock.

## 4. References

[1]. S.A. Akhmetov, Technology of oil and gas deep processing, Ufa: Guillem, **2002**.
[2]. G. Caeiro, A.F. Costa, H.S. Cerqueira, P. Magnoux, J. M. Lopes, P. Matias, F.R. Ribeiro, *Applied Catalysis A: General,* 320 (**2007**), 8 – 15.
[3]. Yingrong L., Wei W., Qiuling H., Yuxia Z., Jinghui D., Songbai T., *China Petroleum Processing and Petrochemical Technology,* 14 (**2012),** 18 – 24.
[4]. Cerqueiraa H.S., Caeiro G., Costa L., Ribeiro F. R., *Journal of Molecular Catalysis A: Chemical,* 292 (**2008**), 1 – 13.
[5]. Xinjin Zhao, A.W. Peters, G.W. Weatherbee, *Ind. Eng. Chem. Res*., 36 (**1997**), 4535 – 4542.
[6]. A.V. Glazov, V.N. Generalov, V.I. Gordenko, V.P. Doronin, I.V. Dubkov, *Russian chemical journal,* 51 (**2007**), 57 - 59.

# Towards optimization of carbon nanotube properties via *in situ* studies of growth mechanism

D.V. Krasnikov[§ 1,2], V.L. Kuznetsov* [1,2]

[1] *Boreskov Institute of catalysis SBRAS, 630090 Novosibirsk, Lavrentieva pr. 5, Russia*

[2] *Novosibirsk State University, 630090 Novosibirsk, Pirogova str. 2, Russia*

[§] krasnikovdmitry@gmail.com * kuznet@catalysis.ru

*Keywords: carbon nanotubes, in situ methods, catalysis*

Multi-walled carbon nanotubes (MWCNTs) are known as one of the most promising components for numerical materials due to their remarkable mechanical, chemical, and electronic properties [1-3]. At the same time, properties of MWCNTs significantly depend on their structure (defect concentration, diameter distribution, morphology of agglomerates, concentration of impurities and etc.), which, in turn, depends on the type of catalyst, reactor type, reaction parameters used for the production and on aftertreatment techniques [4-7]. The nature of catalyst (active component composition, preparation technique, supports, metal-support interaction, and the effect of promoters) is the most important factor for synthesis of MWCNTs by catalytic CVD techniques. The analysis of potential and achieved applications, such as catalyst supports, fillers of composites varnishes and lubricants, shows that each very application requires its own set of nanotube properties:

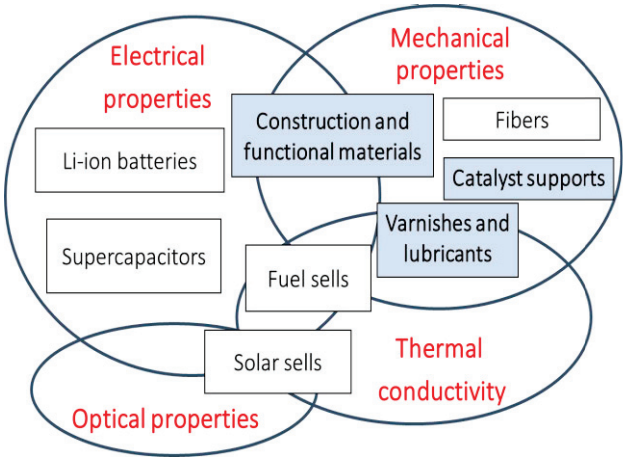


Fig.1. Diagram of potential (colorless rectangles) and already achieved (dark rectangles) applications of MWCNT with respect to their properties (ellipses).

Along with growing number of nanotube applications toxicity of MWCNTs as any other nanomaterials is one of the most discussed and urgent questions [8]. MWCNTs are a diverse group of materials and vary with regards to its diameter, length, defectiveness, surface chemistry, catalyst and organic impurities and morphology. Thus, MWCNT interacts with living systems not only as single cylinders of rolled graphene sheets but also as container with metal catalyst contaminations and light polyaromatic hydrocarbons (PAHs) remains, with acidic of basic surface groups such as carboxyl, carbonyl or phenyl. Also, it must be noted, that single nanotubes can be obtained only in very dilute suspensions. Presence of μm-sized agglomerates of entangled MWCNTs is much more possible in real systems. Therefore, to reach full understanding of mechanisms of MWCNT influence on living beings we should try to separate all abovementioned factors and investigate impact of each of them. To solve this issue MWCNTs with tailored properties must also be obtained.

However, mechanism of MWCNT growth is still not totally understood. This is a key issue which should be solved to obtain MWCNTs with tailored characteristics. Recent development of *in situ* methods of study allowed obtaining much more data on MWCNT growth mechanism [9].

In the present work the formation of the active component of the bimetallic Fe-Co catalyst during MWCNT growth was studied using *in situ* synchrotron radiation (SR) XRD analysis [10, 11]. The *in situ* SR XRD data in combination with the results of other physical methods (HRTEM, NMR)

can be used for the development of kinetic model and the optimization of the synthesis conditions to produce MWCNTs with controlled properties. On the basis of obtained data we show possibilities of tuning such parameters of MWCNTs as diameter, catalyst remains and defect concentration.

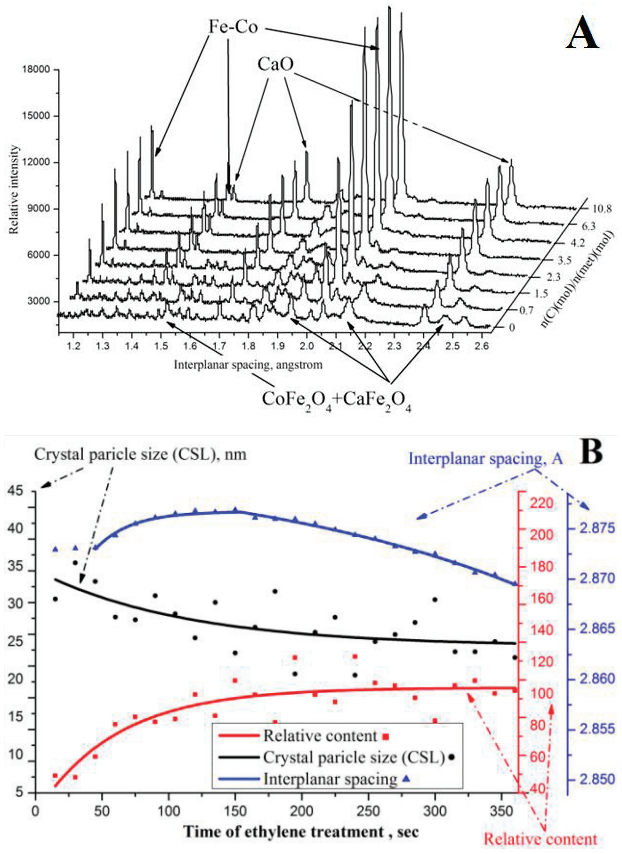


Fig.2. A - Typical *in situ* XRD patterns of Fe–Co/$CaCO_3$ catalyst evolution at reaction temperature during ethylene treatment (iron and cobalt spinel-structured oxides transform to metal alloy). B - Evolution of the Co-Fe alloy (110) bcc reflections (integrated intensity, interplanar spacing and CSL) in C2H4/N2 (20% 1.4 sccm) flow

Also this work summarizes our results achieved on aftertreatment techniques with particular focus on nanotube structure and properties (mechanical, electrical and chemical). Such techniques as carbon flake deposition via hydrocarbon decomposition on MWCNT surface, which also proceeds via formation of light PAHs, and high temperature treatment nanotubes are discussed from their influence on MWCNT toxicity point of view.

## References

[1] M. S. Dresselhaus, G. Dresselhaus, P. C. Eklund, Science of Fullerenes and Carbon Nanotubes. *Academic Press,* 1996

[2] L. Dai, Carbon Nanotechnology. *Elsevier, Amsterdam,Oxford,* ISBN-13:978-0-444-51855-2. 2006

[3] K. J. MacKenzie, O. M. Dunens, A. T. Harris, *Ind. Eng.Chem. Res*. **49** (2010) .5323.

[4] A. Szabó, et al., *Materials*. **3** (2010). 3092

[5] A.I. Romanenko, V.L.Kuznetsov, A.N. Usoltseva, et al., *Phys. Status Solidi B*, **246** (2009) 2641

[6] S.N. Bokova, E.D. Obraztsova, V.L. Kuznetsov et al., *Phys. Status Solidi B*, **247**, (2010) 2827

[7] V.L. Kuznetsov, K.V. Elumeeva, A.V. Ishchenko et al., *Phys. Status Solidi B*, **247** (2010) 2695

[8] C.P. Firme III, P.R. Bandaru / *Nanomedicine: Nanotech., Biol. and Med*. **6** (2010) 245

[9] M. Weckhuysen *In situ* spectroscopy of catalysts ASP 2004

[10] V.L. Kuznetsov, D.V. Krasnikov, A.N. Shmakov et al*., Phys. Status Solidi B* **249** (2012), 2390

[11] D.V. Krasnikov, A.N. Shmakov, V.L. Kuznetsov et al., Bull. of RAS: physics **77** (2013),155

# Low Temperature Synthesis and Characterization of Nanoscale Rutile $TiO_2$

Z. Ismagilov [1,2], N. Shikina[1], E. Bessudnova[1*], V. Ushakov[1], N. Rudina[1]

[1] *Boreskov Institute of Catalysis SB RAS, pr.Akad. Lavrentieva, 5, Novosibirsk, 630090*
[2] *Institute of Coal Chemistry and Material Science SB RAS, Pr. Sovetskiy, 18, Kemerovo, 650000*
[3] *Affiliation 3, institution, department, postal address (font style: Times italic 10pt)*

(*) corresponding author: bev@catalysis.ru

*Keywords: rutile, nanoparticles, thermolysis of $TiCl_4$, physicochemical methods)*

## 1. Introduction

Nanoscale titanium dioxide is a promising object of investigation in various fields: photocatalysis, electrochemistry, optics, microelectronics, production of pigments, ceramics, cosmetics, gas sensors, inorganic membranes, dielectrics, synthesis of mesoporous film coatings and catalysts for environmental remediation and nanobiomedicine [1, 2]. In most cases, $TiO_2$ with the anatase structure is the preferable modification. However, the possibility of obtaining nanoscale rutile has attracted particular attention in recent years. In some catalytic processes like oxidation of hydrogen chloride (the Deacon process) on the $RuO_2/TiO_2$ catalyst, rutile is important for raising the reaction efficiency and selectivity, because rutile and the active component have close crystal lattice parameters [3]. Synthesis methods of nanoscale $TiO_2$ with the rutile structure reported in the literature produce mainly a mixture of two or three $TiO_2$ modifications with the rutile phase yield not higher than 60%. The aim of the present work was to develop well reproducible methods for synthesis of nanoscale $TiO_2$ (rutile) with a high specific surface area and 100% yield of the target phase.

## 2. Experimental

### *2.1. Materials and preparation of $TiO_2$ nanoparticles*

Titanium dioxide was synthesized by thermolysis of titanium tetrachloride $TiCl_4$ in water and in an aqueous solution of HCl upon variation of the main synthesis parameters. The effect of synthesis conditions on the structural features of nanoscale titanium dioxide and physicochemical properties of the target rutile phase was studied: the synthesis temperature was varied from 50 to 90°C at a constant value of $[H_2O]/[Ti] = 39$ in 0.5M HCl; the [Cl]/[Ti] molar ratio was varied from 4.0 to 4.8 at a constant $[H_2O]/[Ti] = 39$ (11 wt.% $TiO_2$ in the reaction solution) and a temperature of 70°C; the $[H_2O]/[Ti]$ molar ratio was varied from 39 to 65 in 0.5M HCl at 70°C. In the low-temperature synthesis, formation of the rutile phase (a white precipitate) was accompanied by formation of a highly dispersed anatase sol, which was separated from the precipitate by decantation. $TiO_2$ nanoparticles with the rutile structure were purified by dialysis, dried under a lamp

### *2.2. Physicochemical methods*

X-ray diffraction (XRD) patterns were recorded over a $2\theta$ = 20-85º range using an HZG-4C diffractometer with Co$K_\alpha$ ($\lambda$ = 1.59021 Å) radiation.

Atomic force microscopy images were obtained on a SolverP47Bio atomic force microscope in a semicontact mode.

HR-TEM images were obtained on a JEM 2010 electron microscope with lattice resolution 0.14 nm at accelerating voltage 200 kV.

Scanning electron microscopy study was performed using a JSM 6460LV (JEOL, Japan) microscope with accelerating voltage 25 kV.

The Raman (combination scattering) spectra of titanium dioxide samples were recorded on a Bruker RFS 100/S

spectrometer over a range of 3600-100 $cm^{-1}$ with a spectral resolution of 4 $cm^{-1}$.

To analyze the textural caracteristics of nanotitania, low-temperature (77 K) nitrogen adsorption-desorption isotherms were recorded using a Micrometrics ASAP 2400, isotherms from Hg porosimetry were recorded using a Micrometrics, AutoPore IV 9500, V1.09. To study changes in the texture characteristics, samples of the temperature series were additionally calcined at 100, 300, 500, 700 and 1000°C.

## 3. Results and Discussion

It was found that formation of a certain titanium dioxide modification depends on the balance of interacting parameters of the synthesis. At the chosen constant values of parameters $[H_2O]/[Ti]$ and HCl concentration, yield of the rutile phase increases with the synthesis temperature and attains 3.8, 48, 64, 99 and 100% at 50, 60, 70, 80 and 90°C, respectively. Thus, at temperatures above 80°C the reaction product is represented by monophase rutile. The dependence of the amount of produced rutile on the reactants ratio is a curve with a maximum at $[H_2O]/[Ti] = 67$ for 100% rutile yield and $[Cl]/[Ti] = 4.2$ for 85% rutile yield.

Structural properties of the samples were examined using XRD and Raman spectroscopy. All the precipitates separated at the synthesis step are characterized by the rutile phase. The XRD studies showed that crystallite size of the rutile samples from the temperature series was 55-70 Å along plane 1.1.0, and 140-200 Å along plane 0.0.2. According to HRTEM data, the crystallites formed long filaments constituting fan-shaped agglomerates. Elevation of the synthesis temperature increased length of the filaments and density of the agglomerates. After ultrasonic treatment, the low-temperature samples of rutile (50, 60, 70°C) dissociated into individual filaments and smaller agglomerates, whereas the high-temperature samples (80, 90°C) were resistant to ultrasound. SEM images clearly demonstrate the morphological features of nanorutile samples obtained at different temperatures.

Low temperatures of the synthesis (50, 60, 70°C) lead to the formation of concretions of underdeveloped globules consisting radially of the fan-shaped agglomerates. At the synthesis temperature of 80°C, globules start to separate from each other and form more energetically compensated structures; this process terminates at the synthesis temperature of 90°C.

The study of rutile powders obtained at different synthesis temperatures showed that materials produced over the entire temperature range have a high specific surface area, 110-140 $m^2/g$, and pore volume 0.09-0.12 $cm^3/g$ according to BET or 0.15-0.4 $cm^3/g$ according to Hg porosimetry. Elevation of the synthesis temperature is accompanied by decreasing the specific surface area and pore volume. The rutile samples were shown to have a heterogeneous pore structure including micro-, meso- and macropores. Elevation of the synthesis temperature increased the fraction of mesopores, whereas the fraction of micro- and macropores decreased. The dynamic study of decreasing texture characteristics of nanorutile during its calcination at 100-1000°C revealed that the sample obtained by thermolysis at 90°C is most resistant to sintering.

## 4. Conclusion

The synthesis methods of nanoscale rutile were developed and the regularities of its formation were revealed. Titanium dioxide with the rutile structure has a high specific surface area, up to 140 $m^2/g$, and pore volume up to 0.4 $cm^3/g$; it can be used as a promising support for catalyst preparation.

## 5. References

[1]. Z. Ismagilov, N. Shikina, E. Bessudnova, D. Korneev, A. Ishchenko, Yu. Chesalov, A. Vladimirova, E. Ryabchikova, *Chem. Eng. Trans*., **27** (2012) 241.

[2]. A. Levina, M. Repkova, Z. Ismagilov, N. Shikina, E. Malygin, N. Mazurkova, V. Zinov'ev, A. Evdokimov, S. Baiborodin, *Scientific Reports*, (2012) |2:756| DOI: 10.1038/srep00756.

[3]. Kohei Seki, *Catal. Surv. Asia*, **14** (2010) 168.

# The nanoparticles with core – shell grain creating by plasma of HF – discharges

G. Churilov[1], I. Osipova[1], N. Vnukova[1]*, A. Kolonenko[2]

[1]*Kirensky Institute of Physics, Akademgorodok 50, bld. 38, Krasnoyarsk, 660036 Russia*
[2] *Krasnoyarsk State Pedagogical University, Ady Lebedevoj Str. 89, Krasnoyarsk, 660049, Russia*

(*) corresponding author: churilov@iph.krasn.ru

*Keywords: nanoparticles with a core – shell grain, catalysis, plasma, HF discharge*

## 1. Introduction

Plasma is a substance state with unique properties. A great number of chemical reactions take place in plasma, which do not take place in usual conditions. Plasma is used for the treatment of different surface.

## 2. Experimental

We present two methods of the preparations of particles with a core – shell grain carbon and metal creating by plasma of HF discharges. For the first method we used installation for particle treatments in carbon plasma. Carbon plasma was creation by HF discharges between two graphite rods. The particles are transported across the metal containing plasma by means of a helium flow in a special device. The method is good for creating particles with a carbon shell. When we want to create particles with a metal shell, we can use plasma stream with a metal only (second method). Two plasma streams meet in one area in the installation for this method. For both methods we transport the particles with another gas flow in the middle of plasma area. Scheme of this process presented in fig.1.

## 3. Results

There are numerous reports of the nickel core and carbon shell particles in literature [1, 2]. Our nanoparticles have pure nickel core and carbon shell with complete structure. By electronic microscopy it was shown that fist layer is nickel carbide.

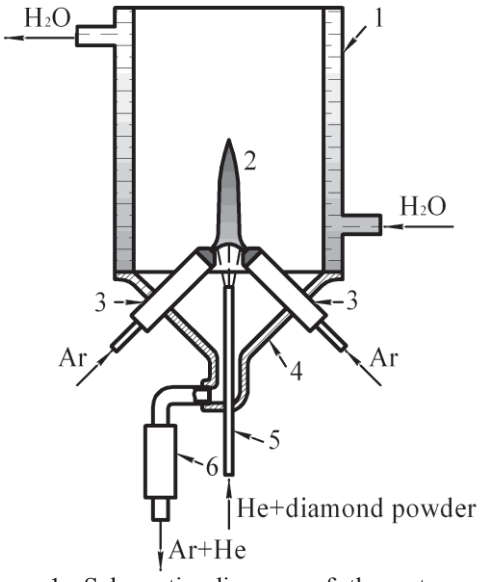


Figure 1. Schematic diagram of the set-up: 1 – chamber, 2 – plasma, 3 – electrodes, 4 – electrode support, 5 – quartz tube, 6 – nitrogen trap

The second layer is diamond and the third ones - graphite. This result was obtained by different analytical methods: Raman spectroscopy (fig.2) and XPS (fig.3).

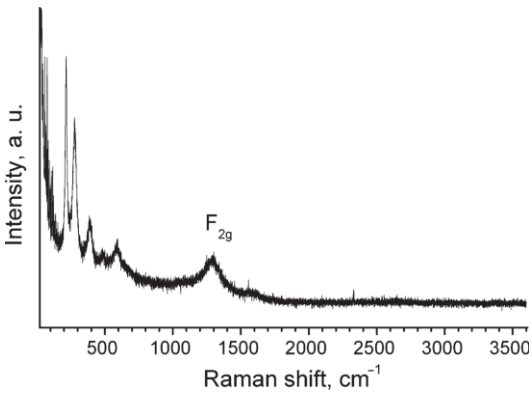


Figure 2. Raman spectrum of nickel-containing carbon particles

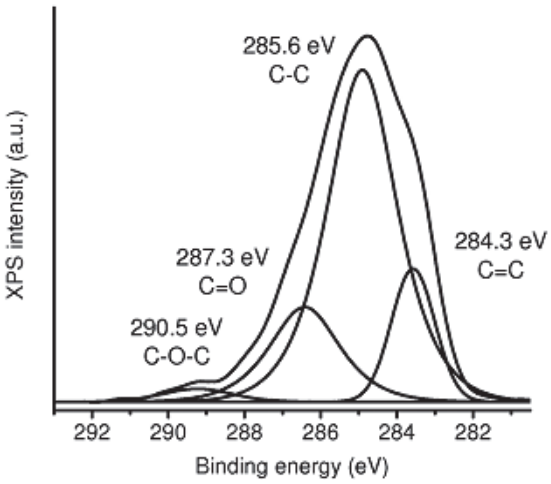


Figure 3. XPS spectra of C1s line for a sample of detonation diamond processed in nickel-containing plasma

Nanodiamonds and technical diamonds were covered by nickel and copper in argon plasma with this metal. The substances investigation was carried out by XPS, X-ray diffraction and electronic microscopy. The spectra of X-ray diffraction showed that metal covered particles have oxygen forms. The annealing under hydrogen allowed to create particles surface from pure metals (fig.4 and fig5).

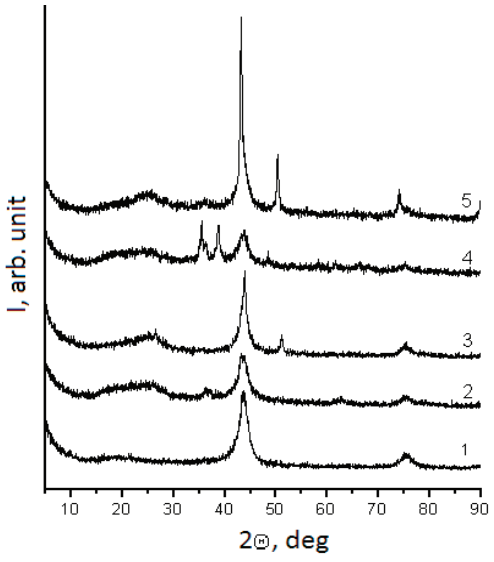


Figure 4. XRD of samples: 1–detonation diamond; 2(4)–detonation diamond, processed in nickel (copper)-containing plasma; 3(5)–detonation diamond, processed in nickel (copper)-containing plasma annealed in hydrogen flow

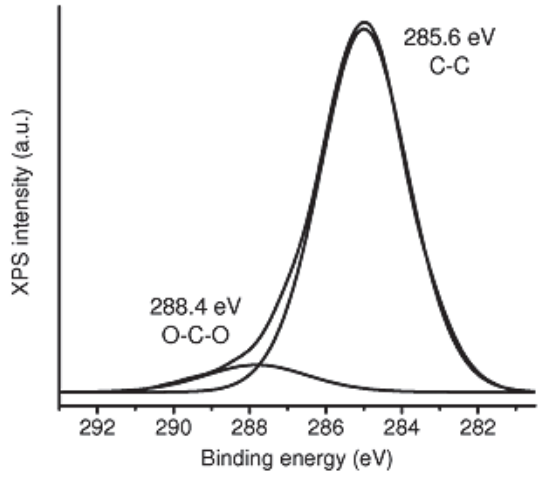


Figure 5. XPS spectra of C1s line for a sample of detonation diamond processed in nickel-containing plasma after annealing in hydrogen flow

## 4. Discussion

Thus it was shown that nanoparticles with a core – shell grain may be creating by plasma of HF discharges.

Further we plan to use high pores powder (such as $Al_2O_3$ for chromatography) as core for particles with a core-shell grain. We can use both metals and non metals as shell for particles.

Catalysis is one of the possible applications of these powders. For example, the powders with different functional groups can be use for various problems of catalysis.

The work was partially supported by the Ministry of Education and Science of Russian Federation, agreement №8194 and 14.B37.21.0163, Russian Foundation for Basic Research project № 12-03-31439, and Russian Academy of Science (Integration project of Belarus NAS and SB RAS №24).

## 5. References

[1] Dong, X. L.; Zhang, Z. D.; et al *Journal of Materials Research* 14 (1782) 1999.
[2] Wang, Han; Guo, Huaihong; et al. *Applied Physics Letters* 101 (083116/1) 2012.

# Immune and Endocrine Responses to Single Intranasal Application of Nanoparticles and Chronic Nanoaerosol Inhalation in BALB/c and C57Bl Mice

G.V. Kontsevaya*, D.V. Petrovski, L.A. Gerlinskaya, S.E. Peltek, M.P. Moshkin

*Institute of Cytology and Genetics, Siberian Branch of the Russian Academy of Sciences, 630090 Prospect Lavrentyeva, 10, Novosibirsk, Russian Federation.*

(*) corresponding author: @E-mail address: g-kon@ngs.ru

*Keywords: nanoparticles, lungs, immunity, Th1/Th2 balance*

## 1. Introduction

Respiratory tract are considered as a main target for aerosols containing nanoparticles [1], which become hygienically significant factors of work and home environments due to rising production of nanosized materials. In addition, nanoparticles enter the atmosphere as a byproduct of burning diesel fuel [2]. Moreover, the inhalation of nanoparticles, which are either independent therapeutic agents or carriers of certain drugs, is increasingly used in medical practice [3]. Therefore, wide spread occurrence of nanoparticles cause necessity in developing approaches to the integrated assessment of potential risks for organisms. Despite the rapid growing of publication in the field, one extremely important aspect of the problem of nanosafety associated with individual susceptibility to the action of the nanoparticles has yet to be uncovered. Primarily this refers to the genetically determined prevalence of Th1- or Th2-types of immune response, which affect the activity and reactivity of mucosal immunity [4].

## 2. Experimental

### 2.1. *Preparation of nanomaterial*

Tarkosil 25 (OOO NPF Quartz) is inorganic nanoparticles of silica dioxide with average particle sizes of 20-30 nm according to the manufacturer. It was used as a model nanomaterial. An investigation of an aqueous suspension of Tarkosil 25 showed that the aggregates ranging in size from 10 to 500 nm are formed during the usual mixing. Individual particles with sizes reaching 5 μm were also present in the preparation. Therefore, the suspension was treated using a CPX 130 ultrosonic disperser (Cole Parmer, USA). The first dispersion was performed in 2 h 12-14 h before use. Then, for 1 h prior to the administration of the suspension, it was redispersed again within 30 min. During such processing, a preparation with particles smaller than 100 nm was obtained.

### 2.2. *Animals*

The study was carried out in the CCU SPF-Vivarium at the Institute of Cytology and Genetics SB RAS using inbred BALB/c and C57Bl male mice of SPF-status aged 3-4 month, which are considered a prototypical Th2- and Th1-type mouse strains, respectively. They were kept in standard housing conditions in individually ventilated cages (IVC, Tecniplast, Italy) supplied with filtered air and access to water and food pellets *ad libitum*. Mice were kept on a 12 h day/night cycle, humidity was maintained at 40-50 % and the temperature was 22-24˚C.

### *2.3. Experimental design*

In the first experiment to study acute immune reaction to nanoparticles male mice of the both strains were treated with intranasal application of 25 ml of suspensions containing either nonosized

(nanoT) or microsized (microT) Tarkosil 25 particles (in concentration 2 μg/ml both) or saline, as a control. Four hours later mice were sacrificed and blood and bronchoalveolar lavage (BAL) were collected.

In the second experiment to study effects of chronic exposition we used nanoaerosol inhalation as a more natural way which nanoparticles penetrates organism. Aerosol generation and inhalation were performed using installation constructed in our laboratory. The aerosol for inhalation had a count median diameter of about 100 nm and a mean number concentration of $1{,}8\times10^5$ nanoparticles/$cm^3$. Male mice of both strains were exposed 10 times for 3 h to aerosol containing Tarkosil 25 nanoparticles. As a control we used distilled water. Next day after the last inhalation mice were sacrificed and blood, BAL and olfactory bulb, kidney, liver, heart, spleen and testicles were collected.

## 3. Results

A single intranasal application of Tarkosil 25 suspensions shows that only nonosized particles result in significant immune reaction. Thus, in BALB/c mice leukocyte and platelet number in BAL significantly increased after application of nanoT. Whereas in C57Bl mice nanoT resulted in increased number of leukocytes in blood. Such effects were not shown for microT. Neither nanoT nor microT have any influence on protein concentration or peroxidase activity in BAL of the both mouse strains. Effects of nanoT were accompanied by elevation of plasma corticosterone, which indicate stress-reaction developing.

Analysis of content of Si in tissues shows that 30 h Tarkosil 25 nanoaerosol inhalation result in 3.5-fold increasing of its concentration in olfactory bulb and only 1.4-fold in the other organs. Chronic inhalation of nanoparticles invoked leukocyte influx in lung of mice regardless of strain but not affected on BAL protein concentration and peroxidase activity. In relation to blood parameter there were no any significant effects of treatment or interstrain differences.

## 4. Discussion

A comparison of the immune response to the intranasal application of nanoT and microT showed that only a suspension containing nanoparticles of Tarkosil 25 causes a significant increase in BAL cells in BALB/c mice and leukocytes in blood in C57Bl mice. Thus, animals, which characterized by a predominance of the Th2 and Th1 immune response, shows different patterns of reacting. As regards endocrine response nanoparticles cause stress-reaction in mice irrespective genetic background.

A chronic effect of nanoparticles inhalation shows significant accumulation of Si in olfactory bulb and slight activation of mucosal immunity in mice of the both genotypes.

## 5. Acknowledgements:

Study was supported by the Interdisciplinary integration research grants from the Siberian Branch of the Russian Academy of Sciences (grants no. 57, 60, 61, 108 and 122) and by grant of Russian Foundation for Basic Research (grant no. 11-04-00414-a).

## 6. References

[1]. M. Geiser, W. Kreyling, *Part. Fibre Toxicol*. **7** (2010), 1.
[2]. T.W. Hesterberg, C.M. Long, C.A. Lapin et al., *Inhalation Toxicol*., **22** (2010), 679.
[3]. I. Roy, N. Vij, *Nanomedicine*, **6** (2010), 237.
[4]. H. Watanabe, K. Numata, T. Ito et al., *Shock*, **22** (2004), 460.

# MWCNT exposure assessment in occupational settings

T.O. Khaliullin[*,1], R.R. Zalyalov[1], A.A. Shvedova[2] E.M. Birch[3], L.M. Fatkhutdinova[1]

[1] *Kazan State Medical University, department of hygiene, occupational medicine, 49 Butlerova str., Kazan, Russia 420012*

[2] *National Institute for Occupational Safety and Health, Health Effects Laboratory Division, Pathology and Physiology Research Branch, 1095 Willowdale road, Morgantown, WV 26505, USA)*

[3] *National Institute for Occupational Safety and Health, Division of Applied Research and Technology, 4676 Columbia Parkway, Cincinnati, OH 45226, USA*

(*) corresponding author: khaliullin.40k@gmail.com

*Keywords: carbon nanotubes, exposure assessment, elemental carbon, TEM*

## 1. Introduction

Multi-walled carbon nanotubes (MWCNTs) production steadily increases all around the world. Unique properties of these nanoparticles are in demand by construction, mechanical engineering, energy-producing industry, medicine etc. [1] However, recently accumulated data suggest that there is a risk to human health upon the occupational contact with carbon nanotubes [2, 3]. The aim of this study was to evaluate the real occupational exposure to MWCNT at the Russian producing facility.

## 2. Experimental

### *2.1. MWCNT production facility*

MWCNTs are produced using the catalytic vapor deposition method [4]. The technological process includes synthesis in reactor, raw product harvesting, optional grinding/disintegration and functionalization or acid treatment.

### *2.2. Sampling*

Sampling was performed during the main operations (harvesting, disintegration, packaging, laboratory handling) throughout the whole technological process using conventional area and individual samplers. For EC analysis air samples were gathered on ultraclean 25 mm quartz filters (Pallflex Tissuquartz®). For TEM characterization mixed cellulose ester (MCE) filters (SKC inc.) were used. Sampling was conducted in workers' breathing zone with and without cyclone. Blank samples were acquired from "clean" rooms as well.

### *2.3. Elemental Carbon analysis*

Elemental carbon analysis was performed using modified NIOSH 5040 method for diesel particulate matter [5].

### *2.4. TEM analysis*

TEM analysis was performed using modified NMAM 7402 method [5] on JEOL 2100F transmission electron microscope. Elemental spectra were obtained using energy dispersive x-ray analysis (EDXA).

## 3. Results

### *3.1. MWCNT concentrations.*

The highest MWCNT aerosol short-term concentration was registered during the reactor cleanout process, reaching 157 ug/m3. Time-weighted average (TWA) concentration was respectively 29,6 ug/m$^3$ for the 8-hours shift.

Respirable fraction TWA concentrations (obtained using the cyclone) for EC at different workstations ranged from 0,53 to 6,11 ug/m$^3$.

### *3.2. TEM data*

TEM microphotographs has showed the presence of MWCNT-containing agglomerates at all technological process stages. The agglomerates consisted either of interspersed carbon nanotubes and matrix (see Fig.1) or MWCNTs only (Fig.2). Agglomerates size ranged from 1 to 10 um, and no individual MWCNTs were found. Cobalt and nickel used as catalysts were found in agglomerates using EDXA analysis

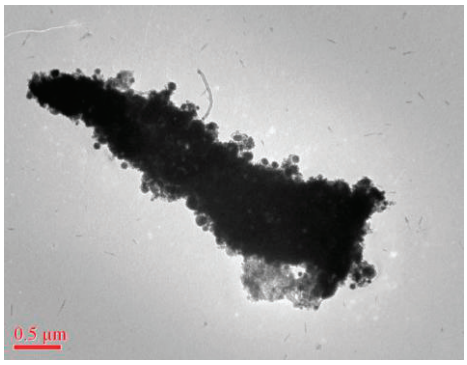

Figure 1 MWCNT agglomerate, product harvesting stage

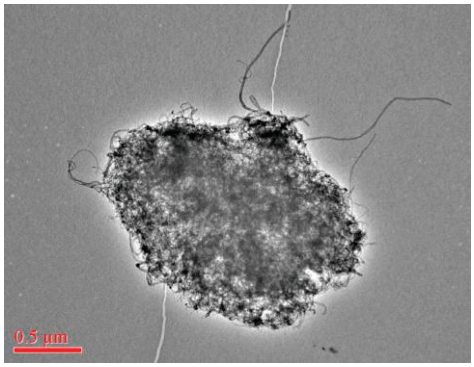

Figure 2 MWCNT agglomerate, product disintegration stage

## 4. Discussion

### *4.1. Exposure assessment*

Our data show that workers are clearly at risk of exposure to MWCNT aerosol at their workplaces. The highest EC values were found in samples obtained during reactor cleanout and harvesting, whereas laboratory handling produced the least MWCNT aerosol mass concentration values.

With no relevant occupational exposure limit currently set in Russia we have compared the maximum 8-hr TWA concentrations with NIOSH recommended exposure level (REL) – 1 ug/m$^3$. Based on latest investigations [6, 7], 10% risk of minimal adverse lung effects development is associated with 0,5 to 4 ug/m$^3$ working lifetime 8-hr TWA concentration.

The 6,11 ug/m$^3$ EC 8-hr TWA mass concentration value measured during product harvesting shows that exposure controls implementation is indeed required to lower the risk of adverse health effects in workers. Previously traditional exposure control measures such as local exhaust ventilation and PPE were found to be quite effective [8].

### *4.2. Future directions.*

Repeated exposure assessment is required after exposure controls installation. Direct-measuring online particle counters should be also used for number concentrations mapping and identification of critical exposure points.

## 5. References

[1]. Lux Research. The Nanotech Report. 5th ed. New York, NY: *Lux Research*; 2007.

[2]. Morimoto Y, Horie M, Kobayashi N, Shinohara N, Shimada M. Inhalation Toxicity Assessment of Carbon-Based Nanoparticles. *Acc Chem Res.* 2012 May 11.

[3]. Kim J.S., Song K.S., Lee J.K. et al. Toxicogenomic comparison of multi-wall carbon nanotubes (MWCNTs) and asbestos. // *Arch Toxicol*. 2012 Apr. №86(4). PP.553-62.

[4]. Cassell, A.M.; Raymakers, J.A.; Kong, J.; Dai, H.J., Large scale CVD synthesis of single walled carbon nanotubes. *J Phys Chem B*, 1999, 103,

[5]. NIOSH Current intelligence bulletin 65: Occupational exposure to carbon nanotubes and nanofibers. [Электронный ресурс] URL:http://www.cdc.gov/niosh/docs/2013-145/

[6] Ma-Hock L, Treumann S, Strauss V, Brill S, Luizi F, Mertler M, Wiench K, Gamer AO, van Ravenzwaay B, Landsiedel R. Inhalation toxicity of multiwall carbon nanotubes in rats exposed for 3 months. *Toxicol Sci.* 2009 Dec;112(2):468-81.

[7] Pauluhn J. Subchronic 13-week inhalation exposure of rats to multiwalled carbon nanotubes: Toxic effects are determined by density of agglomerate structures, not fibrillar structures. *Toxicol Sci.* 2010 113(1):226–242.

[8] Methner MM. Engineering case reports. Effectiveness of local exhaust ventilation (LEV) in controlling engineered nanomaterial emissions during reactor cleanout operations. *J Occup Environ Hyg*. 2008 Jun;5(6):D63-9.

# Investigation of dehydrated, oxide and hydrated phases derived from Mg-Al and Mg-Ga hydrotalcites by different X-ray diffraction approaches

Leontyeva N.N. [1*], Cherepanova S.V.[2], Drozdov V.A.[1], Belskaya O.B.[1], Talsi V.P.[1]

[1] *Institute of Hydrocarbons Processing SB RAS, Omsk, Neftezavodskaya, 54*
[2] *Boreskov Institute of Catalysis SB RAS, Novosibirsk, Lavrentiev avenue, 5*

(*) corresponding author: n_n_leonteva@list.ru

*Keywords: hydrotalcite, layered defect spinel, x-ray diffraction, interstratified phase, Rietveld refinement*

## 1. Introduction

During last decades the attention of scientists is devoted to Layered Double Hydroxides (LDHs) also well known as the anionic clays or hydrotalcites. This fact is connected with unique properties of their oxides prepared by calcination in temperature range of 450-700 °C. The most important property of oxides is the «memory effect» that is the capability of some cationic compositions to restore the layered structure from oxides in contact with water. This property opens a wide range of LDH applications, such as anion exchangers [1], adsorbents, nanocomposites, functional materials for different purposes [2], including catalysts synthesis [3, 4]. In the common case, LDHs may be described by $\left[M^{2+}_{1-x}M^{3+}_{x}\ OH\ _2\right]^{x+}\left[A^{n-}\right]_{x/n}\cdot yH_2O$, where $M^{2+}$ and $M^{3+}$ are the bi- and tri-valent metal cations, $A^{n-}$ - is interlayer anion. To date the crystal structure of many hydrotalcites with different cationic and anionic compositions [5] as well as their thermal decomposition process were investigated. However, there are some opposite opinions that requires a detailed study. So the structure of Mg-Al and Mg-Ga dehydrated phase arised at 200 °C is not clear. Furthermore, the phase composition and structure of the mixed oxides derived from the hydrotalcites at 550-600 °C are the matter of discussions. Also there is no information about influence of Mg:Al and Mg:Ga ratio on the products of hydration of the mixed oxides in water.

## 2. Experimental

X-ray diffraction (XRD) was the main method of investigation. Diffraction patterns were recordered on a X-ray diffractometer D8 Advance (Bruker) in monochromatic Cu-$K_\alpha$ radiation. The Rietveld refinement was made with using TOPAS 3.0 software (Bruker). Simulation of XRD patterns for the one-dimensionally (1D) disordered crystals was made with using DIFFaX program [6]. The additional methods confirmed suggested models were HRTEM, $^{27}$Al NMR, $^{71}$Ga NMR.

## 3. Results and discussion

It was shown that the removal of water molecules from the interlayers of Mg-Al and Mg-Ga hydrotalcites at 200-350 °C leads to the transformation of initial 3-layer polytype $3R_1$ (AC=CB=BA=AC…) that leads to the shift of 003 and 006 peaks towards the higher angles as well as to the change of the intensity ratio of these peaks (Fig.1). Also there is the intensity redistribution of other peaks.

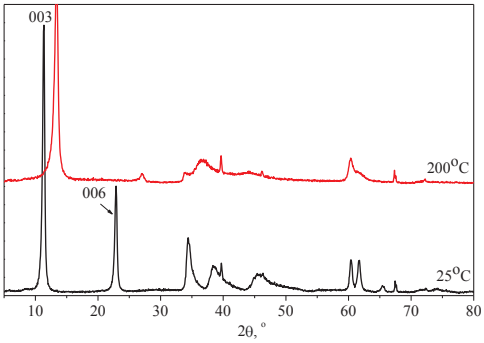


Fig.1. Polytypic transformation of Mg-Al hydrotalcite at 200 °C.

Simulation of the XRD patterns on the base of the model of the 1D disordered crystal showed that structure of Mg-Al and Mg-Ga dehydrated phases is similar: all possible sequences AC-CB-BA, AC-BA-CB and AC-AC-AC are present with equal probabilities and there is some part of turbostratic disorder.

It is interesting that stability of the mixed dehydrated phases is different. Cooling from 200 $^{o}$C to room temperature remains Mg-Ga phase without changes, but Mg-Al one catches water from air and fully recovers the initial hydrotalcite structure.

Calcination at 600 $^{o}$C leads to the formation of Mg-Al and Mg-Ga oxides. Some authors suppose that oxide's structure is close to the MgO (periclase) structure (space group Fm3m). But the Rietveld refinement does not give any satisfactory results in this assumption because of failing of additional peak at 2θ=35.5$^{o}$ presented on the experimental XRD pattern.

The better correspondence in the frame of Rietveld analysis (Fig.2,3) is achieved by the considering the oxides in Fd3m space group intrinsic to spinel-type structure. But in Mg-Al and Mg-Ga oxides along with total filling of 16d sites (as in spinel) another set of octahedral holes (16c) is partially occupied. Spinel tetrahedral positions (8a) are occupied only in part. Such preferable occupation of octahedral positions in mixed oxides can be explained by the structure of the precursor (hydrotalcite) where cations occupy only octahedral sites.

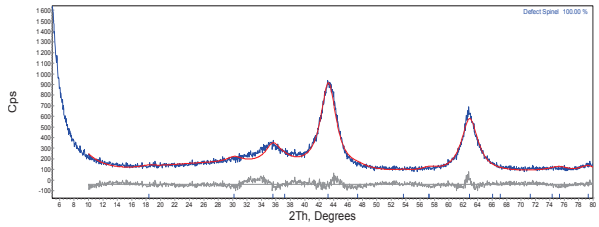


Fig.2 Rietveld analysis of Mg-Al oxide (S.G. Fd3m)

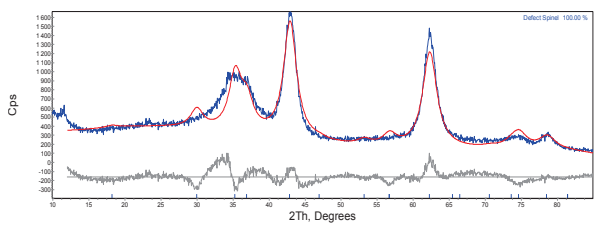


Fig.3 Rietveld analysis of Mg-Ga oxide (S.G. Fd3m)

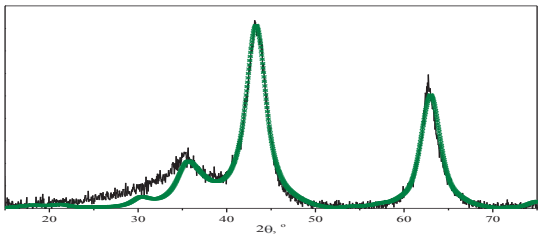


Fig.4 Simulation of the X-ray diffraction pattern for Mg-Al oxide on the base of a defective layered spinel

So it is clear that oxide's structure is some intermediate state between spinel structure and periclase one where all octahedra are occupied. We assumed that oxides inherit the layered structure of hydrotalcites and considered model of so called defective layered spinel consisted of the octahedral (periclase-like) and mixed octahedral-terahedral (spinel-like) layers. Such a model shows the best correspondence (Fig.4) and can explain «memory effect».

It was shown that during hydration the full reconstruction of layered structure of Mg-Al and Mg-Ga hydrotalcites takes place only at high content of trivalent cations (x=0.33). Decrease in Al (Ga) leads to the some loss of trivalent cations and Mg enrichment probably on the calcination stage. It doesn't prevent from formation of layered structure but along with mixed hydrotalcite layers the pure $Mg(OH)_2$ ones are also present. Both types of layers coexist inside of the interstratified phase that was confirmed by the simulation of the XRD partterns.

This work was supported by RFBR grant № 12-03-90812-mol_rf_nr.

## References

[1] F. L. Theiss, S.J.P., G.A. Ayoko, R.L.Frost, Journal of Thermal Analysis and Calorimetry. **107** (2012) 1123.

[2] Li F., D.X., In X. Duan, in *Structure and bonding*, D.G. Evans, Editor, Sringer, NY, USA.(2006) 193.

[3] Palomares, A.E., A. Uzcátegui, and A. Corma, Catalysis Today. **137** (2008) 261.

[4] Sychev, M., et al., Applied Clay Science. **18** (2001) 103.

[5] D. G. Evance, R.T.S., Springer-Verlag Heidelberg: Berlin, Germany. (2006) 87.

[6] Treacy, M.M.J., J.M. Newsam, M.W. Deem, Proceedings of the Royal Society of London. Series A: Mathem. Phys. Sciences. **433** (1991) 499

# The pathway to the self-supported mesoporous mesophase materials

E.A. Mel'gunova*, M.S. Mel'gunov

*Boreskov Institute of Catalysis SB RAS, pr.Akad. Lavrentieva, 5, Novosibirsk, 630090*

(*) corresponding author: melena@catalysis.ru

*Keywords: Mesoporous mesophase materials, MCM-41, SBA-15, self-supported, shaping, nanomaterials, texture*

## 1. Introduction

Since their discovery the mesoporous mesophase materials (MMMs) type of MCM-41, SBA-15, etc. are considered as promising adsorbents and catalysts, materials for medical, optical, and electronics applications. However, to transform from promising to real, the material should fulfill several requirements, one of which is preparation in a shaped form. Usually, MMMs are prepared in a form of powder. Special procedures basing on evaporation induced self-assembly (EISA) technique are elaborated to prepare thin (50 – 500 nm) films over flat solid supports. As well, known are the ways to prepare macroscopically homogeneous monoliths through EISA or sol-gel approach at the presence of macropore forming agents such as polyethylene glycol. But, EISA monoliths have usually low degree of ordering, crack easily during drying and calcination. Sol-gel approach assumes pseudomorphic transformation of a xerogel macroporous monolith into a MMM one, which usually proceeds with conversion significantly below 100%. Shaping of MMMs with mineral binders that are traditional for catalysts is not suitable, because of low apparent density of MMMs. To prepare self-standing SBA-15 containing monolith one should add a binder, which mass usually significantly exceeds the mass of the mesophase. Thus, elaboration of principle for MMMs shaping is still an unresolved task.

In our work we propose a pathway to shaped MMMs through utilization of organic glues that can simultaneously be binding, plasticization and, macropore forming agents. The key idea of the process is utilization of thermally shrinking glues, which attract MMM microparticles one to another and enforce their bonding during drying (glue polymerization) and calcination.

## 2. Experimental

### *2.1. MMM powders preparation*

Aerosil A-300 was used as silica source. It was dissolved in 1M NaOH solution. The Si/Na ratio in final silica source solution was 1. Other chemicals were used as-received.

Silica source was added to the surfactant solution under vigorous stirring. Table 1 shows mixtures mass composition before aging.

Table 1. Synthetic mixture compositions.

| Sam-ple | Surfac-tant | $Na_2Si_2O_5$ | Water | HCl |
|---|---|---|---|---|
| 1 | CTAB 15,0 | 10 | 200 | 150 |
| 2-4* | P 123 25,0 | 10 | 200 | 150 |

* 40 g of mesethylene as swelling agent was added to the synthetic mixture for sample 4.

After preparation the mixtures were aged during 72h at 25 °C (Samples 1 and 2), and 90 °C (Samples 3 and 4) to form pores of different diameters. Than the precipitates were filtered and dried during 12h at 100 °C.

### *2.2. Shaping procedure*

The prepared dry powders were mixed with an organic glue in a proportion suitable for extrusion through the 2 mm round hole of a syringe. The resulting cylinders were left to polymerization for 24 h and than heated under atmospheric conditions to 650°C with the ramp of 1 °C/min.

### *2.3. Characterization*

The prepared shaped MMMs were characterized by means of nitrogen adsorption at 77 K measured on ASAP-2400 (Micromeritics) setup. The samples were degassed under vacuum for 14h at 200 °C before the measurements. Surface area was calculated according to BET procedure, pore volume-size distributions (PVSDs) were calculated in BJH model of cylindrical pores. The mean mesopore size was calculated as a first moment (mathematical expectation) of PVSD.

## 3. Results and discussion

Figure 1 shows shaped SBA-15 rods (sample 4) after calcination. Due to burning off of all organic binder the rods consist only of SBA-15 phase. Their characteristic diameter decreased from 2 mm before calcination to 1,5 mm. After calcination the materials easily withstand washing with water and dilute acids followed by successive calcination. The approximate strength of the rods is 3 MPa, which allows their utilization in fixed bed adsorbers and reactors. Unfortunately, the attrition strength of the rods is low.

Fig. 1. Shaped SBA-15 cylinders after calcination.

$N_2$ adsorption isotherm for sample 3 and corresponding PVSDs calculated for adsorption and desorption branches of the isotherm are shown in Fig.2. One can observe typical for mesoporous mesophases sharp step on both branches of the isotherm that indicates presence of uniform mesopores, which overcame the shaping procedure.

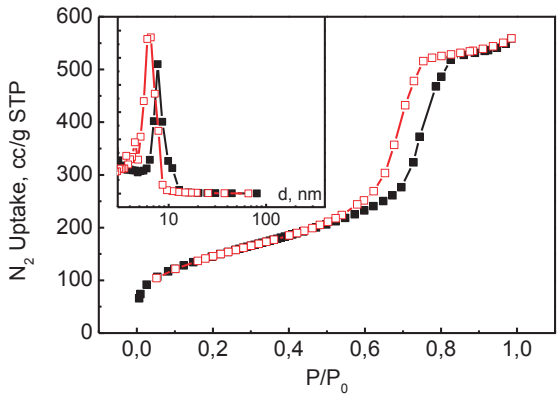


Fig. 2. $N_2$ adsorption isotherm for sample 4 and corresponding PVSDs calculated for adsorption and desorption branches in BJH model.

Textural characteristics for shaped samples 1-4 are shown in Table 2.

Table 2. Textural characteristics for the shaped mesoporous mesophase materials.

| Sample | $A_{BET}$, $m^2/g$ | $V_{pore}$, $cm^3/g$ | $d^*_{pore}$, nm | $h_{wall}$, nm |
|---|---|---|---|---|
| 1 | 883 | 1,09 | 2,02 | 1,0 |
| 2 | 491 | 0,37 | 4,85 | 1,9 |
| 3 | 524 | 0,79 | 6,83 | 1,7 |
| 4 | 387 | 1,30 | 22,4 | 2,3 |

* from adsorption pore volume-size distributions.

One can observe that according to the proposed procedure the shaped mesoporous mesophase materials can be prepared with various pore sizes. As well the thickness of walls between mesopores can be estimated ($h_{wall}$ in Table 2). These values are typical to hydrothermally stable mesophases of corresponding type.

## 4. Conclusion

The idea of application of an organic glue as binding agent to prepare self-supported shaped mesoporous mesophase materials is shown to be prospective. The resulting shaped materials can be used as adsorbents or catalysts supports in traditional fixed bed processes.

## 5. Acknowledgements

The work was supported by Russian Academy of Sciences Presidium grant # 43.

# Synthesis and stabilization of nanosized silicon dioxide

S. Lazareva[1*], Z. Ismagilov[1,2], L. Simonova, A. Ishchenko

[1] *Boreskov Institute of Catalysis SB RAS, Prosp. Akademika Lavrentieva 5, Novosibirsk 630090, Russia*
[2] *Institute of Coal Chemistry and Material Science, SB RAS, Prosp. Sovetsky 18, Kemerovo 650000, Russia*

(*) corresponding author: @E-mail address: ksv@catalysis.ru

*Keywords: $SiO_2$ nanoparticles, hydrolysis, tetraethyl orthosilicate*

## 1. Introduction

Silica nanoparticles (colloidal silica, silica gels, pyrogenic silica, and precipitated silica) are used in production of electronic substrates, thin film substrates, electrical insulators, thermal insulators, humidity sensors, organic catalysts [1-3].

In our work for preparation of aqueous dispersions of silica particles having size ranging from 20 to 150 nm we used the Stober process- hydrolysis and condensation of tetraethyl orthosilicate (TEOS) [4]. The variation of the reaction temperature and reagents ratio were needed to produce dispersions with the different size of particles.

## 2. Experimental

### *2.1. Preparation of sols*

High purity reagents were used for the synthesis. Distilled water was deionized just prior to use.

Silica nanoparticles were prepared by hydrolysis and condensation of TEOS in ethanol in presence of ammonia as catalyst. The solution containing appropriate amounts of ethanol, ammonia and deionized water were stirred and heated to 50-70$^o$C. Then a proper amount of TEOS in ethanol was added to the above solution and the reaction conducted at 50-70$^o$C. Thereafter the colloidal solution was concentrated by evaporation at 80-85$^o$C.

Table 1. Chemical compositions of reaction systems used in this work.

| Sample | T, $^o$C | TEOS, mol | $H_2O$, mol | Ethanol | $NH_3$ |
|---|---|---|---|---|---|
| **1** | 50 | 1 | 21 | 20 | 1.5 |
| **2** | 70 | 1 | 21 | 20 | 1.5 |
| **3** | 70 | 1 | 21.6 | 57 | 2 |
| **4** | 70 | 1 | 4.8 | 33 | 0.2 |

The chemical compositions of the reaction systems (samples 1-4) and reaction temperatures are presented in table 1.

### *2.2. Characterisation techniques*

HR-TEM analysis of silica particles were carried out using JEM – 2010 (JEOL) electron microscope. Samples were supported by ultrasonic disperser on holey carbon films on a copper grid and placed into the microscope chamber.

The IR spectra were recorded by FT-IR spectrometer BOMEM MB102 in the region of 200 – 4000 cm$^{-1}$. The samples were deposited to the optical glasses.

## 3. Results and discussion

### *3.1. Effect of temperature on silica sols properties*

Experiments were carried with the same molar ratio of the reagents (TEOS : $H_2O$ : ethanol : $NH_3$ = 1 : 21 : 20 : 1.5) at 30, 50 and 70$^o$C. The silica sols prepared at 30$^o$C are not stable – $SiO_2$ particles form precipitates in 12 hours after reaction. The silica sols prepared at 50$^o$C and higher demonstrated stability for several months. Figures 1 and 2 show that the increase of reaction temperature results in the decrease of particle size. The size of particles prepared at 50$^o$C (table 1, sample 1) is 100-150 nm (Fig. 1, a).

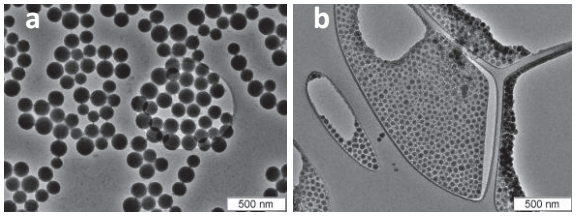


Figure 1. TEM images of $SiO_2$ nanoparticles prepared at 50$^o$C (a) and 70$^o$C (b).

The increase of reaction temperature to 70°C at the same molar ratio of the reagents (table 1, sample 2) results in the decreases of particle size to 40-60 nm (Fig. 1, b). It is associated with the hydrolysis reaction rate, which was observed to decrease significantly at lower temperatures [5].

Futher experiments were carried at 70-75°C varying the ratio of the reagents.

### *3.2. Effect of reagents ratio on size of particles*

In order to obtain smaller particles the amount of the ethanol was increased (table 1, sample 3). In this way $SiO_2$ concentration was decreased and particles with size 25-30 nm were obtained (Fig. 2, a).

The smallest particles were obtained with decrease of water and ammonia concentrations (table 1, sample 4). The TEM image of these particles with size 20 nm are presented in Fig. 2, b.

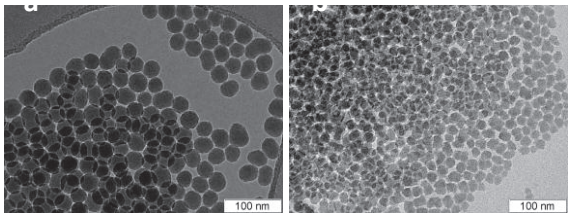


Figure 2. TEM images of $SiO_2$ nanoparticles: sample 3 (2a) and sample 4 (2b).

Thus, particle size of silica depends on the amount of the water and ammonia used in reaction.

### *3.3. FT-IR study*

Figure 3 shows the spectra of TEOS and silica sol, prepared at 50°C (table 1, sample 1). The peaks at 460, 794, 956 $cm^{-1}$ and peaks in the region of 1100-1200 $cm^{-1}$ can be attributed to Si-OH or Si-O-Si [6] The peaks at 2899 and 2983 $cm^{-1}$ can be attributed to the unhydrolysed TEOS, because they correspond to symmetrical C-H stretching vibration and asymmetrical C-H stretching vibration in $CH_3$ respectively. The presence of unreacted TEOS in silica sol can leed to deterioration of its properties (stability, uniformity) and quality. Therefore necessary to achieve a fully completed hydrolysis by varying reaction conditions such as increase of aging time.

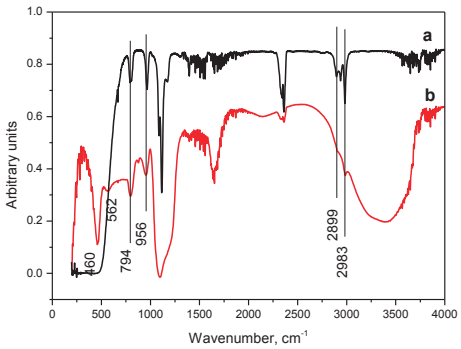


Figure 3. IR spectra of TEOS (a) and silica sol (b).

### *3.4. Stabilization of silica sols*

It was shown that the most stable silica sols have pH 7-9. In the our synthesis process the pH is maintained in the range of 8-10. Below pH 7 the silica sols fall into the fast flowing gel formation process, in highly alkaline medium the rate of depolymerization increases [7]. Since the high temperature of the reaction enhances rapid volatilization of ammonia, the pH is controlled by continuous addition of an aqueous ammonia solution.

## 4. Conclusions

$SiO_2$ nanoparticles were prepared from the hydrolysis and condensation of TEOS. The properties of $SiO_2$ nanoparticles were controlled by varying the reaction temperature and molar ratio TEOS : $H_2O$ : ethanol : $NH_3$. It was shown that the size of $SiO_2$ particles decreases with increase of the reaction temperature and decrease of amount of water and ammonia used. The most important result demonstrated by this study is possibility to synthesize the stable silica sols with narrow distribution of the particle size in the range of 20 to 150 nm.

## 5. References

[1]. R.K. Iler, The Chemistry of Silica, Wiley, New York, 2-nd edition, 1979.
[2] S. Sadasivan, D.H. Rasmussen, F.P. Chen, R.K. Kannabrian, *Coll. Surf., A,* 132 (1998) 45-52.
[3] I. Ab Rahman, V. Padavettan, *J. Nanomater.,* vol. 2012, Article ID 132424, 15 pages.
[4] W. Stober, A. Fink, E. Bohn, *J. Coll. Inter. Sci.,* 26 (1968) 62-69.
[5] C.G. Tan, B.D. Bowen, N. Epstein, *J. Coll. Inter. Sci.,* 118 (1987) 290-293.
[6] P.Y. Chu, D.E. Clarck, *Spectr. Lett.,* 25 (1992) 201-220.
[7] N.A. Shabanova, P.D. Sarkisov. The Fundamentals of sol-gel technology of nanodispersed silica. Moscow. 2004.

# The modified carbon-mineral sorbent for platinum (IV) selective sorption

T. Didenko, L. Adeeva*

*Omsk State University n.a. F.M. Dostoevsky, Chemical Department, Mira avenue, 55A*

kovalenko_85@list.ru

*Keywords: carbon-mineral sorbent, modification, platinum (IV)*

## 1. Introduction

The direction on synthesis and modification of sorbents for sewage treatment and water conditioning in recent years develops by Chair of inorganic chemistry of Omsk State University. Raw materials for sorbents is sapropel. It is renewed widespread raw materials. As a result of the carried-out work, a number of sorbents is developed for the solution of problems of water treatment. Also the sorbents are developed for selective extraction of valuable elements, for example, platinum metals, from the spent technological solutions.

## 2. Experimental

We developed carbon-mineral material with meso-macro-porous structure [1–3] therefore is promising for modification. High mechanical strength of this material predetermines its use as the carrier for receiving other sorbents. The surface of the carbon-mineral material is modified by polyaniline [4]. Polyaniline is transferred to an emeraldin-basis form by processing of 0.2 M by solution of ammonia. On a surface of the sorbent there are secondary amino groups that gives to the modified sorbent anion-exchange properties. The optimal quantity of polyaniline on a sorbent is equal 10-15%.

Sorption of platinum (IV) carried out in static conditions at a temperature 298 K from model solutions with concentration 0.08-1.0 mg $ml^{-1}$, volume of solution of 10.0 ml. The mass of a sorbent made 0.100±0.002 g.

Solutions after sorption separated centrifugation and defined the content of platinum. The content of platinum in solution determined by a spectrophotometric method with tin chloride.

Desorption of Pt (IV) carried out hydrochloric acid and muriatic solution of thiourea (100 mg $ml^{-1}$ of thiourea and 5 mg $ml^{-1}$ of HCl) at temperatures of 298 and 333 K. Duration of desorption made 24 h.

## 3. Results

Influence of amount of the deposit polyaniline being in a form of the emeraldin-basis, on the size of sorption of platinum (IV) is investigated (tab. 1). Sample of sorbent was contacted for 24 hours with solution of platinum (IV) with concentration 1.0 mg $ml^{-1}$ and pH 0.6. Experimental results are presented in tab. 1.

Table 1. Value of platinum sorption depending on contents of deposit polyaniline

| Contents polyaniline, % | Value of sorption, mg $g^{-1}$ |
|---|---|
| 1 | 4.25 ± 0.4 |
| 5 | 13.9 ± 0.1 |
| 10 | 42.6 ± 0.3 |
| 15 | 62.1 ± 0.3 |

Dependence platinum extraction by the modified sorbent from duration of phases contact shows that the maximum value of sorption is reached in 3 hours, and time of semi-sorption makes 20 min.

Studying of dependence of platinum (IV) sorption from solution acidity was carried out on a sorbent containing 15% of the modifier, at duration of contact of phases 3 hours. It is shown that the maximum value of sorption are reached at pH 0-1.0 (tab. 2).

We received an isotherm of sorption of platinum (IV) on the modified sorbent with the maintenance of the modifier of 15% at pH 0, duration of contact of phases 3 hours. Experimental data are well described

by Lengmyur's equation. The calculated sorption capacity on platinum (IV) makes 62 mg $g^{-1}$.

Table 2. Dependence of platinum sorption size from pH

| pH | C eq, mg $ml^{-1}$ | Value of sorption, mg $g^{-1}$ |
|---|---|---|
| 0 | 0.48 | 62.3 ± 0.5 |
| 1 | 0.51 | 59.9 ± 0.2 |
| 3 | 0.78 | 33.3 ± 0.2 |
| 5 | 0.80 | 30.7 ± 0.4 |
| 7 | 0.84 | 27.3 ± 0.2 |

Weak technological solutions in practice contain a large number of foreign ions. Therefore we made experiments on studying of influence of several ions on sorption platinum efficiency. Solutions contained 1 mg $ml^{-1}$ of platinum and 10 mg $ml^{-1}$ of an ion of interfering metal. Data are provided in tab. 3.

Table 3. Value of platinum (IV) sorption in the presence of interfering ions on the modified sorbent (content of polyaniline of 10%)

| Interfering ion | Value of sorption, mg $g^{-1}$ | |
|---|---|---|
| | on interfering ion | on platinum |
| be absent | be absent | 42.2±0.2 |
| $Cu^{2+}$ | not sorb | 41.2±0.2 |
| $Ni^{2+}$ | not sorb | 42.3±0.2 |
| $Fe^{3+}$ | not sorb | 42.3±0.2 |

From tab. 3 follows that ions of copper (II), nickel (II), iron (III) on the modified sorbent aren't occluded, and sorption value of platinum (IV), in the presence of these ions, makes 42 mg $g^{-1}$, that is doesn't decrease.

For practical use clarification of possibility of a desorption of metal from a surface of the modified sorbent is important. Desorption is carried out with 2 M HCl solution and muriatic solution thiourea (100 mg $ml^{-1}$ thiourea and 5 mg $ml^{-1}$ of HCl) in a static mode at 298 and 333 K. The smallest degree of a desorption is observed when using 2 M of HCl that indirectly confirms that sorption of Pt (IV) has no ion-exchange character.

At a desorption muriatic solution thiourea at a temperature of 298 K for two cycles degree of a desorption made 45%. Big efficiency of a desorption is observed when using muriatic solution thiourea at a temperature of 333 K, for two stages degree of a desorption made 80%. The regenerated sorbent was used repeatedly. The volume of platinum sorption is 56 mg $g^{-1}$ that makes 90% from initial capacity.

## 4. Discussion

With increase in percentage of the deposit polyaniline on a sorbent, sorption size on platinum (IV) increases. At the content of polyaniline of 15%, the size of sorption made 62.1±0.3 mg $g^{-1}$. The further increase in the content of polyaniline at surfaces of the modified sorbent has to be accompanied by increase of concentration of aniline in a reactionary mix at synthesis. However, in practice such increase of concentration of aniline leads to its fast polymerization in volume of solution, instead of on a sorbent surface.

Dependence of platinum from duration of phases contact allows to draw a conclusion that the received sorbent has good kinetic characteristics.

Platinum in solution at pH 0-1 is in a form $[PtCl_6]^{2-}$. It is known that increase pH value platinum (IV) changes a stay form in solution, than it is possible to explain decrease in size of sorption at increase pH.

It is shown the modified carbon-mineral sorbent selectively takes Pt (IV) from the solutions containing ions of Cu (II), Ni (II), Fe (III) in the concentration, platinum much exceeding concentration. The modified by polyaniline carbon-mineral sorbent in the form of the emeraldin-basis is perspective for extraction of platinum (IV) of difficult technological solutions.

## 5. Acknowledgment

Work is performed with financial support of the Ministry of education and science of RF within "Scientific and scientific and educational staff of innovative Russia" for 2009-2013. Agreement No. 14.B37.21.1197.

## 6. References

[1]. L. Adeeva, T. Kovalenko. Patent 2414430, RF. Published 20.03.2011. Bull. 8.

[2]. T. Kovalenko, L. Adeeva. *Chemistry for Sustainable Development*. **2** (2010). P. 189.

[3]. L. Adeeva, T. Kovalenko. *Journal of applied chemistry*. **4** (2012). P.535.

[4]. L. Adeeva, A. Fisuk, T. Kovalenko, A. Kostushenko. Patent application №2012115046. Filing date 16.04. 2012.

[5]. T. Kovalenko, L. Adeeva. *Butlerov communications*. **1** (2013). P. 104.

# Study of selectivity of the Suzuki-Miyaura reaction with aryl bromides using Pd on micro- and mesoporous activated carbons: evidences for nanocatalysis

A.A. Kurokhtina[1], E.V. Larina[1], A.F. Schmidt[1], M. Kozlowski[2]

[1] *Irkutsk State University, Chemical Department, Russia, 664003, Irkutsk, K.Marx st., 1*
[2]*Faculty of Chemistry, Adam Mickiewicz University, Grunwaldzka 6, 60-780 Poznan, Poland*

(*) corresponding author: kurokhtina@chem.isu.ru

*Keywords: Suzuki reaction, palladium, mechanism, heterogeneous catalysis, reaction selectivity*

## 1. Introduction

The palladium-catalyzed Suzuki-Miyaura reaction between arylboronic acids and aryl halides draws great attention of scientists. The key feature of the reaction is interconversion of different palladium forms (Pd complexes in solution, nanoparticles and bulk Pd) during the catalytic process. As a result the clarification of active catalyst origin is the very complicated issue [1]. The results of different tests performed to discriminate between homogeneous and heterogeneous mechanisms of catalysis are ambiguous on such situation. In our opinion the possible way to resolve the problem is the study of differential selectivity of the catalytic system instead of catalytic activity. As opposed to catalytic activity the differential selectivity of catalyst does not depend on its quantity and is determined by the nature of active species only. So a comparison of differential selectivities of the reactions using different conditions capable of change of either catalyst form state allows drawing a conclusion about its participation in catalysis.

## 2. Experimental

### *2.1. Catalysts preparation*

The catalyst supports were micro- (average pore diameter 1.96-1.99 nm) and mesoporous (average pore diameter 3.86-4.72 nm) activated carbons.

### *2.2. Preparation of microporous carbons*

Activated microporous carbon samples were prepared from plum stones. After preliminary mechanical treatment to the grain size of ≤0.4 mm, the material was subjected to chemical activation by solid KOH in Ar (sample marked as S(KOH)). Then the samples were subjected to modifications with concentrated $HNO_3$, $(NH_4)_2S_2O_8$ in 1 M $H_2SO_4$ (ammonium peroxydisulfate—APS) and air. Depending on the reagent, temperature and time of treatment the obtained samples were marked as S-$HNO_3$-60°C-8h, S-AIR-300°C-8h, S-APS-30°C-24h.

### *2.3. Preparation of mesoporous carbons*

Activated mesoporous carbons were prepared from oak wood. The raw material was subjected to impregnation with $CaCl_2$, carbonization and activation with $CO_2$ (marked as TD). Then TD samples were modified at different temperatures with $NH_3$. Depending of temperature of treatment the samples obtained were marked as TD-$NH_3$-750, TD-$NH_3$-850, TD-$NH_3$-950.

### *2.4. Preparation of Catalysts*

Pd/C (C is micro- and mesoporous carbon samples) was prepared by impregnation with $Pd(OAc)_2$ (4 wt%) with following reducing by formic acid to form nanoparticles. Resulting catalyst was filtered and washed with acetone. The catalysts were used after drying in vacuum.

### *2.5. Catalytic runs*

To study the influence of catalyst precursor nature on differential selectivity in Suzuki-Miyaura reaction with aryl bromides competitive experiments were carried out (Figure 1). $PhB(OH)_2$ (5 mmol), bromobenzene (S1), 4-bromoacetophenone (S2) and 1-bromo-4chlorobenzene (S3) (1.5 mmol of each), NaOAc (6.5 mmol) as base,

Pd/C (0.08 mmol of Pd, 1.6 mol.%), naphthalene (1 mmol) as internal standard for GC analysis were added to 5 ml of DMF in a glass reactor fitted with a magnetic stirring bar and septum inlet. The reactor was placed into a pre-heated oil bath (140ºC) and the reaction mixture was stirred. Small samples for GC were taken at different moments of the reaction.

## 3. Results

### *3.1. Selectivity of the Suzuki-Miyaura reaction using different catalyst precursors*

The rates of product formation in the competitive reactions were estimated using steady-state segments of kinetic curves and they were used for calculation of catalyst differential selectivity using standard equation:

$$S_{Si} = \frac{r_{Si}}{\sum r_{Si}}$$

where $r_{Si}$ is the rate of formation of products from the substrate $S_i$.

The obtained selectivity values are presented in Figure 2 and Figure 3.

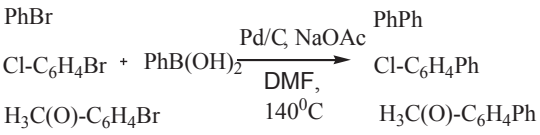


Figure 1. Competitive Suzuki-Miyaura reaction.

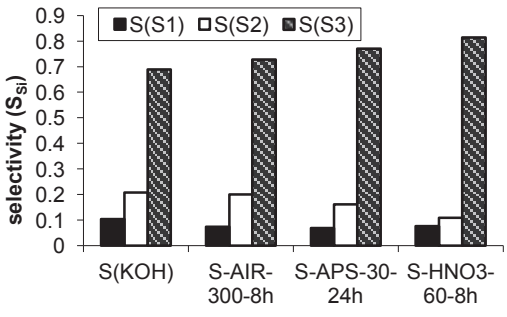


Figure 2. Differential selectivities ($S_{S1}$, $S_{S2}$ and $S_{S3}$) of palladium catalysts deposited on microporous activated carbons in competitive Suzuki-Miyaura reaction.

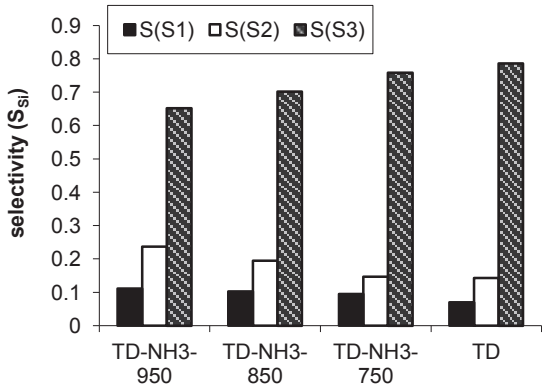


Figure 3. Differential selectivities ($S_{S1}$, $S_{S2}$ and $S_{S3}$) of palladium catalysts deposited on mesoporous activated carbons in competitive Suzuki-Miyaura reaction.

## 4. Discussion

In the case when catalysis is of heterogeneous character the catalyst precursor becomes one of the most apparent factors capable of influence on the nature of active catalyst formed in the system. It has been established that differential selectivities of formed *in situ* catalyst in the competitive reaction of three aryl bromides with phenylboronic acid using a set of heterogeneous precursors with different structure and chemical composition of support do not coincide (Figures 2, 3). It is in agreement with the exclusively heterogeneous catalysis on the surface of Pd nanoparticles located on the precursor support because of the properties of the support used were found to influence on selectivity value. This finding is validated by good correlation of selectivity value with the average diameter of pores of support in the catalyst samples having close chemical composition but different structure. In our opinion the latter can be considered as direct evidence for heterogeneous mechanism of Suzuki-Miyaura catalysis on the Pd nanoparticles located in activated carbon mesopores.

This work was supported by the Russian Foundation for Basic Research (No. 12-03-31166) and the Ministry of Education and Science of the Russian Federation (No. 14.B37.21.0795).

## 5. References

[1]. A.F. Schmidt, A.A. Kurokhtina, *Kinet. Catal*. **6** (2012) 714.

# Influence of silver nanoparticles on the conformational changes of cyanine dye thin films under laser irradiation

N. Toropov*, T. Vartanyan

*St. Petersburg National Research University of Information Technologies, Mechanics and Optics*
*Laboratory of Surface Photophysics, 49 Kronverkskiy pr., St. Petersburg, Russia, 197101*

(*) corresponding author: nikita.a.toropov@gmail.com

*Keywords: cyanine dyes, silver nanoparticles, conformational changes, laser irradiation*

## 1. Introduction

The metallic NPs have unique properties in the visible range of spectrum due to collective electronic excitation. Localized surface plasmon resonances in Ag nanoparticles (NPs) are an attractive object for investigations. They are employed for SERS, enhancement of absorption and fluorescence of organic molecules [1, 2], as well as in many other existing and emerging areas. Bright optical properties of NPs form the basis of many applications, such as optical switching devices, chemical sensors, optical memory devices, spasers [3], photodetectors etc.

At this work we proposed and demonstrated the new phenomena of the influence of localized surface plasmon resonances of Ag NPs on photoinduced rearrangements of the cyanine dye molecular layers. Absorption spectrum of cyanine dyes spread over the solid surface is more broadened than the absorption spectrum of cyanine dyes in solution. This broadening of the spectrum is due to the formation of a larger number of isomers and aggregates, which can form due to interaction of molecules with the surface and each other. The laser irradiation of molecular layers leads to transformations of the components.

The transformations of molecular components in the cyanine dye layer with Ag NPs under cw and pulse laser irradiation were registered via optical means. We had to take into account the difference between the optical properties of organic dyes at the bare dielectric surface and surface with silver NPs. For this purpose the influence of the localized surface plasmon resonances of silver NPs on absorption properties of cyanine dye layers was investigated by us earlier [1].

## 2. Experimental

### *2.1. Preparation of samples*

Ensembles of silver NPs were prepared under high vacuum conditions by deposition of silver atoms on a substrate (sapphire, silica) at different temperatures (20–200 °C). The growth process proceeds without forming of the continuous wetting layer and with random appearance of islands at the imperfections of the sapphire surface. Obtaining of island metal film under these conditions leads to polydispersity of the ensembles of nanoparticles of their shapes and sizes.

We used the 3,3'-diethyl thiadicarbocyanine iodide molecules which consist of –CH= chain connecting two end groups. Cyanine dye molecules were spread over the silver NPs array using by spin-coating technique. To achieve the homogeneity of the molecular layers the substrate were rotated with the rate of 4000 rpm. The dye layer thickness was set by the concentration of the ethanol solution used for spin-coating. The dye layer thickness in our experiments varied up to 15 nm.

### *2.2. Photoinduced modification*

For photoinduced modification of the component composition we used cw and pulse laser (optical parametric oscillator pumped by Nd:YAG laser with pulse duration 10 ns). The wavelengths of photoexcitation were laid in absorption band of all-trans-isomers of the dyes. Preliminary, we studied the photoinduced modification of

molecular layers and Ag NPs on the substrate separately.

## 3. Results

### *3.1. Conformational changes in molecular layers without Ag NPs*

Thin films of dicarbocyanine dyes consisted of 3 isomers, dimers and J-aggregates. Under 1-3 hours cw laser irradiation the components of thin films of the dyes were destructed. The destruction of all molecular components was uniformed.

Under pulsed laser irradiation the optical density of the bare molecular thin films changed too small. Figure 1 shows the results of photomodification of dicarbocyanine layer (concentration of dye solution was $3 \cdot 10^{-4}$ mol/l) by laser pulses (wavelength 665 nm).

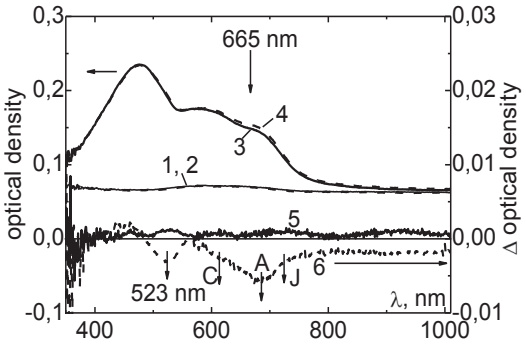


Figure 1. Photoinduced modification of dicarbocyanine thin films on the sapphire substrate (1, 2) and layers on the sapphire substrate with silver NPs (3, 4). The optical density of layers before (1, 3) and after irradiations (2, 4). The curve (5) plots the difference between (1) and (2); the curve (6) plots the difference between (3) and (4). A – all-trans-isomer, C – cis-isomers, J – J-aggregates.

### *3.2. Photoinduced modification of Ag NPs and hybrids*

The shape of the metal NPs has the major effect on their absorption spectra. According to the results of the microscopic research the shape of silver NPs is spheroidal. The frequency of the localized surface plasmon resonances is determined by the axial ratio of the spheroidal particles. The shapes and broadening of the Ag NPs spectrum may be decreased under heating. At the same time an intensive laser irradiation also can lead to the changes of the NPs shapes but selectively [4]. In this case the interpretation of the photoinduced modifications of molecular layers in the presence of NPs was difficult. To overcome it the ensembles of NPs were illuminated by laser pulses. It is found that at energy density less than 8.5 mJ/cm$^2$ selective heating is not observed.

The optical density of cyanine dye thin films without Ag NPs differs from thin films with NPs. Cw laser irradiation of layers with NPs also lead to the destruction of molecular components. But the optical density of layer with NPs decreased larger.

Under pulsed laser irradiation (wavelength 665 nm, the total energy density for 15 pulses was 37.4 mJ/cm$^2$) the optical density of the molecular thin films with Ag NPs changed by 4 times larger than in the layer without NPs.

## 4. Discussion

About 4 times larger changes of the optical density of molecular layers after irradiation were observed in the presence of silver NPs due to 2 processes which may be clearly seen in curve 6. The first of them was the destruction of dimers (minimum at 523 nm) and enhancement of plasmon absorption. The second of them was cis-to-trans-isomerization of molecular components.

## 5. References

[1]. N.A. Toropov, E.N. Kaliteevskaya, N.B. Leonov, T.A. Vartanyan, *Optics and Spectroscopy*. **113(6)** (2012) 616–620

[2] N.A. Toropov, N.B. Leonov, T.A. Vartanyan, *Bulletin of the Russian Academy of Science: Physics.* **76(12)** (2012) 1306–1309

[3] M.A. Noginov, G. Zhu, A.M. Belgrave, et al. *Nature.* **460** (2009) 1110–1112

[4] C. Heindrich, J. Bosbach, T. Vartanyan, et al. *Phys. Rev. Lett.* **89(25)** 57404-1-4

# Fine mechanisms of the interaction of silver nanoparticles with the cells of *Salmonella typhimurium* and *Staphylococcus aureus*

A. Grigor'eva[1*], A. Safonov[2]

[1] *Institute of Chemical Biology and Fundamental Medicine, Siberian Branch of Russian Academy of Science, Novosibirsk, Lavrent'eva Av., 8, 630090. Russia.*
[2] *Kutateladze Institute of Thermophysics, Siberian Branch of Russian Academy of Science, Novosibirsk, Lavrent'eva Av., 1, 630090. Russia.*
(*) -corresponding author: a.e.grigoreva@gmail.com

*Key words: silver, nanoparticles, Salmonella typhimurium, Staphylococcus aureus, electron microscopy*

## 1. Introduction

Antibacterial effect of metal silver is known since ancient times, and development of nanotechnologies has led to emergence of silver nanoforms which found an application in various fields of medicine and hygiene. Sizes of nanoparticles (NPs) and bacteria call for the application of electron microscopy for direct visualization of their interaction. The aim of our study was to obtain direct evidence of the penetration of Ag-NPS into cells of Gram-negative bacterium *S. typhimurium* and Gram-positive bacterium *S. aureus*, and to study cell responses to Ag-NPs. Our study of ultrathin sections directly showed penetration of Ag-NPs in bacterial cells and different response of *S. typhimurium* and *S. aureus* to the nanoparticles.

## 2. Experimental

### *2.1 Nanoparticles*

The Ag-NPs used in this study were a nanocomposite of silver and fluoropolymer matrix (polytetrafluoroethylene), obtained by gas-jet method. Physicochemical characteristics, details of nanocomposite formation and data of antibacterial activity were published earlier [1].

### *2.2 Bacteria cultivation and characterization*

Bacteria strains *Salmonella enterica*, subspecies *typhimurium*, CEMTC 30, (*S.typhimurium*) and *Staphylococcus aureus,* CEMTC 33, (*S. aureus*) were obtained from the Collection of Extremophilic

Microorganisms and Type Cultures of Siberian Branch of Russian Academy of Science (Novosibirsk, Russia). Overnight bacteria cultures grown on beef extract-peptone medium were resuspended in a sterile 0.9% solution of NaCl (saline). The portions of saline (4 ml) containing $7.81 \times 10^7$ CFU of *S. typhimurium,* or $8.96 \times 10^7$ CFU of *S. aureus* were incubated with 4 $cm^2$ of bandage covered by Ag-NPs in an orbital shaker at 190 rpm, 37°C.

Incubation medium contained 0.05 mg/l of silver to data of atomic emission spectrometer with excitation in the inductively coupled plasma (ICP-AES) with an attachment for a spark sampling iCAP - 3500, "ThermoElemental", U.S.

### *2.3. Electron microscopy*

Bacteria cells were fixed by 4% paraformaldehyde solution and postfixed with 1% osmium tetroxide, dehydrated under standard scheme and embedded into a mixture of epon-araldite (SPI, USA). Ultrathin sections were prepared with ultratome Ultracut-6 (Reichert-Young, Austria); some were contrasted with uranyl acetate and lead citrate, and some were not contrasted. Usage of non-contrasted sections allowed us differentiate Ag-NPs from occasional dense granular structures in bacterial cells. Ultrathin sections of bacteria samples were examined in transmission electron microscope JEM 1400 (Jeol, Japan). Digital images were collected by side-mounted camera Veleta (SIS, Germany).

## 3. Results

### *3.1 Interaction of silver nanoparticles with cells of S. typhimurium and S. aureus*

Individual Ag-NPs on ultrathin sections had roundish shape (most were

8-12 nm), fluoropolymer matrix looked as amorphous substance of low electron density around dense silver particles. The Ag-NPs formed friable aggregations (50-200 nm). Individual Ag-NPs and aggregations were observed on the surface of outer membrane of S. typhimurium, and cell wall of S. aureus already after 0.5 h of incubation with the NPs. Some cells of S. typhimurium showed dense layer of Ag-NPs on the outer membrane. Few individual electron dense particles were found in cytoplasm of *S. typhimurium* cells after 0.5 h of incubation, and only after 1.5 h in cells of S. aureus. Ag-NPs were located separately from each other inside microbial cells. We examined non-contrasted ultrathin sections to be sure that Ag-NPs really get inside cells.

### *3.2 Response of microbial cells to the influence of Ag-NPs*

Incubation of S. typhimurium with Ag-NPs arrested division of the cells after 2 h of incubation. In contrast, cells of S. aureus continued to divide during whole period of incubation. The responses of S. typhimurium to Ag-NPs included damage of cytoplasmic membrane, nucleoid and cytoplasm, deformation of the cells, and formation of outgrowths. Outer membrane maintained integrity during whole period of the incubation. Damage of the cytoplasm in the cells of S. typhimurium started with formation of small electron lucent areas in cytoplasm after 0.5 h of the incubation, which increased in number during the incubation. Then cytoplasm became clumpy and electron dense and accumulated on cell periphery. Nucleoid of intact cells of S. typhimurium is composed of thin fibers and spread in large area of cytoplasm. Incubation with Ag-NPs induced condensation of DNA fibers, the nucleoid became compact and located in electron lucent space, which was clearly separated from the cytoplasm. The response of S. aureus to Ag-NPs developed slowly, than in S. typhimurium, and included deformation of cell wall, damage of cell membrane, cytoplasm and nucleoid. After 23 h of incubation the cells lost their characteristic roundish shape and became “shrunk”, but thickness and structure of the wall remained unchanged. The cytoplasm became amorphous; it lost “grainy” appearance which is typical for intact cells, however lysis of the cytoplasm was not observed. Fibers of DNA, often covered by Ag-NPs, were located in amorphous material having low electron density and irregular shape.

## 4. Discussion

Study of ultrathin sections in electron microscope allowed to visualize the penetration of Ag-NPs (diameter 5-12 nm) into the cells of Gram-negative *S. typhimurium* and Gram-positive *S. aureus*. The Ag-NPs overcame the barrier of two membranes in the first, and barrier of cell wall and membrane in the second, and then accumulated in the cytoplasm. It should be noted that Ag-NPs did not induce visible changes of surrounding cytoplasm.

Of course, the microbial cells can not be indifferent to Ag-NPs adsorbed on the surface and getting inside. Cell responses of S. typhimurium and S. aureus differed morphologically, and mainly were represented by damage of cell structures. Evidently, Ag-NPs adsorbed on cell surface and located inside the cytoplasm affect bacterial metabolism. However, any preparation of Ag-NPs contains silver ions, and it is impossible definitely separate their action. We believe that both silver ions and Ag-NPs themselves interact with bacteria cells and induce the changes. The obtained results showed how different could be the responses induced by the same NPs in relatively simple prokaryotic cells. It is evident, that NPs are “active players” which directly interact with macromolecular structures of living cells and are able to exert an active influence on them, and this should be taken into account in the development of NPs and their implementation in practice.

## 5. References

[1]. A. Rebrov, A. Safonov, N. Timoshenko, V. Varnek, I. Oglezneva, S. Kosolobov, *J of Appl Mech & Tech Phys* **51** (2010) 4.

# Antimicrobial Properties of Silver Nanobiocomposites with Natural Polysaccharide Matrixes

G. P. Aleksandrova[1], M. V. Lesnichaya[1*], T. V. Fadeeva[2], B. G. Sukhov[1], and B. A. Trofimov[1]

[1.] *A. E. Favorsky Irkutsk Institute of Chemistry, Siberian Branch of the Russian Academy of Sciences, 1 Favorsky st., 664032 Irkutsk, Russian Federation. Fax: +7 (395) 241 9346.*

[2.] *Scientific Center of Reconstructive and Restoring Surgery, East Siberian Scientific Center, Siberian Branch of the Russian Academy of Medical Sciences,1 Bortsov Revolusion st., 664003 Irkutsk, Russian Federation.*

(*) corresponding author: @E-mail address: alexa@irioch.irk.ru

*Keywords: nanoparticles, nanocomposites, silver, polysaccharides, arabinogalactan, carrageenan*

## 1. Introduction

The most important factor for the increasing biological activity of the silver preparations is the enhancement of their transmembrane permeability, which makes it possible to substantially decrease the therapeutic dose and thus diminish the drug load on the organism. One of the promising methods of achieving transmembrane permeability can be the transformation of silver into the nanosized state with the simultaneous inclusion of silver nanoparticles into matrices of polysaccharides arabinogalactan and carrageenan, which impart water solubility and higher biocompatibility to the constructed materials. The purpose of this work is the synthesis and study of the structure and antimicrobial properties of the hybrid nanocomposites based on biocompatible galactose containing polysaccharides: arabinogalactan and carrageenan.

## 2. Experimental

### 2.1. *Analytical technique*

The electronic absorption spectra of 0.04% aqueous solutions of nanocomposites were recorded relative to $H_2O$ in the ultraviolet and visible spectral regions on a Perkin Elmer Lambda 35 spectrophotometer. Micrographs of the nanocomposite samples were taken with a Leo 906 transmission electron microscope at an accelerating voltage of 80 kV. The particle size was determined by the statistical processing of the electron micrographs.

### 2.2. *Synthesis of the silver containing nanocomposites.*

Arabinogalactan (20 kDa) and carrageenan (1800 kDa) were used. An aqueous solution (10 mL) of (0.04—0.33 g) $AgNO_3$ was added dropwise to a solution of arabinogalactan or carrageenan (1 g) in (30 mL) $H_2O$, and then a 1 *M* solution of NaOH (3 mL) was added. The reaction time was 20 min, temperature was 90 °C, and the nanocomposites were precipitated by the addition of fourfold excess of ethanol. The yield was near 94%.

*2.3. Determination of the antimicrobial activity of argentoarabinogalactan and argentocarrageenan* containing 4.0% silver nanoparticles was carried out by the method of serial dilutions using reference cultures of *Escherichia coli ATCC 25922*, *Pseudomonas aeruginosa ATCC 27853*, *Staphyllococcus aureus ATCC 25923*, and *Bacillus subtilis* and *Salmonella typhimurium.*

## 3. Results

The silver containing nanocomposites based on arabinogalactan and carrageenan were synthesized using a procedure of nanoparticle formation in the matrix of the polysaccharide developed by us earlier [1]. As a result of the reactions of silver nitrate with polysaccharides in an aqueous-alkaline medium, we obtained a

series of water soluble nanocomposites, whose structures combine the above mentioned polysaccharides and silver in the amount from 2.5 to 20.9%

The process of formation of the silver-containing nanocomposites is based on the redox reaction occurring in an aqueous alkaline medium of silver ions with the hydroxyl groups of polysaccharides [2]. The simultaneous stabilization of the formed nanoparticles of reduced silver occurs, probably, due to form the stable metallic nanophase. The spectra of aqueous solutions of the prepared silver containing nanocomposites have an intense absorption maximum caused by the collective excitation of silver conductivity electrons (plasmon resonance) at the wavelength 410 and 411 nm for argentoarabinogalactan and argentocarrageenan, respectively. This effect reliably confirms that the obtained silver containing nanocomposites contain silver in the zero valent state [2]. The size of the prepared silver containing nanocomposites was studied by transmission electron microscopy. The size of the resulting nanoparticles varies from 10.3 to 12.0 nm.

The antimicrobial activity of the silver containing nanocomposites was determined on the reference strains using the method of serial dilutions in a liquid medium. The studies of argentoarabinogalactan and argento-carrageenan containing 10.0 and 4.0% silver showed its high antimicrobial activity against a series of microorganisms: *Escherichia coli*, *Pseudomonas aeruginosa*, *Staphyllococcus aureus*, *Salmonella typhimurium* and *Bacillus subtillis*. The minimum inhibition concentrations (MIC) with respect to these microorganisms are listed in Table 1. Depending on the type and strain of the microorganism, the values of MIC range from 1 to 50 mkg/mL, which is similar to the activity of the recently patented nanosilver preparations [3].

Table 1. Antimicrobial properties of the silver containing nanocomposite

| **Microorganisms** | **MIC, mkg/mL** | |
|---|---|---|
| | Argentocar-rageenan | Argentoara-binogalactan |
| *E. coli* | 10 | 1.0 |
| *S .typhimurium* | - | 1.0 |
| *P. aeruginosa* | 25 | - |
| *S. aureus* | 50 | 100.0 |
| *B. subtillis* | 50 | 50.0 |

It is also known that the acute toxicity ($LD_{50}$) of the silver containing argentoarabinogalactan nanocomposite is 11600±4500 mg/kg, which allows one to assign this drug to the class IV of low dangerous substances.

## 4. Discussion

Thus, the water soluble nanocomposites consisting of silver nanoparticles and stabilized by the arabinogalactan and carrageenan polysaccharide matrices were prepared for the first time. The polysaccharide based nanocomposites were found to manifest the antimicrobial activity against a series of nosocomial microorganisms, which is the basis for the subsequent development of preparations of medical design from these nanocomposites.

This work was supported by Russian Foundation for Basic Research (grant 12-03-90433-Ukr_a), SB RAS (integration projects No. 85, 134, interdisciplinary projects of SB RAS and the Mongolian Academy of Sciences and the Ministry of Education, Culture and Science of Mongolia's No. 4, 14

## 5. References

[1]. Pat. RF 2278669; *Inventionts Bulletin*, 2006, 18.
[2]. B.G. Sukhov, G.P. Aleksandrova, L.A. Grishchenko, *J. Struct. Chem*. 2007, **48**, 922.
[3] M.V. Lesnichaya, G.P. Aleksandrova, T.V. Fadeeva, B.G. Sukhov, and B.A. Trofimov. *Russian Chem. Bull.*, **59**, 12, 2266-2271.

# Magnetic sorbents based on hypercrosslinked polystyrenes for removal of toxic organic compounds

K. I. Lubentsova, A. V. Pastukhov, V. A. Davankov*

*Nesmeyanov Institute of Organo-Element Compounds, Russian Academy of Sciences, Vavilova St. 28, Moscow, 119991 Russia*

(*) corresponding author: davank@ineos.ac.ru

*Keywords: hypercrosslinked polystyrene, composite sorbents, iron oxides*

## 1. Introduction

Among various technologies of removing toxic or recovering useful components from liquid or air flows, sorption methods have found wide application, in particular, due to the development of new sorbents. Providing sorbents with magnetic properties can significantly widen their efficient use, since it would make it possible to introduce the sorbents into the desired environment as a dispersed phase with controlled interphase contact surface and then recover the sorbents from the environment by using magnetic separation method.

## 2. Experimental

For the obtaining of new magnetic sorbents, as a starting porous polymer matrix, various types of commercial hypercrosslinked polystyrene sorbents ("Purolite") [1], namely, nonionic microporous hypercrosslinked polystyrenes MN-270, biporous MN-200 and carboxylated ion exchanger MN-600, as well as mesoporous polydivinylbenzene sorbent Amberlite XAD-4 were used. For providing magnetic properties to these sorbents, magnetic iron oxides in the amount from 13 to 17 mass-% were introduced into the hypercroslinked polystyrene interior by means of the chemical deposition method (Elmore's reaction) [2, 3]:

$$FeCl_2 + 2FeCl_3 + 8NH_4OH \rightarrow \downarrow Fe_3O_4 + 8NH_4Cl + 4H_2O$$

## 3. Results and discussion

It was found, that the composite sorbents obtained are characterized by low density **d** from 0.6 to 0.7 g/sm$^3$ and by high internal specific surface area $\mathbf{S}_{in}$ from 500 to 1100 m$^2$/g (Table 1).

Table 1. Basic physical properties of magnetic composite sorbents.

| **Sorbent** | **Fe**, mass. % | **Iron oxides,** mass. % | **d**, g/cm$^3$ | $\mathbf{S}_{in}$, m$^2$/g | **σ**,* Gs cm$^3$/g |
|---|---|---|---|---|---|
| MN270 | - | - | 0.60 | 1300 | - |
| **MMN270** | 10.6 | 14.1 | 0.70 | 1150 | 7.0 |
| MN200 | - | - | 0.48 | 1100 | - |
| **MMN200** | 11.9 | 16.2 | 0.58 | 915 | 10.6 |
| MN600 | - | - | 0.54 | 700 | - |
| **MMN600** | 10.8 | 16.8 | 0.66 | 530 | 11.0 |
| XAD-4 | - | - | 0.52 | 860 | - |
| **MXAD-4** | 9.6 | 13.1 | 0.61 | 670 | 5.6 |

* - specific magnetization in a magnetic field with an intensity of 2.5 kGs

Magnetic composite sorbents (Fig. 1) retain high sorption capacity for toxic organic compounds. It was found that inserting nanodisperse particles of iron oxides into the porous structure of the initial polymer sorbents reduces their ability to absorb low-molecular-weight organic compounds to a small extent, only (Table 2).

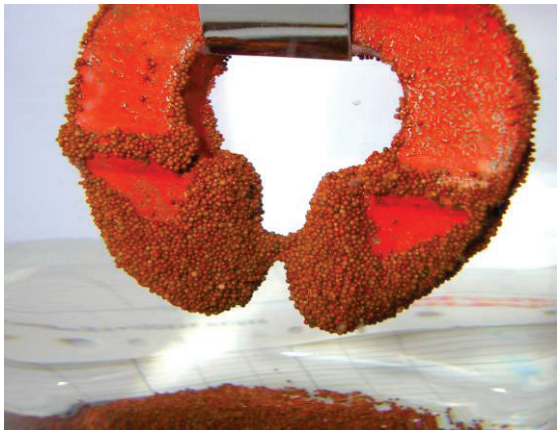

Figure 1. Magnetic nanocomposite MMN200 based on biporous commercial sorbent.

To examine the sorption properties of the produced composite materials, the method of static sorption of saturated vapors of various organic solvents was used. The amount of sorbate uptake was determined by the increase in the weight of the sorbent after certain intervals of time. This method permits to follow the sorption kinetics and determine the maximum equilibrium sorption capacity of the volatile low molecular weight compounds. As was determined, this value for the porous materials examined is practically equal for both sorption from the liquid phase and from saturated vapors of organic compounds.

Table 2. Maximal sorption of organic solvents and their saturated vapors.

| **Sorbent** | **toluene**, ml/g | **heptane**, ml/g | **dichloro-ethane**, ml/g | **dioxane**, ml/g | **ethanol**, ml/g |
|---|---|---|---|---|---|
| MN270<br>**MMN270** | 1.33 (1.38)*<br>1.06 | 1.25<br>1.00 | 1.26<br>1.04 | 1.21<br>1.01 | 1.29<br>1.08 |
| MN200<br>**MMN200** | 1.94 (1.92)*<br>1.25 | 1.83<br>1.23 | 1.88<br>1.26 | 0.89<br>0.83 | 1.83<br>1.26 |
| MN600<br>**MMN600** | 1.44 (1.44)*<br>1.09 | 1.39<br>0.99 | 1.48<br>1.10 | 0.77<br>0.64 | 1.42<br>1.10 |
| XAD-4<br>**MXAD-4** | 1.46 (1.54)*<br>1.06 | 1.43<br>1.07 | 1.48<br>1.09 | 1.42<br>1.05 | 1.47<br>1.07 |

* - swelling in liquid solvent

Thus, our work results in the optimization of the method of producing magnetic hypercrosslinked polystyrene sorbents and determination of their basic chemical and sorption properties. Nanocomposite hypercrosslinked polysterynes with iron oxides are efficient magnetic sorbents for removing toxic compounds from fluids, for the fast absorption of toxic liquids and their vapors, followed by the collection of the sorbent from the contaminated surface with the use of a magnet. It is also promising to use the sorbent for the direct extraction of target components from aqueous suspensions, for example, in the microbiological production of biologically active compounds.

## 4. References

[1]. Hypersol-Macronet™ Sorbent Resins, Purolite Technical Bulletin, The Purolite Company, UK, **1995**, 11p.

[2]. A. V. Pastukhov, V. A. Davankov, V. V. Volkov, K. A. Dembo, Y. V. Zubavichus, A. A. Korlyukov, A. G. Filatova, *Bulletin of the Russian Academy of Sciences: Physics.* **73** (2009), 471.

[3]. A.V. Pastukhov, V.A. Davankov, *Bulletin of the Russian Academy of Sciences. Physics*. **75** (2011), 1248.

# Palladium nanoparticles: effects on macrophages and epithelial cells

K. Razum*[1], S. Trouzhkyi[2], V. Bukhtiyarov[2], E. Ryabchikova[1]

[1] *Institute of Chemical Biology and Fundamental Medicine SB RAS, Russia, Novosibirsk, Lavrentiev Ave. 8*
[2] *Boreskov Institute of Catalysis SB RAS, Novosibirsk, Russia, Novosibirsk, Lavrentiev Ave. 5*

(*) corresponding author: kk-kristina@mail.ru

*Keywords: palladium nanoparticles, toxicity, cellular uptake*

## 1. Introduction

Palladium nanoparticles (Pd-NPs) are byproduct of automobile catalytic converters, which is released into the atmosphere from the exhaust. The content of Pd-NPs increases in the environment over time and can be harmful for humans [3]. Studies of Pd-NPs influence on cells were not studied enough. The aim of this work was to examine the effect of Pd-NPs on the epithelial cells MDCK and primary mouse macrophages. These nanoparticles were similar to those emitted from motor vehicle exhaust gases.

## 2. Experimental

### *2.1. Synthesis and preparation of Pd-NPs*

The Pd-NPs used in this study were synthesized using the intermediate synthesis polynuclear hydroxocomplexes of palladium (II) [5]. The resulting preparation represented a suspension of Pd-NPs in PBS (pH 7.3-7.5, concentration 0.05 g/mL). Pd-NPs were dispersed in conditioned cell culture Dulbecco's Modified Eagle Media (DMEM, Gibco) with 10% heat-inactivated fetal bovine serum (FBS, Gibco). The medium was collected after 48h cultivation of Madin-Darby Canine Kidney Epithelial Cells (MDCK). The resulting suspension was subjected to ultrasonic exposure (240 V, 50/60 Hz) in an ultrasonic bath (Bandelin DT31, Germany) for 15 minutes and then was added to the cells.

### *2.2. Characterization*

The morphology and size of Pd-NPs were examined by transmission electron microscope (TEM) JEM 1400 (JEOL, Japan) supplied with a digital camera Veleta (SIS, Germany). The average size of Pd-NPs was determined by measurement of 100 particles with sharp edges, using image analysis (iTEM, Version 5.2).

### *2.3. Cell culture*

MDCK cells were cultured in DMEM (pH 7.4) in humidified incubator (37 °C, 5% CO2). The DMEM was supplemented with 10% FBS and 1% penicillin/streptomycin. MDCK cells ($2\times10^5$ in 1 mL) were spread into one of 6-wells tissue culture plate (TTP, LabTech) and allowed to grow for 24 h.

Primary peritoneal macrophages (PMs) were obtained by washing of peritoneal cavity of mice, and were cultured in Iscove's Modified Dulbecco's Medium (IMDM, Gibco) with 10% FBS and 1% penicillin/streptomycin. Cells were spread into 38 mm Petri dish (Nunc, Denmark) ($3\times10^6$ in 3.5 mL per dish), and allowed to grow for 24 h.

### *2.4. Uptake and toxicity studies*

Both PMs and MDCK were incubated with Pd-NPs (3.5 mg/mL and 1.1 mg/mL respectively) for 10, 30 min, 1, 3, 5, 7 and 24 h. The samples were prepared on coverslips for light microscopy and for TEM according to standard protocols. The viability of MDCK cells treated with Pd-NPs was assessed after 24, 48 and 72 h of incubation by MTT-test using 100-fold serial dilutions of the original suspension (50– $5x10^{-11}$ mg/mL). Untreated cells served as a control.

## 3. Results

Ultrathin sections of culture samples showed Pd-NPs (5.76 ± 1.61 nm) with irregular shape close to spherical, and particle aggregates (100-500 nm in size).

Pd-NPs actively adsorbed on the plasma membrane of MDCK cells and penetrated into the cells across the plasma membrane, without formation of endocytotic vesicles. Single nanoparticles or small groups (up to 10) were detected in the cytosol, Golgi apparatus, mitochondria, endoplasmic reticulum, endosomal-lysosomal structures, near the nuclear envelope, in perinuclear space and nucleus. During the incubation Pd-NPs accumulated in lysosomes and in the nucleus. Active penetration of Pd-NPs into epithelial cells was observed during the whole period of incubation. The toxic effect of Pd-NPs was represented by alteration of the integrity of plasma membrane and membranes of organelles. Cell organelles became swollen, and structure of cytoplasmic and nuclear matrix was broken. MDCK cells incubated with Pd-NPs during 24 h showed cell viability of 20-60% at a concentration of nanoparticles in culture medium 50 - $5x10^{-11}$ mg/ml. Thus, Pd-NPs showed evident toxicity toward MDCK epithelial cells and penetrated freely into their cytoplasm and nucleus. Toxicity of Pd-NPs increased with their concentration in culture medium.

Interaction of Pd-NPs with PMs differed from the interaction with MDCK cells. Macrophages actively phagocytized clusters of Pd-NPs which were found inside the cells in phagosomes and lysosomes. Pd-NPs were also detected in early endosomes and multivesicular bodies, indicating that Pd-NPs entered the cell by microendocytosis. Pd-NPs were not found in the cytosplasm and nucleus of PMs. During the incubation Pd-NPs accumulated in lysosomes, and remained enclosed in membrane vesicles. Thus, primary PMs showed ability to capture Pd-NPs and neutralize them by storage in lysosomes.

## 4. Discussion

We examined the toxicity and interaction of Pd-NPs (size about 5 nm) with mammalian cells. Primary PMs were chosen as the cells responsible for the capture and neutralization of foreign substances in organism. Treatment of MDCK cells by Pd-NPs modeled interaction of lung epithelium with inhaled Pd-NPs which are present in exhaust gases.

The results of our study showed that epithelial cells are unable to prevent penetration of Pd-NPs into the body. Similar results were obtained in study of Pd-NPs interaction (10 nm) with Primary Bronchial Epithelial Cells (PBEC). The epithelium of upper respiratory tract (model PBEC) was more sensitive to the toxic effects of Pd-NPs than epithelium of lower respiratory tract (cell culture A549) [6].

We found that Pd-NPs penetrate in MDCK nonspecifically and damage cell membranes. We did not observe signs of damage in PMs treated by Pd-NPs. The uptake of Pd-NPs by macrophages occurred by endocytosis. Membranes of PMs showed resistance to the action of Pd-NPs, and ability to isolate nanoparticles from the contents of cells.

Thus, interaction of Pd-NPs with mammalian cells is complex and specific. Differences of the interaction of MDCK cells and PMs with Pd-NPs were related with cell specialization and functions.

## 5. References

[1]. Trouzhkyi SY, Chuvilin AL, Kotchoubey DI, Novgorodov BN, Kolomiychuk VN, Likholobov VA. The structure of polynuclear hydroxo palladium (II), formed by alkaline hydrolysis of its chloride complexes. *Russ. Chem. Bull* 1995, **44**(10), 1822-1826.

[2]. Wilkinson KE, Palmberg L, Witasp E, Kupczyk M, Feliu N, Gerde P, Seisenbaeva GA, Fadeel B, Dahlén SE, Kessler VG. Solution-engineered palladium nanoparticles: model for health effect studies of automotive particulate pollution. *ACS Nano*. 2011, **5**(7), 5312-24.

[3]. Wiseman CL, Zereini F. Airborne particulate matter, platinum group elements and human health: a review of recent evidence. *Sci Total Environ*. 2009, 1, 407(8), 2493-500.

# Physicochemical Characterization of Nanoparticles in Physiological Solutions

E. Yunda[*1], A. Godymchuk[1,2], D. Kuznetsov[2], A. Gusev[2,3], N. Kosova[4]

[1] *National Research Tomsk Polytechnic University, Institute of High-Technology Physics, Department of nanomaterials and nanotechnologies, 634034 Lenina ave., 30, Tomsk, Russia*
[2] *National University of Science and Technology "MISIS", Department of functional nanosystems and high-temperature materials, 119049 Leninsky pr., 4, Moscow, Russia*
[3] *Tambov State University named after G.R. Derzhavin, Centre "Nanotechnologie and Nanomaterials", 392000 Internationalnaya str., 33, Tambov, Russia*
[4] *National Research Tomsk State University, Laboratory of catalytic research, 634050 Lenina ave., 36, Tomsk, Russia*

(*) corresponding author: eny@tpu.ru

*Keywords: nanoparticles, dissolution, aggregation, toxicological testing*

## 1. Introduction

The production of nanoparticles actively grows due to the widespread application of nanomaterials. For example, in a small Siberian city of Tomsk (Russia) since 1998 the annual production of nanopowders has reached more than 2 tons [1]. Owing to a small size nanoparticles are capable to release into the ambient air and enter living organisms including human body.

When passed through nanoborder (less than 100 nm), particles remain molecular properties, meanwhile their reactivity considerably grow up, that is explained with heightened part of surface and subsurface atoms in comparison with number of bulk atoms. What is more, because of the raised reactivity and small size nanosized particles may demonstrate highly toxic effects, this fact has become a major cause for concern from the viewpoint both of occupational and environmental health [2].

The review has shown that while evaluating the health effect of nanomaterials scientists associate nanoparticles toxicity mostly with the initial parameters of samples, not taking into account nanoparticles degradation in terms of their composition and properties in physicochemical solvents [3]. However, solubility and changes in acomposition, morphology, size of the particles together determines the migration activity and the accumulation degree of nanoparticles in tissues and cells either with amplification or weakening the toxicity. For instance, soluble nanoparticles entering a biological liquid may be a sources of heavy metal ions, most of which are highly toxic when accumulated in the body [4]. When nanoparticles dissolve till molecules and ions, their environmental migration, particularly in human body, becomes much easier.

In the opposite case, when released into the environment insoluble solid particles typically form lyophobic disperse systems, where heightened aggregation of nanoparticles is observed. In terms of toxicity evaluation the observed toxic effect is better to be balanced with aggregates size but not with the size of the initial particles.

Therefore, the accumulation of information on the physicochemical properties of nanoparticles in physiological fluids is obviously an urgent problem. Since 2006 our research group has been implementing a project aimed at the study of the properties of fine systems formed by nanoparticles in liquid media of the environment.

## 2. Experimental part

### *2.1. Objects of study*

As objects of study we use metal containing nanoparticles (Zn, Ni, Al, Cu, $Al_2O_3$, ZnO) obtained by electric explosion of conductors, and metal oxide nanoparticles

($Al_2O_3$, $ZrO_2$, $TiO_2$, ZnO, $Y_2O_3$) obtained by plasmochemical synthesis. In numerous experiments we prepare suspensions based on chosen nanoparticles and physiological solutions (physiologically favorable media: phosphate buffered saline, solutions of saccharides, solutions of ionic and nonionic surfactants, solutions of different salinity, lung fluid etc.). All components of the solutions are the elements of biological fluids of living organisms.

### *2.2. Experimental techniques*

Initial nanoparticles and products formed after their interaction with the solutions are studied with the help of the techniques shown in table1.

Table 1. Techniques Used for Studying the Physicochemical Properties of Suspensions.

| Parameter | Technique for assessing |
|---|---|
| Composition | X-ray analysis<br>Infrared spectroscopy |
| Morphology | Scanning and transmission electron microscopy |
| Dispersity | Method of laser diffraction, dynamic light scattering |
| Solubility | Stripping voltammetry, atomic absorption speroscopy |
| Electrokinetic properties | Electroacoustic and conductometric methods, dynamic light scattering |

## 3. Results

### *3.1. Reactivity of metal nanoparticles*

According to the experimental data the dissolution degree of metal nanoparticles (Zn, ZnO, Cu, Ni, NiO, etc.) in physiological saline solutions (e.g., PBS) may reach 14-50 wt.%, whereas in pulmonary fluid the dissolution degree of the nanoparticles increases till 70-99 wt.%. The oxidation of nanoparticles in simple physiological solution, like PBS, was established to be accompanied by formation of solid products with new composition and morphology, which did not separate from the particles surface.

While dissolved in pulmonary fluid Zn and Ni nanoparticles resolve into stable complexes of metals with carboxylic acids that were proved by thermodynamic analysis.

### *3.2. Aggregation stability of oxide nanoparticles*

The experiments with insoluble nanoparticles are carried out to study electrokinetic characteristics and aggregation stability of nanoparticles sols and suspensions. For particles of $Al_2O_3$, $ZrO_2$, $Y_2O_3$ the aggregation and sedimentation stability was calculated. It has been demonstrated that sols with high aggregation and sedimentation stability (2-3 days) had been formed in the solution of certain saccharides (glucose, $C_6H_{12}O_6$), in which the dispersed phase was represented by the colloids with micelle structure $d_{av}$ = 100...300 nm.

## 4. Conclusion

In summary, numerous experiments have shown a high reactivity of nanoparticles in physiological solutions. Thus, products formed during dissolution may jointly exert influences onto living organisms. The development of adequate methods for nanomaterials testing is complicated without the data on the physicochemical properties of nanoparticles.

Due to dynamic changes in the properties of nanoparticles the following milestone of our project is to link physicochemical degradation and toxicity of nanoparticles.

This work was supported by the Russian Ministry of Science and Education (contract No.13.G25.31.0021; state assignment "Science").

## 5. References

[1]. ADVANCED POWDER TECHNOLOGIES LLC, Tomsk, Russia, Web-page http://www.nanosized-powders.com.

[2] G. Oberdörster, E. Oberdörster, J. Oberdörster, *Environmental Health Perspectives*. **113** (2005) 823.

[3]. X. Zhu., L. Zhu, Y. Chen, S. Tian, *Journal of Nanoparticle Research*. **11** (2009) 67.

[4]. A. Ivask, O. Bondarenko, N. Jepihhina, A. Kahru, *Analytical and Bioanalytical Chemistry*. **398** (2010) 701.

# Expression of apoptosis protein bsl-2 innerve cells induced by silver nanoparticles encapsulated in polymer matrix

Novikov M.A. [1]

[1] *Institute of Occupational Health & Human Ecology FSBI «ESSC HE» SB RAMS (Angarsk), Russia*

(*) corresponding author: novik-imt@mail.ru

*Keywords:* nanocomposites with silver nanoparticles, bcl-2 protein cells

## 1. Introduction

Currently, the world has been an increased interest in development of preparations containing inorganic nanoparticles and organic nature, especially with use of natural or synthetic polymersas nanostabilizingmatrices. One of such polymer is poly-1-vinyl-1,2,4-triazole (PVT), which has managed a complex of properties such as high hydrophilicity and chemical stability, biocompatibility, heat resistance, and can be used in the development of new forms of medical synthetic drugs. Earlier histological studies of synthesized in the Favorski Irkutsk Institute of Chemistry ISC SB RAS nanocomposites with silver nanoparticles (Ag NP's) (AgPVT, size of 2-10 nm, stabilized by PVT) are pointed to damaging effect of Ag NP'scontained in this nanocompositein subacute introduction of there in the brain tissue of white rats. In particular, There are marked a perivascular edema of brain vessels, and swelling of conductive fibers in subcortical structures.Administration of PVT without Ag NP's addition revealed no deviations from control animals, except for a small vascular stasis. In this regard, it was necessary to evaluate the intracellular effect of Ag NP'son the nervous tissue. As one of parameters, we used the expression bsl-2 protein as a nonspecific inhibitor of apoptosis, whose synthesis is induced by the tumor suppressor protein p53, which will assess the activity of apoptotic process in a cell.

## 2. Experimental

A total of 32 healthy male outbred rats obtained from the Laboratory Animal Center (Eastern-Siberian Scientific Center, Angarsk). The rats nearly of the same age (12 weeks old) and weighing 220-240 gm. Animals were randomly divided into 4 groups, 2 AgPVT – treated groups, 1 PVT – treated group and control group. Test substances were administered orally in rats for periods 9 days as shown in Table 1.

Table 1. The oral administration of test substances in rats for periods of 9 days

| **Groups** | **Phase-in substance** | **Dose of substance** | **Number of animals** |
|---|---|---|---|
| **Control (C)** | saline solution | 0,5 ml | N=8 |
| **G1** | PVT | 100 µg | N=8 |
| **G2** | AgPVT | 100 µg/kg* | N=8 |
| **G3** | AgPVT | 500 µg/kg* | N=8 |

*Administration of 100 and 500 µg silver per kilogram of rat's body weight in a volume of 0.5 ml

The rats were maintained on standard laboratory rodent diet pellets and were housed in humidity and temperature-controlled ventilated cages on a 12 h day/night cycle. All animals were killed by dislocation of the next day after the end of treatment. The studies were conducted in accordance with the rules adopted by the European Convention for the Protection of Vertebrate Animals used for Experimental and other purposes (Strasbourg, 1986). Working with laboratory animals was carried out according to the study protocol in accordance with the Geneva Convention of 1985 on international principles of biomedical research using animals and the

Helsinki Declaration of 2000 on humane treatment of animals. Fresh portions of the brain from each rat were cut rapidly, fixed in neutral buffered formalin (10%), then dehydrated, with grades of ethanol (70, 80, 90, 95 and 100%). Dehydration was then followed by clearing the samples in 2 changes of xylene. Samples were then impregnated with 2 changes of molten paraffin wax, then embedded and blocked out. Paraffin sections (4-5 μm) were placed on polizinglasses (Menzel, Germany) and stained for antibody to bsl-2 apoptosis protein (Monosan, Netherlands) according to manufacturer's suggested protocol. Then they were stained with thionin colourant. Stained sections were controls and treated rats were examined by the number of nerve cells and cells overexpressing bcl-2 protein. Statistical value calculated by Statistica 6.1 Mann-Whitney test.

## 3. Results and discussion

According to the study of brain sections using the above system analysis revealed that the introduction of studied doses of nanocomposite was not significantly affected by total number of nerve cells. We assume that this is due to insufficient exposure time of injected substance on brain cells. However, the results of counting the number of nerve cells overexpressing bsl-2 compared to total number of nerve cells in 60 fields of view revealed a significant increase in the number of cells with increased expression of a group of animals exposed to various doses of nanocomposite (G1,G2). Also showed an increase compared to the control cells by overexpression in brain sections of G1 group (PVT without Ag NP's adding) which, in our opinion, associated with the response of neurons to administration of the foreign agent (Table 2).

Thus, the percentage of cells with high expression was significantly increased with introduction of Ag NP's, which is connected with the development of apoptotic cells in the process, in our opinion. In brain slices animals exposed PVT without Ag NP's addition was observed minimum number of cells with high expression, indicating that the polymer matrix HTP has no significant effect on brain cells. Conversely, in sections of the brain of animals exposed nanobiocomposites with Ag NP's was revealed significant increase in number of overexpressing bcl-2 protein cells compared with the control and detected a direct correlation between the dose of Ag NP's and change in the number overexpressing cells. All this suggests that the 9-day administration of nanocomposites is run apoptotic process, which leads to activation of apoptosis inhibitor protein Bcl-2. To minimize the effects of the impact of the test substance should be further study of the effect on the functional systems of the body.

Table 2. Expression bsl-2 protein in the brain tissue under the influence of the test substances.
Med (Q25 - Q75) n = 60

| Groups | Total number of nerve cells (Nt) | Number of overexpressing bcl-2 protein cells (No) | % number of overexpressing cells to total number, (No/Nt) |
|---|---|---|---|
| Groups | Nt | No | No/Nt |
| **C** | 287,5 (264-306) | 11,6 (2-18) | 1,02 |
| **G1** | 232,3 (196-271) | 10 (4-11)* | 2,8* |
| **G2** | 281 (275-308) | 17,9 (4-22)* | 4,3*# |
| **G3** | 313,6 (276-350) | 7 (5-9)* | 6,9*#● |

Note: * - the difference is statistically significant when compared with the control group ($p < 0.05$); # - differences are statistically significant when compared to group G1 ($p \leq 0,05$); ● - differences are statistically significant when compared to group G2($p \leq 0,05$).

# Effect of Serial Administration of Titanium Dioxide on Locomotor and Brain Activity Locomotor and Activity Aggressive Behavior of Wistar Rats

M. Khodanovich, N. Krivova, A. Zelenskaya, O. Zaeva, D. Sukhanov, E. Gul

*Tomsk State University*

*Keywords: titanium dioxide; TiO2; behavior; EEG.*

## 1. Introduction

Titanium dioxide (titania, or $TiO_2$) has been used in industry since 1930. Nowadays this substance in the form of nanoparticles is among the most widely used nanomaterials. Mainly titanium dioxide is used as a white pigment due to its high reflective index and white color [8]. In particular, titanium dioxide is applied as a pigment to provide whiteness to such products as paints, paper, foodstuffs (flour, sugar, milk), medicines (pills, tablets), toothpastes, etc.

However, exactly these properties of nanoparticles of titanium dioxide have a negative effect on biosystems. Injected or inhaled $TiO_2$ can migrate to any organ [6] and cause an inflammation, DNA [3] or enzyme [9] injury, oxidative stress [4], which may lead to a cell death [2] or development abnormalities [1]. Although titanium dioxide is less toxic than other materials [7], it is used much more widely, so a study of the physiological reactions to its introduction is essential.

Abnormalities on cellular and mediator levels as well as behavioral disorders are evidence of versatile targeting of $TiO_2$, which convinces to explore its impact, using different methods, on different levels of the CNS organization.

## 2. Experimental

### *2.1. Chemicals*

The $TiO_2$ nanoparticulate anatase was produced with the plasmochemical method (MACH I, USA).

### *2.2. Animals and treatment*

Two groups of ten Male Wistar rats were housed in a ventilated room with controlled environmental conditions: light (automatically controlled light-dark cycles 12:12, 8AM – 8 PM), temperature of about 20 ºC, a standard vivarium diet (granulated food) with food and water being ad libitum. All animals were handled in accordance with the European Convention on the Vertebrate Animals Used for Experimental and Other Research Aims Protection.

Twenty rats were randomly divided into two groups: the experimental group was receiving nano-$TiO_2$ for 7 days at morning hours with attractive food (pancakes with a surface of about 20 $cm^2$), and the control group was receiving only attractive food. Each rat received 50 mg (250 mg/kg) of nano-$TiO_2$ per a day. Apart from the receiving of the experimental material, the rats were fed as usual.

Before and after the experiment the EEG was registered. The EEG signal was registered monopolarly in the range of 0.16-70 Hz. We analyzed EEG indexes of main rhythms in an audio stimulation mode.

A daily video recording of two cages with control (n=10) and experimental (n=10) animals was carried out in the course of the experiment. The video files were analyzed by means of «Mouse Express» software. The «Mouse Express» software automatically calculates the moving activity value in relative units by evaluating the differences between frames.

## 3. Results

### *3.1. EEG indexes*

The comparative analysis of EEG power spectra was carried out in the control group and in the group which received nano-$TiO_2$. It was found that the means of the main rhythms power before and after the experiment did not differ in the control group. At the same time, the power of alpha and beta rhythms in the animals which received nano-$TiO_2$

decreased both in the background and stimulation mode in comparison with the EEG power before the experiment. The changes of the EEG power in the experimental group were observed, mainly, in the right hemisphere. The EEG power of other rhythms and in the left hemisphere also decreased, but the difference was not significant.

### *3.2. General locomotor activity*

The state of the central nervous system was estimated on the diurnal calm-activity dynamics and on the dynamics of the average activity of an animal.

The analysis of the diurnal dynamics of the locomotor activity shows three peaks in both groups of animals. At 7 time points, we observed a significant decrease of the general locomotor activity of rats receiving nano-$TiO_2$ with food, compared to the control group. ANOVA showed significant effect of factors "group" ($F(1, 162)=51.418$, $p=0.00000$) and "time" ($F(23, 162)= 5.8014$, $p=0.0000$) and no interaction of factors "group" and "time" ($F(23, 162)=0. 50708$, $p=0. 97079$)/

A similar situation was observed in the dynamics of the experiment, such as a significant decrease of the locomotor activity was revealed during the 7 days of the experiment. ANOVA showed significant effect of factors "group" ($F(1, 288)=12.054$, $p=0.0006$) "time" ($F(23, 288)=9.6768$, $p=0.0000$) and significant interaction of factors "group" and "time" ($F(23, 288)=2.084$, $p=0.003$).

## 4. Discussion

The rats which were given nano-$TiO_2$ showed a shift of the EEG spectra to low frequencies, which is consistent with behavioral data. Daily monitoring showed a reduction in the general locomotor activity of animals treated with nanosized titanium dioxide. Our studies also showed disorders of the bioelectrical brain activity associated with the general depression of the central nervous system. These results are consistent with the behavioral changes that revealed themselves in the reduction of locomotor activity. Taking into account the EEG data, this type of behavior probably should be regarded not as a calmer one but as a more depressed behavior.

The depressive effect of titanium dioxide nanoparticles on the CNS observed in our study might be related to neuronal damage caused by an increase in ROS as well as the impairment of synaptic transmission. [4]. Some studies show connection between amount of ROS and depression of long-term potentiation [10].

## 5. References

**[1]** Fedulov, A.V., Leme, A., Yang, Z., Dahl, M., Lim, R., Maria{Bibliography}ni, T.J., Kobzik, L., 2008. Pulmonary exposure to particles during pregnancy causes increased neonatal asthma susceptibility. American journal of respiratory cell and molecular biology 38, 57-67.

**[2]** Jin, S., Mo, B., Joon, Y., Hee, S., Won, H., Kang, S.J., Kim, B.M., Lee, Y.J., Hong, S.H., Chung, H.W., 2009. Titanium dioxide nanoparticles induce apoptosis through the JNK/p38-caspase-8-Bid pathway in phytohemagglutinin-stimulated human lymphocytes. Biochemical and biophysical research communications 386, 682-7.

**[3]** Li, N., Ma, L., Wang, J., Zheng, L., Liu, J., Duan, Y., Liu, H., Zhao, X., Wang, S., Wang, H., Hong, F., Xie, Y., 2009. Interaction Between Nano-Anatase TiO(2) and Liver DNA from Mice In Vivo. Nanoscale research letters 5, 108-115.

**[4]** Long, T.C., Saleh, N., Tilton, R.D., Lowry, G.V., Veronesi, B., 2006. Titanium Dioxide (P25) Produces Reactive Oxygen Species in Immortalized Brain Microglia (BV2): Implications for Nanoparticle Neurotoxicity. Environmental Science & Technology 40, 4346-4352.

**[5]** Long, T.C., Tajuba, J., Sama, P., Saleh, N., Swartz, C., Parker, J., Hester, S., Lowry, G.V., Veronesi, B., 2007. Nanosize Titanium Dioxide Stimulates Reactive Oxygen Species in Brain Microglia and Damages Neurons in Vitro. Environmental Health Perspectives 115, 1631-1637.

**[6]** Nemmar, A., 2002. Passage of Inhaled Particles Into the Blood Circulation in Humans. Circulation 105, 411-414.

**[7]** Soto, K.F., Carrasco, A., Powell, T.G., Garza, K.M., Murr, L.E., 2005. Comparative in vitro cytotoxicity assessment of some manufactured nanoparticulate materials characterized by transmission electron microscopy. Journal of Nanoparticle Research 7, 145-169.

**[8]** Swiler, D.R., 2005. Inorganic pigments, in: Kirk-Othmer Encyclopedia of Chemical Technology. John Wiley & Sons, Inc., Hoboken, NJ, USA.

**[9]** Zhu, R.-R., Wang, W.-R., Sun, X.-Y., Liu, H., Wang, S.-L., 2010. Enzyme activity inhibition and secondary structure disruption of nano-TiO2 on pepsin. Toxicology in vitro: an international journal published in association with BIBRA 24, 1639-47.

**[10]** Ott, M., Gogvadze, V., Orrenius, S., Zhivotovsky, B., 2007. Mitochondria, oxidative stress and cell death. Apoptosis 12, 913–922.

# Investigation of UV induced detoxication of chlorinated herbicides

N. Vershinin[*,1], I. Sokolova[*,1], O. Tchaikovskaya[1]

[1] *National Research Tomsk State University, Russia, Tomsk, Lenin Av. 36*

(*) N.Vershinin: nik_vershinin@mail.ru

(*) I.Sokolova: sokolova@phys.tsu.ru

*Keywords: Detoxication, herbicides, irradiation, exilamps*

## 1. Introduction

The use of herbicides in agriculture is accompanied by the rise of a wide range of environmental problems connected with their intake from soil into ground and surface waters. The application of a combination of physical-chemical methods and biodegradation is an advanced technology for destruction of organic compounds. Since the degradation processes of organic compounds can lead to the formation of substances with similar or greater toxicity than the organic matters, the need arises in search of more effective processes of transformation of pollutants into non-toxic matters or their mineralization [1].

## 2. Experimental

The degradation of herbicides 2,4-dichlorophenoxyacetic acid (2,4-D) and 3,6-dichloro-2-methoxybenzoic acid (dicamba) in water by combination of UV-irradiation and humic acids has been studied. The following lamps were used as radiation sources for photochemical studies: KrCl ($\lambda_{rad}$ = 222 nm), XeCl ($\lambda_{rad}$ = 308 nm) and $Xe_2$ ($\lambda_{rad}$ = 172 nm) exilamps [2]. The irradiation time of aqueous solutions was 1 – 60 min.

Electron absorption and fluorescence spectra of studied solution before and after irradiation were recorded with a UV spectrophotometer (Thermo Evolution 600 firm, United States) and a Cary Eclipse spectrophotometer (Varian firm, Australia).

In order to evaluate the toxicity of aqueous solutions, in this study we used a Microbiosensor bioassay on the basis of lyophisically dried Photobacterium phosphorium luminescent bacteria, which was performed at the Institute of Biophysics, Siberian Branch, Russian Academy of Sciences (Krasnoyarsk). The bioluminescent measurements were performed according to a standard technique, with a Cary Eclipse spectrophotometer in the bioluminescence mode. The toxicity of the photoproducts obtained was also examined by standard procedures adopted in the risk assessment (daphnids, algae) [3].

The chromate-mass-spectrometric analysis of samples for determining the concentrations of final products of phototransformation of pollutants after the UV treatment was performed using a Finnigan instrument of the Trace DSQ model (Thermo Electron Chromatography and Mass Spectrometry Division firm, United States). *Organizing Committee*

## 3. Results

The intensity ratio ($I/I_0$) at the maximum of the absorption bands of 2,4-D before and during the irradiation ($I_0$ = 222 nm) was determined for express quantitative assessment of the loss effectiveness of organic pollutants in water. It was also determined that the most effective reduce of the concentration of 2,4-D occurred when the Xe2 excilamp was active for 30 min.

Standard indicator such as the index of biodegradability (BI) defined by the ratio of biochemical oxygen demand (BOD5/COD) was used to assess the biodegradability of solutions of pollutants after physicochemical treatment.

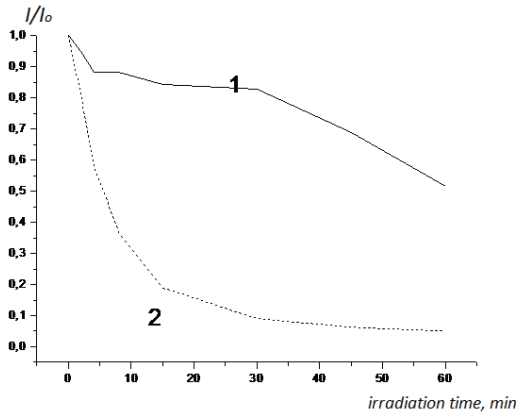


Figure 1. Kinetic curves of the loss in 2 x $10^{-5}$ M 2,4-D under irradiation KrCl (1) $Xe_2$ (2) exilamps.

Solutions are considered to be biodegradable at the extent of BOD5/COD ≥ 0,4. The value of BOD5/COD for irradiated solutions significantly increased as compared to unexposed one. However these values were below 0.4, i.e. the UV irradiation of the solution is 2.4-D for 120 minutes did not increase of the biodegradability.

This is because of several reasons. First of all, the complete transformation of 2,4-D does not occur within the specified time. Secondly, the main photoproducts that accumulate in the solution are a 2.4-dichlorophenol (2,4-DCP) which biological waste also requires some time for adaptation of the microorganisms-destructors.

Table 1. Values of the bioluminescence index BI of 2,4-D (C = 2 x $10^{-5}$ M)

| | **BI** |
|---|---|
| 2,4-D | 0,78 |
| 2,4-D + 60 min KrCl | 0,83 |
| 2,4-D + 120 min KrCl | 0,79 |

## 4. Discussion

Thus, we examined the adaptation method of the photochemical reactor in order to study the effect of different sources of UV radiation on subsequent biodegradation of organic compounds. The reactor is simple in design and does not require the addition of any chemicals and other oxidants, which is an integral part of the existing current oxidation technologies that involve the creation of hydroxyl radical. We obtained the following results:

Radiation of Xe2 excilamp allowed to mineralize 2,4-D and dicamba for 60 min.

Basic photoproducts were studied after irradiation by different sources of UV.

The assessment of the toxicity of solutions before and after UV treatment was provided.

## 5. References

[1]. G. Matafonova, V. Batoev, Chemosphere. **89** (2012) 637–647

[2] E. Sosnin, T.Oppenländer, V. Tarasenko, Photochem. Photobiol. C: Photochem. Rev., **7** , (2006) 145–163

[3] O. Tchaikovskaya, I. Sokolova, V. Svetlichnyi, E. Karetnikova, E. Fedorova, N. Kudryasheva, Luminescence. **22** (2007) 29 – 34

# DOS and electrical resistivity in disordered graphene at low temperatures

V. Egorushkin[1], N. Melnikova[2],A. Ponomarev[1], N. Bobenko[1*]

[1] *Institute of Strength Physics and Materials Science, Laboratory of Physics of Nonlinear Media, 2/4, pr.Akademicheski, 634021,Tomsk*

[2] *V.D. Kuznetsov Siberian Physical Technical Institute of Tomsk State University, Laboratory of newperspective materials. 1, ploschad' Novosobornaya, Tomsk 634050, Russia*

(*) corresponding author: @nlitvin86@mail.ru

*Keywords: graphene, low temperature, electronic transport properties*

## 1. Introduction

The low-temperature behavior of electrical resistance and electron density of states (DOS) in non-ideal graphene is shown to depend on its structure peculiarities such as concentration of impurities and structural defects of different types [1]. Doping and degassing also influences on the temperature dependence of DOS and resistivity and even may change the type of conductivity (semiconductor-metal) in graphene [2]. The study of DOS and resistivity in graphene is necessary to understand the processes of electron transport in graphene.

## 2. Calculations

### *2.1. Relaxation time*

The low-temperature peculiarities of electrical resistivity and DOS in graphene may be described in the frame of the temperature Green functions (GFs) method [3, 4]. The calculations of contribution to DOS and resistivity were carried out in the relaxation time approximation taking into account the multiple elastic scattering of electrons by impurities and structural inhomogeneities of short-range order. The obtained expression for the relaxation time is the following:

$$\frac{1}{2\tau} = \frac{1}{2\tau_{imp}}\left[1+\frac{1-c}{N}\sum_{i=0}^{N}\alpha_i BT\right].$$

Here $c$ is the concentration of impurities, $\alpha_i$ are the short-range order parameters, $N$ is the number of atoms in the range of structural inhomogeneity, $B = \pi\frac{R^2 m}{\hbar^2}k \approx 0.1\ \mathrm{K}^{-1}$, $N$ - number of atoms in the range of structural inhomogeneities, $R$ is the radius of the first coordination sphere and $m$ is electron mass. The inverse relaxation time of electron scattered only by impurities $\frac{1}{\tau_{imp}}$ is in order of $2\cdot 10^{15} s^{-1}$.

### *2.2. DOS*

The contribution to DOS in graphene is defined as follows

$$\Delta\nu = -\frac{1}{\pi}\mathrm{Im}\,Sp(\langle G\rangle - G_0),$$

where $G_0 = (\varepsilon - \varepsilon_p + i0)^{-1}$ is the electron GF in a perfect graphene, $\langle G\rangle$ is the averaged GF in a disordered graphene. Calculating $\langle G\rangle$ we also took into account the multiple elastic electron scattering by impurities and structural defects of short-range order type. Finely, $\varepsilon_p = \hbar k \upsilon_F$ is the electronic spectrum in ideal graphene plane near $\varepsilon_F$, and $\upsilon_F \approx 10^6 m/s$ [5].

The resulting expression of contribution to DOS in disordered graphene consists of two terms:

$$\Delta\nu = \frac{1}{\hbar^2 \upsilon_F^2}\left[\frac{\hbar}{2\tau}\ln\left(1+\frac{p_0\upsilon_F(p_0\upsilon_F-2\varepsilon))}{\varepsilon^2+\left(\hbar/2\tau\right)^2}\right)+ 2\varepsilon arctg\left(\frac{p_0\upsilon_F\left(\hbar/2\tau\right)}{\left(\hbar/2\tau\right)^2+\left(\varepsilon-p_0\upsilon_F\right)\varepsilon}\right)\right],$$

where $p_o$ is the Fermi momentum.

*2.3. Electrical resistivity*

Contribution to resistivity from electron scattering by impurities and structural inhomogeneities obtained with the help of the Drude formula is the following:

$$R(T) = \frac{m}{e^2 n}\left(\frac{1}{\tau_{imp}} + 2\pi U_0^2 \nu_0 \frac{c(1-c)}{N}\sum_i \alpha_i BT\right),$$

where $\nu_0 = \frac{m}{4\pi\hbar^2}$ is DOS at the Fermi level in ideal graphene (without defects), $U_0$ is the effective electron potential.

## Results

The resulting expressions for the contribution to DOS and electrical resistivity depend on concentration of impurities and the parameters of short-range order (structural heterogeneity). Analyzing these expressions we concluded the following:

1. Gas adsorption in graphene leads to appearance of a gap in the DOS at the Fermi level, which can be explained by the negative contribution to DOS from multiple elastic electron scattering by structural inhomogeneities of short-range order.

2. Change in the defect structure of graphene results in metallization of disordered graphene due to the increasing contribution to DOS at the Fermi level from the electron scattering by structural inhomogeneities of short-range order. This result is in a good agreement with data [2].

3. The value of $\Delta\nu(\varepsilon_F)$ increases when temperature rises in graphene without impurities (the case of metallization) and decreases in graphene saturated gas [6].

4. The sorption of gases results in the inverse temperature dependence of resistivity at low temperatures. This is in a good agreement with data [6].

5. The variation of the impurities concentration does not change the type of electrical resistivity in graphene - this is in a good agreement with data [7].

## 3. Discussion

The results of our calculations showed that the low-temperature behavior of electrical resistivity and DOS is determined by the short range ordered structure of non-ideal graphene. At the same time the change in concentration of impurities does not strongly influence on the low-temperature electrical resistivity and DOS.

## References

[1]. S.Yu. Davydov, *Physics and Technics of Semiconductors* . **46**, No **2**, PP 204-209 (2012).

[2]. S.Dröscher, P. Roulleau, F. Molitor, P. et all**,** *Appl. Phys. Lett*., **96**. PP. 152104-1-152104-3. (2010).

[3]. A.A. Abrikosov, L.P. Gorkov, I.E. Dzyaloshinskii, *Methods of quantum field theory in statistical physics,* (1962).

[4] V.E. Egorushkin, N.V. Melnikova, A.N. Ponomarev et al., *.J. Physics: Conference Series,* **248** PP. 012005 (2010).

[5]. P.R. Wallace, *Phys. Rev.,* **71**, PP. 622–634 (1947).

[6]. Y.-W. Tan, Y. Zhang, H.L. Stormer et all. *Eur. Phys. J. Special Topics,* **148**, PP. 15–18 (2007).

[7]. S.V. Morosov et al., *PRL,* **100**, PP 016602 (2008).

# Metal Nanoparticles Supported by Nanodiamonds as Novel Catalysts for Steam Ethanol Reforming Reaction

M.N. Efimov*, E.Yu. Mironova, M.M. Ermilova, N.V. Orekhova, L.M. Zemtsov, G.P. Karpacheva

*A.V. Topchiev Institute of Petrochemical Synthesis RAS, Leninskiy Prospekt 29, Moscow, 119991, Russia*

(*) corresponding author: efimov@ips.ac.ru

*Keywords: metal nanoparticles, nanodiamonds, catalyst, steam ethanol reforming*

## 1. Introduction

The method for the formation of metal-carbon catalysts with VIII group metals nanoparticles, fixed on detonation nanodiamonds (DND), for steam reforming of ethanol was developed. DND as the support for ethanol steam reforming catalysts are observed for the first time.

## 2. Experimental

Formation of metal-carbon catalyst occurs via IR pyrolysis of precursor. The compositions based on compounds of Pd, Ni, Ru (dissolved in DMFA) and DND were employed as the precursors. The sources of metals were Pd $(CH_3COO)_2$, $NiCl_2$, $RuCl_3$. The precursor was treated by ultrasonic during 2 hours. IR pyrolysis of precursor was carried out in a pulse photon annealing laboratory device at 700 °C for 2 min in an inert atmosphere.

## 3. Results and discussion

Infrared radiation can significantly reduce the time of pyrolysis (20-30 min), excluding the complex equipment and significantly reduce energy costs. Thus, the developed method of forming metal-carbon nanocomposites based on DND and metals of VIII group is effective and energy efficient.

The formation of chelate between metal ions and ether bonds presented on the surface of DND was shown with IR Fourier spectroscopy for nanocomposite DND/$NiCl_2$ which was taken as example. The distribution of metal particles was studied by transmission electron microscopy. It was shown that metal particle size depended on metal concentration in the precursor. Thus there were only very small metal particles (about 0.5–1.5 nm) in DND/Pd-Ru(1%) (fig. 1).

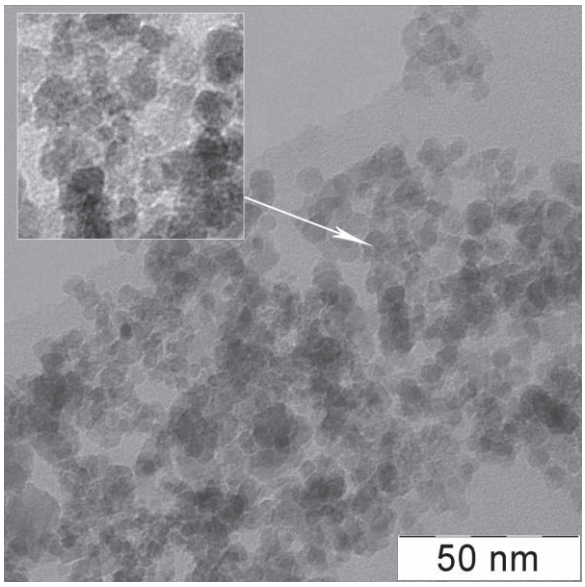


Figure 1. TEM image of DND/Pd-Ru(1%) sample.

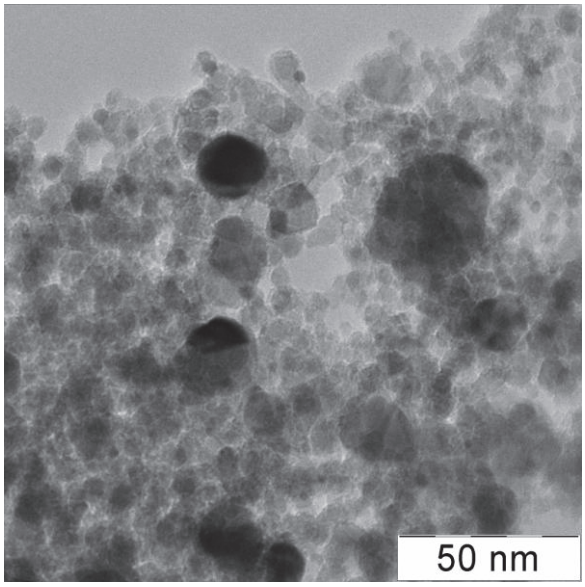


Figure 2. TEM image of DND/Pd-Ru(20%) sample.

And there were both types of nanoparticles in DND/Pd-Ru(20%): 1 nm and 15-20 nm (fig. 2).

The X-ray diffraction showed that there are reduced metals in the prepared nanocomposite for nanocomposites (for example DND/Pd and DND/Pd-Ru were taken). There were an alloy nanoparticles in the nanocomposite in case of the presence of two metals in the precursor (fig. 3).

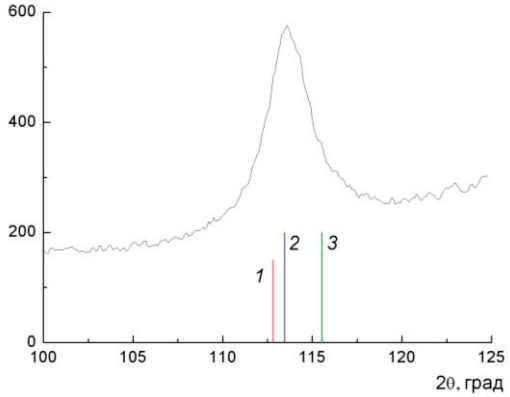


Figure 3. Part of X-ray diffraction pattern for DND/Pd-Ru(20%) sample. There is bar chart for Pd (*1*), $Pd_9Ru$ (*2*), $Pd_2Ru_{75}$ (*3*) phases.

The calculations of the structural characteristics of the metallic phase in nanocomposites were performed. And the Pd-Ru alloy is very similar to the intermetallic compound $Pd_9Ru$ (Table 1).

Table 1. Lattice spacing values of the metallic phase for bulk samples taken from the tables of ASTM and for nanoscale metal particles obtained by authors.

| **Sample** | **Lattice spacing *a*, E** |
|---|---|
| Pd (bulk) | 3.889 |
| $Pd_9Ru$ (bulk) | 3.875 |
| $Pd_2Ru_{75}$ (bulk) | 4.286 |
| DND/Pd | 3.881 |
| DND/Pd-Ru | 3.872 |

Applying metal-carbon nano-composite DND/Pd as heterogeneous catalyst in the reaction of steam reforming of ethanol caused considerable increase of ethanol conversion from 60 up to 90% in the temperature range 400–600 °C. The highest yield of hydrogen was achieved at 600 °C and it was 1.83 mol $H_2$/ mol EtOH. The catalyst DND/Pd-Ru was proved to be more effective than DND/Pd. The catalyst DND/Pd-Ru showed almost total conversion of the ethanol at temperature above 500 °C.

## 4. Acknowledgement

This work has been supported by the Russian Foundation of Basic Research, project 12-03-31432.

# Organoboron nanoparticles: size, geometry, electronic structure and chemical properties on the example of interaction with $ND_3$.

Slutsky V.G. [1], Grishin, M.V. [1], Kharitonov V.A. [1,*], Gatin A.K. [1], Shub B.R [1]

[1] *N. N. Semenov Institute of Chemical Physics, RAS,*

(*) corresponding author: vch.ost@mail.ru

*Keywords: carborane, organoboron, nanoparticles, STM, scanning tunnelling spectroscopy*

## 1. Introduction

Organoboron nanoparticles (OBN) are non-toxic, stable under normal conditions boron compounds. The physical properties of boron, for example, a large neutron capture cross section, or chemical properties of borohydrides such as high energy density at virtually any size of particles open up a wide range of possibilities for their use in the detection of neutron radiation [1], cancer treatment [2], creation of catalysts [3] and additives increasing energy density of fuels [4].

## 2. Experimental

In this study we explored size, geometry and electronic structure of individual organoboron nanoparticles synthesized from carborane $C_2B_{10}H_{12}$ by high-temperature pyrolysis of its vapors [4]. We also studied physical and chemical properties of nanostructured coatings based on organoboron nanoparticles. Mass-average size of single synthesized nanoparticles was 15.3 nm [5]. The elemental composition of synthesized OBN can be described as $C_{1.9\pm0.1}B_{10}H_{4.1\pm0.2}$ which fairly well-defined corresponds with given in [4,5] analytic expression $C_2B_{10}H_4$. The study of synthesized OBN was performed by use of ultra-high vacuum analytical complex which includes scanning tunneling microscope (STM), Auger spectrometer, mass spectrometer and accessories. Measurements were carried out under base pressure of 2 x $10^{-10}$ Torr at a temperature of 300 K. OBN nanoparticles were adsorbed on hot (T = 375 K) surface of highly ordered pyrolytic graphite (HOPG) from lyosol ($CCl_4$ solvent) in the air. Using of such techniques allowed us to create on the surface of graphite both uniform coating consisting of isolated nanoparticles and OBN films. Interaction of nanostructured surfaces with ammonia molecules ($ND_3$) at T = 700 K was also studied by means of analytical complex. Vladivostok, Russia).

## 3. Results and discussion

As a result of studies three types of OBN were observed on the graphite surface: spherical (75 - 80% of total) with diameter of 10 nm, concave lenticular (15 - 20%) of 22 nm and shapeless (less than 5%) with a typical size of about 50 nm. The "fine" texture in increments of about 1.5 nm is observed for first two types of OBN, which corresponds to the size of a single molecule of carborane $C_2B_{10}H_{12}$. Spectroscopic measurements in the STM revealed that spherical and lenticular OBN have metallic conductivity and OBN of third type has the semiconductor type. On the basis of data on the structure and electronic properties of each type of particle it is shown that spherical and lenticular OBN consist of partially dehydrated carborane molecules, and OBN of third type consist of carbon depleted carborane decomposition products.

Auger and mass spectroscopic investigation of interaction between the HOPG surface coated with an OBN film consisting mainly of particles of the first two types, with the $ND_3$ molecules was carried out. Experiment showed that at T = 700 K the decomposition of ammonia accompanied by the formation of molecular nitrogen $N_2$ and hydrogen in forms of $D_2$, DH, $H_2$ takes place in the processing chamber. In this case, the $D_2$ molecule consists of deuterium

atoms that were part of the ammonia molecule while DH and $H_2$ appear due to the partial substitution of protons in OBN by deuterium. Furthermore, some of the protons apparently either replaced by nitrogen atoms, or a $NH_2$ group. Though the electronic structure of the OBN films during the reaction remains unchanged which suggests maintaining the structure of OBN in reactions of this type.

## 4. References

[1].Caruso A. N., Billa R. B., Balaz S., Brand J. I., Dowben P. A. / / J. Phys.: Condens. Matter. 2004. V. 16. P. L139.

[2].Genady A. R. / / European Journal of Medicinal Chemistry. 2009. V. 44. P. 409.

[3].Zhao J., Huang P., Chen G., Zhan M. / / Inorganic Chemistry Communications. , 2012. V. 15. P. 321.

[4].Slutsky V.G., Tsyganov S.A., Severin E.S. et. al. / / Propulsion, Explosives, Pyrotechnics. 2005. V. 30. Number 4. P. 303.

[5]. Slutsky V.G. Grishin, M.V., Kharitonov V.A., Gatin A.K., Shub B.R., Ciganov S.A. / / Chem. Physics. 2013. In print.

# Electron traps in nanostructured oxides of tin and zinc

A.A. Kirsankin*, M.V. Grishin, L.I. Trakhtenberg, B.R. Shub

*Institut of chemical physics RAS, Moscow*

(*)corresponding author: kirsankin@mail.ru

*Nanostructure, adsorbtion, scanning tunnelling microscopy, surface*

## 1. Introduction

The sensitivity of up-to-date gas detectors based on films of semiconductors such as tin oxide ($SnO_2$) and zinc (ZnO) is determined by the change in the number of charge carriers, which occurs in the process of adsorption and desorption. Conduction electrons appear in process of thermal ionization of oxides structural defects whose energy levels are close to the bottom of the semiconductor conduction band. Formed by dissociative adsorption oxygen atoms capture electrons from the conduction band of the semiconductor, which reduce its conductivity. During the adsorption of gas molecules needed to be detected the reaction between them and oxygen adatoms take place. It forms desorbed oxygen molecules and electrons which enter conduction band. The current then increases, which is a sign of the presence of analyzed gas in the atmosphere. Consequently, the sensitivity of the sensor is determined by characteristics of the semiconductor layer such as position of energy level of the electron traps (correlating with structural defects and adatoms) and their rate of recharge. The most likely candidate for the role of electron trap in the oxide is an oxygen vacancy.

## 2. Experimental

Nanostructured film of oxides of tin ($SnO_2$) and zinc (ZnO) were prepared from the concentrated aqueous suspensions deposited to the surface of quartz glass. Structural features of the films were defined by use of atomic force microscopy. The characteristic size of tin oxide nanoparticles is approximately 100 nm. The film of zinc oxide has a similar structure, while there is a sufficiently large variation of ZnO nanoparticles size in a range of 100-200 nm. The film is non-uniform and has a large number of pores up to 500 nm.

To determine the physical characteristics of the electron traps based on oxygen atoms current-voltage dependence of the tunneling current were measured, which allowed to establish the position of the energy level and the recharging point dependence on the STM bias voltage. Given that in the spectroscopic measurements bias voltage $U$ is a linear function of time $t$ (i.e. $U = U_0 + \beta t$, where $\beta$ is scan speed voltage), the current-voltage dependences of the tunnel current can be converted into a current versus time.

## 3. Results

In our conditions for the electron trap (oxygen adatoms) located in a nanostructured film of tin dioxide at $\beta_1$ = 278 V / us, one can determine the position of energy level $E_e \approx 1$ eV and the characteristic time of the trap emptying $\tau \approx 2$ milliseconds. The same way as for the electron trap based on a structural defect in the zinc oxide film reduced in hydrogen one can set the position of energy level $E_e \leq 0.1$ eV and the characteristic emptying time $\tau \approx 20$ milliseconds.

This work was supported by RFBR grants 12-03-31411, 11-03-00342 and 13-03-00391.

# Low-temperature thermopower in disordered carbon nanotubes

V. Egorushkin[1], N. Melnikova[2], A. Ponomarev[1*], N. Bobenko[1]

[1] *Institute of Strength Physics and Materials Science, 2/4, pr.Akademicheski, 634021,Tomsk*
[2] *V.D. Kuznetsov Siberian Physical Technical Institute of Tomsk State University, 1, sq. Novosobornaya, 634050,Tomsk*

(*) corresponding author: alex@ispms.tsc.ru

*Keywords: carbon nanotubes, low temperature, electronic transport properties*

## 1. Introduction

One of the most attractive properties of electron transport in carbon nanotubes (CNTs) is thermoelectric power, which is very sensitive to the mechanisms of electron transport (ballistic, diffusive, hopping, etc.). We can say unequivocally that the low-temperature behaviour of thermoelectric power in the disordered carbon nanotubes has the following features:

• Thermopower increases nonlinearly with increasing temperature (at temperatures up to ~ 100 K).
• Saturation of the CNTs with nitrogen or oxygen changes the sign of thermopower, and the subsequent degassing of nanotubes by annealing at high temperatures again leads to a change in the sign of thermopower.
• The change in concentration of impurities and defects in the structure of the tube or the tube diameter, which is directly proportional to the chirality of the CNT, leads to the deviation of temperature dependence from the linear dependence which may be pronounced in different degrees.

## 2. Calculations

Let us use a well-known formula for thermopower given by

$$S = -\frac{\pi^2 T}{3e}\frac{d\ln J}{d\varepsilon_F}, \qquad (1)$$

where $J = \int \tau \vec{v}\vec{v}\frac{\partial f_0}{\partial \varepsilon}\frac{d\vec{p}}{(2\pi)^3}$, $\tau$ is the electron relaxation time, $\vec{v}$ is electron velocity, $\varepsilon_F$ is the Fermi energy and $\frac{\partial f_0}{\partial \varepsilon} \sim \delta(\varepsilon - \varepsilon_F)$.

The electron relaxation time and contribution to the electronic density of states (DOS) in the disordered carbon nanotubes were calculated in [1, 2] using the temperature Green's function taking into account the multiple elastic electron scattering on defects. The relaxation time and DOS depend on temperature, impurity concentration, short-range order parameters and chirality of CNTs.

We have obtained the following expression for thermopower of the disordered carbon nanotubes:

$$S(T) = -\frac{\pi k}{6e}\left[\left(\frac{a\gamma_0}{2\sqrt{3}C_h kT} - 1\right)^{-1} - \left(1 + \frac{1}{BT^{1/2}}\right)^{-1}\right], \qquad (2)$$

where $k$ is the Boltzmann constant, the chirality $C_h = a\sqrt{n^2 + mn + m^2}$ is connected with the diameter of nanotube $d$ as follows: $C_h / \pi = d$, $(n, m)$ are the indexes of chirality. Then $a$ is the lattice constant and $\gamma_0$ is the transfer integral between the first neighbor $p_z$ orbitals. Finally $B = \frac{2\sqrt{2\pi}(1-c)m^{3/2}}{\nu_0 N}\sum_i \alpha_i$, where $\alpha_i$ are the short-range order coefficients [3], $N$ is the number of atoms inside the structure inhomogeneity of the short-range order type, $m$ is mass of electron and $\nu_0 = \frac{p_0}{\pi^2\sqrt{3}a\gamma_0}\sqrt{p_0^2 - \left(\frac{2}{3d}\right)^2}$ is the density of states at the Fermi level and $p_0$ is the Fermi momentum for an ideal CNT.

The first term in (2) is connected with the contribution from DOS and the second term is connected with the contribution from electron relaxation time. These contributions have different signs and one of them increases and another one decreases when temperature rises. That is why in curve S(T) there is a maximum

which takes place when the velocities of change of these contributions are equal.

## 3. Results

Analyzing Eq. (2) we have found that at $\Sigma\alpha_i < 0$ (when S(T)<0) the derivative $\partial S(T)/\partial T$ does not have real (physical) roots that is why there are no any bending points in S(T). This result is in a good agreement with the experimental data [4] - the negative thermopower never has maximum or minimum in its temperature dependence!

Temperature of maximum in S(T) differs for different CNTs and depends on chirality and parameters of short-range order as it is shown in the Table 1.

Table 1. Temperature of maximum in S(T), in Kelvin, depending on parameter of short-range order $\Sigma\alpha_i$ and index of chirality $n$ (c=0.1).

| n \ $\Sigma\alpha_i$ | 0.05 | 0.1 | 0.15 | 0.2 | 0.25 |
|---|---|---|---|---|---|
| **6** | 70 | 87 | 88 | 85.6 | 82.1 |
| **8** | 48.3 | 63.7 | 66.4 | 65.4 | 63.4 |
| **10** | 35.8 | 49.8 | 52.9 | 52.8 | 51.6 |
| **12** | 27.9 | 40.5 | 43.8 | 44.1 | 43.5 |
| **16** | 18.5 | 28.9 | 32.2 | 33 | 33 |

From Table 1 one may see that the value of temperature of maximum $T_{max}$ decreases dramatically when index of chirality increases at the fixed $\Sigma\alpha_i$ and $T_{max}$ increases more slowly when $\Sigma\alpha_i$ rises at the fixed $n$. It means that the negative "structure" contribution defined by chirality, increases quicker than the contribution determined by the short-range ordering.

Thermoelectric power S(T) calculated for the (10,10) CNT for the different values of short-range order parameters and concentration of impurities, is shown in Fig. 1. As it was mentioned above the sum of parameters of short-range order is determined by the different types of defect structure of CNT and it may be as positive as negative, depending on what coordination sphere (the first or the second one) will be occupied by atoms of impurity or defects. From our data it is seen that thermopower is positive when defects are located mainly in the first coordination sphere and thermopower becomes negative at $\Sigma\alpha_i \le 0.1$ when the most defects are pushed out from the first coordination sphere.

Finally in the samples degased fully, thermopower becomes negative [4]. However we have found that the tendency to decreasing of S(T) takes place only for decreasing parameter of short-range order. As for concentration of impurities then the opposite effect occurs: S(T) is higher for CNTs with the lower concentration of impurities. It may mean that annealing regulates the short-range ordered structure of CNTs more strongly than the concentration of impurities.

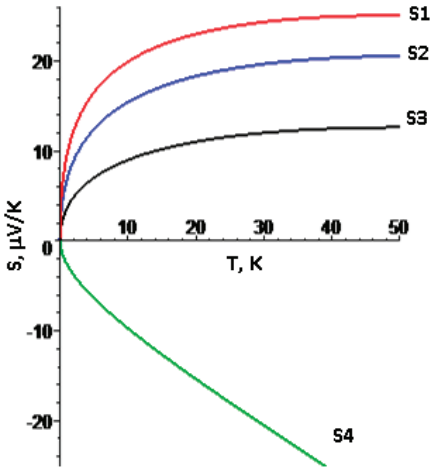


Figure 1. Temperature dependence of thermopower of the CNT (10,10), calculated for different values S(T) of short-range order: $\Sigma\alpha_i$=0.3 (S1), $\Sigma\alpha_i$=0.2 (S2), $\Sigma\alpha_i$=0.1 (S3) and $\Sigma\alpha_i$=-0.1 (S4).

## 4. Discussion

The results of our calculations showed that:

- The non-linear temperature dependence of thermopower is due to electron scattering on structural defects of CNTs. In an ideal CNT the dependence S(T) is linear.
- Decreasing of short-range order parameters results in the decreasing of a slope in the curve S(T) and even in the change of the sign of thermopower. These results correspond to the experimental data.
- Position of the bend or maximum with a subsequent change in the slope of the curve S(T) to the temperature axis is determined by chirality of CNTs and types of structural defects of nanotube.

## References

[1] V Egorushkin, N Mel'nikova, A Ponomarev and N Bobenko, *J. Mat. Sci. Eng.*, **1** PP. 161 (2011)

[2] V Egorushkin, N Mel'nikova, A Ponomarev and N Bobenko, *Phys Sci Appl*, **2**, PP. 224 (2012)

[3] V I Iveronova and A A Katsnelson, Short-range ordering in solid solutions (Moscow: Nauka) P. 256 (1977)

[4] R Jin, Z X Zhou, D Mandrus et al., *Physica B*, **388** PP. 326 (2007)

# Application of laser diffraction for evaluation of surfactants effectiveness in graphene nanoparticles aqueous suspensions stabilization

A.V. Nikolaeva[1], E.A. Danilov[*,1], V.M. Samoylov[1], L.S. Bekhli[2], V.P. Melnikov[2]

[1]*JASC "NIIgraphit" of Rosatom State Corp.,111524, 2, Elektrodnaya St., Moscow, Russia*
[3] *The Semenov Institute of Chemical Physics of RAS, 119991, 4, Kosygina St., Moscow, Russia*

(*) danilovegor1@gmail.com

*Keywords: graphene, graphite exfoliation, graphene nanoplatelets, laser diffraction, graphene suspensions*

## 1. Introduction

Numerous recently published studies([1],[2]) were aimed to obtain graphene particles via surfactant-assisted exfoliation of carbon materials aqueous suspensions via ultrasonication are of great interest as this technique is not only economically attractive but also facilitates further processing of the as-prepared graphene into various functional materials. Surfactants can however possess different effectiveness in terms of both stabilization and exfoliating strength.

In the present study laser diffraction technique was used to estimate the effectiveness of different surfactants for natural graphite exfoliation and stabilization of the respective aqueous suspensions.

## 2. Experimental

Pristine natural graphite (particle mean size 3 μm) was used as source material. Graphite was gas-thermally treated (ash content <0.01 mass.%). In order to investigate the influence of chemical structure on the exfoliation process three types of surfactants were used: aromatic cycle-containing (i.e. 3,4-diaminobenzene sulfuric acid (DABSA)), aliphatic (dioctylsulfosuccinate sodium salt (SDOSS)) and fluorinated aliphatic (1,1,11-trihydroeicosofluor sodium undecanolate polyglycidile ether (PGE-THEFU)) molecules, concentrations up to 0.6 mg/ml.

Fritsch Analisette A-22 laser diffraction particle size distribution device was used to evaluate the time stability of the graphene aqueous suspensions (residence time 1 to 90 minutes). Effectiveness of the surfactants was estimated using the differential particle size distribution curves evolution.

Exfoliation process was carried on using a horn-type ultrasonication device (output power 100W at 22.5 KHz) for 10 minutes to obtain 6 mg/ml aqueous suspensions.

## 3. Results

In order to investigate the influence of surfactants' hydrophobic part structure on the effectiveness of graphite exfoliation the stability of graphene suspensions 3 categories of surfactants were used. Particle size distribution curves and their evolution provide valuable information on graphene platelets mean size as well as on the process of their agglomeration.

As can be seen from Fig.1 (a) and (b), using aromatic surfactants (DABSA) nice relatively sharp distribution about 3 μm was obtained leading to only modest agglomeration within 90 min (slight shift of the main peak to around 9μm with only a small additional peak at over 100 μm). This behavior does not significantly depend on the number of aromatic rings in the molecule.

Both anionic and non-ionic fluorinated surfactants (i.e. PGE-THEFU) behaveanalogously (see Fig.1 (c), (d)). The difference in the extent of fluorination leads however to the difference in suspension stability: the less fluorine atoms surfactant molecule contains the worse the stability.

Non-fluorinated aliphatic surfactants of low molecular weight show poor

effectiveness as both exfoliating (wide distribution on fig.1 (e)) and stabilizing (large fraction of agglomerates with mean size of over 500 μm on fig. 1 (f)) agents which is in respect with other studies ([3]).

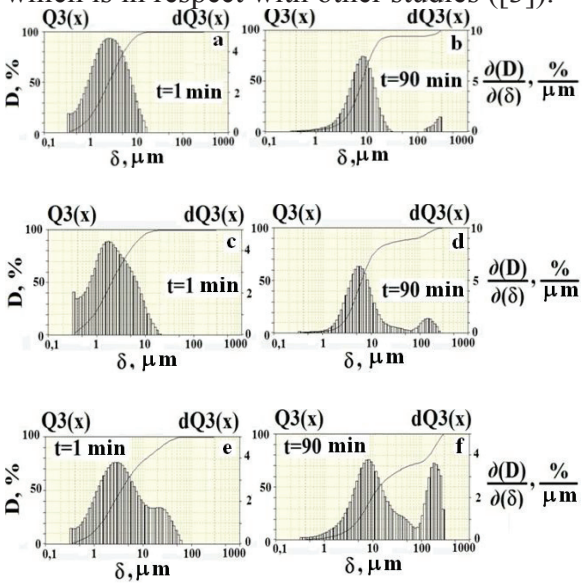


Figure 1. Graphene nanoplatelets particle size distribution curves within: (a), (c), (e) – 1 min.; (b), (d), (f) – 90 minutes after the sonication. Curves (a), (b) – DABSA, (c), (d) – PGE-THEFU, (e), (f) – SDOSS (see text).

In order to access whether the miccellization or surface charge creation are responsible for the surfactant's effectiveness surface tension tests were carried on for aqueous solutions of the studied surfactants. Fig.2 clearly shows that this is not the case. Best stabilizers possess insignificant surface tension depression whereas SDOSS having rather low surface tension in water solutions is a weak stabilizer for graphite exfoliation. It is thus crucial to consider the chemical interactions between the hydrophobic part of the surfactant molecule and graphene plane to be able to predict the effectiveness of the surfactant for natural graphite exfoliation.

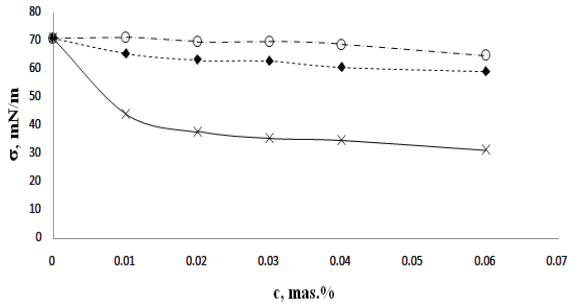


Figure 2. Specific surface tension for different surfactants aqueous solutions: ○-PGE-THEFU, ♦-DABSA, ×-SDOSS.

Figure 3 reveals the morphology of the obtained particles. From the left side of the picture it can be clearly seen that the product obtained via exfoliation is indeed a suspension of few-layered graphene platelets with the mean size of about 1-3 μm. Electron diffraction pattern supports this point as it can be concluded [4] that nanoplatelets consist of 2-5 graphene sheets.

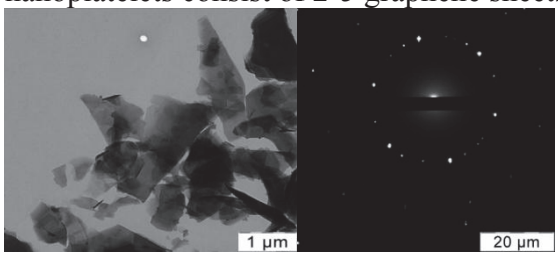


Figure 3.TEM image (left) of the obtained graphene nanoplatelets and electron diffraction pattern for one of the platelets (right).

## 4. Discussion

As a result of studying particle size distribution curves and their evolution via laser diffraction technique for surfactant-assisted graphene platelets aqueous suspensions preparation we were able to conclude that the best surfactants should contain either aromatic or fluorinated fragments in the hydrophobic part of the molecules as it should increase the energy of interaction between the surfactant and graphene plane. Specific surface tension of surfactants is not too significant a factor for consideration. Therefore, estimation of the effectiveness of surfactants for graphite exfoliation in aqueous suspensions should be based on direct observation of particle size distribution rather than on the properties of the isolated surfactants. The advantage of laser diffraction technique is that it is an express and direct method for such type of analysis.

## 5. References

[1]. Y.Sim, J. Park, Y.J. Kim et al.*J.Kor. Phys. Soc.* **58 (4)** (2011) pp. 938 – 942

[2]. S.Lin, C.J.Shih, M.S. Strano, D. Blankschtein. *J. Am. Chem. Soc.***133 (32)** (2011) pp.12810–12823

[3]. M.J. Fernandez-Merino, J.I. Paredes, S. Villar-Rodil et al. *Carbon* **50** (2012) pp.3184-3194

[4]. H.J. Park, J. Meyer, S. Roth, V. Skakalova. *Carbon* **48 (4)** (2010) pp.1088-1094

# Size-effects in catalytic properties of nanoparticles of silver and gold in reaction of hydrogen isotopic exchange

M.O. Sergeev[1], A.A. Odintsov[1], A.V Malyutin[1], A.G. Koshkin[1], E.Y. Lieberman[1], A.A. Revina[1.2], K.N. Zhavoronkova[1], O.A. Boeva[1]

[1]*Russian University of chemical technology of D. I. Mendeleev*
[2] *Institute of physical chemistry and electrochemistry of A. N. Frumkin, RAS*

*Keywords: 6 maximum, one single line maximum (font style: Times italic 10pt)*

## 1. Introduction

The size effects in the properties of nanostructures means their reactivity is different from the reactivity of solid metal, and the bigger, the smaller the particle size [1].

As objects of study the metals of IB group were chose, namely silver and gold. As it well known, a massive noble metals studied previously in the form of films, prepared by evaporation from sample and deposition in high vacuum, don′t adsorb hydrogen at below room (or more high) temperatures, and thus do not catalysis the reaction of H − D exchange at low temperatures on metals.That′s why it was interesting to know if there is a size influence on catalytic activity of this metals.

To study the size effects in catalytic properties of metals is hydrogen isotope exchange reaction of $H_2$+ $D_2$ ↔2HD was used, as a structurally sensitive reaction, as well as the simple and convenient enough for studies of catalytic properties of nanostructured composite systems. In addition, hydrogen isotope exchange reaction can be seen as a test for the characteristics of the activity of the catalytic systems for other reactions, involving hydrogen.

To get the metal nanoparticles with a narrow size distribution used the synthesis of particles in reverse micelles [2, 3].

Silver nanoparticles obtained by radiation-chemical and chemical methods of reduction of metal ions in reverse micelles solutions (RMS) $AgNO_3/H_2O$/Bis(2-ethylhexyl) sulfosuccinat sodium (AOT)/isooctane with different values for the coefficients solubilisation ω = 1, 2, 4 and 8. Solubilisation factor ω represents the ratio of the number of moles of water to moles number of surface active substance (SAS). Nanoparticles of Au obtained by a chemical reduction process in a SID $AuCl_3$ /$H_2O$/AOT/isooctane with ω = 1, 3 and 5.

In a chemical way NP in RMS as a reductant used quercetin is a substance of class of flavonoids with high rehabilitation potential.

The radiation-chemical method reduction of metal ions occurs by ion and radical particles that are generated by ionizing of γ- radiation $^{60}Co$ source.

Formation, stability over time and changing the content of NP as a result of adsorption in contact with support controlled by spectrophotometry on the Hitachi U-3010 by the presence of characteristic peaks for silver and gold nanoparticles in optical absorption spectra.

Size and differential distribution by size of NP were determined by atomic force microscopy (AFM) on the Enviro Scope 5.30 (Bruker). Resolution on an axis Z is 0.1 NM Dimensions of NP are presented in table 1. Solubilization factor increases − the size of nanoparticles Ag in RMS increases, and increases the size of nanoparticles and Au when increasing ω from 1 to 4 is growing disproportionately, and a value of ω = 5 size nanoparticles Au in reverse micelle drops to 1 nm.

For study of adsorption and catalytic properties of nanoparticles of silver and gold they were put on the surface of the γ-$Al_2O_3$ (mark "Shamrock", $S_{sp}$= 220 $m^2/g$, Redkinskij catalyst plant).

Table 1. Dependence of size of NP on ω

| ω | Diameter of NP Ag, nm | | Diameter NP of Au, nm |
|---|---|---|---|
| | First peak | Second peak | |
| 1 | 0.6 | 1.1 | 0.9 |
| 2 | 1.3 | 1.7 | 3.4 |
| 3 | - | - | 4.1 |
| 4 | 4.4 | 5.6 | 18 |
| 5 | - | - | 1.0 |
| 8 | 12 | 27 | |
| 20 | 20 | | |

Specific surface area of nanoparticles was measured by hydrogen hemosorbtion (77 K). Isotherms of adsorption of hydrogen on NP are expressed plateau at sufficiently high equilibrium pressure– $10^{-2} \div 10^{-1}$ Torr, which is unusual for massive metals.

Catalytic studies were carried out in the temperature range of 77-300 K.

Viewed:

1. Reducing the size of massive silver and gold to size of nanoparticles 30 nm or less results in the appearance of fine silver and gold adsorption and catalytic properties at low temperatures.

2. At temperatures 150 – 77 K isotope exchange reaction to molecular hydrogen leaks practically with no activation energy, in temperatures from 150 to 300 K the activation energy is 8-12 kJ/mol.

3. With the increase in temperature the hydrogen adsorption decreases on the surface of the nanoparticles.

4. When reducing the size of silver nanoparticles from 20 up to 1 nm specific catalytic activity increases several times, the dependence of the Kud from nanoparticles.

5. Catalytic systems based on Ag and Au nanoparticles in their specific catalytic activity is approaching to high active platinum catalysts.

This work is supported by RFBR grant 11-03-90738.

## 2. References

[1] Сергеев Г.Б. Размерные эффекты в нанохимии//Рос. хим. ж. 2002, т XLVI, №5. С. 22-29.

[2] Ревина А.А. Препарат наноразмерных частиц металлов и способ его получения. Патент РФ №2312741. Бюл. 35. 2007.

[3] Ревина А.А. Препарат наноструктурных частиц металлов и способ его получения. Патент РФ №2322327. Бюл. 11. 2008.

# The role of lithium tetrahydroaluminate in the formation of nanoscale hydrogenation catalysts

Yu.Yu. Titova[1*], L.B. Belykh[1], F. K. Shmidt[1]

*Irkutsk state university, catalysis laboratory, Russia, 664003, Irkutsk, K.Marx st., 1*

(*) corresponding author: ytitova60@gmail.com

*Keywords: $LiAlH_4$, hydrogenation, catalysis, nanoparticles, reduction, activation*

## 1. Introduction

Among the many catalytic hydrogenation systems special place is occupied by the systems comprising available complex hydrides, in particular, $LiAlH_4$ and its derivatives as reducing agents. Despite $LiAlH_4$ is used as the reducing agent more than a half century, the data concerning the properties of formed in conjunction with $LiAlH_4$ metallic catalysts in the literature is scattered and often contradictory. The report presents the results of the study of formation mechanism, nature and properties of nanoscale catalytic hydrogenation catalysts based on nickel, cobalt and palladium acetylacetonates in combination with $LiAlH_4$ and alkoxyhydride derivatives.

## 2. Experimental

Solvents, substrates and reagents were purified by standard procedures used for handling of organometallic compounds. For more thorough drying, benzene and toluene were additionally distilled over $LiAlH_4$ on a rectification column and stored under argon in sealed tubes over molecular sieves 4Å. THF after removal of peroxides was successively distilled over sodium, $LiAlH_4$ and benzophenone ketyl, and stored under argon in sealed tubes. All the prepared and synthesized reagents were kept under argon in sealed ampoules. Standard vacuum techniques were used in the manipulations of volatile and air-sensitive materials.

Catalytic reactions were carried out in a thermostated vessel of the "duck" type at starting pressure of hydrogen of 2 Torr. The process of hydrogenation was followed by dropping of pressure using manometer and by GC method.

$^{1}H$, $^{31}P$, $^{27}Al$ NMR spectra were registered on a pulse spectrometer VXR-500S Varian. IR spectra were taken in KRS (0.2 mm thickness) or KBr (0.112 mm thickness) cuvettes pre-blown with argon, on a FT-801 IR. UV spectra were recorded with an "SF-2000" spectrometer. Size and nature of nanoscale particles was studied by X-ray phase analysis (DRON-3M) and TEM (Philips EM-410).

## 3. Result

The basic factors that influence on the properties of Ni, Co, Pd nanoparticles formed under the action of $LiAlH_4$, in the alkenes hydrogenation have been studied. Extreme nature of the TOF dependence on the reagent ratio $LiAlH_4$ / M (M = Pd, Co) has been established (Fig. 1).

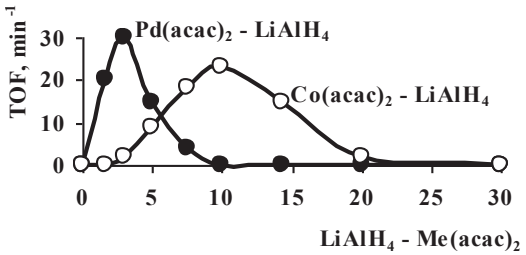


Figure 1. Dependence of the catalytic activity of the Pd and Co catalysts in styrene hydrogenation on the ratio $LiAlH_4$ /M ($C_M$ = 5 mmol/l, [substrate]/M(acac)$_2$ = 170, solvent – benzene, T = 30 $^0$C, = 1 atm).

It has been shown that using reagents purified from water and other impurities it is impossible to obtain a hydrogenation catalyst in the Ni(acac)$_2$ - $LiAlH_4$ system in benzene-THF mixture at any ratio of reagents.

A promoting effect of proton donating compounds on the properties of $M(acac)_2$ - $LiAlH_4$ systems has been revealed (Fig. 2).

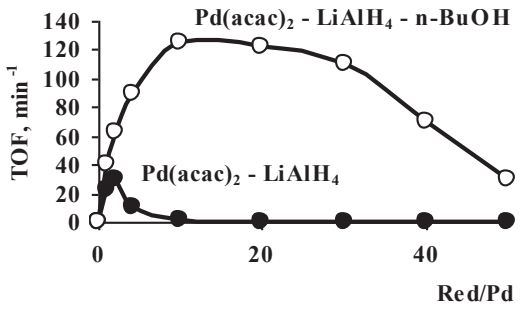


Figure 2. Hydrogenation of styrene in the presence of $Pd(acac)_2$ –Red catalytic systems ($C_{Pd}$ = 5 mmol/l, [substrate]/$Pd(acac)_2$ = 170, solvent – benzene, T = 30 $^0$C, $P_{H_2}$ = 1 atm).

Among the tested proton donors (alcohols, acids, phenol), *n*-butanol has the largest promoting effect. As a result of activation of metal nanoparticles by alcohols the $LiAlH(OR)_3$ formation is registered in the reaction system.

According to the TEM results, nanoparticles of 2-5 nm in diameter are formed as a result of metal acetylacetonates reaction with $LiAlH_4$. The amount of hydrogen liberated in the redox process in 2-8 times higher than the theoretically predicted one:

$$M(acac)_2 + 2LiAlH_4 = 1/n(M_n)_{coll.} + 2Li(acac) + 2AlH_3 + H_2$$

The $^{27}$Al NMR method shows that the $LiAlH_4$ alcoholysis leads to a mixture of $LiAlH_{4-x}(OR)_x$. Composition of alcoholysis products depends on the nature and concentration of alcohol (x=0-4).

The order of the reducing ability and inhibiting effect of $LiAlH_4$ and it alkoxyhydride derivatives on TOF is $LiAlH_4$ >> $LiAlH_2$(*tert*-BuO)$_2$ > $LiAlH$(*tert*-BuO)$_3$.

## 4. Discussion

Analysis of the above catalytic experiments indicates the inhibitory effect of $LiAlH_4$ excess. The reason is that nanoparticles catalyze the decomposition of not only the formed alane to elements:

$$[AlH_3]_n \xrightarrow{M} nAl + \frac{3n}{2}H_2$$

but also $LiAlH_4$:

$$LiAlH_4 \xrightarrow{Ni} LiH + AlH_3$$
$$\underline{LiAlH_4 + 2LiH \xrightarrow{Ni} Li_3AlH_6}$$
$$3LiAlH_4 \xrightarrow{Ni} Li_3AlH_6 + 2AlH_3$$

Thus, the $LiAlH_4$ function is not only reduction of the metal precursor. Tetrahydroaluminate anions act as stabilizers for the metal nanoclusters adsorbing on its surface. The tetrahydroaluminate anions and, probably, the products of its catalytic decomposition block active sites of the surface being the catalytic poisons.

The activating effect of proton donating compounds is caused by the chemical bonding of catalyst poisons in the $LiAlH_4$ alcoholysis.

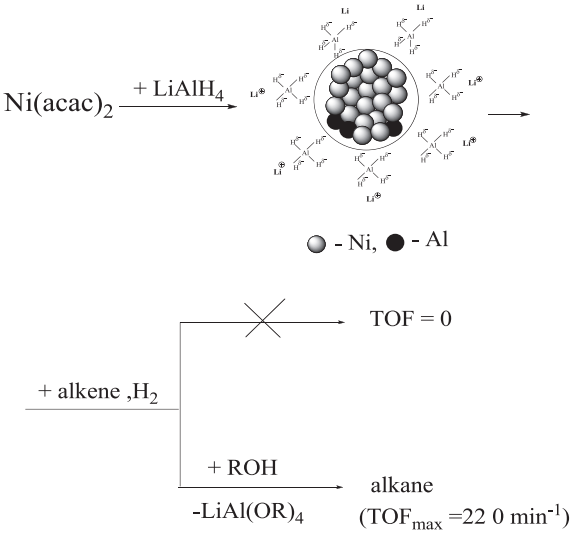


The strategy allowing obtaining good reproducible and highly efficient nanoscale catalysts on the base of nickel, cobalt and palladium acetylacetonates and $LiAlH_4$ has been proposed. The obtained nickel catalysts substantially exceed not only the similar systems based on the Fe triad, but also the palladium catalysts in activity in the alkenes hydrogenation [1].

The study was supported by The Ministry of education and science of Russian Federation, project 14.B37.21.0795.

## 5. References

[1]. Belykh L.B., Titova Yu.Yu., Umanets V.A., Rokhin A.V., Schmidt F.K. // Applied Catalysis A: General. – 2011. – Vol. 401. - P 65– 72.

# The interaction of nanocluster polyoxometalates with different substances

M. Tonkushina[1,2], A. Ostroushko[1], N. Moricheva[1], A. Safronov[1]

[1] *Ural Federal University named after First President of Russia B.N. Yeltsin, Institute of Natural Science, 620002, ul. Mira, 19, Ekaterinburg, Russia*

[2] *Institute of Immunology and Physiology, Russian Academy of Sciences Ural Branch, 620049, ul. Pervomayskaya, 106, Ekaterinburg, Russia*

(*) corresponding author: Rita-zar@yandex.ru

*Keywords: polyoxometalate, enthalpy, nanocluster, polymer-salt composition, calorimetry.*

## 1. Introduction

Nanocluster polyoxometalates on the basis of molybdenum represent a continuously inriched class of compounds, attracting the attention of scientists from different countries by its highlysymmetric structure and huge for inorganic molecules size. There is a possibility of easy modification of their structure that allows to control physical and chemical properties. Representatives of this class can be divided according to the form of the molecule on the spherical (or close to it) and toroidal [1].

Such clusters are composed of oxygen-molybdenum polyhedra and other metals, and stabilizing ligands – organic and inorganic acids, water. Their synthesis is performed by selfaggregation in aqueous solution. Thanks to its structure, nanocluster polyoxometalates are perspective as catalysts of fine organic synthesis, sorbents and molecular sieves (due to the presence of pores in the surface of the strictly a certain size), as components of the sensors and functional materials. The availability of the internal cavity, allows to consider them as nanocontainer.

The unique structure generates the unique physico-chemical properties of such compounds, but they are studied not sufficiently. From already known, I would like to note the unique structure of water in spherical nanoclusters, the ability of nanoclusters to aggregate in the solution into the hollow spherical globules of sizes ranging from 50 to 1000 nm, photo and thermal stabilization of polymers, the ability to form complexes with surface-active substances and water-soluble polymers.

## 2. Experimental

Synthesis of polyoxometalates $(NH_4)_{42}[Mo^{VI}_{72}Mo^{V}_{60}O_{372}(CH_3COO)_{30}(H_2O)_{72}]\cdot 300H_2O\cdot 10CH_3COONH_4$ ($Mo_{132}$) and $[Mo_{72}Fe_{30}O_{252}(CH_3COO)_{12}\{Mo_2O_7(H_2O)\}_2\{H_2Mo_2O_8(H_2O)\}(H_2O)_{91}]\cdot 150H_2O$ ($Mo_{72}Fe_{30}$) was performed according the method described in the papers [2,3]. Ammonia heptamolybdate $(NH_4)_6Mo_7O_{24}\cdot 4H_2O$ (chemically pure), hydrazine sulfate $N_2H_4\cdot H_2SO_4$, ammonium acetate $CH_3COONH_4$ (reagent grade), sodium chloride NaCl (pure for analysis), glacial acetic acid, sodium acetate $CH_3COONa$ (analytical grade), hydrochloric acid HCl (special purity), and iron (III) chloride $FeCl_3\cdot 6H_2O$ (Panreac, main matter content 97-102 mass percent) served as initial agents.

To obtain polymer compositions polyvinylpyrrolidone (K 29-32, Acros Organics) was taken. The compositions were prepared by drying the nanocluster-polymer water solutions.

Thermal effects were measured by the method of isothermal calorimetry with the help of microcalorimeter DAK-1-1.

Enthalpies of dissolution of the nanocluster–polymer compositions were determined calorimetric. Then they were recalculated into the enthalpies of interaction by the following formula:

$$\Delta H_{int.} = \omega_1 \Delta H_1 + (1-\omega_1)\Delta H_2 - \Delta H_3,$$

where $\Delta H_1$, $\Delta H_2$ and $\Delta H_3$ - enthalpies of dissolution of the polyoxometalate, polymer and composite film, respectively; $\omega_1$ - mass fraction of cluster in this film.

## 3. Results

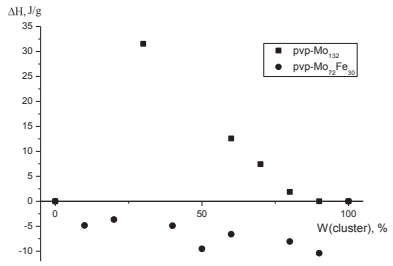


Figure 1. The enthalpy of interaction of $Mo_{132}$ and $Mo_{72}Fe_{30}$ with polyvinylpyrrolidone.

Table 1. Enthalpy of interaction of $Mo_{132}$ with organic compounds.

| Растворитель | enthalpy of interaction (J/g) | molecular weight (g/mol) |
|---|---|---|
| water | -38,1 | 18 |
| ethanol | -24,3 | 46 |
| n-butanol | 0,2 | 74 |
| t-butanol | 5,8 | 74 |
| carbon tetrachloride | 2,7 | 154 |
| hexane | 11,6 | 86 |

## 4. Discussion

As can be seen from the figure 1, interaction of polyoxometalates with polyvinylpyrrolidone occurred in different ways from the thermodynamics point of view. The enthalpy of interaction of $Mo_{132}$ with polyvinylpyrrolidone is positive in all the range of compositions, which speaks of energy unprofitableness of formation of the complex cluster – polymer. The enthalpy of mixing of $Mo_{72}Fe_{30}$ with polyvinylpyrrolidone is negative. If we turn to the structure of nanoclusters, we can see that they are very similar. The difference is the presence in the $Mo_{72}Fe_{30}$ oxygen polyhedra of iron, which causes the differences in interaction with polymer. As we know from the literature, terminal oxygen ligands belonging to the molybdenum are inactive and are not inclined to protonation. Surface oxygen, associated with iron is a part of the water molecules, or OH groups:

$$\cdots Fe^{III}(OH_2) + H_2O \Leftrightarrow \cdots Fe^{III}(OH)^- + H_3O^+,$$

such surface groups are much more inclined to associate with polymer molecules. The introduction of iron–oxygen polyhedra in a cluster framework is a modification of the surface of the cluster, which entails the change of the properties of the whole cluster. Thus, we get an opportunity to control the properties of the surface of the nanocluster by the introduction of the hetero elements in the composition.

It is also interesting to study the interaction of nanocluster polyoxometalates with organic compounds. Earlier the ability of nanocluster $Mo_{132}$ to absorb organic solvents from the vapor phase of both surface and internal cavity was shown [7]. In the internal cavity the organic compounds are held better and are only removed when heated. In this paper, we continue the study of the interaction of nanocluster polyoxometalates with a number of organic solvents, polar and non-polar but now they are in a liquid state. Nanocluster was dried at the temperature of $100^0$C, to remove the water, both from the surface and from the internal cavity, without destroying the structure. The data obtained are presented in the table 1. From the table it can be seen that the energetically favourable interaction occurs with water and ethanol. The value of enthalpy of interaction depends on the molecular weight and surround the size of the molecule of organic compound. In a series of water, ethanol, n-butanol enthalpy is growing. Also occurs for n-butanol, t-butanol. Positive enthalpy of interaction of nanocluster with non-polar compounds is also clear. Sorption is possible due to physical factors, but there are no possibilities to the formation of chemical bonds.

## 5. References

[1]. Müller A., Gouzerh P., Chem. Soc. Rev. 41 (2012) 7431-7463.
[2]. Müller A., Krickemeyer E., Bögge H., Schmidtmann M., Peters F., Angew. Chem. Int. Ed. 37 (1998) 3360–3363.
[3]. Müller A., Sarkar S., Shah S.Q.N., Bögge H., Schmidtmann M., Sarkar Sh., Kögerler P., Hauptfleisch B., Trautwein A.X., Schünemann V., Angew. Chem. Int. Ed. Engl. 38 (1999) 3238–3241.

# Mechanochemical synthesis of $Mo_2C$-carbon composite powders

A. Vasilevich*, O. Baklanova, A. Lavrenov, O. Knyazheva, E. Buluchevskii, N. Leontyeva, V. Likholobov

*Institute of Hydrocarbons Processing SB RAS, 644040 st. Neftezavodskaya, 54, Omsk, Russia.*

(*) corresponding author: vasilevich.ihcp@mail.ru

*Keywords: mechanosynthesis, molybdenum carbide, carbon black.*

## 1. Introduction

Transition metal carbides are considered as the new promising catalysts and have been widely investigated in recent years because of their unique electronic structure and high performance [1]. Molybdenum carbides, with their resemblance in electronic structure to noble metals [2], have similar catalytic properties to noble metal catalysts in various organic chemical reactions [3]. It makes molybdenum carbides be a promising substitute for noble metal catalysts in the future. These catalysts show good catalytic activity and selectivity in hydrogenation, hydrodesulfurization, and hydro-denitrogenation in petroleum refining [4].

The main method for synthesizing such molybdenum carbides currently is temperature-programmed reaction method via carbonization of molybdenum trioxide with gas hydrocarbon, such as methane, ethane, butane and their gas mixtures. In this work of molybdenum carbides were prepared using the mechanosynthesis. The structure and catalyst activity of the molybdenum carbides were also studied.

## 2. Experimental

### *2.1. Mechanosynthesis under air atmosphere*

Molybdenum (VI) oxide, zinc and carbon black powders with a molar ratio as shown in Table 1 were ball milled using a АГО-2 type planetary ball mill with stainless steel vials and balls under air atmosphere. The rotation speed of the mill was 1000 rpm and the ball-to-powder mass ratio was about 40:1.

Table 1. Composition of obtained samples.

| № | Molar ratio of powders | | |
|---|---|---|---|
| | $MoO_3$ | C | Zn |
| S1 | 1 | 1.34 | 3 |
| S2 | 1 | 46.4 | 3 |
| S3 | 1 | 7.8 | 3 |
| S4 | 1 | 1.34 | - |

### *2.2 Mechanosynthesis under argon atmosphere*

Sample S5 was prepared using the standard incipient wetness method. Molybdenum was impregnated at 10 wt. % on carbon black using a aqueous solution ammonium heptamolybdate tetrahydrate (Aldrich, 99.98%) $(NH_4)_6Mo_7O_{24}\cdot 4H_2O$ then the sample was dried at 120°C. Obtained sample was performed in a planetary ball mill under argon atmosphere. The rotation speed of the mill was 1000 rpm and the ball-to-powder mass ratio was about 40:1. Sample was heat treated at 800 °C for half an hour in an argon atmosphere.

Sample S6 was obtained by mechanosynthesis of ammonium heptamolybdate tetrahydrate and carbon black powders with a molar ratio of Mo:C as 1:3.6.

All obtained samples were characterized by XRD using a D8 Advance Bruker (40 kV and 40 mA) diffractometer with Cu Kα radiation (λ = 0.154 nm).

### *2.3 Measurements of catalyst activity for dibenzothiophene hydrodesulfurization*

The model feedstock was a heptane solution of 1 % 1-methylnaphtalene and 1 % dibenzothiophene. The model reaction was performed at 320°C, under a hydrogen atmosphere of 3.5 MPa.

## 3. Results and discussion

The diffractograms of the samples obtained by ball milling for 0.5 h under air atmosphere are shown in Fig. 1.

The stoichiometry of Mo:Zn:C=1:3:1.34 is molar ratio and selected to give the $Mo_2C$ carbide on the following reaction:

$$MoO_3 + 3Zn = Mo + 3ZnO$$

$$2Mo + C = Mo_2C$$

The diffraction patterns of samples S2, S3 and S4 were not observed $Mo_2C$ phase.

Fig. 2 shows the XRD patterns of the S5 and S6 samples after milling under argon atmosphere for 0.5 h. XRD data confirmed the presence of the expected $Mo_2C$ phase only in case of S1 and S5 samples.

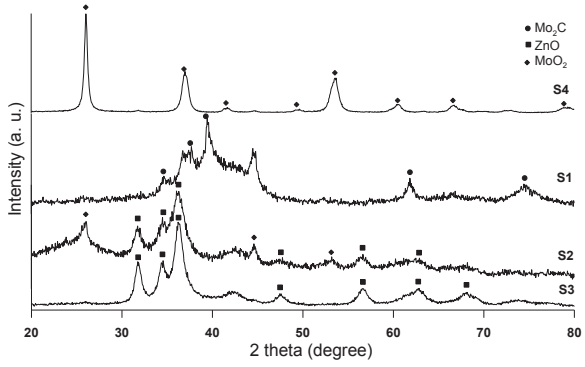


Figure 1. XRD patterns of samples S1 to S4.

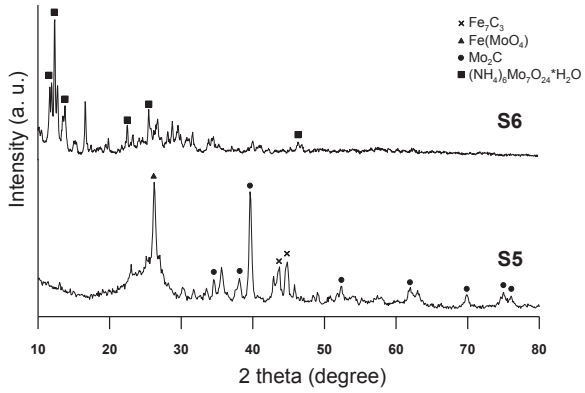


Figure 2. XRD patterns of samples S5 and S6.

Table 1 shows the activity for hydrotreating of 1-methylnaphthalene and dibenzothiophene.

All catalysts demonstrated high hydrodesulfurization activity conversion of dibenzothiophene about 90-93%.

It should be noted, that the hydrogenation activity for catalysts (S1 and S5) has very low.

Table 2. Distribution of products from hydrotreating of model feedstock

| **Catalyst** | **S1** | **S5** |
|---|---|---|
| Hydrodesulfurization, % | 92.8 | 89.5 |
| Hydrogenation, % | 4.0 | 18.7 |
| Distribution of products, % | | |
| Alkanes ($C_7$) | 0.2 | 0.3 |
| Cycloalkanes ($C_7$) | 0.5 | 0.4 |
| Toluene | 5.1 | 4.9 |
| Biphenyl | - | 0.4 |
| Methylnaphthalene | - | 0.3 |
| Dibenzothiophene | 0.1 | 0.1 |
| 1-methylnaphthalene | 0.9 | 0.7 |
| Heptane | 93.2 | 92.9 |

## 4. References

[1]. Jin Guangzhou, Zhu Jianhua, Fan Xiuju, et. al., *Chinese Journal of Catalysis.* V. 27, Is.10 (2006).

[2]. Z.P. Xia, Y.Q. Shen, J.J. Shen, et. al., *Journal of Alloys and Compounds.* 453 (2008), 185-190.

[3]. J.X. Wang, S.F. Ji, J. Yang, et. al., *Catalysis Communications.* 6 (2005), 389.

[4]. Q L Zhu, X T Zhao, Zh X Zhao, et. al., *Chinese Journal of Catalysis.* 26(12) (2005), 1047.

# Nanographites, their compounds and film structures

A.M. Ziatdinov

*Institute of Chemistyr, Far Eastern Branch of the Russian AS.*
*690022 Vladivostok, Russia*

E-mail: ziatdinov@ich.dvo.ru

*Keywords: nanographite, intercalation, electronic structure, magnetic properties*

## 1. Introduction

In this paper, the results of investigations by complementary physical methods of structure and properties of nanographites (the structural blocks of activated carbon fibers - ACFs), their intercalation compounds and films are presented. It was shown that presence of nano-sized π-electron conjugated system and edge electronic state allow to consider the nanographite as a new mesoscopic system with specific characteristics, which distinguish it both from the bulk graphite, and fullerenes and carbon nanotubes. Due to their intermediate position between the bulk graphite and aromatic molecules, nanographites are potential source of new chemical substances and films with unusual electronic and magnetic properties.

## 2. Results and Discussion

The X-ray diffractograms of ACFs show very broad peaks around $20^0$ and $45^0$ (Fig. 1). From the width of (002) peak around $20^0$, we find a grain thickness $L_c \approx 1{,}2$ nm. We deconvulate the broad feature around $45^0$ into (100) and (101) peaks on the assumption that each peak originates mostly from a single component. The obtained contribution to the (100) peak gives an estimate of the in-plane size of $L_a \approx 2$ nm. From the centre of (002) peak the interlayer distance between graphene sheets in evacuated samples are estimated as 0,4 nm, which are considerably longer than the interlayer distance of 0.3354 nm for bulk regular graphite. From nanographite sample thickness and interlayer distance between graphene sheets, the number of graphene sheets is estimated as 2-4.

The C1s spectrum of ACFs consists only of a single peak with the binding energy 284,4±0,1 eV. The lineshape parameters of signal considered are near the same for bulk graphite. This fact testifies to absence or negligible amount of functional groups in ACFs.

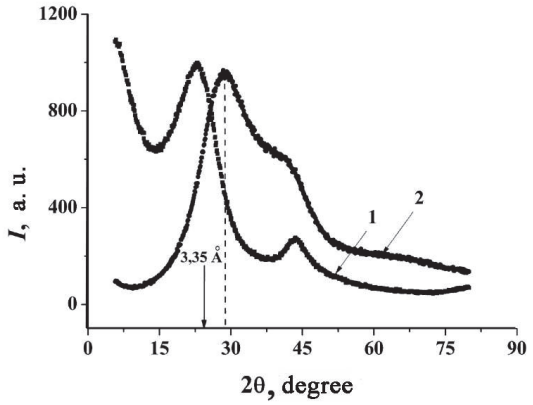


Figure 1. The X-ray diffractograms of ACFs.
1 – initial, 2 – after adsorption of water molecules.

The EPR spectrum of initial ACFs in atmosphere consists of two slightly asymmetric signals of different width (Fig. 2). The values of the asymmetry parameter *A*/*B* and *g*-factor are the same for both signals and are respectively 1.15 and 2.0027. As the temperature decreases the width of broad signal increases, while the width of the narrow signal does not change (Fig. 2). Temperature changes of the asymmetry parameters and *g*-factors values of both signals are within the errors of their determinations. The width of broad signal from conduction electrons decreases to 0.78 mT without changing the value of *g*-factor in evacuation the tube with sample. Ratio of the integral intensity of the conduction ESR signal before and after evacuation is near 0,75.

The magnetization curve shows the absence of the residual magnetization at different constant magnetic fields. The temperature dependence of the magnetic susceptibility $\chi_g$ for ACFs investigated is well described by the expression $\chi_g$=1.318e-5/($T$+0.9)-0.61e-6. From the value of Curie constant, it follows that one localized spin approximately per 2500 carbon atoms (or 1 localized spin per ≈10 nanographites) are presented in fibers at low temperatures.

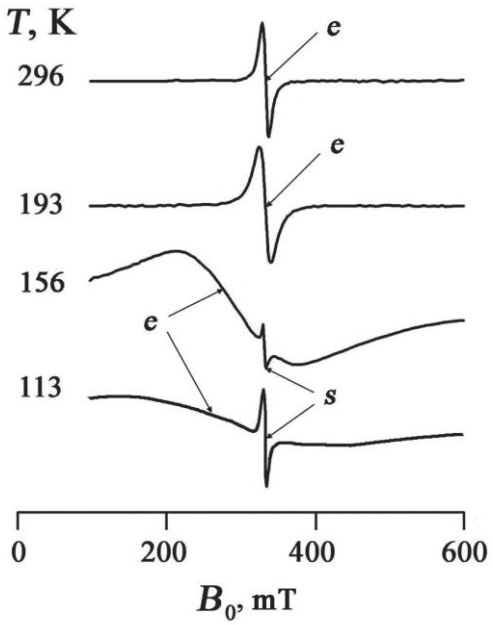


Figure 2. EPR spectrum of ACFs.
Signals "e" and "s" correspond to the conduction electrons and the localized spins, respectively.

From comparison of integral intensities of signals from conduction electrons and localized spins (the concentration of latter is known from the magnetic susceptibility data), the density of states near the Fermi level in nanographites was estimated. Such calculations show, that it is more than one order of magnitude larger than in bulk regular graphite at the same value of Fermi energy [1]. The results obtained unambiguously indicate the presence of an additional band around the Fermi energy in nanographites that was proposed theoretically [2]. Another reason of considered phenomenon is the deeper position of Fermi level in nanographite, than that in bulk regular graphite. Such displacement of the Fermi level in nanographites may be as the result of interaction of surface carbon atoms with some adsorbed molecules, such as water and oxygen. We shall note, that in acceptor graphite intercalation compounds a similar situation are realized and the value of displacement of the Fermi level may be significant (≈1 eV [1]). Obviously, at the validity of the model considered, the position of the Fermi level in nanographites (as well as the sign and the value of charge on graphene layers) may be controlled by adsorption on their surface of different molecules.

In ACFs studied the position of (002) reflex shifts at the adsorption of water molecules (Fig. 1), nitric acid, chlorine and some other molecules. The possible reasons for this are 1) the insertion of molecules into the interlayer space of nanographite or 2) superposition of nanographite reflex with the reflex of absorbed molecules in the pores of the fiber. The chlorine absorption is accompanied by an decrease in the concentration of localized spins and is not convertible. It specifies that some of absorbed chlorine molecules form covalent bonds with edge carbon atoms of nanographites. The absorption of oxygen leads to a reversible increase in the concentration of mobile spins 1.2 times.

Using above new knowledge a principally new, simple and inexpensive method of growing nanographite films with predominantly zigzag edges was proposed and realized. In this procedure, the activated carbon materials are used as a source of nanographites. We also found methods to modify the activated carbon materials and regimes of growing of nanographite films, in which a nanosized carbon structures of certain type are formed in the films.

This work was supported by grants of the Far Eastern Branch of the Russian Academy of Sciences (No. 12-I-П8-10 and 12-I-OXHM-03).

## 3. References

[1] M.S. Dresselhaus, G. Dresselhaus. *Adv. Phys*. Vol. 30. P. 139-326 (1981).

[2] M. Fujita, K. Wakabayashi, K. Nakada, K. Kusakabe. *J. Phys. Soc. Jpn.* Vol. 65. P. 1920-1923 (1996).

# Investigation of composition, structure and morphology of cenospheres and possibility to obtain thermostable $Fe_2O_3$ films on their surface

O.A. Mikhaylova*, E.V. Rabchevskiy, E.V. Fomenko

[1] *Institute of Chemistry and Chemical Technology of SB RAS, Siberian Branch, Russian Academy of science, Akademgorodok 50/24, Krasnoyarsk, 660036 Russia*

(*) corresponding author: mikhaylovaolgaa@mail.ru

*Keywords: cenospheres, catalysis, deep oxidation, methane, thermostable film*

## 1. Introduction

Fly ashes produced from the pulverized coal combustion contain a few microspherical components with valuable characteristics that determine the possibility of their use in different fields of industries.

Among microspherical components of fly ashes are hollow aluminosilicate microspheres with a low bulk density (0.2-0.8 g/cm$^3$), namely, cenospheres. The formation of cenospheres occurs as a result of thermochemical and phase transformations of the mineral components of coal during combustion process. Their granulometric, chemical, and phase compositions depends on the composition of the original coal, the type of combustors used, and the conditions of cooling of the melt drops.

Cenosphere narrow fractions with certain composition and specific shell structure with predictable properties are very interesting to create new functional materials [1-3]. Hollow aluminosilicate cenospheres are valuable because of high strength, thermostability, acid resistance, and regular porosity of glass-crystal shell. One of the perspective applications of cenospheres is their use as supporting material for catalytic active components.

There are a lot of examples the use of iron-containing catalysts [4, 5]. Their catalytic activity depends on active component state. One of the methods to obtain catalysts with high surface is deposition of active component as thin film. This method allows raising dispersity of active component and providing avaibility of active centers for reacting components.

## 2. Experimental

The narrow cenosphere fractions have been separated from concentrates of cenospheres of fly ash produced via the pulverized combustion of Kuznetsk and Ekibastuz coal. The technological scheme [6] used for separating of low-density nonmagnetic non-perforated cenosphere fractions includes stages of grain-size classification, gravitational separation, magnetic separation with the subsequent hydrostatic isolation of the destroyed globules. Each cenosphere fraction was characterized by a set of physical-chemical parameters, which included the chemical and phase composition, bulk density, size distribution, the average diameter of the globules, the apparent thickness of the shell, and the content of globules of certain morphological types.

To obtain iron-containing films on the cenosphere surfaces we used the method of thermal decomposition of iron compounds on the support surface. This method includes cenosphere impregnation with aqueous solution of iron nitrate (III) with different concentration and subsequent drying at 110-120°C. Decomposition of iron nitrate (III) was carried out at 500 °C during 2 hours with following burning at 600, 700, 800, 900 °C during 6 hours. As a result, the iron oxide – cenospheres systems containing from 1 to 10 wt % of $Fe_2O_3$ were obtained.

Catalytic properties of cenospheres with iron-containing deposited films were investigated in a microcatalytic set-up in the reaction of deep oxidation of methane (mixture $CH_4$:$O_2$= 98:2 %wt). The rates of products formation in deep oxidation were determined under steady-state condition for

methane and oxygen conversions of less than 5%. Activation energy were determined in the temperature range 357-637 °C and calculated by the least-squares method from dependence lnW-1/T.

## 3. Results and discussion

It has been established that low-density nonmagnetic non-perforated cenosphere fractions are multicomponent $SiO_2$–$Al_2O_3$–$Fe_2O_3$–CaO–MgO–$Na_2O$–$K_2O$–$TiO_2$–$SO_3$–MnO–$P_2O_5$ system with content of $Al_2O_3$ from 20 to 38, $SiO_2$ from 56 to 68 and low content of $Fe_2O_3$ from 1 to 3.5 %wt. Phase composition of cenospheres includes glass phase from 57 to 93 %wt, crystal phases of mullite (1-42 %wt) and quartz (1-7 %wt). Moreover, the cenosphere fractions include the impurity phases of calcite and ferrospinel, whose concentrations do not exceed 1.8 and 0.5 %wt, respectively. Cenosphere specific surface area is 0.2-1.5 $m^2/g$.

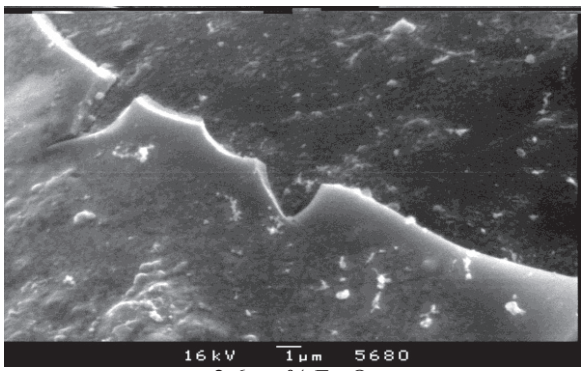


2.6 wt % $Fe_2O_3$

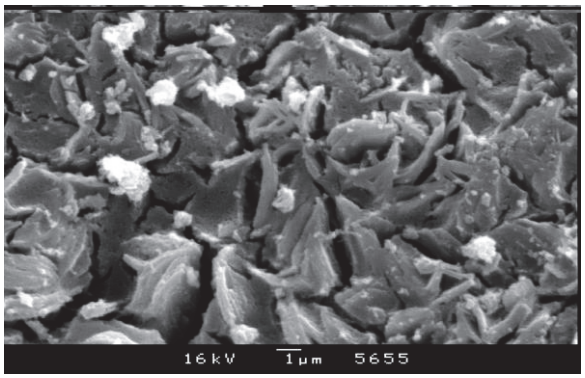


10.1 wt % $Fe_2O_3$

Figure 1. SEM images of iron oxide–cenospheres systems with different content of $Fe_2O_3$ after treatment at 500 °C.

The specific surface area of deposited iron-containing component depends on concentration of iron oxide and pretreatment temperature and change in the range from 10 to 200 $m^2/g$. That indicates about possibility to obtain thin deposited films on the cenosphere surface. One of the morphological properties of deposited $Fe_2O_3$ is tendency to change its two-dimensional crystallization to three-dimensional with increasing concentration on the cenosphere surface (Fig. 1).

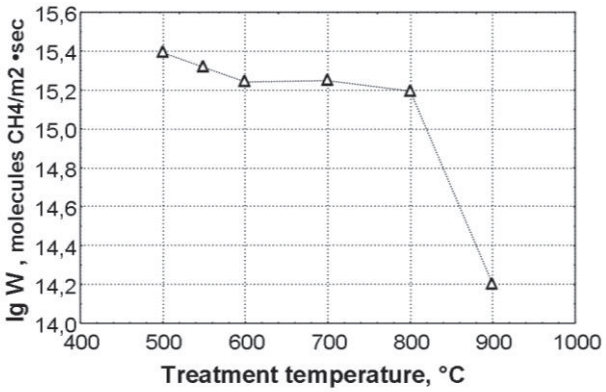


Figure 2. Dependence of catalytic activity in reaction of methane deep oxidation (T=400 °C, $CH_4$:$O_2$ = 2:98) and treatment temperature of iron oxide–cenospheres systems ($Fe_2O_3$–10 %wt).

Investigation of catalytic properties of iron oxide–cenospheres systems in the reaction of deep oxidation of methane (Fig. 2) demonstrated their thermostability in the temperature range of 500-800 °C.

This study was supported in part by the Siberian Branch of the Russian Academy of Science (Interdisciplinary Integration Project Nos. 52 and 91).

## 4. References

[1]. Fomenko, E.V.; Anshits, A.G.; Bobko, A.A.; Khramtsov, V.V.; Salanov, A.N.; Kiriluk, I.A.; Grigor`ev, I.A. *Russ. Chem. Bull*. **2008**, 57, 493-498.

[2] Fomenko, E.V.; Anshits, N.N.; Pankova, M.V.; Solovyev, L.A.; Vereschagin, S.N.; Anshits, A.G.; Fomin V.M. *Dokl. Phys. Chem*. **2010**, 57, 202-204.

[3] Pankova, M.V.; Fomenko, E.V.; Anshits, N.N.; Vereschagina, T.A.; Anshits, A.G. *Chem. Sustainable Dev.* **2010**, 18, 509-516.

[4] Torres Galvis, H.M.; Bitter, J.H.; Khare, C.B.; Ruitenbeek, M.; Dugulan, A.I.; de Jong, K.P. *Sci. Technol. Catal*. **2012**, 18, 835-838.

[5] Wang, Xu.; Wang, A.; Li, N.; Wang, Xi.; Liu, Z.; Zhang, T. *Ind. Eng. Chem. Res*. **2006**, 45, 4582-4588.

[6] Anshits, N. N.; Mikhailova, O. A.; Salanov, A. N.; Anshits, A. G. *Fuel* **2010**, 89, 1849-1862.

# Irreversible and reversible aggregation of nanoparticles in physiological solutions

E. Karepina[1*], A. Godymchuk[1,2], D. Kuznetsov[2], S. Senatova[2], M. Umrikhina[3]

[1] *Tomsk Polytechnic University, Russia, Tomsk, Lenina str., 30, 634050*
[2] *National University of Science and Technology "MISIS" Russia, Moscow, Leninsky pr., 4, 119049*
[3] *Tambov State University named after G.R. Derzhavin, Russia, Tambov, Internationalnaya str., 33, 392000*

(*) corresponding author: karepina_ee@mail.ru;

*Keywords: nanoparticles, aggregation, toxicology*

## 1. Introduction

Wide application and considerable interest in aluminum oxide nanoparticles has increased their manufacturing for the last 10 years [1]. Boost production provokes the release of nanoparticles into the environment and interaction between the nanoparticles and including human's body. Due to the fact that nanoparticles are characterized by a large surface area and high reactivity, they their biological effect like toxicity has become a major cause for concern [2].

Recently, it has been shown that nanoparticles $Al_2O_3$ can accumulate in organisms and cause dysfunction of organs or death of *Daphnia magna* daphnia [3]. Another authors has demonstrated that chronic exposure of *Caenorhabditis elegans* to $Al_2O_3$ nanoparticles leads defeat of their nervous system of roundworm's [4]. Therefore, the growth of nanoparticles emission and their potential high toxicity are the basis to detailed study of the environmental, occupational and health impact of nanoparticles [5].

When entering the liquid environment nanoparticles change their properties dramatically. Because of its high reactivity and high surface energy nanoparticles tend to aggregate in the aqueous medium [6].

Low aggregation stability of nanoparticles creates a number of difficulties in analytical testing of nanomaterials in toxicology, because toxicity assessment of nanoparticles is primarily based on data about their dispersity (particle size distribution, the average diameter, specific surface).

Nanoparticles are capable of forming stable colloidal solutions of micelle in solutions of humic acids, salts of carboxylic acids, saccharides, as was shown by different authors [7]. Although these processes were mainly applied for the synthesis of nanoparticles, for the use of dispersants in nanotoxicology have been considered insufficiently for engineered nanoparticles and preparation of nanoparticles lyosols.

The aim of this study was to determine the aggregation stability of $Al_2O_3$ nanoparticles in aqueous suspensions for making recommendations about the composition of the sols used in toxicology.

## 2. Experimental part

In this study $Al_2O_3$ nanoparticles (Nanostructured & Amorphous Materials Inc, USA) obtained by precipitation from aqueous solution ("wet" chemistry, fig.) were investigated. For study we prepared nanoparticles suspensions (0,010-0,15 wt.%) in aqueous solutions of tricarboxylic acid and synthetic alveolar fluid, wherein the main component was tricarboxylic acid from the first solution and the rest - the sodium, magnesium and calcium salts [8].

The transmission electron microscope JEM-2100 Jeol was used to study particles morphology. The specific surface area was determined by low-temperature nitrogen adsorption on the BET installation Quantachrome NOVA 1200e. The composition of powder was identified with X-ray diffractometer XRD-7000S Shimadzu.

Aggregation stability of suspensions was assessed during continuous stirring by the change of dispersion with the use of laser diffraction analyzer SALD-7101 Shimadzu. The data were measured after 1, 2, 5, 10, 15, 20, 25, and 30 – minute-stirring. The data used to build a distribution of particle size at each point of time, and to calculate an average size of particles/aggregates ($d_{av}$).

## 3. Results

According to TEM-images the shape of $Al_2O_3$ nanoparticles is close to a sphere, the average diameter ≈ 20 nm. The particles form aggregates 100 - 800 nm with coagulation bond. The specific surface of the nanopowder is 8 $m^2/g$.

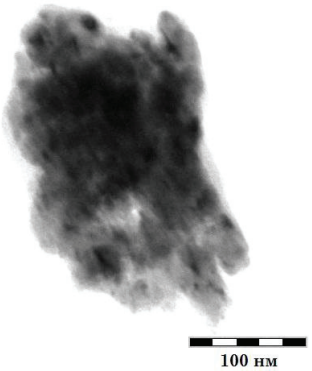


Fig. 1 .TEM-image of aggregates of nanoparticles $Al_2O_3$.

The size distribution of $Al_2O_3$ nanoparticles in tricarboxylic acid after 10-minute incubation is shown on figure 2. According to the data this suspension is characterized by a monomodal distribution in the range of 0.3 ... 6 μm.

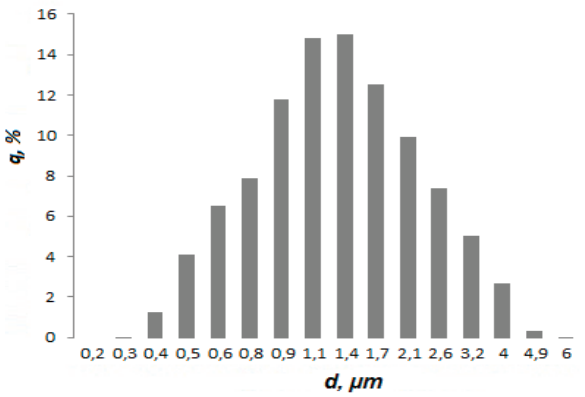


Fig. 2. Average size distribution of the $Al_2O_3$ particles/aggregates in tricarboxylic acid after 10 - minute incubation.

It has been revealed that suspensions based on synthetic alveolar fluid save its dispersion during 10 minutes: average particle size ($d_{av}$) retains its original size (20-23 nm). After 15 minute incubation $d_{av}$ increased in more than 100 times ($d_{av}$ = 3,5 μm). Further stirring of suspension does not provoke great changes in dispersion. That is why despite the large content of carboxylic groups the aggregation of the particles is irreversible in alveolar fluid.

During the stirring of suspension prepared on the basis of the aqueous solution of a tricarboxylic acid, a strong aggregation was fixed for 5 minutes: the average particle size increased from 23 nm to 1.8 μm. Thus, the dispersion of suspension decreased in 75 times. Further exposure of nanoparticles has provoked a complete deaggregation and the formation of a stable sol with $d_{av}$ 23 nm.

Thus, it has been shown irreversible aggregation in suspensions based on synthetic alveolar fluid and reversible aggregation of the nanoparticles in aqueous suspensions prepared with addition of tricarboxylic acid.

## 4. References

[1]. O. Salata, *Journal of Nanobiotechnology*. **2** (2004) 1-6.
[2]. H. Warren, *Journal of the Minerals, Metals and Materials Society*. **56** (2004) 13-18.
[3]. X. Zhu, L. Zhu, Y. Chen, S. Tian, *Journal of Nanoparticle Research*. **11** (2009) 67–75.
[4]. Y. Li, S. Yu, Q. Wu, M. Tang, Y. Pu, D. Wang, *Journal of Hazardous Materials*. **219-220** (2012) 221-230.
[5]. V. Colvin, *Nature Biotechnology*. **21** (2003) 1166–1170.
[6]. M. Pettitt, J. Lead, *Environment International*. **52** (2013) 41-50.
[7]. M. Baalousha, *Science of the Total Environment*. **47** (2005) 2093-2101.
[8]. K. Midander, J. Pan, C. Leygraf, *Journal of Environmental Monitoring*. **9** (2007) 74–81.

# Electrosurface properties of nanoparticles in solutions of ionic surfactants

A.S. Komutova[1*], A.Y. Godymchuk[1,2], D.V. Kuznetsov[2], S.I. Senatova[2]

[1]*Tomsk Polytechnic University, Russia, Tomsk, Lenina str., 30, 634050*

[2] *National University of Science and Technology «MISIS», Russia, Moscow, Leninsky pr., 4, 119049*

(*) corresponding author: ainagul_komutova@mail.ru

*Keywords: surfactants, metal nanoparticles, zeta-potential, particle/aggregate size*

## 1. Introduction

Despite the innovative potential of nanomaterials, in the literature there are more works proving the high toxicity of nanoparticles while releasing into the living organisms and other objects of the environment. Nanoparticles are potentially more toxic than their bulk counterparts because of the high reactivity, small size and high surface energy.

Thus, Cu and Zn nanoparticles cause high sensitivity on cyanobacteria [1], Zn nanoparticles cause earthworms mortality after 96 hours exposure in high concentrations [2], Cu nanoparticles can cause significant increase in cell death of Xenopus laevis (A6) (African frog) [3].

Currently, in order to determine a toxic dose of nanomaterials all approaches in nanotoxicology are based on a key factor - "dispersion", that is effected with both concentration and surface of the test sample. However, the difficulty in preparing nanoparticles suspensions with high aggregation stability remains one of the largest analytical difficulties, and therefore determines the adequacy of the methods and approaches in nanotoxicology.

Among all the methods of stable suspensions preparation (sonication, stirring, addition of stabilizers), only the latest allows to control the dispersion of suspensions for a long time and do not require extensive sample preparation [4]. In this case, one of the main requirements to the stabilizer in toxicology is the lack of toxicity.

There is a data in literature about the synthesis of nanoparticles from solutions with addition of non-toxic ionic surfactants [5, 6]. In this work the approach for the preparation of aggregative stable suspensions of industrial nanoparticles with the physiologically absorbable substances addition was proposed to use.

## 2. Experimental

The objects of the study were electroexplosive Cu and Zn nanoparticles with the average surface diameter ~ 50 nm. Suspensions were prepared by mixing the 5 mg of nanoparticles and 50 ml of solution with different surfactant concentrations (20, 100 mg / l).

The weight of powder was measured by laboratory scale ANDGR-202 (Germany). As surfactant sodium citrate ($Na_3$-$C_3H_5O(COO)_3$•$2H_2O$), sodium acetate ($CH_3COONa$•$3H_2O$) were used. The suspension was stirred for 5 minutes, and then the coarse phase was removed by 2-hours decantation. In the suspension zeta-potential and average particle/aggregate size was measured by Zetasizer Nano ZN, Malvern (UK).

## 3. Results

According to experimental data aggregation stability of the suspension varies in time and depends on the type and concentration of used surfactant [7]. Sodium acetate adding leads to significant reduction of the particles Zeta-potential absolute value in time, that in 48 hours are almost neutral: -2.47 mV and -1.44 mV for Cu and Zn nanoparticles respectively (fig.1,2). However, the surfactant concentration has a significant effect only in the first 2 hours, what can be explained by the process of carboxyl groups sorption-desorption on the

particles surface. Further, the increase of the Zeta-potential absolute value does not depend on the content of $CH_3COO^-$-group. These data conform to the results of hydrodynamic diameter of the suspensions measurements. For example, after 10 hours-standing for the surfactant concentrations 20, 100 mg/L the average particle size in Cu-suspension was 590, 951, 1344 nm, in Zn-suspensions 585, 300, 403 nm.

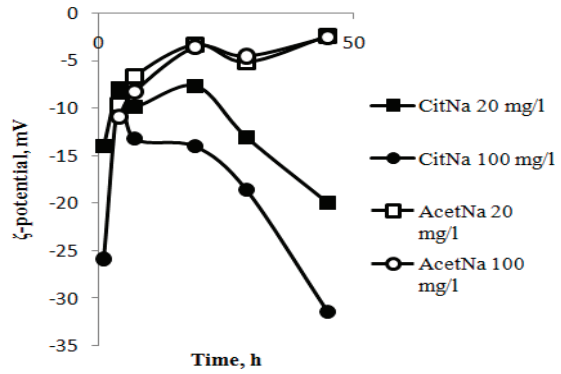


Figure 1. Change of zeta-potential of Cu particles in suspensions stabilized with sodium citrate (CitNat) and sodium acetate (AcetNa) at 20 and 100 mg / l.

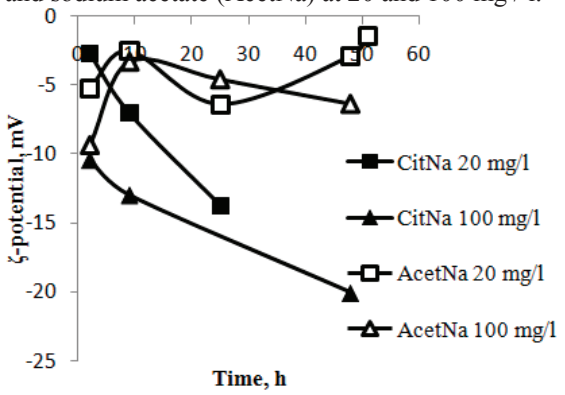


Figure 2. Change of zeta-potential of Zn particles in suspensions stabilized with sodium citrate (CitNat) and sodium acetate (AcetNa) at 20 and 100 mg / l.

In suspensions containing citrate ions, the tendency in changing of particles electrosurface properties is different: the stability of colloids in suspension increases in time (fig.1,2).

Thus, from the practical point of view it is important to note that in the non-toxic ionic surfactant solutions metal-containing nanoparticles may form both stable and unstable dispersions. This fact is highly important in the development of methods for dispersing nanoparticles in toxicological studies.

From a fundamental point of view it is interesting to study the influence of the surfactant nature and the particles material on the properties of suspension.

For Zn and Cu as basic metals the affinity to negatively-charged carboxyl groups is typical. So $OH^-$-groups adsorbed in water will be substituted by carboxyl ones. The difference of zeta-potential for used surfactants suspensions can be explained: $C_3H_5O(COO)_3^{3-}$-groups have more electronegative charged groups in comparison with $CH_3COO^-$-groups, adsorption of which the particle charge tends to zero value.

## 4. References

[1]. Chakraborty P., Baby R., Acharyya T., Bandyopadhyay D. Chemosphere (2010).
[2]. Li L-Z., Zhou D-M., Peijnenburg W., Gestel., C., Jin S-Y., Wang Y-J., Wang P. Environment International (2011).
[3]. Thit A., Selck H., Bjerregaard H. Toxicology in Vitro (2013).
[4]. Farré M., Gajda-Schrantz K., Kantiani L., Barceló D. International Journal of Refrigeration (2011).
[5]. Leeuwenburgh S., Ana I.D., Jansen J.A. ActaBiomaterialia (2010).
[6]. Sadiq M., Pakrashi S., Chandrasekaran N., Mukherjee A. J Nanopart Res. (2011).
[7]. Sallam K.I. Science direct. (2007).

# Silver-containing nanocomposites on the basis of humic substances and their antioxidant activity

M. V. Lesnichaya[1*], G. P. Aleksandrova[1], G. Dolmaa[2], B. G. Sukhov[1], D. Regdel[2] and B. A. Trofimov[1]

[1.] *A. E. Favorsky Irkutsk Institute of Chemistry, Siberian Branch of the Russian Academy of Sciences, 1 Favorsky st., 664032 Irkutsk, Russian Federation. Fax: +7 (395) 241 9346.*

[2.] *Institute of Chemistry and Chemical Technology, Mongolian Academy of Sciences, 210351, Enkhtaivan avenue, 13330, Ulaanbaatar, Mongolia*

(*) corresponding author: @E-mail address: mlesnichaya@irioch.irk.ru

*Keywords: nanocomposites, silver, humic substances, antioxidant activity*

## 1. Introduction

Humic substances (HS) are organic compounds complex of polyaromatic and carbohydrate nature. They are formed in soils and sediments as a result of microbial decomposition of plant and animal organisms. Functional composition of humic substances contains by characteristic polar functional groups -COOH, -OH, -CO, -$NH_2$, and long alkyl side chains of fatty acid residues [1,2]. It defines prospects of use of humic substances as a reducing and stabilizing matrix for the synthesis of nanocomposites. Besides, such polyfunctional of macromolecules humic substances and metal nanocomposites based on them determines their valuable biological properties, including antioxidant activity.

## 2. Experimental

### 2.1. *Analytical technique*

The transmission electron microscopy measurements were performed on Leo 906 E microscope operated at an accelerating voltage of 120 kV. The particle size was determined by the statistical processing of the electron micrographs. The absorption spectra of the nanocomposite aqueous solutions were recorded relative to $H_2O$ on a Perkin Elmer Lambda 35 spectrophotometer in quartz cell d=1 cm. Metal content in the nanocomposites was determined by atomic absorption analysis using a Perkin Elmer Analyst 200 spectrometer.

### 2.2. *Synthesis of the silver containing nanocomposites.*

Humic substances of therapeutic muds of the Gurvan-Nuur Mongols Lake were used. An aqueous solution (10 mL) of (0.08—0.2 g) $AgNO_3$ was added dropwise to a water-alkaline solution of humic substances (3 %). The reaction time was 20 min, temperature was 90 °C, and the nanocomposites were precipitated by the addition of fourfold excess of ethanol. The yield was near 90 %.

### *2.3. Determination of the antioxidant activity of humic* substances *and silver containing nanocomposites based on them*

The antioxidant activity was determined by measuring the inhibitory effect of the antioxidant potential *in vitro* to simulated processes of $Fe^{+2}$ - ascorbate-induced oxidation of Tween-80 by the oxygen air to malondialdehyde [3].

## 3. Results

Silver-containing nanocomposites (content of silver ranging 6-15 %) were synthesized by hydrothermal reduction of $AgNO_3$ in aqueous-alkaline medium in the presence of a humic substances matrix. The generation of Ag nanoparticles was monitored by appearance of the intensive plasmonic absorption of the silver metal nanoparticles formed in visible range of spectrum (410 - 415 nm). According to data of transmission electron microscopy, nanocomposites are formed as nanoparticles

of almost spherical shape and relatively narrow size range incorporated in the humic substances matrix (Fig. 1).

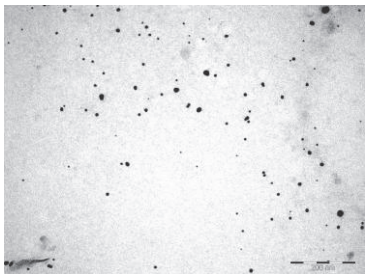

**Figure 1.** TEM image of nanoparticles in the silver - containing nanocomposites

The study of antioxidant activity of humic substances, and nanocomposites of silver (silver content 6.5, 9.8, 14.7 %) established that all samples *in vitro* inhibit of the oxidative processes within 28-46 % (Fig. 2).

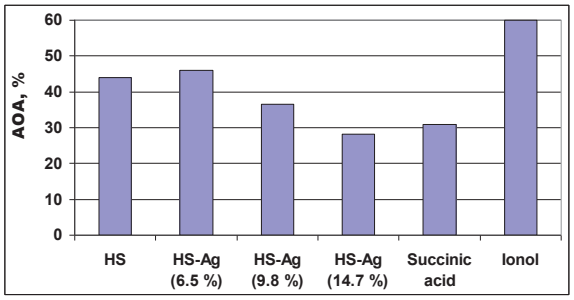


**Figure 2.** Antioxidant activity (AOA) of the humic substances and silver-containing nanocomposites in comparison with known antioxidants

## 4. Discussion

We developed new humic substances preparations containing silver nanoparticles and characterized them by complex of physicochemical methods.

The data show that the greatest inhibition of the accumulation of lipid peroxidation products (up to 46 and 44%) (Fig. 2) was observed in the case of using a silver-containing nanocomposite, with a silver content of 6.5 % and an initial of humic substances. Slightly less pronounced antioxidant activity (43 %) have nanocomposites containing 9.8 % silver. Least inhibitory effect (28 %) demonstrated nanocomposites containing 14.7 % silver.

Unequal antioxidant activity of humic substances and nanocomposites based on them, probably due to the difference in their functional composition. In general, despite the pronounced (up to 18 %) difference, the antioxidant activity of all samples is relatively high and comparable with the value of the known antioxidants - succinic acid and ionol.

This work was supported by Russian Foundation for Basic Research (grant 12-03-90433-Ukr_a), SB RAS (integration projects No. 85, 134, interdisciplinary projects of SB RAS and the Mongolian Academy of Sciences and the Ministry of Education, Culture and Science of Mongolia No. 4, 14).

## References

[1]. Chilom G., Rice J.A., *Langmuir*. 2009, **25**, 16. C. 9012 - 9015.

[2]. Aleksandrova G.P., Dolmaa G., Enkhbadral U., Grishenko L., Tserenpil Sh., Sukhov B.G., Regdel D., Trofimov B.A. A new humic acid remedy with addition of silver nanoparticles. *Mongolian Journal of Chemistry*. 2012, 13(39) P.7-11.

[3]. Fedoseeva A.A., Lebedkova A.S., Kanibolotskaya L.V., Shendric A.N. *Chemistry of plant resourse,* 2008, **3**, C. 123 - 127.

# Compared effects of silver pharmaceuticals and silver nanoparticles suspensions *in vitro* on microorganisms

E. N. Petritskaya*, O. D. Smirnova, D. A. Rogatkin, L. Ph. Abaeva, E.V. Rusanova

[1] *Moscow Regional Research and Clinical Institute named after. M.F. Vladimirskiy, Moscow, Russia*

(*) corresponding author: medphys@monikiweb.ru

*Keywords: silver nanoparticles, nitrate, antibacterial silver pharmaceuticals, Klebsiella pneumoniae Escherichia coli, Staphylococcus aureus, Candida albicans*

## 1. Introduction

There is a strong opinion about the antibacterial activity of silver based on which pharmaceutical on the basis of $AgNO_3$ and new products containing silver nanoparticles are used in medicine. Some publications reported on the toxicity of silver nanoparticles [1, 2]. The aim of our study was to investigate the possible bactericidal effect of colloidal solutions of silver nanoparticles on the activity of microorganisms in comparison with well-known antiseptics, including silver-containing pharmaceuticals.

## 2. Experimental

### *2.1. Materials and methods*

We used *Escherichia coli* (E.coli) as gram-negative strain (ATCC number 26941) and *Klebsiella pneumonia* (K.pneumoniae) (ATCC number is 43062), which have a capsule. Out of gram-positive we chose Staphylococcus aureus (*Staphylococcus aureus* (*S.aureus 209 P*), as the strain with the highest pathogen effect compared to other staphylococci. As for the fungi clinical strains of Candida albicans (C.albicans) were used.

The main object of our research was colloidal suspension of silver nanoparticles "Silver Shield" produced by "Fractal-M" Ltd., with nanoparticles concentration of 50 mg/l and 100 mg/l and a particle diameter of about 15±5 nm.

For comparison we used a solution of silver ions, obtained by the appliance "George" at a concentration of 0.5 mg/l, 1% solution Protargolum, platelets from whole pieces of silver, furacillinum 1:5000 and various antibiotics (amoxicillin, ampicillin, cefotaxime, imipenem).

For the isolation role of nitrate anions and silver ions in pharmaceuticals effect of Protargol was compared to aqueous solutions of nitrates of other metals - $NaNO_3$, $Sn(NO_3)_2$, $Co(NO_3)_2$ and $Zn(NO_3)_2$ in silver equimolar Protargol concentrations on Gram-positive bacteria (*S.aureus*) and Gram-negative (*E.coli*).

### *2.2. Experiment organizing*

The main study of the colloidal solution of nanophase silver and objects of comparison was carried out in 2 series with 3 tests in each series. During the first series of experiments we used the slurry with optical turbidity standard of 5NTU derived from daily agar culture emulsified in saline. The resulting slurry was uniformly seeded on the Petri dishes containing blood agar for culturing *S.aureus, E.coli, K.pneumoniae* and with Sabouraud medium for *C.albicans*. Then the dishes were labeled and separated into sectors with numbers. One sector was always used for control, other sectors were used as experimental. The cups were placed in an incubator for 24 hours at 37 ºC.

During the second series of experiments we used the slurry with the optical turbidity standard of 5NTU derived from daily agar culture emulsified in a solution of silver nanoparticles with 50 mg/l and 100 mg/l. The resulting suspension was plated onto agar immediately after preparation, after 2 hours and after 24 hours incubation at 37 ºC. Then cups were placed in an incubator for 24 hours.

To test the specificity of the effect of silver ions $AgNO_3$-based pharmaceutical

and role of nitrate anions we used reference solution containing 0.052 – Molar methals nitrates: $Sn(NO_3)_2$, $Co(NO_3)_2$, $Zn(NO_3)_2$, $NaNO_3$.

Native cultures in this case were inoculated on blood agar in Petri dishes with initial concentration of $5 \cdot 10^5$ CFU. Plates were divided into four sectors, in the centre of each sector over the seeded surface of the bacterial culture one of the 4 solutions in the amount of 30 μl was placed. The experiment was repeated three times for reliability.

## 3. Results

### *3.1. Colloidal silver nanoparticles*

At the end of incubation uniform growth in all the seeded sectors was observed with no visible differences from the control sector, regardless of the choice of culture *S.aureus*, *E.coli*, *K.pneumoniae* or *C.albicans*. No growth was reported on blood agar which was not seeded with microbial culture. Thus, the examined colloidal solutions of silver nanoparticles with concentrations of 50 and 100 mg/l in this case had no bactericidal effect on microorganisms in the frames of the experiment.

There was no bactericidal effect of silver ion solution which was obtained with the help of "George" device in the mode of intensive saturation of water with silver ions at the concentration of 0.5 mg/l and also for pure silver plates laid on agar.

### *3.2. Comparators*

Comparative experiment on agar with discs of all of the antibiotics presented a distinct inhibition zone around the disc of bacterial growth. A similar distinct zone of inhibition of microbial growth was detected in the experiment with Protargol and a very weakly expressed one in an experiment with furacillinum solution 1:5000 (fig.1).

### *3.3. Substitution solutions*

The growth of both bacterial cultures (*S.aureus, E.coli*) was completely suppressed in areas of the dropping of 0.052 - molar solution of metal nitrates studied, which also was confirmed by additional cultivation of these microorganisms in liquid media.

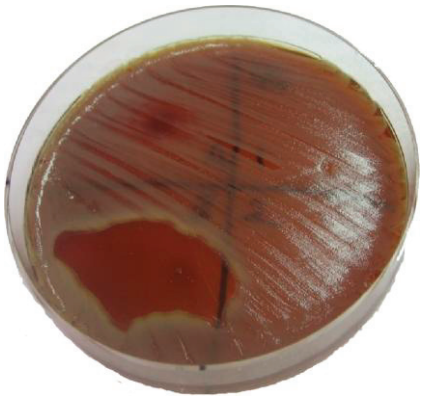

**Fig.1**. Results of 24-hours cultivation of *E.coli* on agar with 100mg/l silver nanoparticles (top right sector), control (down right sector), Protargol (down left) and furacillinum (top left).

## 4. Discussion

So, colloidal solutions of silver nanoparticles with concentrations up to 100 mg/l do not show any antibacterial activity. Protargol with dilution of 1% has an alkaline reaction and an expressed bacteriolytic property. Equimolar on silver by 1% Protargol nitrates of other metals - sodium, zinc, cobalt and tin - have expressed strong anti-bacterial properties. Silver ions of standard pharmaceuticals most probably inhibit growth of bacteria due to the activity of their anions. Pure silver, including nanophase silver is ineffective as an antimicrobial agent.

## 5. References

[1]. *Singh M., Singh S., Prasad S., Gambhir I.S. Nanotechnology in medicine and antibacterial effect of silver nanoparticicles* // Digest Journal of Nanomaterials and Biostructures . Vol. 3, № 3, September 2008. p. 115–122.

[2]. *Shrivastava S., Bera T., Roy A., Singh G., Ramachandrarao P., Dash. D. Characterization of enhanced antibacterial effects of novel silver nanoparticles* // Nanotechnology, 2007, №18. p. 1–9.

# Protonation effect on photochromic properties of chromenes in solution and polymer films

O.V. Venidiktova*, V.A. Barachevsky, A.M. Gorelik

*Photochemistry Center, Russian Academy of Sciences, 119421, Novatorov str., 7a, Moscow*

(*) corresponding author: wolga@photonics.ru

*Keywords: photochromism, chromenes, protonation, merocyanine form, spectral characteristics*

## 1. Introduction

Among the rapidly developing fields of application of photochromic organic compounds (optoelectronics, optical memory, photocontrolled nanostructured materials, etc.) photocontrolled chemosensors, in particular for determination of solution acidity, occupy an important place.

This paper presents study results of photoinduced protonation of photochromic chromenes tested reversible transformstions under light from the colorless cyclic form A into the colored merocyanine form B:

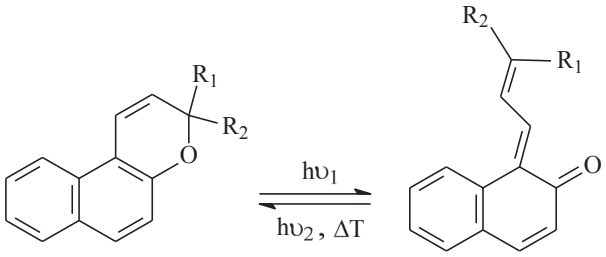


A B

Photochromic chromenes are characterized by photoinduced absorption in the spectral range of 400-500 nm

## 2. Experimental

As the objects were used two synthesized chromenes, namely 3,3-bis(4-methoxyphenyl)-3H-naphtho-[2,1-b]-pyran (**I**) и 2,2`-bis-(4-methoxyphenyl)-8-(2-fluorophenyl)-8`-(4-methoxyphenyl)-1,7-dioxachrysene (**II**).

Investigations were carried out in acetonitrile without and at presence of perchloric acid. Spectral characteristics of compounds **I** and **II** were measured before and after UV irradiation.

The spectral properties of the polymer film prepared by casting of solution of a polyvinyl butyral binder and chromenes **I** and **II** in chloroform-chlorobenzene (1:1) were investigated too.

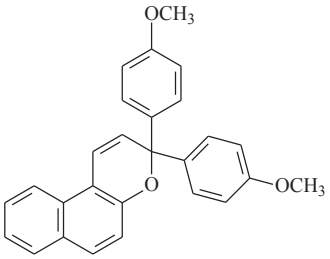


I

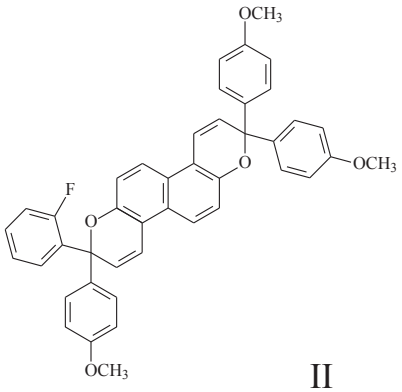


II

To study the interaction of photochromic compounds with acid the photochromic film was immersed into acetonitrile solution of perchloric acid for 1 min. Molecules of chromenes partially passed from the polyvinyl butyral film into solution. Transfer efficiency chromenes into solution was monitored by the absorption spectra of photochromic films and acid solution.

## 3. Results

As a result of the carried out spectral research it is revealed, that at presence of a perchloric acid absorption spectra of chromenes in acetonitrile contain new intensive absorption bands in the long-wave spectral range (Fig.1). These absorption bands were absent in absorption spectra of solutions without acid (Fig. 1 and Table 1). From these data it is seen that position and

intensity of new absorption bands essentially depend on the structure of compounds. The maximum of the absorption band for bischromene **II** is displaced on 56 nm in the long-wave spectral area in comparison with a monomer analogue **I**. However intensity of the absorption band was below at identical concentrations of these compounds in solution.

Alongside with long-wave absorption bands short-wave absorption bands of the photoinduced merocyanine forms of chromenes which have not formed interacted with a perchloric acid are present at the same spectra. Particular emphasis is an insignificant bathochromic spectral shift for maxima of these absorption bands (on 15 nm only) at transition from **I** to **II** compounds.

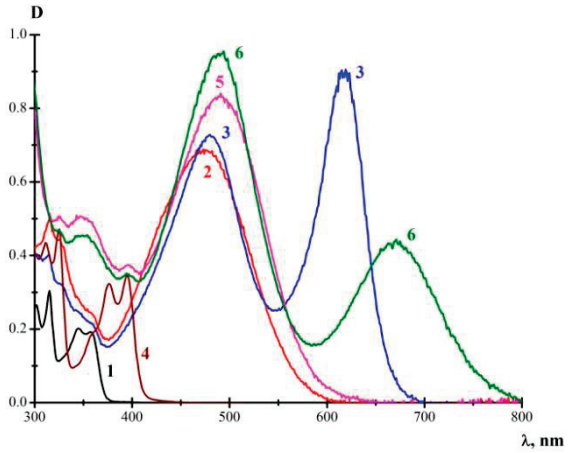


Fig.1 Absorption spectra for chromenes **I** (1-3) и **II** (4-6) in acetonitrile before (1,4) and after (2,3,5,6) UV irradiation without (1,2,4,5) and at presence (3,6) of perchloric acid.

At immersing photochromic polymer films containing chromenes **I** or **II** into solution of perchloric acid in acetonitrile diffusion of molecules of photochromic chromenes from polymer films to solution was observed. It follows from the absorption spectrum of solution after extraction of polymer film containing chromene **I** from solution (Fig.2, Table 1). This spectrum is similar on what has been received in acetonitrile solution (compare appropriating curves on Fig.1 and 2)

The spectral study of photochromic polymer films taken of solutions has shown that its absorption spectra contain absorption bands of photoinduced merocyanine forms only (Fig.2, curve 5).

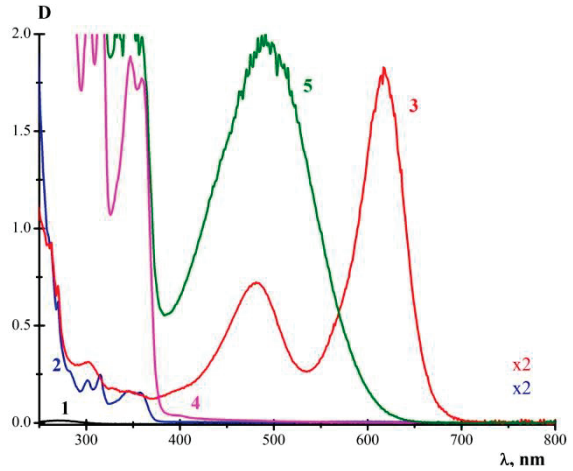


Fig.2. Absorption spectra for perchloric acid in acetonitrile before (1) and after immersing the photochromic polymer film containing chromene **I** into solution before (2) and after (3) UV irradiation; for photochromic film extracted from solution before (4) and after (5) UV irradiation

Table 1. Spectral characteristics

| sample | | $\lambda_A^{max}$, nm | $D_A^{max}$ | $\lambda_B^{max}$, nm | $D_B^{max}$ |
|---|---|---|---|---|---|
| I | - | 345<br>358 | 0,2<br>0.19 | 475 | 0,69 |
| | $H^+$ | 345<br>358 | 0,2<br>0.19 | 480<br>619 | 0,73<br>0,9 |
| II | - | 377<br>395 | 0,31<br>0,33 | 490 | 0,84 |
| | $H^+$ | 376<br>395 | 0,32<br>0,34 | 494<br>671 | 0,96<br>0,45 |
| pvb-I after $H^+$ | | 347<br>359 | 1,89<br>1,77 | 491 | 2,04 |
| pvb-II after $H^+$ | | 378<br>398 | 2,1<br>2.26 | 510 | 2,27 |
| Solution $H^+$ after pvb-I | | 345<br>357 | 0,08<br>0.08 | 481<br>617 | 0,36<br>0,91 |
| Solution $H^+$ after pvb-II | | 376<br>394 | 0,02<br>0,02 | 487<br>670 | 0,08<br>0,08 |

Note: $\lambda_A^{max}$ and $\lambda_B^{max}$ – wave-lengths of absorption band maxima for initial and photoinduced forms, accordingly; $D_A^{max}$ and $D_B^{max}$- optical densities at absorption band maxima for initial and photoinduced forms, accordingly.

## 4. Conclusions

Presented data show that in acid acetonitrile solutions there are photoinduced protonation merocyanine forms of chromenes with characteristic long-wave absorption bands in spectra.

Photochromic polymer films containing chromenes can be used as chemosensors for definition of a proton content in solutions.

# Noncovalent functionalization of single-walled carbon nanotubes with plasma proteins regulates their interaction with platelets and neutrophils in blood

I.I. Vlasova[1*], A.A. Gusev[1], E.A. Arifulin[2], V.A. Kostevich[1,3], A.V. Sokolov[1,3], S.A. Gusev[1]

[1] *Research Institute for Physico-Chemical Medicine, FMBA, ul. M. Pirogovskaya 1, Moscow, Russia.*
[2] *A.N. Belozersky Institute of Physico-Chemical Biology, MSU, Leninskye gory1- 40, Moscow, Russia*
[3] *Institute of Experimental Medicine, RAMS, akad. Pavlov Str. 12, Saint Petersburg, Russia*

(*) corresponding author, E-mail: irina.vlasova@yahoo.com.

*Keywords: carbon nanotubes, albumin, fibrinogen, immunoglobulin G, platelet aggregation, blood biocompatibility.*

## 1. Introduction

Single-walled carbon nanotubes (SWCNTs) are very promising nanomaterial for diagnostics, targeted drug delivery and cancer therapy.[1] When in contact with blood, CNTs adsorb plasma proteins. As known, adsorption of plasma proteins on a surface is useful to regulate the interaction of this surface with blood cells.[2-3] Here, we demonstrated that pretreatment of SWCNTs with the major plasma proteins, namely human serum albumin (HSA), fibrinogen (Hfg) and immunoglobulin G (IgG), may be useful to regulate interaction of SWCNTs with platelets and neutrophils in blood.

## 2. Experimental

Carboxylated (c-) SWCNTs and c-SWCNTs covalently functionalized by PEG (PEG-SWCNTs) were obtained from Carbon Solutions Inc. (USA).[4] Treatment with a protein was carried out by incubating SWCNTs at 37°C for 0.5 h with an aqueous protein solution at the concentration of proteins comparable to those in plasma.

Citrated blood samples were incubated (at 37°C) with c-SWCNTs or PEG-SWCNTs untreated or treated with proteins, and smear slides for light microscopy were prepared at different time point. For myeloperoxidase (MPO) and SH-groups measurements, the blood was centrifuged to obtain plasma. MPO concentration was quantified using ELISA. The concentration of SH-groups was measured with DTNB. TEM images were acquired by the use of a microscope JEM-1400, JEOL Ltd (Japan).

## 3. Results

### *3.1. Effect of SWCNTs on platelets*

Upon addition of SWCNTs to blood samples, the number of single platelets in blood sharply decreased. At the same time, dose- and time-dependent formation of agglomerates of SWCNTs and platelets was demonstrated, Figure 1A. The TEM images of agglomerates showed evidence of the activation-related morphological changes in the adhered platelets, Figure 1B.

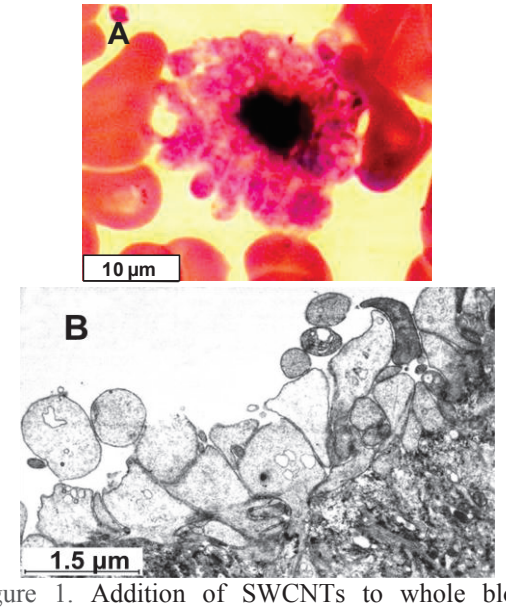


Figure 1. Addition of SWCNTs to whole blood resulted in formation of platelet-SWCNT agglomerates and platelet activation.
(A) - Micrograph of an agglomerate among erythrocytes in a blood smear made at 30 min after addition of PEG-SWCNTs (75 µg/ml) to blood.
(B) – TEM image of a part of an agglomerate.

Pretreatment of SWCNTs with albumin suppressed the formation of platelet-SWCNT agglomerates. As a result, blood samples incubated with HSA-PEG-SWCNTs contained more single platelets and the agglomerates had much smaller size (Table 1). A similar effect was observed when PEG-SWCNTs were treated with IgG. On the contrary, addition of Hfg-PEG-SWCNTs to blood caused immediate formation of the large platelet-SWCNT agglomerates.

### *3.2. Effect of SWCNTs on blood cells*

SWCNTs added to blood caused activation of neutrophils and, to a lesser extent, of monocytes in a dose- and time-dependent manner. Erythrocytes and lymphocytes were not affected.

Morphological changes typical of activated neutrophils were observed after 0.5h of blood incubation with SWCNTs. Data for 1 h incubation are presented in Table 1. Neutrophil activation was evidenced by an increase of MPO concentration in plasma. Oxidative stress caused by neutrophil activation was manifested by the decrease of free thiols.

Pretreatment of SWCNTs with albumin or fibrinogen did not affect substantially the activation of neutrophils. Functionalization of nanotubes with IgG resulted in increase of MPO concentration by about 1.5 times and decrease of SH-groups.

## 4. Discussion

Thrombus formation as well as slow biodegradation in the body are among the adverse effects of CNTs. A search for an appropriate functionalization of carbon nanotubes to overcome these negative events is urgently needed in view of biomedical applications of SWCNTs.

Functionalization with PEG is widely used to improve biocompatibility of SWCNTs. The effects of PEG-SWCNTs used in our study on blood cells and platelets were the same as those of c-SWCNTs. SWCNTs induced platelet aggregation and activated myeloid immune cells. Activation of myeloid cells may be important for *in vivo* biodegradation of SWCNTs.[3-5]

In the present work, we evaluated the impact of the major plasma proteins on the ability of PEG-SWCNTs to activate blood cells. The results of our study suggest that serum albumin is a good candidate for noncovalent functionalization of SWCNTs to impart them lower thrombogenicity. Modification of PEG-SWCNTs with IgG may serve to enhance neutrophil activation.

The work was supported by grant 12-04-01293 from RFBR.

## 5. References

[1]. F. Liang, B. Chen, *Curr. Med. Chem.* **17** (2010), 10-24.

[2]. C.J. Nonckreman, S. Fleith, P.G. Rouxhet, C.C. Dupont-Gillain, *Colloids Surf. B Biointerfaces* **77** (2010), 139-149.

[3] V.E. Kagan, N.V. Konduru, W. Feng, B.L. Allen, J. Conroy, et al., *Nat. Nanotechnol.* **5** (2010), 354-359.

[4] I.I. Vlasova, T.V. Vakhrusheva, A.V. Sokolov, V.A. Kostevich, A.A. Gusev, et al., *Toxicol. Appl. Pharmacol.* **264** (2012), 131-142.

[5] A.A. Shvedova, A. Pietroiusti, B. Fadeel, V.E. Kagan, *Toxicol. Appl. Pharmacol.* **261** (2012), 121–33.

Table 1. Assessment of platelet and neutrophil activation after incubation of the whole blood samples with c-SWCNTs, PEG-SWCNTs or with PEG-SWCNTs treated with plasma proteins.

| Parameter | Control | c-CNTs | PEG-CNTs/- | /+HSA | /+IgG | /+Hfg |
|---|---|---|---|---|---|---|
| aggregate size, $\mu m^2$ | 0 | 290 ± 40 | 244 ± 33 | 14 ± 5 | 43 ± 11 | 320 ± 70 |
| single platelets * | 57 ± 5 | 0,07 ± 0,01 | 0,15 ± 0,01 | 23 ± 2 | 15 ± 3 | 0 |
| % activated neutrophils | 4.2 ± 0.5 | 37 ± 6 | 32 ± 7 | 35 ± 9 | 57 ± 12 | (-) |
| myeloperoxidase, ng/ml | 69 ± 10 | 295 ± 12 | 270 ± 11 | 240 ± 17 | 440 ± 22 | 271 ± 11 |
| SH-groups, μM | 530 ± 16 | 454 ± 15 | 485 ± 14 | 480 ± 18 | 309 ± 14 | 445 ± 16 |

*Number of single platelets per 1,000 erythrocytes; (-) parameter was not measured. In the control sample, the blood was supplemented with water instead of nanotubes. All values are averages of three replicates (± S.D). The data represent the results of a typical experiment among at least 4 independent experiments. SWCNTs were added to the blood at concentration of 35 μg/ml. Incubation time was 30 min for platelets, and 60 min – for neutrophils.

# The oxidized carbon-mineral sorbent

T. Didenko*, O. Verevkina, D. Platonova, L. Adeeva

*Omsk State University n.a. F.M. Dostoevsky, Chemical Department, Mira avenue, 55A*

kovalenko_85@list.ru

*Keywords: carbon-mineral sorbent, oxidation, carboxyl groups, ion-exchange capacity*

## 1. Introduction

Carbon-mineral material (CMM) is developed by carbonization of natural renewable raw materials sapropel [1] at the Department of Inorganic Chemistry, Omsk State University. It is established that the received material is capable to take ions of metals thanks to silanol groups on its surface consisting of mineral and carbon fragments [2]. The ion exchange capacity of this material may be enhanced by the formation of functional groups on the surface of the carbon component. CMM has a high mechanical strength, meso-macroporous structure [3] and can be used as a basis for the sorbent with the higher capacitance characteristics. The aim of this work is the modification of carbon-mineral material by oxidizing the surface to increase the capacity for metal ions.

## 2. Experimental

CMM received by carbonization of sapropel at 700°C was chosen for modification. Initial sapropel belongs to siliceous type and incorporates 64 % mass. inorganic substances. CMM characteristics: the total pore volume is 0,2 $cm^3$ $g^{-1}$, specific surface is 60 $m^2$ $g^{-1}$, mechanical strength is 65 MPa.

Oxidation of CMMs surface is carried out by nitric acid and hydrogen peroxide within 20 hours at a temperature of 20°C, solid:liquid = 1:10 [4]. Efficiency of oxidation estimated on concentration of the oxygen-containing functional groups (OCFG) which was determined by titration by Boehm's technique [5].

The initial and oxidized sorbents were applied for sorption copper (II) ions. Process of sorption carried out from solution with copper(II) concentration of 2,0 mg $ml^{-1}$, pH 3,8, duration of contact 24 hours.

We studied the dependence of the sorption of copper (II) from pH. Series of solutions at a concentration of copper ions 2.0 mg $ml^{-1}$ and pH ranging from 1 to 5 was prepared for this goal. Liquid was separated by centrifugation and analyzed after contact phase lasting 24 hours.

Dependence of sorption value of copper (II) from equilibrium concentration is also studied on the oxidized sorbent. Solutions of copper ions with concentration of 0,1–2,5 mg $ml^{-1}$ and constant value pH = 4,0 were prepared for this purpose. The contact phase was 24 hours.

Kinetic characteristics were studied by varying the duration of contact between the phases from 15 minutes to 24 hours. The copper ion concentration was 2 mg $ml^{-1}$, pH 4.0. Concentration of copper (II) ions is determined by spectrophotometric analysis with sodium diethyldithiocarbamate [6].

## 3. Results

Data on the content of OCFG on a surface of initial CMM and on a surface of the sorbents received by its oxidation are obtained. Results are presented in the table 1.

Table 1. Assessment of oxidation efficiency of a sorbent by various oxidizers

| Sample | Content of OCFG, mmol $g^{-1}$ | |
|---|---|---|
| | carboxyl | lactone |
| Initial CMM | 0,03±0,01 | 0,06±0,01 |
| CMM oxidized 30% $HNO_3$ | 0,12±0,01 | 0,06±0,01 |
| CMM oxidized 10% $H_2O_2$ | 0,08±0,02 | 0,06±0,01 |
| CMM oxidized 20% $H_2O_2$ | 0,09±0,01 | 0,06±0,01 |
| CMM oxidized 30% $H_2O_2$ | 0,13±0,02 | 0,07±0,01 |

Increase of concentration of peroxide of hydrogen with 10 to 30% causes increase in the content of OCFG. For oxidation of a surface of CMM is chosen solution of hydrogen peroxide with concentration 30%.

For this oxidizing agent dependence of the content of OCFG on a surface from duration of oxidation process is established. It is shown that the increase in duration of contact of CMM and peroxide solution from 1 to 7 hours results in an rise of OCFG concentration. At further increase in duration of oxidation the content of OCFG doesn't change and makes 0,20±0,02 mmol $g^{-1}$.

On the surface of the oxidized sorbent are thus not only silanol, but carboxyl groups that will improve exchange properties as compared with the initial CMM.

Determination of the copper (II) sorption on the initial sorbent and sorbent oxidized is conducted. The sorption value of ions of copper (II) made 31,1±0,7 mg $g^{-1}$ on an initial sorbent. Under identical conditions the sorption value of ions of copper (II) was 60,4±1,3 mg $g^{-1}$ on the oxidized sorbent.

It is shown that an increase in the pH range from 1 to 5 copper sorption value increases (table 2). This dependence can be explained by an increase in the degree of dissociation of weakly acidic carboxyl groups with increasing pH. For further experiments, we selected a pH of 4.0.

Table 2. Dependence of sorption value of copper (II) on the oxidized sorbent from pH solution

| pH | Sorption value, mg $g^{-1}$ |
|---|---|
| 1,0 | 4,5±0,3 |
| 2,0 | 23,2±1,0 |
| 3,0 | 41,5±1,7 |
| 4,0 | 54,5±2,0 |
| 5,0 | 57,8±2,7 |

The received isotherm of copper sorption on the oxidized sorbent represents a convex curve. This isotherm refers to the Langmuir type. After linearization of the experimental data, we calculated the constant $A_\infty$ and K, as well as found the Langmuir equation, which describes the data satisfactorily. The calculated ion-exchange capacity of the oxidized sorbent on ions of copper (II) makes 61,0±1,7 mg $g^{-1}$.

Kinetic studies have shown that the equilibrium sorption of copper on oxidized sorbent is achieved h hours. Sorption half time is less than 15 minutes.

## 4. Discussion

Oxidation by hydrogen peroxide and nitric acid leads to formation of mainly carboxyl groups on CMM surface while the content of lactone groups practically doesn't change. As a result of processing by nitric acid and hydrogen peroxide the maintenance of KFG on a surface of a sorbent makes approximately the same size.

The double increase of sorption value confirms expediency of oxidation of an carbon-mineral material for improvement its cation-exchange properties. Oxidized carbon-mineral sorbent has a high kinetic characteristics.

Thus, the oxidized carbon-mineral sorbent has high ion-exchange capacity, comparable with synthetic ion-exchange resins. However renewability and universal prevalence of initial raw materials for its receiving in combination with high capacitor characteristics does the oxidized sapropel carbon-mineral sorbent one of the perspective material for purification of the industrial sewage polluted by ions of heavy metals.

## Acknowledgment

Work is performed with financial support of the Ministry of education and science of RF within "Scientific and scientific and educational staff of innovative Russia" for 2009-2013. Agreement No. 14.B37.21.1197.

## 5. References

[1]. L. Adeeva, T. Kovalenko. Patent 2414430, RF. Published 20.03.2011. Bull. 8.

[2]. L. Adeeva, T. Kovalenko. *Journal of applied chemistry*. **4** (2012). P.535.

[3]. T. Kovalenko, L. Adeeva. *Chemistry for Sustainable Development*. **2** (2010). P. 189.

[4]. Tarkovsky I.A. *The oxidized coal*. Kiev: Scientific thought, 1981. 200 p.

[5]. Boehm H.P. *Catalysis. Stereochemistry and mechanisms of organic reactions*, 1968. P. 186–288.

[6]. Novikov Yu.V., Lastochkin K.O., Boldin Z.N. *Methods of definition of harmful substances in water of reservoirs*. M: Medicine, 1981. 376 p.

# Preparation of $Pd_{core}Cu_{shell}$ Nanoparticles: Catalytic Reduction of $Cu^{2+}$ Ions by Hydrogen

E.V. Abkhalimov[*,1], R.D. Solovov[1,2], B.G. Ershov[1]

[1] *Institution of Russian Academy of Sciences - A.N. Frumkin Institute of Physical Chemistry and Electrochemistry of RAS, 31-4, Leninsky ave., 119071 Moscow, Russian Federation*

[2] *Lomonosov Moscow University of Fine Chemical Technology, 86, Vernadskogo ave, 119571 Moscow, Russian Federation*

(*) corresponding author: abkhalimov@ipc.rssi.ru

*Keywords: copper, nanoparticle, hydrogen, reduction, palladium, bimetallic*

## 1. Introduction

In the recent years, metal nanoparticles (NPs) have received a great interest for their unique properties and catalytic performance [1-3]. It is known that Cu-M (M – noble metals) nanocomposites along with eco-friendliness and cheapness exhibits high catalytic activity in hydrogenation and oxidation reactions [4-6].

In this work we investigated the reduction of Cu(II) ions by hydrogen in aqueous solution which have been catalyzed by Pd NPs.

## 2. Experimental

### *2.1. Materials*

Copper (II) perchlorate hexahydrate ($Cu(ClO_4)_2 \cdot 6H_2O$, 98%), Polyethyleneimine (PEI, $M_w$=60000, 50wt% aqueous solution) from Acros Organics, Tetraammine palladium (II) chloride monohydrate ($Pd(NH_3)_4Cl_2 \cdot H_2O$, 99.99%) from Sigma-Aldrich, polyacrylic acid sodium salt (SPA, $M_w$=2100) from Fluka, Isopropyl alcohol (IPA, 99.5%) and pure hydrogen ($H_2$, 99,999%) were used without further purification.

All glassware and Teflon-coated magnetic stirrer bar were cleaned with aqua regia, followed by copious rinsing with purified water. Solutions were prepared in distilled water, which was additionally deionized with a "Vodoley" water system and had a conductivity of no higher than 0.056 μS/cm.

### *2.2. Characterization*

UV–vis absorption spectra were recorded on Varian Cary 100 spectrophotometer with water-cooled Peltier accessory.

The sizes of NPs were determined in the colloidal solution by dynamic light scattering technique (DLS). The measurements were carried out on the Beckman Coulter Delsa$^{TM}$Nano C particle analyzer at a wavelength of 658 nm.

### *2.3. Synthesis procedure*

#### *2.3.1. Pd nanoparticles*

A Pd hydrosol was obtained by photo-induced method [7]. A 20 ml 0.2 mM aqueous Pd(II) was mixed with 80 ml of 0.25 mM sodium polyacrylate solution. The solution was deaerated and irradiated by pulse UV lamp with stirring and cooling in photochemical reactor. The mean size of the synthesized spherical particles is 22.7 nm.

#### *2.3.2. Cu@Pd nanoparticles*

A Pd hydrosol prepared as above was used as a seed of particles core for preparation of a series of Cu/Pd bimetallic NPs with core-shell structure and varying thicknesses of Pt shells. A core-shell Cu@Pd NPs was prepared as follows: 2 ml of 1 mM fresh Cu(II) aqueous 2.5 ml of 2 mM PANa solution and 0.5 ml water was mixed, and then it was added to 5 ml of 0.2 mM Pd hydrosol. The resulting solution was stirred with a magnetic stirrer for one hour, and then it was deaerated and saturated with hydrogen to form the core-shell particles. Analogously, Cu@Pd NPs with other molar ratios were prepared.

## 3. Results and discussion

In the absence of Pd NPs, a Cu(II) ions are not reduced by hydrogen in aqueous solution. Palladium NPs were used as seed to start the reduction of Cu. Spectra of optical absorption of a Cu(II) solution, containing Pd NPs, at various time after saturation by hydrogen are shown in fig. 1.

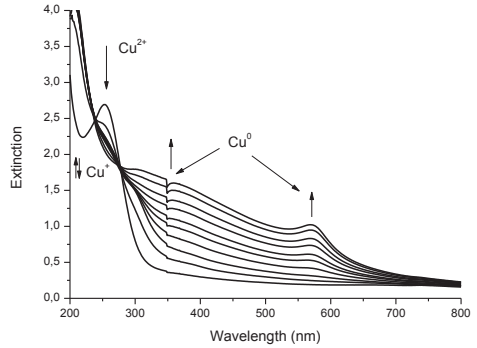


Figure 1. Changes in optical spectrum during the formation of Cu@Pd NPs.

The band with a maximum at 272 nm, is due to the presence of Cu(II)-PEI complex. The saturation of the solution by hydrogen leads to reduction Cu(II) to Cu(I). Its accomplishes by disappearing of Cu(II)-PEI complex's band at 272 nm and increasing absorbance of the hidden band at 214 nm that belongs already to Cu(I)-PEI complex [8]. After the completion of the process, a broad absorption band of colloidal metal with unclear maxima at 300 and 565 nm is fixed in the optical spectrum. The absorption instantaneously disappears when the system is in contact with air oxygen, which is caused by the oxidation of copper.

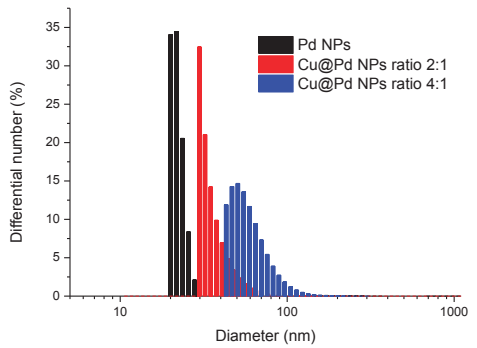


Figure 2. The size distribution histograms of a Pd and Cu@Pd various molar ratio NPs.

Table 1. The theoretical and experimental sizes of Pd and Cu@Pd NPs.

| Sample | Mean size(Exp./Theor.) |
|---|---|
| Pd | 22.7 ± 7.3 /– |
| Cu@Pd 2:1 | 36.1 ± 9.2 / |
| Cu@Pd 4:1 | 60.2±17.1 / |

## 4. Conclusions

The new green method of synthesis Cu@Pd NPs was developed. It is shown that the saturation of an aqueous solution containing Cu(II) with hydrogen in the presence of 22 nm Pd NPs leads to the reduction of copper on the Pd surface and the formation of Cu@Pd core-shell NPs. The UV-Vis DLS, and theoretical data confirms a formation of Cu@Pd core-shell NPs.

The authors thank Sergei Abramchuk for technical assistance in the TEM experiments. This work was supported by the Russian Found of Basic Research (Project Grant Nos. 12-03-00449-a).

## 5. References

[1]. J. Belloni. Catal. Today. **113** (2006) 141.

[2]. J. Santhanalakshmi, L. Parimala. J. Nanopart. Res. **14** (2012) 1090.

[3]. E.V. Abkhalimov, R.D. Solovov, B.G. Ershov, N.Yu. Kozitsyna, I.A. Yakushev, and M.N. Vargaftik. Coll. J. **74** (2012) 415.

[4]. S. Chen, H. Zhang, L.n Wu, Y. Zhao, C. Huang, M. Ge and Z. Liu. J. Mater. Chem. **22** (2012) 9117.

[5]. A. Hussain. J. Phys. Chem. C. **117** (2013) 5084.

[6]. X. Li, S. See Soon Fang, J. Teo, Y. L. Foo, A. Borgna, M. Lin, and Z. Zhong. ACS Catal. **2** (2012) 360.

[7]. J. Barta, M. Pospisil, V. Cuba. J. Radioanal. Nucl. Chem. **286** (2010) 611.

[8]. B.G. Ershov, E.V. Abkhalimov. Coll. J. **71** (2009) 487.

# Express-evaluation of industrial catalysts efficiency in the lower paraffin hydrocarbons aromatization process

G.V. Akimochkina, V.M. Kirilets

*Institute of Chemistry and Chemical Technology, Siberian Branch of Russian Academy of Sciences*

*Keywords: associated gas, aromatization, propane-butane fraction, BTX- fraction.*

## 1. Introduction

The current annual burnout of associated petroleum gas (APG) in Russia is estimated around 20 billion cubic meters, thus creating environmental problems (about of 500 thousand tons of tar and soot particles, and more 50 million tons of $CO_2$ are being released into the atmosphere) due to irrational using of valuable petrochemical raw material. /1/

The purpose of this work is to search economically effective method of deep APG processing with high content of "fat" part (percentage of the propane-butane fraction in APG more 20%) under conditions where food transporting is possible only through the oil pipeline. In this paper, the approach of recovery “oil-like fluid” (mixture of aromatic hydrocarbons) from propane-butane fraction, which is easily transported with raw oil through the oil pipeline is considered. This fluid will slightly decreases the viscosity of oil, and increases its quantity without loss of raw materials quality. Aromatization process of the propane-butane fraction commercially realized by leaders of world oil processing (that are BP-UOP firms) and named as CYCLAR /2/.This approach isn't intended for field conditions, but as compared with Fischer-Tropsch process, it’s less demanding to structure of raw materials and to qualification of the personnel /3/ and from our point of view, under certain conditions, this processing method may be realized in the small remote regions, where the "fat” component of associated gas constitute the essential part.

The essence of the CYCLAR process is transformation of propane-butane fraction on high-silica metal-loaded zeolite catalysts –ZSM-5 (known in Russia as “pentansil”), which also be modified by other transitional metals from the second or third periodic table groups. These zeolites are nanocrystal aluminosilicates or element-aluminosilicates with estimated pore size of channels about 5Å. These modified zeolite catalysts exhibit high activity in the lower paraffin hydrocarbons aromatization reactions because of their unique pore structure and low density of acid sites (Si/Al > 10) – factor that considerably reduce the deactivation rate of catalyst /4/. The incorporating of Zn or Ga ions in ZSM-5 increases the selectivity of aromatization process. The Russian catalytic factories have been released the industrial batches of catalysts – a pentansil-like zeolites modified by Zn.

The aim of this work is to evaluate efficiency of industrial catalysts in the lower paraffin hydrocarbons aromatization process and assess the profitability of plant with production rate of 20 thousand tons per year in the calculation of raw material.

## 2. Experimental

Experimental tests were conducted with five catalysts: (i) PGB-A and AGF-4 that supplied by «AZK&OS» company (Angarsk, Russia), (ii) AG-3 and BAK-70U supplied by «Nizhegorodskie sorbents» company (Nizhni Novgorod, Russia) and (iii) IK-17M supplied by Institute of Catalysis SB RAS (Novosibirsk, Russia). The main differences of these catalysts are in the features of their preparing techniques and the amount of zinc incorporated as promoter.

Carrying out of the aromatization reaction was used the liquefied hydrocarbonic fuel gas (a mixture of propone and butane according to GOST 20448-90). The ratio of gases $C_3H_8$:$C_4H_{10}$ was used as 1:1.

The transformation process of propane-butane mixture was carried out in a catalytic high-pressure laboratory apparatus with 100ml continuous flow, fixed bed reactor at thermo-programmable mode. The experiments was performed in the temperature range of 450-580 º C, at 10 atm., and volumetric feed rate of raw material was 2 $hour^{-1}$.

Composition of a gaseous and liquid fraction of products were determined by using a gas chromatography method. The quantity of liquid fraction was measured by direct weighting.

The economic evaluations were calculated by using «Project Expert ver.6.0» program package. Capital investments have been estimated on the assumption of the cost of stainless steel and ferrous metalwares required for our installation. Consumption parameters per tonne of production were as follows: the electric power consumption was 13 kW/h, the cost of catalyst was 325 RUR, the wages is 460 RUR, nitrogen and air consumption was 20 RUR. The cost of the product was 10000 RUR per tonne, which correspond to oil price in the oil fields. The price of raw material was 400 RUR per tonne.

## 3. Results and discussion

During transformation of propane-butane fraction in pentansil-like zeolite catalysts were obtained gaseous and liquid hydrocarbons. The gaseous products consisted of hydrogen, methane and ethane (their sum > 90 %).

The yield of liquid fraction increases with temperature rise. The catalyst AGF-4 was proven to appear the highest productivity in yield of liquid product (31-37wt.%). Reducing of pressure down to 5 atm. leads to increase of liquid yield up to 40 wt.%, but increasing of retention time allows to obtain a liquid product up to 48 wt.% .

During conversion of initial propane-butane mixture the composition of obtained liquid product were benzol (5-10%), toluene (of 25-30%) and xylol (20-30%). The temperature rise of process have been conducted to increases the bicyclic hydrocarbons (naphthalene and replaced alkylnaphthalene) up to 20 wt.%.

The estimation of investment project for enterprise with performance up to 20 thousand tonnes (on raw material) has been performed. The acceptable economic efficiency in existing conditions was shown to have been achieved at the capital investments in 10000 RUR per tonne of product, at sufficiently high internal norm of profitability in IRR = 37.44 % and at the discount factor in 20% for 2,5 years starting from the commencement of construction works date.

## 4. Conclusions

1. The actuality of this work has been corroborated. It is shown that in suitable conditions the processing of APG can be useful at the fields.
2. The experiments to assess effectiveness of the different industrial Russian catalysts in conversion process of associated gas "fat" part to aromatic hydrocarbons mixture were performed.
3. The maximum amount of liquid aromatic products were recovered by using of AGF-4 zeolite catalyst with the percentage of incorporated zinc ions 3 wt.%. Processing of "fat" gases at the modular installations with simplified construction has been suggested. Processing of fat part (heavy oil) to the mixture aromatic hydrocarbons by using of catalysts manufactured in Russia and its transporting through oil pipelines with oil were purposed.

## 5. References

1. Andreeva N.N. Modern state of the use of passing petroleum gas in the light of increasing state requirements // Material conferences. Khanty-mansiysk, 2008
2. http://www.uop.com Open information on the official web-site of company UOP
3. Maurs R.F. Basic processes of the oil processing. Reference book. trudged. with the eng of 3th publ. Under Glagoleva's supervision - SPb 2011 - 944c
4. H.M.Minachev, A.A.Dergachev Aromatization of low-molecular paraffin's on the pentasil-like zeolite families Successes of chemistry (in Russian), 1990, Tom 59, Number 9, With1522-1554

# Method for obtaining of carbon nanotubes-filled carbon materials

E.A. Danilov*,1, Yu.V. Gavrilov2, N.Yu. Beilina1

[1]JASC "NIIgraphit" of Rosatom State Corp.,111524, 2, Elektrodnaya St., Moscow, Russia
[3] D.I. Mendeleev University of Chemical Technology of Russia, 125047, 9, Miusskaya Sq., Moscow, Russia

(*) <danilovegor1@gmail.com>

*Keywords: carbon nanotubes, MWNT, carbon materials, carbonization, coke, carbon black*

## 1. Introduction

Carbon nanotubes-based materials have been attracting tremendous research effort recently [1-2]. This is justified by their unique properties (high heat and electrical conductivity, mechanical properties, aspect ratio) promising substantial modification of the properties of existing materials. The main difficulty in manufacturing of such materials is to achieve homogeneous dispersion of carbon nanotubes (CNT) in the matrix as they tend to agglomerate, thus leading to decreased effects of reinforcement with respect to expected. Low bulk density (0.01-0.05 g/cm$^3$) of the CNT poses a problem of mixing them with conventional matrix materials (polymeric, ceramic, metallic) in CNT contents over 2-5%, [3-4] although, provided the mixing was achieved, these highly-filled materials might be of great interest.

In the present study we report manufacturing of carbon materials with high content of multi-walled carbon nanotubes (MWNT) using coal tar pitch and petroleum pitch as binders, carbon black and petroleum coke – as basic fillers. The as-obtained composite materials possess high porosity accompanied by low specific electrical resistance as well as improved heat conductivity and microhardness.

## 2. Experimental

MWNT were obtained via catalytic chemical vapor deposition (CVD) using methane as carbon precursor. The process was carried out at 700 C over the iron-group based porous catalysts and is described in detail elsewhere [1]. The main drawback of such CVD-technique is high degree of agglomeration of the product and relatively high content of impurities. On the other hand, this route allows for obtaining relatively cheap product suitable for most composite applications. To assess the influence of the mixing technique on the properties of the materials two routes were utilized: direct mechanical mixing and disintegration using a laboratory Bosch knife-type miller and solvent-based mixing (preparation of CNT-filler-binder suspension in acetone followed by refluxing for 1 hr.; the solvent was then evaporated under vacuum, and the product dried and milled). Green bodies were obtained via room-temperature molding in steel press moulds (inner diameter 20 mm) using an M-10 machine. Carbonization was carried out in a laboratory muffle-type oven at temperatures up to 1000 C. To exclude the access of air the samples were put into a stainless steel container under a layer of fine-grained calcined coke. Electrical conductivity measurements were carried out using an E-7 RCL-measuring device (2-point protocol). Porosity and specific surface area measurements were performed using a ASAP 2020 (nitrogen adsorption, BET model).

## 3. Results

One of the most serious drawbacks of the CVD-technique using porous catalysts is that the degree of agglomeration is relatively high. As can be seen from fig.1, the size of agglomerates exceeds several microns.

The most crucial issue in obtaining carbon nanotubes-filled composites is to achieve high degree of dispersion. This can be done using several techniques. In the present study we propose boiling acetone as a good dispersion phase for CNT

suspension. Apart from improved MWNT-disentanglement, this route of mixing is very cost effective as compared to ultrasonication, cryomilling etc. and solves the problem of obtaining high-degree-of-filling composites which is challenging using conventional techniques as carbon nanotubes possess very low bulk density. Additionally, solution-based mixing provides more homogeneous distribution of the binder. Using laser diffraction technique it was shown that using boiling acetone it is possible to reduce the particle size from 3-6 μm down to less than 0,4 μm.

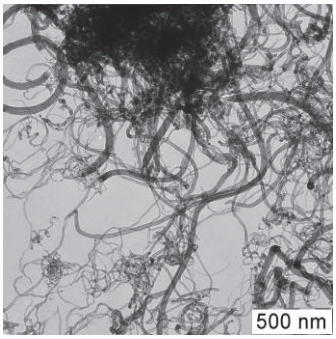


Figure 1. TEM image of MWNT agglomerate obtained via CVD-technique

Further steps for obtaining carbon composites followed traditional procedures such as milling, molding, carbonization (see experimental).

It was shown that by varying of the filler:binder proportion we were able to obtain composiiton with specific surface areas of up to 650 $m^2/g$ (55-70 wt.% of the filler). The results of their sorption activity tests were very promising.

On the other hand, different filler:binder proportions (1:4-2:3) can lead to obtaining of strong (compression strength 60-80 MPa) compositions with very low specific electrical resistance of 2-4 μΩ·m. This might open a whole new area of application of such materials as novel electrodes, functional composites etc.

## 4. Discussion

Obtaining next generation carbon materials is very unlikely to omit the use of carbon nanoparticles (CNT etc.); therefore, it is very interesting to study the mechanisms of their synthesis and properties formation today.

The present study shows that traditional techniques for obtaining of carbon compositions can be modified to allow for CNT to be used as a filler material which leads to light-weight highly electrically conductive high-performance materials for various applications.

## 5. References

[1]. M.S. Senthil Saravanan, S.P. Kumaresh Babu, K. Sivaprasad, M. Jagannatham. // Int. J. of Eng., Sci.&Tech. 2010. Vol. 2. No. 5. P. 100-108.

[2]. Kumar, Y. Ando. // J. of Nanosci.&Nanotech. 2010. Vol.10. P. 3739-3758.

[3]. A. Krueger. Carbon materials and nanotechnology. Weinheim (FRG): Wiley-VCH Verlag GmbH&Co. KGaA. 2010. 476 p.

[4]. S.J. Tong. Carbon nanotube reinforced composites. Metal and Ceramic Matrices. Weinheim (FRG): Wiley-VCH Verlag GmbH&Co. KGaA. 2009. 228 p.

# Some characteristics of the humic acids emitted from sapropel of the Omsk region

L. Adeeva*, D. Platonova, T. Didenko

*Omsk State University n.a. F.M. Dostoevsky, Chemical Department, Mira avenue, 55A*

kovalenko_85@list.ru

*Keywords: humic acid, sapropel, thermogravimetry, IR-spectroscopy*

## 1. Introduction

Humic acids are widespread in environment, have a large number and a variety of the functional groups into their structure. Humic acids are perspective for use when developing new materials, including sorbents for extraction of heavy metals from the polluted industrial drains of metallurgical and instrument-making materials. As sorbents humic acids can be used as independently, and put on a mineral substrate [1].

One of sources of the humic acids is sapropel. The Omsk region is one of the largest sapropelic regions of the country. It is known 162 lake fields with total stocks of 156.7 million tons [2].

## 2. Experimental

In this work humic acids were isolated from the lake sapropel Puchay, Omsk region. The maintenance of organic part in sapropel makes 54%, mineral - 46%. This sapropel belongs to siliceous type.

For humic acids sapropel treated with alkali. Then the nonhydrolyzable residue (humin) was separated by filtration. Precipitation of humic acids from the filtrate was carried out at pH 1 and separated from the mother liquor by centrifugation. Ash removal treatment of humic acids by HCl and HF in a boiling water bath was carried before the study. The residue was diluted with water and washed free of ions $F^-$ and $Cl^-$. The thus obtained humic acids were dried in a drying oven at a temperature of 60-70°C.

Thermal analysis was performed on Simultaneous Thermal Analyzer STA 449C Jupiter (NETZSCH) with free access of air into the furnace space. The rate of temperature rise of 5°C per minute.

IR spectra were recorded on a Fourier-IR spectrometer «Spectrum One FT-IR» firm Perkin-Elmer (USA) in the frequency range 4000-400 $cm^{-1}$ and the number of scans 32.

Sapropel was processed alkali for receiving humic acids. Then nonhydrolyzable residue (humin) was separated by filtering. Sedimentation of humic acids from a filtrate was carried out at pH 1 and separated from mother waters by centrifugation. Before the study ash removal of humic acids was conducted by repeated treatment with a solution of HCl and HF in a boiling water bath. The residue was diluted with water and washed free of ions $F^-$ and $Cl^-$. The thus obtained humic acids were dried in an oven at a temperature of 60-70°C.

## 3. Results

It was established that the greatest impact on completeness of humic acids allocation from sapropel has temperature (the studied interval 25 – 75°C) and concentration of alkali (0,5 – 3,5 %). It is noted that the ash content of the selected humic acid increases with increasing temperature and alkali concentration. Thus at 75°C and the alkali concentration 0.5% mass of ash in humic acids is 27%. While the alkali concentration 3.5% at the same temperature mass of ash is 52%. Thermal analysis with mass spectrometry control exhaust gases have been studied conversion humic acids sapropel air in the temperature range 40 – 1000ºC.

The endothermic effect was observed at 40 – 140°C on the thermogram. This effect may be due to removal of adsorption water

and the cleavage of the skeleton of humic acid molecules in the peripheral portion. This is evidenced by a weight loss. DTA curve is characterized by the presence of exothermic effects observed in a wide range of temperatures (140 – 500°C).

The first exothermic effect is observed at low temperatures from 140 – 240°C, corresponding to the destruction of the molecular periphery of sapropel humic acids. This effect is fixed a distinct peak in the DTG curve at 140 – 220°C. The second distinct exothermic effect on derivatograms at 240 – 500°C are explained further degradation of humic acid molecules. High-temperature effects are observed at temperatures above 500oC. These effects are associated with the collapse of the most stable structures, which can be attributed aromatic ring of humic acids.

IR-spectroscopy of the isolated sapropel humic acid allows to determine the presence of functional groups which define areas of application. On the obtained IR spectrum is noted intensive absorption in 3434 and 3200 $cm^{-1}$, which may be due to the presence of –OH and –C=NH group and intermolecular hydrogen bonds. Absorption in the 2920–2521 $cm^{-1}$ indicates the participation aliphatic CH groups. An absorption band with a frequency of 1723 $cm^{-1}$ characterizes the carbonyl group. Absorption in the 1643 $cm^{-1}$ may be attributed to the presence of primary amides, which manifests itself due to the amide carbonyl group or a group O=C–H. This fact testifies to the preservation of individual molecules of humic acid fragments of proteins. In addition to the primary amide, absorption in this field indicates the presence of quinone bonds, ketones, carboxylic and carbonyl groups, C=C aromatic skeleton, the shift to shorter wavelengths requires a multicore structure [3].

The aromatic nature of humic acids detected thanks to the absorption maximum caused by the stretching vibrations of the conjugated carbon bonds at 1579–1660 $cm^{-1}$. This is due to stable aromatic C=C bonds and the bending vibrations of the $CH_2$– and $CH_3$-groups.

Band of anti-symmetric stretching vibrations appears in 1450 $cm^{-1}$. Weak band symmetric vibrations appears around 1421 $cm^{-1}$, which indicates the presence of carboxylate-ion.

Slight uptake observed in the 826 – 703 $cm^{-1}$ and even less intense in the 688 $cm^{-1}$ due to the presence aromatic groups in the molecule, alcohol and ester groups, phosphate groups and band out of plane deformation CH-group [3].

## 4. Discussion

Feature of the method of alkaline extraction of humic acids from sapropel is a shift in the solution of large quantities of mineral substances. This fact leads to high ash in humic acids. This can be used a method of producing supported sorbents.

Thermogravimetric study ashless humic acids shows two district of their decomposition, wherein the weight loss in the temperature range 140 - 500°C is 35.9% and the weight loss in a high temperature region (more 500°C) is 44,3%. The results show a high proportion of peripheral chains.

IR spectroscopic studies confirmed the presence of various functional groups on the surface of sapropel humic acids. Determination of oxygen-containing functional groups by selective neutralization by Boehm demonstrated that the hydroxyl content is 2.8 meq $g^{-1}$ carboxylic acid is 2.2 meq $g^{-1}$ and a lactone is 0.2 meq $g^{-1}$ Significant amounts of carboxyl and hydroxyl groups confirm the perspective of the use of sapropel humic acid to create sorbents.

## 5. Acknowledgment

Work is performed with financial support of the Ministry of education and science of RF within "Scientific and scientific and educational staff of innovative Russia" for 2009-2013. Agreement No. 14.B37.21.1197.

## 6. References

[1]. I. Perminova, D. Zhilin. *Green Chemistry in Russia*. 2004. P.146.

[2]. P. Shmakov, A. Tretyakov, V. Levitsky. *Resources of Western Siberia and their management.* 2005. P.51.

[3]. D. Orlov, A. Rozanova, S. Matyukhina // *Soil science*. **1** (1962). P. 17.

# Development of nanostructured Si (111) surfaces

K. S. Ermakov[1], A. V. Ognev[1,2], A.S. Samardak[1,2], L. A. Chebotkevich[1,2]

[1] *Far Eastern Federal University, 8 Sukhanova st.,Vladivostok, 690095 Russia*
[2] *Institute for Automation and Control Processes, Far East Branch, Russian Academy of Sciences, 5 Radio st., Vladivostok, 690041 Russia*

(*) corresponding author: Ermak_ph@mail.ru

*Keywords: nanostructures, copper silicide, silicon*

## 1. Introduction

The development of nano-sized structures preparation technology requires to carry out the fundamental research in the field of nanofabrication. These nanostructures include ultrathin films, nanowires, nanoislands and quantum dots [1, 2].

Problems of self-organized growth and stability of metal silicide nanoislands on a semiconductor substrate are actual for microelectronics and intensively studied in recent years [3-6]. These nanostructures are potential candidates for electronic and optical devices and for metamaterial fabrication.

In this paper we investigated the characteristics of the growth processes of single crystal nanoislands of copper silicide on the surface of Si (111) substrate.

## 2. Experimental

The experimental samples were prepared by molecular beam epitaxy in ultra-high vacuum on the Si substrates with (111) surface orientation. To obtain an atomically clean surface substrates, they were pre-heated for 8 hours at temperature of 500 - 550 oC and immediately warmed up to ~ 1200 ° C passing DC current during 2 min.

Copper was deposited from an effusion cell on atomically clean surface of Si (111) 7□7 at substrate temperature ~ 550 °C. The pressure during deposition process does not exceed 5 × 10-10 Torr. The deposition rate was 1 nm/min. The thickness of Cu was varied from 2 to 96 monolayer (1 monolayer (ML) = 0,3615 nm). The thickness was controlled by quartz crystal calibrated using the oscillation of spot intensity in the reflection high-energy electron diffraction (RHEED) patterns.

The deposited structures were investigated by RHEED with electron beam energy of 15 keV and by scanning tunneling microscope (STM) with applied voltage ± 2.0 V and tunneling current 1 nA. Surface morphology was studied ex situ by scanning electron microscope (SEM) and atomic force microscope (AFM). All measurements were performed at room temperature.

## 3. Results

Formation of epitaxial copper silicide nanostructures on the surface of semiconductor substrate was observed after deposition of 0.5 - 1 ML of Cu. STM study confirmed that at initial stages the layer of stable quasi-periodic phase of Si (111) - 5.55×5.55-Cu was formed and then grown as three-dimensional islands of copper silicide [7, 8].

Diffraction patterns obtained from this sample after the deposition of copper were very complicated. There was the superposition of reciprocal lattices, which indicated the presence of several phases of copper silicide. For instance, the RHEED pattern from the sample with the thickness 24 ML of copper consists of extended reflection spots from the flat parts of the surface, and reflexes of transmission diffraction from the three-dimensional copper silicide nanoislands.

At Cu thicknesses from 2 to 4 ML the epitaxial nanoislands of β-phase copper silicide were triangular and polygonal. The edges of nanoislands oriented along the <110> directions of the Si substrate. The crystallographic plane of copper silicide nanoislands (111) was parallel to (111) Si.

At copper thicknesses from 4 to 24 ML we observed the perfectly aligned η-

phase copper silicide nanowires which growth between nanoislands, Fig. 1. In the η-phase of copper silicide the crystal plane was oriented parallel to the Si (111). The inset of Fig. 1 shows that the longest side of nanowires is oriented along the crystallographic direction <110> Si. We believe that this effect is due to anisotropy of crystal lattice mismatch between copper silicide and Si substrate. Thus, the mismatch of the lattice parameters of copper silicide $Cu_3Si$ and Si (111) along the directions <110> and <112> Si were 1.8% and 6.7%, respectively.

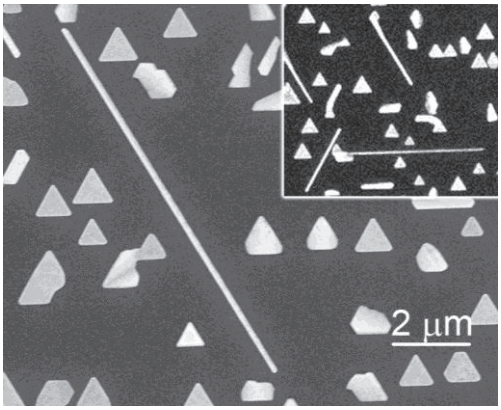


Fig. 1. SEM image of copper silicide nanostructures after deposition of 12 ML of Cu on Si (111). The size of the insert is 12x12 $\mu m^2$.

The maximum value of nanowires observed at thickness ~ 8 ML of Cu was 12% from total area of nanoislands.

The experimentally determined maximum length and width of nanowires were 12 μm and 100 nm, correspondingly.

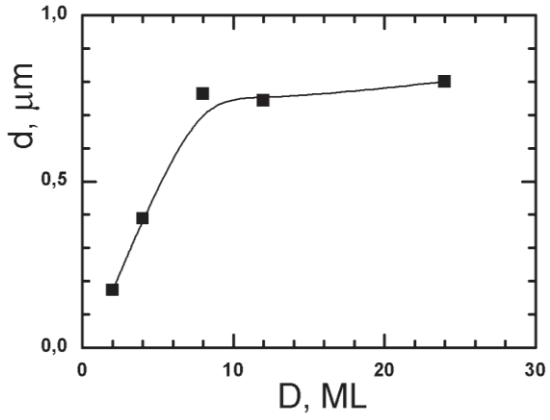


Fig. 2. The dependence of $Cu_3Si$ nanoisland diameter on thickness of Cu deposited on Si (111).

The next step of our study included of the investigation of a nanoisland size dependence on thickness of Cu coverage. The statistic analysis of nanoislands distribution was done with Lispix software [9]. We defined that with increase of Cu thickness the average diameter (D) of copper silicide nanoislands increased to cover the 8 ML, Fig. 2. After further Cu deposition D was unchanged, but the density of the islands increased. At the coverage thickness more than 25 ML the coalescence of nanoislands and nanowires were observed. In this case, statistical analysis did not reflect a real picture.

However, the increasing of islands density led to the coalescence of nanoislands with nanowires. The driving force of this process is a change of surface energy. The mass transport at the coalescence was due to the bulk and surface diffusions.

## 4. Conclusions

Our study of the growth processes of copper silicide nanostructures on Si (111) reveals that: at substrate temperature of 550°C the nanoislands and nanowires with a perfect facing are formed; - the long side of nanowires orients along the crystallographic directions <110> Si; - the maximum concentration of nanowires occurs at thickness of coverage near 8 ML; - at Cu thickness more than 25 ML the coalescence of the islands and nanowires are performed.

Authors acknowledge the support of the Russian Ministry of Education and Science under government contracts 16.552.11.7059, 2.8649.2013.

## 5. References

[1] FG Staros Cybernetics. Development prospects. Nauka, Moscow (1981) 203.
[2] Nanotechnology Research Directions: IWGN Workshop Report. Vision for Nanotechnology R&D in the Next Decade. / Edited by MC Roco, RS Williams, and P Alivisatos. – Kluwer
[3] Academic Publishers. – 2000. – 292 p.N. Motta. J. Phys.: Condens. Matter **14**(2002)8353.
[4] F.J. Walker, E.D. Specht, R.A. McKee. Phys.Rev. Lett. **67** (1991)2818.
[5] Z.H. Zhang, S. Hasegawa. Surface Science **415**(1998)363.
[6] A.V. Zotov a,b,c, D.V. Gruznev a, O.A. Utas a, V.G. Kotlyar a, A.A. Saranin. Surface Science **602**(2008)391.
[7] M. Mundschau, E. Bauer, W. Telieps, and W. Świch. J. Appl. Phys. **65**(1989) 4747.
[8] T. Yasue, T. Koshikawa, M. Jalochowski, E. Bauer. Surface Science 493(2001)381.
[9] http://www.nist.gov/lispix/

# Evaluation of topography of the kinks of high strength steel at the nanoscale using atomic force microscopy

A.V. Pogodaev, V.P. Pogodaev

[1] *FEFU, School of Engineering, Sub-Department of Welding production, city Vladivostok*

*Keywords: atomic force microscopy*

## 1. Introduction

Analysis of failure of turbine engines having in operation shows that the majority of fatigue failures were initiated by mechanical damage and erosion.

Providing guaranteed work of weld element is based on the solution of problems of prediction of individual resource-specific objects in the specified operating conditions. For predicting of diagnostic information serves as a basis about the state of the metal object. The quality of steel is laid at the atomic, nano- and mesolevel formation of its structure. It is therefore of particular interest to study the fine structure of the metal in its destruction.

Currently, several authors considered the main types of macro-and microstructure of fractures and fracture mechanisms of metallic materials in single (static, shock and high-speed switching) and cyclic types of loading, as well as methodological breaks research methods macro- and microfractography and X-ray analysis. A study on nanolevel are not considered.

The aim of our study was to evaluate the fracture surfaces of static high-reinforcing steel by atomic force microscopy.

We used the integrated studies using optical and fractographic methods. The study was conducted at the Laboratory of Physical and mechanical methods of research welds and coatings (Head of the Laboratory Prof. Pogodaev V.P.) FEFU using a scanning atomic force microscope (SPM-9600, Shimadzu, Japan) for the visual and digital assessment of surface roughness at the nanoscale.

Using an atomic force microscope studied five different portions kink valves, each of which was carried out 15 scans at intervals of 0,25 μm (micrometers). Area scanned plots was 20x20 μm, 10x10 μm and 7x7 μm. Further, when a computer program with subsequent digital processing surface roughness was calculated.

Visual and digital assessment of fracture surfaces using SPM-9600 showed that the average depth of the surface roughness are 0,35-2,08 μm.

From the study it can be concluded that the atomic force microscope scanning allows to objectively assessing visual and digital fracture surfaces.

The work was performed as part of the event 1.3.2. Federal Target Program "Research and scientific-pedagogical personnel of innovative Russia" for 2009-2013. The agreement № 14.132.21.1571 from “01” October 2012.

# Preparation of Ag(0)-nanocomposites based on sulfated arabinogalactan

T.V. Ganenko, A.P. Tantsyrev, B.G. Sukhov, B.A. Trofimov

[1] *A.E. Favorsky Irkutsk Institute of Chemistry, Siberian Branch of the Russian Academy of Sciences, 664033 Irkutsk, Russian Federation*

(*) corresponding author: irk_inst_chem@irioch.irk.ru

*Keywords: sulfated arabinogalactan based nanocomposites*

## 1. Introduction

The development of metal-containing polysaccharide silver-based nanocomposites is the urgent challenge for the design of multipurpose substances and materials.

Ag(0)-based nanocomposite materials are intensively used in medicine, optoelectronics, nanophotonics and etc. due to their the superpolarizability, active highly-developed surface, catalytic activity as well as antimicrobial and antiviral properties [1].

Our study aim was to develop the simple, feasible and efficient methods for the silver nanocomposites preparation on the basis of sulfated arabinogalactan, and also the study of the conditions to form the metal nanoparticles and water-soluble nanosized composites.

Natural polysaccharide arabinogalactan, isolated from Siberian larch wood, combines the water solubility with the unique immunomodulatory and membranotropic properties. Thus, it profitably differs from the other natural macromolecules. Chemically modified arabinogalactan (AGS) sulfate is a potential heparinoid and independent antimicrobial agent [2].

The achieved results in the treatment of some infectious diseases can be predictive for the high competitiveness of sulfated arabinogalactan as a new type of antibacterial systems with prolonged action effect. The high viricidal action of nanostructured silver preparation attracts an ever-growing research interest of drug designers [3].

We have studied the methods of recovery (chemical dispersion of metallic silver particles into a modified polymer matrix, microwave assistance, mechanical activation) on the final characteristics of the resulting nanosized systems.

We used water and DMSO as the solvents. The spectrophotometry method was applied to control the formation of silver nanoparticles.

The products are water soluble and extracted from aqueous solutions by precipitation in alcohol or acetone, and then can be easily transferred again into aqueous solutions stored for a long time without changing the physical properties. In combination with a biocompatible polymer matrix, they have a great interest for medicine.

The stabilizing effect of sulfated arabinogalactan is observed in a wide range of AGS/AgNO3 ratio and gives the nanocomposites with a silver content of 3.6 to 9.0%.

Thus, stirring AGS/AgNO3 in DMSO at room temperature for 12 h without alkali and heating leads to the product with a silver content of 6.3%. When the ammonia is added (pH=8-9) and the temperature increases up to 50°C for 10 min in DMSO, the nanocomposite AGS with a silver content of 8.1% is formed. Apparently, the ammonia addition facilitates the interaction of silver ions with AGS matrix and prevents the further aggregation of reduced silver nanoparticles. We found that with the extra reaction time the silver content in the product is increased.

The most efficient and rapid method is the microwave initiation of the reaction. At minimum power (100 Wt) for 1 min, the addition of ammonia solution (0.01 ml of 30%) affords composite with 6.2% silver content.

We have studied the possibility to obtain the silver nanoparticles by mechanical activation of the mixture AGS/AgNO3.

The mechanochemical processing of AGS/AgNO3 mixture in a ball mill with the addition of 6.5 wt% KOH for 10 min results in the nanocomposite with the silver containing of 3.7%.

The silver nanoparticles obtained initiates the formation of the absorption band with a maximum at λ=420-445 nm, that corresponds to the numerous data on plasmon absorption in the silver nanoclusters [4].

According to IR spectroscopy, the formation of AGS nanocomposites is not accompanied by the structural changes in the modified polysaccharides.

The above data demonstrate the new perespectives of sulfated arabinogalactan chemistry directly associated with the creation of nanosized materials. It is found that AGS can be successfully applied for formation and stabilization of the nanostructures using facile synthetic protocols.

The real advantage of nanocomposites based on sulfated arabinogalactan will be synergism of the properties peculiar both to modified natural polysaccharide matrix and to the nanosized core that allows realizing the new approaches in therapy and developing the new biomaterials of directed intracellular action.

## 2. Acknowledgments

This work was supported by Russian Foundation for Basic Research (grant 12-03-90433-Ukr_a), SB RAS (integration projects No. 85, 134, interdisciplinary projects of SB RAS and the Mongolian Academy of Sciences and the Ministry of Education, Culture and Science of Mongolia No. 4, 14).

## 3. References

1. Pomogailo A.D., Rosenberg A.S., Uflyand I.E., Metal nanoparticles in polymers. M, Chemistry, 2000, 672 p.

2. Ganenko T.V., Kostyro Ya.A., Sukhov B.G., Trofimov B.A., Fadeeva T.V., Vereshchagina S.A., Koryakina L.B., Silver nanocomposite, based on sulfated arabinogalactan, having antimicrobial and antithrombotic activity and its preparation method. RF Patent 2462254. 2012. – B.I - 2012. - № 27

3. Blagitko E.M., Burmistrov V.A., Kolesnikov A.P., Mikhailov Yu.I., Rodionov P.P. / Silver in medicine. Novosibirsk: Science-Center. - 2004. – 251p.

4. Krutkov Y.A., Kudrinsky A.A., Olenin A.Yu., Lisichkin G.V. Synthesis and properties of silver nanoparticles: achievements and prospects. Russian Chemical Reviews, 2008, T.77, p.242-269.

5 Shurygina IA, Sukhov BG, Fadeeva TV, Umanets VA, Shurygin MG, Ganenko TV, Kostyro Ya.A., Grigoriev EG, Trofimov BA Bactericidal action of Ag (0) - antithrombotic sulfated arabinogalactan nanocomposite: soevolution of initial nanocomposite and living microbial cell to a novel non-living nanocomposite / / Nanomedicine: Nanotechnology, Biology and Medicine. - 2011. - V. 7, N 6. - P. 827-833.

# Grain size dependent magnetic behavior of nanocrystalline Ni films

E.V. Sukovatitsina[1], A.S. Samardak[*,1,2], A.V. Ognev[1,2], A.Yu. Samardak[1], L.A. Chebotkevich[1,2], M.R. Sanaeian[3], F. Nasirpouri[3]

[1] *Far Eastern Federal University, 8 Sukhanova St., Vladivostok 690950, Russia*
[2] *Institute for Automation and Control Processes, 5 Radio St., Vladivostok 690041, Russia*
[3] *Department of Materials Engineering, Sahand University of Technology, Tabriz, Iran*

(*) corresponding author: samardak@dvfu.ru

*Keywords: grain size, anisotropy, nanocrystal, domain wall, coercivity*

## 1. Introduction

Polycrystalline materials with grain sizes less than100 nm are known as nanocrystalline materials [1,2]. These materials in the form of bulk nanostructured structures or films have become important in many technologies due to their improved physical, chemical and mechanical properties [3,4]. Nanocrystalline nickel is an example which has attracted much attention due to its improved surface properties such as hardness, corrosion and wear resistances, and also functional characteristics like magnetic and magentotransport properties [5-8]. Electrodeposition is a common, convenient and flexible method for the production of metal films or like nickel [9].

In this work, nanocrystalline nickel films were deposited from a Watts bath using direct current (DC). Detailed investigations on the effect of deposition conditions on the evolution of microstructure, crystallographic micro-texture and magnetic properties of nickel films are presented.

## 2. Experimental

In this investigation, nanocrystalline nickel films were prepared by electrodeposition in a Watt baths with pure nickel (99.99%) plate (surface Area: 10 $cm^2$) as the anode and copper foil (Surface Area: 1 $cm^2$) as the cathode. The Watts bath consisted of NiSO4.6H2O (265 g/litre of $H_2O$), NiCl2.6H2O (48 g/litre of $H_2O$), and H3BO3(31 g/litre of $H_2O$). Deposition was conduced in a pH of 3.7 and a temperature of 45± 0.5°C. We electrodeposited the series of films using DC.

The films thickness $D$ was calculated using the value of the mass per unit area of the deposited material $m = \rho D = {It}/{F} \times {M}/{z}$, where $\rho$ is Ni resistivity, $I$ is a current density, $t$ is a deposition time, $M$ is Ni molar mass, $z$ is valence number of ions, $F$ is Faraday constant.

Surface morphology was studied by scanning electron microscope (SEM) and roughnesses were measured by atomic force microscope (AFM). Films coercivity was defined from hysteresis loops with home-made vibration sample magnetometer.

## 3. Results and Discussion

Our study shows that with the rise of $D$ the grain size $R$ and amplitude of roughnesses h are increasing, Fig.1.

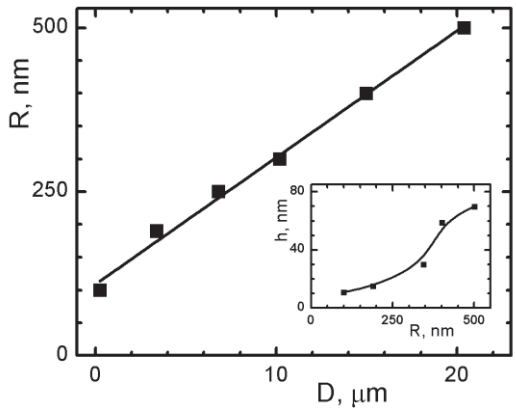


Figure 1. Dependence of the grain size $R$ on the film thickness $D$. The insert consists of the amplitude of roughnesses $h$ on $R$.

Polar diagrams of the remanent magnetization defined from hysteresis loops show the isotropic magnetic properties. We explain this fact by polycrystallinity of the films leading to the negligible value of magnetocrystalline anisotropy. There is no induced magnetic anisotropy in the films.

All the investigated Ni films had grains with size more than 100 nm. At $D$=0.27 μm the average grain size is about 200 nm which is compatible to the Bloch DW width in a single crystal Ni film, Fig.2. One can calculate typical DW width as $\delta = \sqrt{2A/K}$, where $A$=0,9×10$^{-6}$erg/cm is exchange constant, $K$=5×10$^4$ erg/cm$^2$ is magnetocrystalline anisotropy constant. As result δ=190 nm. Grains, which size $R$ is compatible to δ, will be single domain. The DW formation is only possible in films with $D$ > 15 um where $R \geq 400$ nm (grains have two magnetic domains). Therefore, in films with $D$ < 10 um, magnetization reversal occurs through non-coherent rotation of magnetization vectors.

In films with $R \geq 400$ nm remagnetization processes are due to magnetization vectors rotation and DWs displacement. The shape of hysteresis loops supports this statement. These are narrow loops with small remanent magnetization $M_r / M_s = 0.11 \div 0.14$.

The dependence of coercive force $H_c$ on $D$ is represented in Fig.2. $H_c$ non-monotonically decreases with rising of $D$.

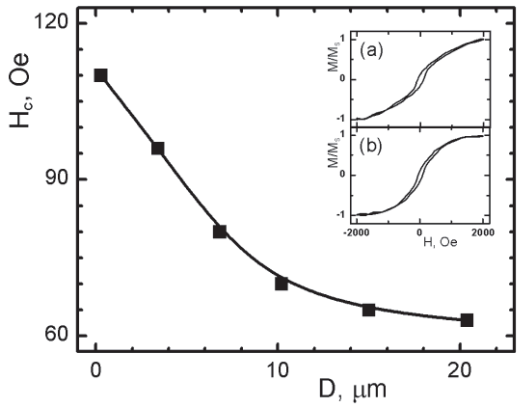


Figure 2. Dependence of coercive force $H_c$ on film thickness $D$. The insert shows hysteresis loops for different films.

Coercive force $H_c$ of polycrystalline Ni films consists of two components stipulated by a local magnetic anisotropy of grains $H_c^K$ [10] and surface roughnesses $H_c^h$ [11]:

$$H_c^K = p_c < K > / M_s \,, H_c^h = C M_s h / l^{4/3} D^{1/3} \,,$$

where $M_s$ is saturation magnetization, $l$ is period of roughnesses which is compatible with a grain size, $p_c$ =0.64 and $C$ are proportionality factors. For all studied films $H_c^K$ = 63Oe. The parameter $h/(l^{4/3} D^{1/3})$ of the component $H_c^h$ decreases with rising of $D$ and $R$, therefore in films with $D$ > 10 um coercive force $H_c$ will be defined only by the component $H_c^K$.

## 4. Conclusion

The study of the nanocrystalline Ni films reveals following:
- with rising of film thickness the grain size and surface roughness increase;
- the coercive force is in strong dependence on film thickness and grain size;
- if the average grain size is compatible to Bloch DW width, magnetization reversal occurs through the non-coherent rotation of magnetization vectors;
- if the average grain size is larger than the DW width, the remagnetization processes are due to coherent rotation of magnetization vectors and DW displacement.

## 5. Acknowledgements

Authors thank the Russian Ministry of Education and Science for financial support under contracts 14.A18.21.1277, 16.552.11.7059, 2.8649.2013, The Scientific Fund of FEFU.

## 6. References

[1] C. Suryanarayana et al., Hyperfine. Interact, 130 (2000) 5.
[2] A.S. Samardak et al., Phys. Met. and Metallog. 101 (2006) 11.
[3] C.C. Koch, J. Mater. Sci. 42 (2007) 1403.
[4] R. Mishra et al., Mat. Science and Eng.A 373 (2004) 370.
[5] A. Ul-Hamid et al., App. Surf. Science 257 (2011) 9251.
[6] A.V. Ognev et al., J. Phys.: Conf. Series 345 (2012) 012010.
[7] O. Sadiku-Agboola et al., Portug. Electrochim. Acta 29 (2011) 91.
[8] F. Nasirpouri et al., JMMM 299 (2006) 356.
[9] F. Nasirpouri et al., Electroanal. Chem. 690 (2013) 136.
[10] G.Herzer, IEEE Trans. On Magn. 26 (1990) 1397.
[11] S.P.Li et al., Phys. Rev. B. 61 (2000) 6871.

# Obtaining graphene nanoparticles aqueous suspensions and their complex investigation

A.V. Nikolaeva[1], E.A. Danilov[*,1], V.M. Samoylov[1], G.A. Erpuleva[1], N.N. Trofimova[1], S.S. Abramchuk[2]

[1]*JASC "NIIgraphit" of Rosatom State Corp.,111524, 2, Elektrodnaya St., Moscow, Russia*
[2] *M.V. Lomonosov Moscow State University, Faculty of Physics, 11999, Leninskie Gory, Moscow, Russia*

(*) danilovegor1@gmail.com

*Keywords: graphene, graphene nanoparticles, graphite exfoliation, graphene suspensions, graphene TEM*

## 1. Introduction

Recent state of modern research in the field of manufacturing novel polymer and ceramic composite materials has a strong tendency to use different nanoparticles that are able to significantly enhance mechanical, adjust electrical and heat conductivity, optical properties. From this point of view, carbon nanoparticles, such as graphene, multi- and single-walled carbon nanotubes, fullerenes etc., seem to be of greatest interest [1]. The aim of the current study was to develop commercially attractive ecologically safe protocols for obtaining stable aqueous suspensions of carbon nanoparticles which serve as a convenient source material for manufacturing of different composites [2].

## 2. Experimental

Graphene suspensions were obtained via natural graphite surfactant-assisted ultrasonication using a horn-type UZDN device (output power up to 200 W). Ultrasonication time varied from 10 to 360 min. Source graphite was milled down to 30 μm particle size and gas thermally treated to lower the ash content down to less than 0.01% (mass.). 3,4-diaminobenzene sulfuric acid (brutto formula $C_6H_8N_2O_3S$) was used as a surfactant. Our technique allowed obtaining of 6-30 mg/ml aqueous suspensions.

## 3. Results

Graphene suspensions were studied using laser diffraction technique. It can be stated (see fig.1) that the correlation between the size of graphene nanoplatelets and time of ultrasonication is almost exponential: size decreases significantly during the initial period with a trend for stabilization at 2.5-3 μm as the time of treatment increases.

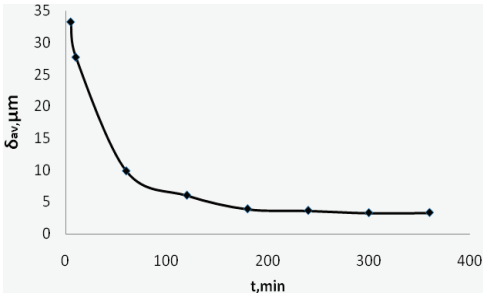


Figure 1. Correlation between mean particle size in graphene suspensions and time of ultrasonication.

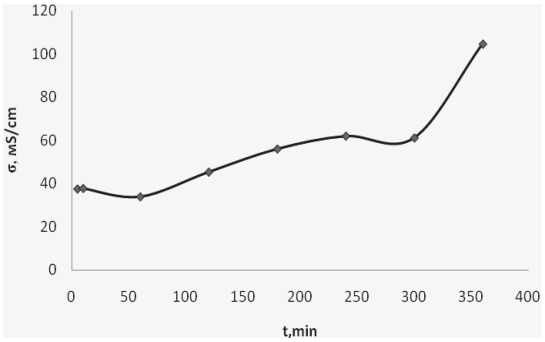


Figure 2. Suspension electrical conductivity as a function of ultrasonication time.

From both solution electrical conductivity and turbidimetry plots versus time of ultrasonication (fig.2 and 3) it is easy to note that, although both conductivity and opacity increase as the particle size decreases, rather drastic accretion occurs only when the particle size has stabilized which might suggest that exfoliation is most effective when particle size reaches certain

critical value allowing for the reduction in the number of graphene sheets without significant layer area decrease.

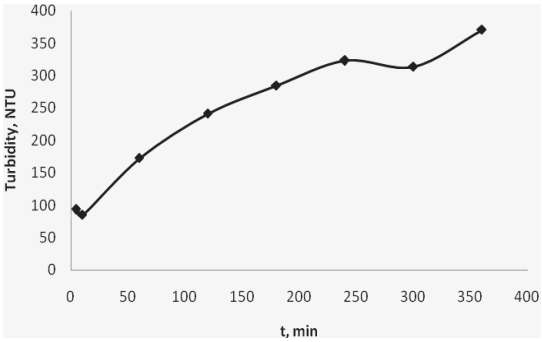


Figure 3. Suspension turbidity as a function of ultrasonication time.

TEM images analysis further supports this statement: increase of the time of ultrasonication leads to obtaining of more few-layered graphene particles (fig. 4).

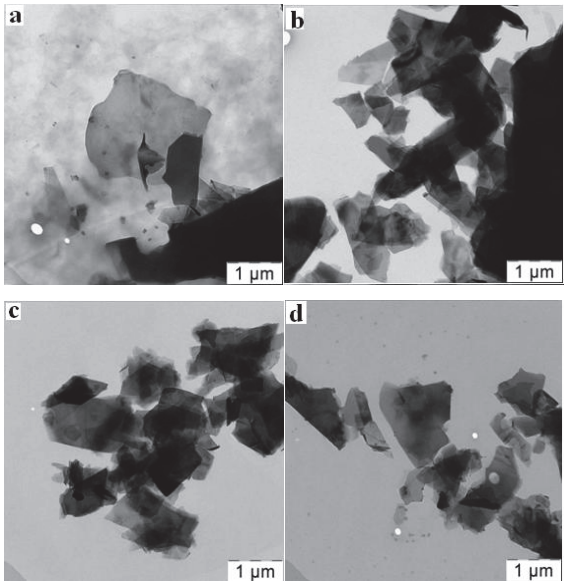


Figure 4. TEM images of ultrasonicated graphite suspensions: (a) 10 min., (b) – 4 hours, (c) – 5 hours, (d) – 6 hours.

On the final stage of ultrasonic treatment formation of folded and rolled graphene structures can be observed (see fig. 5) which is well established for graphene formation via the Hummers method [3].

## 4. Discussion

In the present study laboratory technology for obtaining few-layered graphene particles from graphite aqueous suspensions via direct surfactant assisted ultrasonic exfoliation was proposed. This technology excludes the use of oxidizing reagents, intercalates, reducing processes and does not require additional high-temperature treatment.

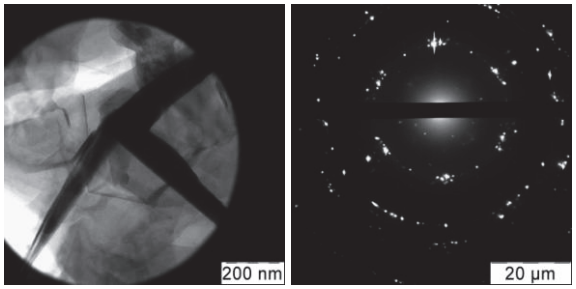


Figure 5. TEM image (left) and electron diffraction pattern (right) of graphene platelet obtained via graphite ultrasonication (6 hours).

Laser diffraction technique enables the estimation of sedimentation stability, whilst TEM – of size and number of layers for graphene nanoparticles suspensions.

Authors are currently designing a complex of laboratory units for manufacturing of experimental batches of graphene suspensions in different liquids. Laser diffraction, turbidimetry, and conductometry are proposed to assess the stability of the process.

Research aimed to apply graphene suspensions for manufacturing of electrically conductive ceramics, plastics and radio-shielding components is currently underway.

## 5. References

[1]. D. Galpaya, M. Wang, M. Liu et al. *Graphene*, **1** (2012) pp. 30-49.
[2]. Y.Sim, J. Park, Y.J. Kim et al.*J.Kor. Phys. Soc.* **58 (4)** (2011) pp. 938 – 942
[3]. I. Zaman, T.T. Phan, H.Ch. Kuan et al. *Polymer* **52** (2011) pp. 1603-1611

# Magnetic properties of nanostructures investigated by the improved magneto-optical Kerr effect method

M.E. Stebliy[1], A.V. Ognev[1,2], A.S. Samardak[1,2], L.A. Chebotkevich[1,2]

[1] *Far Eastern Federal University, 8 Sukhanova st.,Vladivostok, 690095 Russia*
[2] *Institute for Automation and Control Processes, Far East Branch, Russian Academy of Sciences, 5 Radio st., Vladivostok, 690041 Russia*

(*) corresponding author: ognevav@gmail.com

*Keywords: magnetic nanostructures, magnetic anisotropy, magneto-optical effect*

## 1. Introduction

Magnetic nanostructures possess by unique properties depending on the material parameters, size and shape of nano-elements. Using nanostructures it is possible to produce magnetoresistive memory, magnetic logic-in-memory chips and magnetic field sensors. Magnetic anisotropy is one of the key parameters determining magnetic structure and magnetization reversal critical fields. With reduction of the size of nanostructures below 100 nm, the control of their shape becomes more difficult due to the limit of lithography resolution. However, magnetic anisotropy can stabilize magnetic moments and reduce the possibility of thermal fluctuations of magnetization. Therefore, the development of local highly sensitive methods for determination of value and type of magnetic anisotropy is very actual.

In this paper, we propose the improved Kerr effect method for using as the magneto-optical anisometer with the modulated magnetic fields (modulated field magneto-optical anisometry - MFMA [1]). The improvement leads to the more accurate determination of the magnetic anisotropy field (Ha) utilizing MFMA. Moreover we demonstrate the possibility of measurement of the configurational anisotropy of magnetization processes in nanostructure arrays by MFMA.

## 2. Experimental

In this paper the magnetic properties of the films and arrays of nanodisks with a thickness of 20 nm are represented. The samples were prepared by magnetron sputtering. The base pressure in the chamber was $P_{base} = 2\times10^{-8}$ mBar, the working pressure of argon was $P_{Ar} = 3\times10^{-3}$ mBar. The deposition of cobalt was done on naturally oxidized substrate Si (111). The square arrays of nanodisks with diameter 600 nm and distance between centers 900 nm were fabricated using the electron-beam lithography and standard lift-off technique.

Magnetic properties were investigated by high-resolution magneto-optical Kerr effect (MOKE) with the laser spot diameter less than 10 μm. Magnetic anisotropy was measured with the improved MFMA.

## 3. Results

The MH loops showed that the polycrystalline Co film has strong uniaxial anisotropy. The value of $H_a$ was 41 Oe. However, if the MH loop has hysteresis along h.m.a., the value of $H_a$ will be incorrect. This is the case when one can use MFMA.

To measure the value and type of magnetic anisotropy by MFMA, one needs to apply two mutually perpendicular magnetic fields in the sample plane: the big constant field H and the small variable field $H_t$ (see the insert in Fig.1).

The frequency of $H_t$ was 30 Hz. The value of $\Delta M/M$ is depended on H and $H_t$. The set of $\Delta M/M = f(H_t, H)$ curves is represented in Fig.1. There are peaks on the curves at different magnetic fields $H^{max}$. However, in accordance with [1] the maximum value on the $\Delta M/M = f(H)$ curve is corresponding to $H_a$ which have to be constant and does not depend on the magnetic fields.

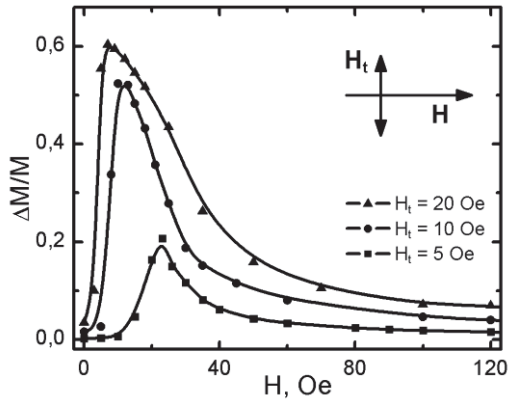


Fig.1. The magneto-optical response ΔM/M as a function of Ht and H. The insert shows magnetic fields configuration

We calculated ΔM/M dependences under variable and constant magnetic fields. We suggested that magnetic anisotropy measurements were done at the fields which were higher than the coercive force. Thus, the ΔM/M value is defined mainly by magnetization rotation. In common, ΔM/M is depended on the energy of anisotropy ($K_a$) and Zeeman energy caused by $H_t$ and H:

$$E = K_a \sin^2 \alpha - H_t M \cos\alpha - HM \sin\alpha$$

For precise experimental measurement of $H_a$ we plotted $H_{max} = f(H_t)$. The $H_{max}$ values were defined from differentiation of $\Delta M/M = f(H_t, H)$ curves. The $H^{max} = f(H_t)$ dependence has a nonlinear character.

We defined $H_a$ by extrapolation the $H_{max} = f(H_t)$ dependence to $H_t = 0$. For the Co film we found $H_a$ = 43 Oe which value is in good agreement with the experimental $H_a$ value.

To determine the anisotropy type, one need to measure the dependence $\Delta M/M = f(\theta)$, where θ is an angle between selected direction in a sample and an applied magnetic field H. The interaction between the shape of nanostructures and anisotropy of magnetization reversal processes was shown in [2] using MFMA method. We propose to utilize MFMA to define the anisotropy of magnetization reversal processes caused by an array configuration.

In this work we present results of the configurational anisotropy study in Co nanodisk array. The circle shape of nanodisks enables to exclude an influence of shape anisotropy.

Measurement results of the magnetization reversal processes anisotropy for the cobalt film and nanodisk array is shown in Fig.2. We found a uniaxial anisotropy of magnetization reversal processes in the film reflected by $H_c = f(\theta)$ и $\Delta M/M = f(\theta)$ dependences, Fig.2 (a,c). For the nanodisk array we observed the four maxima on the $H_c = f(\theta)$ polar diagram which repeat over 60 and 120°. However, the $\Delta M/M = f(\theta)$ polar diagram has the same number of maxima, but they are arranged symmetrically over 90° which corresponds to the symmetry of the square array.

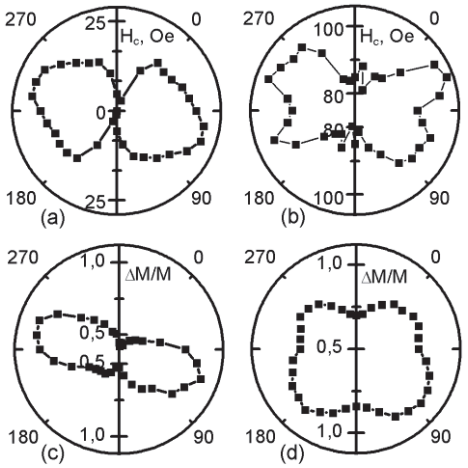


Fig. 2. The polar diagrams Hc = f(θ) (a, b) and ΔM/M= f(θ) (c, d) plotted for Co film (a, c) and nanodisks (b, d).

## 4. Conclusions

As result we have defined following: MFMA is the reliable method to study of magnetic anisotropy in films and nanostructures; to define Ha, one has to measure the set of $\Delta M/M = f(H_t, H)$ curves, find $H_{max}$ and make an approximation of the $H_{max} = f(H_t)$ dependence; utilizing MFMA, one can accurately determine the anisotropy of magnetization reversal processes caused by the dipole-dipole interaction in an array.

Authors acknowledge the support of the Russian Ministry of Education and Science under government contracts 16.552.11.7059, 2.8649.2013, 14.A18.21.1640 and Russian Foundation for Basic Research under project 12-02-31328 mol_a.

## 5. References

[1] R.P. Cowburn, A. Ercole, J. Appl. Phys., 81, pp.6879-6883, 1997.
[2] R.P. Cowburn // J. Phys. D: Appl. Phys. 33 (2000) R1–R16.

# Morphology and particle size of nanosized silica gel, synthesized by micellar technology

R. Romanova*, E. Sitnikova, A. Dresvynnikov

*Kazan National Research Technological University, 420015, Russia, Kazan, K. Marx str., 68;*

*e-mail: romanova_rg@mail.ru

*Keywords: silica, silica gel, micelle, nanosized*

## 1. Introduction

One of the most promising materials used for manufacturing semiconductors, dielectric, piezoelectric, magnetic, and other sintered products [1,2] is based on cordierite ceramic structures $MgO-Al_2O_3-SiO_2$, a phase and chemical composition whose primarily due to chemical composition, morphology and size of the primary particles of the precursors used to obtain it. In this connection the working of technology for ultradispersed precursors, in particular, silica, providing the most definitive phase transformation to the cordierite, is an actual.

In this paper a process for preparing samples of nanodispersed silica gel in nanoreactors, representing the mesophase of surfactant (saturated carboxylic acid composition $C_nH_{2n+1}COOH$ (n = 9,15)) with the ampholytic structure in an organic solvent [3,4], is proposed, and also results of a study of morphology and particle size of the synthesized gel samples are shown.

## 2. Experimental

Samples of silica gel, synthesized in accordance with the proposed procedure, were taken for study. Aqueous solutions of silicate of sodium or potassium (concentration of silica = 0.73-7.30 mol/l) added while stirring to solution of palmatic or n-capric acid (concentration - 0.09 mol/l) in chloroform or hexane. System was emulsified with continuous stirring for 30 seconds, then acetone (20 % vol.) was added – the formed silica gel milky-white color was precipitated to the bottom of the reaction vessel, whereupon was separated by filtration followed by washing with acetone and water. Samples of silica gel were dried in oven at the temperature 100 ± 5°C to constant weight. The synthesis conditions of silica gel samples are presented in Table 1.

Table 1. The synthesis conditions of studied silica gel samples.

| № | Organic acid | Solvent | Silicate type | Concentration of $SiO_2$, mol/l |
|---|---|---|---|---|
| 1 | palmatic | chloroform | $Na_2SiO_3$ | 0.73 |
| 2 | palmatic | hexane | $Na_2SiO_3$ | 2.19 |
| 3 | n-capric | hexane | $Na_2SiO_3$ | 0.73 |
| 4 | n-capric | hexane | $Na_2SiO_3$ | 2.19 |
| 5 | n-capric | hexane | $Na_2SiO_3$ | 7.30 |
| 6 | n-capric | hexane | $K_2SiO_3$ | 1.31 |
| 7 | n-capric | hexane | $K_2SiO_3$ | 2.18 |

Morphology and particle size of the synthesized gel samples were studied by method of transmission electron microscopy (TEM) with use of electron microscope EMMA-4. The preparations were prepared by applying a drop of collodion film on the substrate with a copper mesh and then coated with carbon in a vacuum system VUP-4 at an accelerating voltage of 75 kV.

## 3. Results and Discussion

The obtained results are shown as photomicrographs on Figure 1 and quantitatively described in Table 2.

The study of the synthesized silica gel samples by TEM showed that they are colloidal systems (from sols to gels), formed as an isolated and coagulation (gelatinous) phases with nanosized particles having different morphology. The largest conglomerates are characterized by translucent amorphous structure and sizes ranging from 4 to 25 microns.

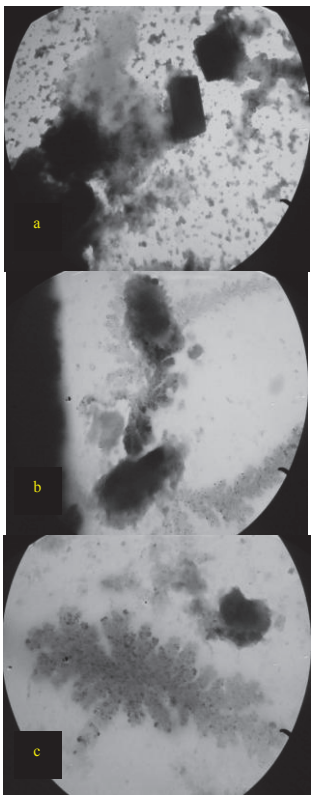


Figure 1. The results of TEM-study for silica gel sample (obtained using n-capric acid, hexane and solution of potassium silicate with silica concentration of 2.18 mol/l) at the different zoom (a - 2000-4000, b - 17000-19000, c - 40000 -55000).

Table 2. Results of study of synthesized silica gel samples by TEM.

| № | Particle size, nm, at the zoom | | |
|---|---|---|---|
| | 2000–4000 | 17000–19000 | 40000–55000 |
| 1 | - | 450-550 | 150-200 |
| 2 | 5000–6000 | 600-650 | 200-250 |
| 3 | 4000–5000 | 450-500 | - |
| 4 | 9000–10000 | 250-500 | 100-150 |
| 5 | 20000–21000 | 250-500 | - |
| 6 | 24000–25000 | 600–650 | 150–220 |
| 7 | 9000-11000 | 600–650 | 150–200 |

Particles with non-isometric lamellar structure with size 250-650 nm are detected at higher zoom. Moreover, as shown in Figure 1, the presence of thin rounded and slightly faceted particles with size 100 - 250 nm, forming the chain of the gel, is characteristically for samples.

This work was financially supported by the Ministry of Education and Science of the Russian Federation within the framework of the state task (PNIL-96-12) and the Federal Target Program "Research and development on priority directions of scientific-technological complex of Russia for 2007-2013" (State Contract 16.552.11.7060)

## 4. References

[1]. I. Trubnikov, Ogneupori i tehnicheskay keramika. 7 (2003) 14.
[2]. N. Shabanov, V. Popov, P. Sarkisov, Khimia I tekhnologiy nanodispersnikh oksidov. M.: Academkniga, 2007. 309 p.
[3] R. Romanova, A. Dresvynnikov, O. Kuz'mina et al, Vestnik KGTU. 8 (2010) 448.
[4] R. Romanova, A. Dresvynnikov, A. Abdullina, Vestnik KGTU. 10 (2010) 680.

# The Formation of TaC Structure from Tantalum Alkylamides

V. V. Shatunov[*,1], G. I. Shcherbakova[1], M. Kh. Blokhina[1], M. S. Varfolomeev[1], D. V. Sidorov[1], P. A. Storozhenko[1], G. Yu. Yurkov[2].

[1] *Federal State Unitary Enterprise "State Research Institute for Chemistry and Technology of Organoelement Compounds", 38, shosse Entuziastov, Moscow, 105118, Russia*

[2] *A. A. Baikov Institute of Metallurgy and Material Science, RAS, 49, Leninsky prospekt, Moscow, 119991, Russia*

(*) corresponding author: sha2nov@rambler.ru

*Keywords: tantalum carbide, tantalum alkylamides, thermal transformation, pyrolysis, ceramic.*

## 1. Introduction

Tantalum carbide is a high-melting compound ($T_{melt}$=3880 °C), which is extremely hard and chemically inert, and possesses phase stability in a wide temperature range and low vapour pressure. A set of those characteristics makes tantalum carbide indispensable in the aerospace industry [1].

Traditional synthesis techniques for nanoscale tantalum carbide (plasma enhanced technique, laser pyrolysis, chemical vapour deposition) [2] are technologically difficult and energy consuming. Recently methods of synthesis via transparent tantalum-carbon containing gels [3], via tantalum pentaethoxide and activated nanocarbon [4] and according to the reaction of metal magnesium with sodium carbonate and tantalum pentachloride have been spread [5].

We suggest a new approach to obtaining tantalum carbide TaC.

## 2. Experimental

All operations with tantalum amides and tantalum containing substrates were carried out in a nitrogen box blown off with dry nitrogen or in the flow of dry nitrogen; utilized solvents were dried over calcium hydride and distilled under vacuum.

10 g (21.346 mmol) of pentakis(dimethylamino)tantalum and 19.15 g (25 ml) of purified and dried tetradecane were put into a 250 ml three-neck flask equipped with a thermometer, a reflux condenser and a vacuum-nitrogen system. The mixture was heated from room temperature to 150 ºC for 30 min. After that it was slowly heated to 170-180 ºC and kept within that temperature range, until gas completely ceased to release. The mixture gets visually black. Then the reaction mass is boiled down for a few hours at tetradecane boiling temperature (254 ºC). Clear tetradecane dripping from the reflux condenser proves that the thermal transformation of tantalum amide has ceased. At the end of this stage the solvent was distilled, and 7.07 g of black high-dispersive powder was obtained. A sample of the powder was put into an alumina tray, where it underwent pyrolysis under dry argon atmosphere up to 1100 ºC being kept at 500 ºC for 2 hours and then at 1100 ºC 2 hours more. Fine brown powder was obtained. A ceramic yield was 77.27%.

## 3. Results

A new approach we suggest to obtaining tantalum carbide TaC consists in thermal transformation of solutions of tantalum amide compounds in high-boiling solvents under inert atmosphere (dry nitrogen or argon), followed by a step pyrolysis of the resultant tantalum containing substrates under inert atmosphere at 1100 ºC to form tantalum carbide TaC.

At the first stage, while solutions of tantalum amide compounds are heat treated, tantalum amides are thermally destructed with a corresponding dialkylamine, depending on the selected object of heat treatment, released, and a tantalum containing substrate is formed. The formation of dialkylamines is confirmed by NMR $^1$H spectroscopy.

At the second stage after solvent distillation the tantalum containing substrate

undergoes a step pyrolysis up to 1100 ºC under dry argon atmosphere. The tantalum containing substrate after pyrolysis under inert atmosphere forms tantalum carbide TaC in the form of fine brown powder. The formation of tantalum nitride was not observed during that process.

SEM/EDS (Fig. 1) and XPA results for ceramic samples we have obtained confirm quantitative formation of tantalum carbide. A SEM image (Fig. 2) is evidence of formation of TaC microspheres (scale 10 μm).

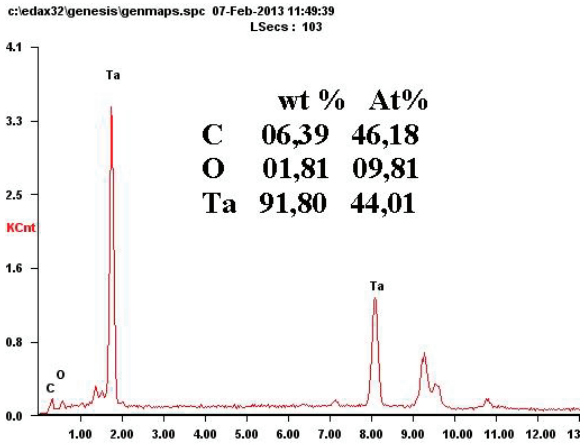


Figure 1. SEM/EDS of the ceramic material sample.

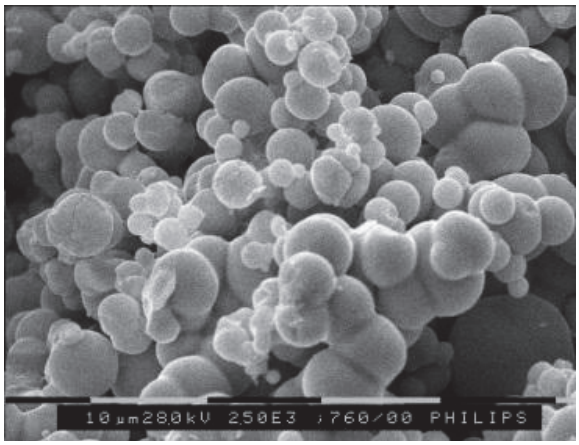


Figure 2. SEM image of tantalum carbide microspheres.

## 4. Discussion

The presence of oxygen impurity contaminates tantalum carbide with tantalum oxides and narrows a range of its end use. Such issue is a technical one, and that is where we currently direct our efforts to.

At present some work is done to increase dispersion ability of the obtained ceramic samples to nanoscale, which in its turn will broaden their application area.

A disadvantage of the technique is rather a high price for initial tantalum amides. That hinders large lot production of tantalum carbide.

## 5. References

[1]. G. V. Samsonov, I. M. Vinnitsky, Tugoplavkiye soedinenia (spravochnik). 2nd edition, M. Metallurgia. 1976. 560 pages.

[2]. V. G. Sevastyanov, E. P. Simonenko, N. A. Ignatov, Yu. S. Yezhov, N. P. Simonenko, N. T. Kuznetsov, *Neorg. Mater. RAS.* **56** (2011) 707.

[3]. V. G. Sevastyanov, E. P. Simonenko, N. A. Ignatov, Yu. S. Yezhov, N. P. Simonenko, N. T. Kuznetsov, *Neorg. Mater. RAS.* **46** (2010) 563.

[4]. M. Ma, W. Shen, P. Zhang, J. Zhang, Q. Wang, C. Ge. *Mater. Lett.* **65** (2011) 96.

[5]. J. Ma, Y. Du, M. Wu, M-C. Pan. *Mater. Lett.* **61** (2007) 3658.

# Chemoselective hydrogenation of o-nitrochlorobenzene in the presence of catalysts based on nanoscale palladium phosphides

N.I. Skripov[1*], T.P. Stepanova[1], L.B. Belykh[1], F.K. Schmidt[1]

[1] *Irkutsk State University, department of chemistry, K. Marks st. 1, Irkutsk, 664003 Russia*

E-mail: nsk7@mail.ru

*Keywords: hydrogenation, catalysis, nanoparticles, palladium, o-nitrochlorobenzene*

## 1. Introduction

In recent years questions of environmental safety get the increasing attention so it is important to find new catalysts and new approaches to synthesize effective catalysts for hydroprocessing: hydrogenation of halonitroaromatics, hydrodechlorination of aryl and alkyl halogenides, hydrodesulfurization and hydrodenitrogenation.

Among the numerous systems based on platinum group metals the most effective in reduction of nitro group and hydrogenolysis of C-Hal bond are palladium catalysts. Despite high activity of palladium in both above reactions, it is possible to produce the palladium catalysts showing a high chemoselectivity to haloanilines by varying the particle size, degree of polydispersity, the nature of the catalyst support, the method of catalyst anchoring or by addition of modifiers based on I-IVB groups metals or Lewis acids.

The report focuses on the study of influence of the size, nanoparticles and surface layer composition on properties of palladium catalysts modified with elemental phosphorus in the reduction of-nitrochlorobenzene.

## 2. Experimental

Solvents, substrates were purified by standard procedures used for handling of organometallic compounds. Catalytic reactions were carried out in a thermostated vessel of the "duck" type at starting pressure of hydrogen of 2 Torr. The process of hydrogenation was followed by dropping of pressure using manometer and by GC method.

Data on surface layer composition, size and nature of nanoparticles were obtained using such methods as X-ray powder diffraction (XPD, DRON-3M), transmission electron microscopy (TEM, Philips EM-410) and X-ray photoelectron spectroscopy (XPS, Riber LAS-3000).

## 3. Results

The major factors influencing activity, selectivity and stability of Pd-containing nanoparticles in o-nitrochlorobenzene hydrogenation are established. These are nature of the precursor, concentration of modifier (elemental phosphorus) and the process conditions.

The selectivity to o-chloroaniline of Pd-blacks obtained from different precursors in hydrogen atmosphere and N,N-dimethylformamide decreases in the series: $Pd(acac)_2$ (76%) > $PdCl_2$ (66%) ≈ $Pd(dba)_2$. Average size of base particles of Pd-blacks varies in the range of $Pd(acac)_2$ (26 nm) > $PdCl_2$ (5-6 nm) > $Pd(dba)_2$ (3 nm).

A symbate relationship between selectivity to the desired product – o-chloroaniline and phosphorus concentration in the range of molar ratios P/Pd = 0-2 was shown. The introduction of phosphorus in catalytic system favors an increase in selectivity to o-chloroaniline from 66-76 to 92%, an increase stability nanoparticles compared with Pd-black, but reduces the turnover frequency of the reaction by an order of magnitude.

At high concentrations of modifier kinetic curves of nitrocompound hydrogenation under the action of $Pd(acac)_2$-P system are S-shaped. When introducing the second portion of substrate S-shaped

form of kinetic curve is not observed, while increasing the time of formation did not eliminate S-shaped form.

The nature of Pd-containing nanoparticles modified with phosphorus is investigated. By XPS, XPD and TEM set the size, the composition of the nanoparticles and the state of the surface layer of palladium catalysts are established. When P/Pd = 0.3 nanoparticles with an average diameter of 5.6 nm consist of phosphide $Pd_6P$ and clusters Pd (0). According to XPS there are both clusters Pd (0) ($BE(Pd3d_{5/2})$=334.5 eV), palladium phosphides ($BE(Pd3d_{5/2})$=336.3 eV; $BE(P2p_{3/2})$=129.5 eV), and ammonium salts – dihydro- and hydrophosphates (phosphites) on the catalyst surface.

With growth of modifier concentration composition and size of nanoparticles are changed. When the ratio P/Pd = 1.0 the nanoparticles with an average diameter of 4.7 nm consist of palladium phosphides $Pd_5P_2$, $PdP_2$. The content of Pd (0) is reduced to 8%.

## 4. Discussion

The reaction of catalytic hydrogenation of o-nitrochlorobenzene under action of molecular hydrogen is usually accompanied by hydrogenolysis of the C-Cl bond, which refers to the structure-sensitive processes. In the case of Pd-blacks derived from different precursors in hydrogen selectivity to o-chloroaniline increases with decreasing catalyst particle size.

However, the particle size is not the only factor determining the selectivity of palladium catalysts. Pd-containing nanoparticles modified with elemental phosphorus commensurable by the size with Pd-blacks (5.6 nm) had significantly higher selectivity and stability.

Improved stability of nanoparticles may be due to elektrosteric factor - the stabilization of nanoparticles with ammonium salts – dihydro- and hydrophosphates (phosphites). The latter are the result of partial hydrolysis of the solvent N,N-dimethylformamide, and formed phosphoric acids accelerate this process. The condition of Pd on a surface of nanoparticles can be other reason of selectivity enhancement. According to XPS, at the surface of the nanoparticles modified with phosphorus, palladium is in two forms: $Pd^0$ and $Pd^{\delta+}$. The acquirement of a positive charge on palladium leads to a weakening of the M-Cl bond and increases the stability of these catalysts in hydrodechlorination, as HCl formed quickly leaves the surface.

## 5. Acknowledgments

This study was financially supported by the Ministry of Education and Science of the Russian Federation, the agreement no. 14.B37.21.0795 and Irkutsk State University grant no. 2012-03-03.

# Evolution of catalytic property of Palladium nanoparticles

R. D. Solovov[1,2*], H. E. Yakimova[1,2], E. V. Abkhalimov[2], B. G. Ershov[2]

[1] *IPCE RAC, Institution of Russian Academy of Sciences Frumkin Institute of Physical Chemistry and Electrochemistry of the Russian Academy of Sciences, 31, Leninsky prospect, Moscow GSP-1, 119071 Russia*
[2] *MITHT, Lomonosov Moscow University of Fine Chemical Technology, 86, Prospect Vernadskogo, Moscow, 117571 Russia*

roman_solovov@mail.ru

*Keywords: nanoparticles, ξ-potential, dynamic light scattering, catalysis*

## 1. Introduction

At the last time a physicochemical property of nanoparticles and dependence on each other are investigated very active. However, there are very few works, which investigates the evolution of these properties in a time.

In this work we investigated the evolution of physicochemical property of palladium nanoparticles in time. A ξ-potential, hydrodynamic diameter and catalytic activity were measured.

## 2. Experimental

### *2.1. Materials, solutions and devices*

In this work tethraaminpalladium dichloride $[Pd(NH_3)_4]Cl_2$ (Aldrich), sodium polyacrylate $(CH_2CHCOONa)_x$ (Fluka), sodium hydroxide NaOH (Fluka), methylviologen dichloride $MVCl_2$ (Acros, 98%) and hydrogen $H_2$ were used. All solutions were prepared with deionized water.

All spectra of absorbance were measured by spectrophotometer Cary Varian 100. ξ-potential and hydrodynamic diameter were measured by device of dynamic light scattering DelsaNano C. Size of palladium nanoparticles were measured by transmission electron microscope Carl Zeiss LEO 912 AB Omega.

### *2.2. Preparation of nanoparticles and their characteristics*

Very stable at during long time nanoparticles were prepared by means of photochemical method. The photochemical method is to irradiation of solution of palladium complexes and stabilizing agent by pulsed xenon lamp. When irradiated of solution, highly active radicals and molecules were produced. They reduced palladium complexes to $Pd^0$.

The formed nanoparticles are monodispersed and have average diameter of 2.5 nm. Absorbance spectra of irradiated solutions for different times (Figure 1a) and histogram of the size distribution of producing palladium nanoparticles (Figure 1b) are showed.

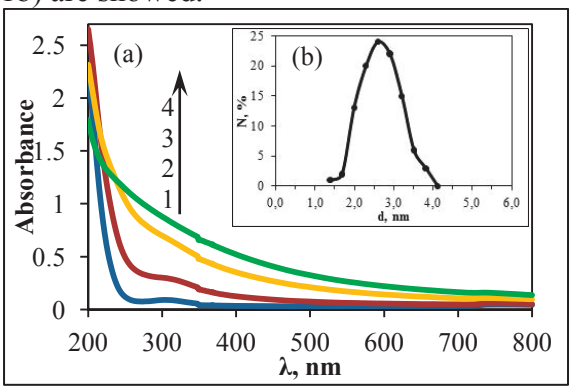


Figure 1. (a) Absorbance spectra of irradiated solutions for different times: 1 – 0 minutes; 2 – 1 minute; 3 – 5 minutes; 4 – 20 minutes
(b) Histogram of the size distribution of producing palladium nanoparticles

### *2.3. Catalytic reaction*

Catalytic activity of palladium nanoparticles was studied in the reaction of single-electron reduction of methylviologen in the alkaline (pH = 11.0) aqueous medium by hydrogen. Standard potential of pair is $E_0(MV^{2+}/MV^{\cdot+}) = -0.450$ V [1]. Potential of hydrogen pair is substantially more negative, namely $E_0(H^+/H_2) = -0.652$ V, because hydrogen ion concentration is low. By these conditions the next reaction becomes possible:

$$2MV^{2+} + H_2 \rightarrow 2MV^{\cdot+} + 2H^+$$

The formed radical cation $MV^{\cdot+}$ is blue, therefore its concentration was measured by spectrophotometry ($\varepsilon_{600}(MV^{\cdot+}) = 1.1\times10^4$ l·mol$^{-1}$·cm$^{-1}$) [2]. This reaction is a reaction of the first order with respect to hydrogen and is described by the next kinetic equation:

$$[MV^{\cdot+}] = [MV^{\cdot+}]_\infty \times e^{-k\tau}$$

## 3. Results

When studying properties of palladium nanoparticles has been shown that the hydrodynamic diameter of the sol increases uniformly in time to 15 nm and then slowly decreases to 14 nm (Figure 2a). However, measured by transmission electron microscope size of nanoparticles were not changed.

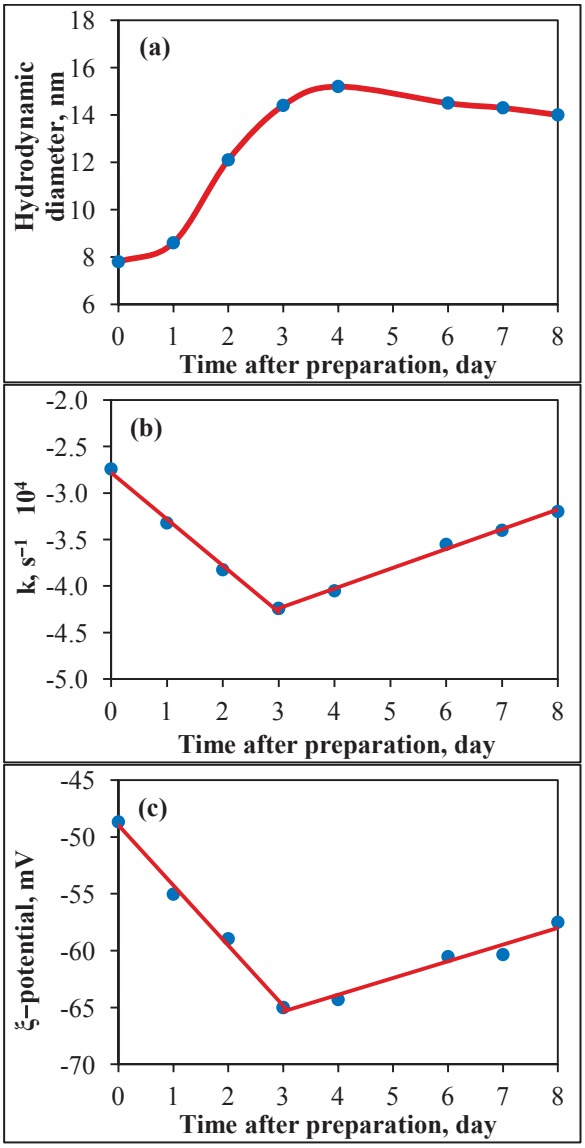


Figure 2. Evolution of hydrodynamic diameter (a), reaction rate constant (b) and ξ-potential (c) in a time.

The dependence between first-order rate constant of reaction (Figure 2b) and zeta-potential (Figure 2c) on one part and time on the other part has a linear form with a kink. Kink of lines occur on the third day after preparation of palladium nanoparticles.

## 4. Discussion

The hydrodynamic diameter is a diameter of light-scattering particles. It is likely to have been increased due to additional adsorption of stabilizing polymer on the nanoparticles surface. The catalytic activity of palladium nanoparticles decreased because the diffusion of hydrogen is complicated to surface of nanoparticles by layers of stabilizing polymer. Therefore, aggregative stability and zeta-potential increased. After three days the adsorption was ended and particles began to lose sedimentation stability. Potential began to increase. Catalytic activity is likely to has been increased due to partial desorption of stabilizing polymer from the nanoparticles surface and due to saturation of nanoparticles with hydrogen.

Thus, the study of the evolution of physical and chemical properties of nanoparticles in time allows to control their catalytic properties.

## 5. References

[1]. Henglein A. // J. Phys. Chem. 1993. V. 97. P. 5457.
[2]. Trudinger P.A. // Anal. Biochem. 1970. V. 36. P 222.

# Synthesis of mixed Mg-Zn oxides fine powders

A.N. Chudinov, T.A. Rozdyalovskaya*, Yu.S Chekryshkin

*Institute of technical chemistry of UB of the RAS*

(*) corresponding author *rozdta@mail.ru*

*Keywords: zinc oxide, magnesium oxide, molten salt oxidation*

## 1. Introduction

Novel approaches for synthesis of nanosized metal oxides are urgent due to unique properties of such materials. Fine dispersed zinc and magnesium oxides can be applied in electronic and pharmaceutical industry, as well as in production of adsorbents, catalysts, sensors, abrasives, and ceramics with excellent operating characteristic.

It was shown, that while feeding of air or oxygen to molten chlorides of magnesium, calcium or zinc reaction of chloride-ion oxidation occurred resulting in formation of corresponding metal oxide and gaseous chlorine [1].

## 2. Experimental

Powders of individual and mixed magnesium and zinc oxides were synthesized bubbling air or oxygen through the molten chlorides (individual and mixed in Mg:Zn 1:1, 1:2, or1:10 molar ratio). Metal oxides generated in such way were retrieved through dissolving of reaction mixture in distilled water followed by centrifugation. Oxides powders were then dried at 100–130 °C and calcined at 300–600 °C.

## 3. Results

XRD analysis data indicated that MgO and ZnO were the only reaction products. Crystalline average size, $D$ (nm), of oxides particles was calculated with Selyakov-Scherrer equation [2]: $D_{MgO}$ = 62 nm; $D_{ZnO}$ = 58 nm. These values of $D$ were practically the same for individual and mixed oxides.

Size of magnesium oxide grain synthesized in the pure $MgCl_2$ was shown to be 2–5 μm (SEM). It was established with the help of atomic-force microscopy that Mg and Zn oxides grain size in their mixture was about 25–100 nm (See fig. 1).

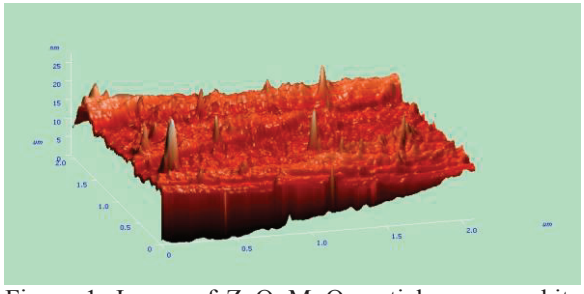

Figure 1. Image of ZnO–MgO particles on graphite substrate.

Specific area values for individual and mixed oxide powders were found to be: MgO – 10,85 $m^2/g$, ZnO – 1,95 $m^2/g$, ZnO–MgO – 20,26 $m^2/g$.

## 4. Discussion

Data acquired allow saying that reaction of molten chloride oxidation is of interest to produce metal oxides. It is possible to synthesize with help of this method nanosized (ZnO) as well as coarse-crystalline, but nanostructured (MgO) metal oxide powders of high purity.

This work had been performed with financial support of RFBR, project No 13-03-00166_a.

## 5. References

[1]. Чекрышкин Ю.С., Чудинов А.Н., Роздяловская Т.А., Федоров А.А. // Журнал прикладной химии. – 2010. – Т. 83. – № 8. – С. 1355–1359.

[2]. Шабанова Н.А., Попов В.В., Саркисов П.Д. Химия и технология нанодисперсных оксидов. М.: ИКЦ "Академкнига", 2007. 309 с.

# Research of nanopowders properties of new the phosphors produced by a method of pulsed electron beam evaporation

M.G. Zuev[1, 3], V.G. Il`ves[2], S.Yu. Sokovnin[2, 3]

[1] *Institute of Solid State Chemistry, Ural Branch, RAS, 91, ul. Pervomaiskaja, Yekaterinburg, Russia; 620990*

[2] *Institute of Electrophysics, Ural Branch RAS, 106 Amundsen St., Yekaterinburg, Russia; 620016*

[3] *Ural Federal University named after First President of Russia B.N. Yeltsin, 19, ul. Mira, Yekaterinburg,620002*

*Keywords: pulsed electron evaporation*

For the first time using pulsed electron evaporation were produced nanopowders (NPs) of phosphors $Sr_2Y_8(SiO_4)6O_2$:Eu with oxyapatite structure with a specific surface to 184 $m^2$/g. Characteristics NPs were studied by methods of XRD, electronic microscopy of the high permission, electrongraphy and photoluminescence (PL).

The analysis of a photoluminescence spectrum of phosphor has shown that the luminescence spectrum has changed in comparison with a micropowder of the same structure. The $Eu^{3+}$ luminescence spectrum containes smaller number of lines, than $Eu^{3+}$ spectrum of the micron size particles. Besides the shift of spectral lines was observed. There was also a reduction of intensity red and increase orange spectrum lines. After roasting on the air the nanophosphor spectrum of luminescence $Eu^{3+}$ has coincided with that one for microparticles. Thus, the effect of quantum restriction on position of power levels was observed, apparently. The size of particles of a phosphor has influenced its spectral structure.

NPs synthesis $Sr_2Y_8(SiO_4)6O_2$: Eu an evaporation method by pulsed electron beam (PEB) in low pressure gas and condensation nanoparticles in vacuum is of interest for use in optoelectronics. Ultrathin oxide NPs and a phosphor are received by PEB evaporation for the first time.

The purpose of the present work consists in research of possibility of reception NPs phosphors on the basis of difficult oxides in vacuum by PEB evaporation and studying of their basic properties.

NPs have been synthesized by PEB evaporation on installation NANOBEAM-2. Targets made from stoichiometric powders of the micron sizes received by solid phase synthesis with specific surface SBET=0,04 − 0,5 $m^2$/g. Pressings from micron powders in diameter of 20-30 mm and thickness of 5-10 mm were preliminary baked at temperature 1400 ºC during 40 h on air to avoid target destruction at PEB evaporation. NPs besieged on not cooled glass substrates of the big area (to 625 $cm^2$) which placed round a target. Gathering NPs made nearby 0,6 g/h.

Structural properties nanopowders defined with use of methods of electronic microscopy (TEM HR, JEM-2100 microscope) and X-ray diffraction (XRD, DRON-2 diffractometer). For measurements of luminescent properties nanopowders used spectrometer MDR-204 (deuterium lamp, Hamamatsu R928 photomultiplier). Specific surface NPs measured by means of BET method on installation TriStar 3000V.

The X-ray phase analysis has shown that all received NPs were amorphous. Data TEM HR has confirmed presence amorphous components oxide NPs. However, given electron diffraction analysis have shown that NPs are not completely amorphous and contain an insignificant share of crystal nanoparticles that follows from presence on separate sites of the sample of reflexes from crystal phases. As a matter of fact, received NPs are amorphous-nanocrystal.

The analysis of spectra of photoluminescence NPs $Sr_2Y_8(SiO_4)6O_2$: Eu has shown that the luminescence spectrum has changed in comparison with a micropowder of the same structure. The

spectrum of PL $Eu^{3+}$ began to contain smaller number of lines, than spectrum $Eu^{3+}$ particles of the micron size. Besides, shift of spectral lines was observed. There was also a reduction of intensity red and increase orange spectrum lines. After roasting nanophosphor on air the spectrum of PL $Eu^{3+}$ has coincided with that for microparticles. Thus, the effect of quantum restriction on position of power levels was observed, apparently. The size of particles of a phosphor has influenced its spectral structure.

Work is partially executed with financial support of the project of Ural Branch of the RAS «Working out and spectral characteristics nanophosphor, the targets received at electronic evaporation on a basis apatite of silicates» № 12-M-23-2007.

# Impact of Fullerene $C_{60}$ on Morphological Properties of Neutrophils

L.A. Sharafutdinova[1], E.N. Gorshkova[2], Z.R. Khismatullina[1]

[1] *Bashkir State University, 32, Validy Str., Ufa, Russia, 450076*

[2] *Lobachevsky National Research University of Nizhni Novgorod, 23, Prospekt Gagarina, Nizhni Novgorod, Russia, 603950*

*Keywords: fullerenes, neutrophils, cytotoxic effect*

Active development of industry and usage of nanomaterials leads to the pollution of the environment, their penetration into living organisms and, finally, to the effect on human's health. Nanoparticles are known to be absorbed and not to be removed from living cells; they change DNA, can cause genetic disorders, damage biomembrane, disturb biomolecules' functioning, make compounds with blood proteins and easily penetrate into all organs. They even can overcome encephalitis haematological barrier, thus, getting into the brain. The investigation of nanomaterials' impact on human's body, nanoparticles' degeneracy while interacting with biological material, their influence on metabolic processes in living organisms and the development of methods that enable to get this information are rather important and topical tasks of the present. The problems of nanotoxicology and biosafety of applied nanomaterials have become issues of primary importance recently which consequently results in the growing number of works in this field. The indices of immunobiological protection can serve as an indicator showing the affect of nanomatetials on human organism.

Aim: To estimate the impact of fullerene $C_{60}$ on morphofunctional properties of neutrophils. To achieve this goal blood neutrophils of apparently healthy donors were isolated by a standard technique in density gradient of Ficoll- Urografin. A suspension of fullerene $C_{60}$ (0.75 mg/ml) was thoroughly mixed and subjected to ultrasonic dispersion. By using a laser particle size analyzer SALD - 7101 (Shimadzu) demonstrated the presence of nanoparticles of 10 to 80 nm in the test suspensions was demonstrated. Neutrophil granulocytes ($2*10^6$ cells/ml) were incubated with fullerene $C_{60}$ (0.75 mg / ml) for 30 min at 37 °C. To study the reactive changes of neutrophil due to fullerene $C_{60}$ effect the scanning of their topography in semi-contact regime was carried out on the installation SOLVER BIOTM (NT-MDT, Zelenograd) using probes DNP (Veeco, USA). To visualize scanned objects the program Nova NT-MDT SPM Software (NT-MDT, Zelenograd) was used. In the software package Statistica (v.6.0), the statistical analysis of the results of measurements was condacted. The nonparametric Mann-Whitney test was used. A statistically significant increase in the diameter and height of the core, the body diameter of neutrophils was demonstrated ($p < 0.01$). Thus, the observed the change of morphometric parameters of neutrophils, such as changing the size of the nucleus and the cytoplasm, is an indication of their increased functional activity and may indicate a cytotoxic effect of $C_{60}$.

# Study of crack growth of nanomodified coatings

V.P. Pogodaev, A.V. Pogodaev, N.V. Tugovikov

[1] *FEFU, School of Engineering, Sub-Department of Welding production, city Vladivostok*

*Keywords: crack growth, nanomodified coatings*

Methods and tools to evaluate the reliability of products have played a role, as being one of the components of the quality of products it describes the ability to perform the functions specified in the conditions of use for a specified time with the preservation of certain properties. One way to improve reliability is to study the material properties and deformation processes occurring in it during the operation and lead to the destruction due to the emergence and development of cracks. The most effective experimental methods for assessing the level of the mechanical properties of welded joints with the required specifications include tests on cracking.

The concept of the fracture toughness of the material in the form of a limit value of stress intensity factor $K_{1C}$ follows from the structure of the stress-strain state arising in the vicinity of the crack tip in plane strain. If the plane strain in the vicinity of the crack tip in this body is not implemented, then the set in such a case, fracture toughness in terms of the stress intensity factor is denoted by $K_c$. Quantitative characteristic of the fracture of the material is a critical factor of intensity/stress in plane strain at the crack tip $K_{1C}$.

$K_{1C}$ determined by testing samples of the special pre-grown fatigue crack (GOST 25506-85). Methods according to GOST 25.506-85 not determine $K_{1C}$ for welds and coatings. The conditions stated by the ratio of the geometric dimensions of the sample. The nature of the material fracture toughness values determined experimentally, is largely dependent on the power circuit failure of the specimen with a crack, which is the basis of the experimental techniques.

To study the coating method is used Microindentation. Microindentation - one of the common methods of non-destructive analysis of the mechanical properties of solids. This method provides a quantitative value of fracture toughness (critical stress intensity factor - $K_{1C}$). For Palmqvist`s cracks fracture toughness value can be determined by $K_{1sp}$ formula:

$K_{1sp} = 0.035\ b_t s^{1/2}\ (E/b_t)^{0,4}\ (C/c\text{-}1)^{-1/2}$,

where c is the size of the print, with the length of Palmqvist`s crack.

For comparison, consider three methods for determining recovery factors:

1. The estimated on the structural parameter by Prof. G.V. Matokhin.

$$K_{1C} = \sqrt{\frac{\left(R_{MCHb} \cdot D\right)^{\left(\frac{1}{m}+1\right)} \cdot \pi \cdot 6{,}18 d_3}{g^{\left(\frac{1}{m}+1\right)} \cdot \sigma_T^{\left(\frac{1}{m}-1\right)}}}.$$

2. By GOST 25.506-85.
3. The method of kinetic indentation.

We can make the following conclusion:

1. Analyzed the methods techniques to determine the critical stress intensity factor.

2. Was developed experimental method of determining the critical stress intensity factor for coatings by kinetic indentation.

3. Conducted debugging techniques to determine the critical stress intensity factor based UltraMicroHardness Tester DUH-211S Shimadzu.

4. The proposed technique gives errors when compared with the GOST 25.506-85 about 10%.

# Molecular dynamics simulations in design of thermally-stable bimetallic clusters based on copper

V.S. Myasnichenko[*,1,2], M.D. Starostenkov [1]

[1] *ASTU, general physics dep., 46 Lenina pr. 656038, Barnaul, Russian Federation*
[2] *TDISIE SB RAS, 41 Russkaya st. 630058, Novosibirsk, Russian Federation*

(*) corresponding author: virtson@gmail.com

*Keywords: copper, bimetallic clusters, stability, molecular dynamics, substitutional atom*

## 1. Introduction

The modern intense researches of the structure and properties of metallic and bimetallic nanometer-sized clusters is motivated by fundamental questions regarding the role of system size and geometry on the properties of matter.

Understanding and controlling the structural properties and mechanical behaviors of these nanostructures are crucial for the practical application, in such areas as the rational design of novel materials with the given mechanical, electrical, magnetic and optical properties, low energy electronic devices and catalytic agents with controlled properties [1-3].

The paper deals with the results of molecular-dynamic simulation of the atomistic structures stability in bimetallic copper-based clusters, using many-body tight-binding interatomic potential.

## 2. Simulation methods

The peculiarities of the melting process for $Me@Cu_{N-1}$ (Me = Ag, Pb, Th, Ca, Sr) clusters with the smooth heating up from 1°K was simulated in a series of computer experiments. Two magic numbers N = 55 and N = 147 in case of which cluster has the cubooctahedron form with the central atom, are considered. This form is one of the least stable for monometallic fcc clusters [4-5].

All simulations have been performed using the Cleri–Rosato tight-binding (TB) interatomic potentials with parameters reported in the work [6]. This potential has been used in several studies of transition- and noble-metal bulk and cluster systems [7-9]. It is derived from Gupta's expression for the cohesive energy of a bulk material [10] and is generated by fitting experimental data to a pair potential containing repulsive pair and attractive many-body terms. The Cleri–Rosato potential parameters for all Me atoms are taken from [11]. The fixed radius of truncating – on the fifth coordination sphere inclusively is applied.

At least five equal experiments were done for each cluster type. The initial cluster arrangement was defined as a block of fcc crystal. The model system was then heated up to the temperature structurally–phase transition. Speed of temperature's change U = 1 K per 1 ps.

Such heating results in the transition of cluster from fcc solid to icosahedral state which was fixed on a saltus of a first coordination number and was confirmed based on the analysis of the radial distribution function of atoms *g(r)*. Symmetry in the immediate environment of atom was calculated by common neighbors analysis method [12].

The temperature in the course of simulation was defined by average of kinetic energy of atoms. The kinetic energy was calculated with a step on h time = 2.5 fs on the basis of high-speed Verlet algorithm [13]. Simulation was carried out in microcanonical ensemble on the basis of the methods explained in [14].

The obtained atoms configurations of the clusters were saved automatically in the database. It made it possible to combine the results obtained simultaneously by several computers and visually analyze the obtained structures. All simulations are executed in an authoring software [15].

## 3. Results

The results of our experiments for $Me@Cu_{54}$ and $Me@Cu_{146}$ clusters also are given in fig.1 and fig.2 respectively.

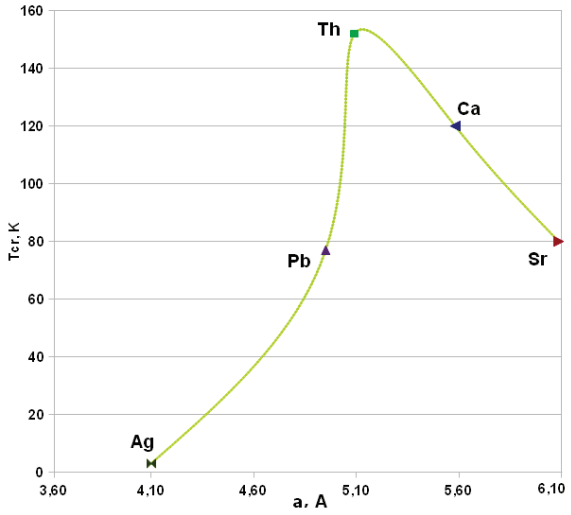


Figure 1. Changing of $T_{cr}$ for 55-atomic cluster.

The substitution of the central atom of copper by metal atom of bigger radius (or lattice constant a in Table 1) increases the critical temperature $T_{cr}$ of structural-phase transition in the fcc copper-based cluster.

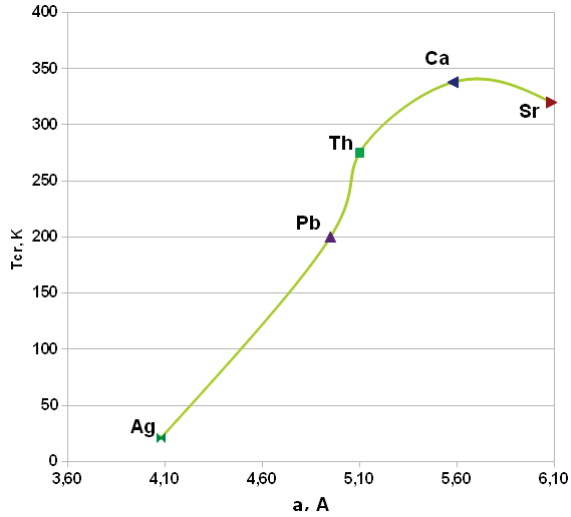


Figure 2. Increasing of $T_{cr}$ for 147-atomic cluster.

It is possible to draw an output that there is an optimum size for a substitutional atom. The maximum $T_{cr}$ value among the considered compositions is reached when using of a certain metal for substitution of central Cu atom. In this case, the formation of the icosahedral core creates more internal stress, then stress in pure copper cluster.

Table 1. Temperatures of structural-phase transition.

| Me | a (Å) | $T_{cr}$ for N=55 | $T_{cr}$ for N=147 |
|---|---|---|---|
| Cu | 3,615 | 2 | 20 |
| Ag | 4,086 | 3 | 21 |
| Pb | 4,950 | 76 | 200 |
| Th | 5,084 | **152** | 275 |
| Ca | 5,582 | 120 | **378** |
| Sr | 6,085 | 80 | 320 |

## 4. Conclusions

The possibility of essential increasing of the structural-phase transition temperature for unstable fcc cluster was shown in the molecular-dynamic research of copper-containing bimetallic clusters.

*This study was partially supported by RFBR, research project No. 12-02-31135.*

## 5. References

[1] A. W. Woods and S.S. Cardoso, *Nature*. **385** (1997) 518.

[2] X. Zheng, X. Shi, Z. Dai, Z. Zeng, *Physical Review B*. **74** (2006) 085418.

[3] V.S. Myasnichenko, M.D. Starostenkov, *Applied Surface Science*. **260** (2012) 51–53.

[4] V.S. Myasnichenko, M.D. Starostenkov, *Fundamental problems of the modern materials science*. **8** (2011) 49–52 [in Russian].

[5] V.S. Myasnichenko, M.D. Starostenkov, *Fundamental problems of the modern materials science*. **9** (2012) 284-286 [in Russian].

[6] F. Cleri, V. Rosato, *Physical Review B*. **48** (1993) 22–33.

[7] G. W. Turner, R. L. Johnston, and N. T. Wilson, *J. Chem. Phys*. **112** (2000) 4773 .

[8] R. Ferrando, A. Fortunelli, R.L. Johnston, *Physical Chemistry Chemical Physics*. **10** (2008) 640.

[9] X. Wu, G. Wu, Y. Chen, Y. Qiao, *The Journal of Physical Chemistry A*. **115** (2011) 13316–23.

[10] R. J. Gupta, *Phys. Rev. B*. **23** (1981) 6265.

[11] M.A. Karolewski, *Radiation Effects and Defects in Solids*. **153** (2001) 239-235.

[12] J.D. Honeycut, H.C. Andersen, *J. Phys. Chem*. **91** (1987) 4950.

[13] D. Frenkel, B. Smit, Understanding molecular simulation: from algorithms to applications. San Diego: Academic Press, 2002.

[14] M.P. Allen, D.J. Tildesley, Computer Simulation of Liquids. Oxford: Clarendon Press, 1987.

[15] V.S. Myasnichenko, Molecular dynamics simulation and bio-inspired optimization of binary and ternary metallic nanostructures, Russian registration certificate № 2011615692, July 20, 2011.

# AUTHOR INDEX

# AUTHOR INDEX

# CONTENT

# CONTENT

# ADVERTISING MATERIALS

**State-of-art QC and research Field-Flow Fractionation systems for nano- and microparticles separation and characterization from FFF-technology inventor and industry leader**

# *AF4 / HF5 / Centri FFF / Thermal FFF / Splitt FFF*

Completely integrated modular systems for a number of up to date techniques for particle separation in the range from couple of nanometers to hundreds of microns based on Field-Flow Fractionation principle invented by Prof. Calvin Giddings.
Based only on simple physical principle, FFF is a family of extremely convenient techniques allowing high-precision separation of particles by their size in the most known solvents without using any columns or other stationary phase systems in metal-free or stainless steel channels.

**Asymmetric Flow Field-Flow Fractionation (AF4)**
in Ambient, Mid-temperature (+5..+90°C) and High Temperature (+20..+200°C) laboratory and semi-preparative versions

**Hollow Fiber Flow Field-Flow Fractionation (HF5)**
made commercially accessible by Postnova only in 2011

**Centrifugal Field-Flow Fractionation (CF3)**
for nanoparticles separation based not only on volume but on mass.

**Thermal Field-Flow Fractionation (TF3)**
for ultra-high mass polymer particles separation in thermal field

**Split Flow Thin Cell Fractionation (SPLITT)**
for preparative high throughput gravity separation of microparticles

System includes eluent preparation and flow organization modules with **FOCUS** and **Slot-outlet** patented technologies, interchangeable FFF-modules and great variety of detectors (UV, DRI, FL, DLS etc.), including recent in house award winning **21-angle MALS**. All of the system modules are controlled by **NovaFFF** software, which allows convenient acquisition of all obtained data.

The systems can be combined with the most known ICP-MS instruments for immediate obtaining elemental composition of particles through the all particle size distribution.

*More information in English: www.postnova.com*

---

**SocTrade** is a Russian company based in Moscow specialized in sales and service of different laboratory equipment in the fields of research and quality control. During more than 25 years of existence we obtain the reputation of a reliable partner for many customers and manufacturers.

**SocTrade** is proud to represent innovative **Postnova Analytics GmbH** FFF-systems in Russia and make any support and promotion for this 21st century technology, as one of the main our task is to introduce newest analytical techniques and technologies to Russian market.

*More information in Russian: www.soctrade.com*

# ООО "Реолгрейд сервис" - авторизированный дистрибьютор компании "Agilent Tehnologies", США.

**Компания “Реолгрейд сервис” осуществляет:**

- комплексное оснащение лабораторий различного профиля аналитическим и вспомогательным оборудованием;
- поставки и запуск оборудования зарубежных производителей, не имеющих представительства в Российской Федерации;
- гарантийное и послегарантийное обслуживание поставляемого оборудования.

**Спектр поставляемого оборудования:**

Agilent Technologies

Широкий спектр самого современного оборудования для молекулярной спектроскопии и хроматографического анализа крупнейшего производителя Agilent Technologies:

- Атомно-абсорбционные спектрометры;
- Оптико-эмиссионные спектрометры;
- ИК-Фурье микроскопы/ИК-Фурье спектрометры;
- Портативные ИК-Фурье анализаторы;
- УФ-Вид спектрофотометры;
- Спектрофлуориметры;
- Газовые, жидкостные и гель проникающие хроматографы;
- Расходные материалы для газовой и жидкостной хроматографии;

RENISHAW apply innovation™

Конфокальные Рамановские микроскопы Renishaw inVia;

DAIHAN Scientific

Общелабораторное оборудование Daihan Scientific.

ООО “Реолгрейд Сервис”
630559 Россия, Новосибирская обл., Наукоград Кольцово ул. Вознесенская, 4 офис 53
тел/факс: (383) 306-37-97, 291-71-05
web: www.reolgrade.ru, e-mail: ovking@yandex.ru, service@reolgrade.ru (сервисная служба).

Reolgrade service

Agilent Technologies

*Авторизированный дистрибьютор*

**ООО “Реолгрейд Сервис” (г.Новосибирск) – аналитическое и лабораторное оборудование**

# СПЕКТРАЛЬНОЕ И ХРОМАТОГРАФИЧЕСКОЕ ОБОРУДОВАНИЕ Agilent Technologies:

## Атомно-абсорбционные спектрометры

Атомно-абсорбционные спектрометры (ААС) Agilent отличаются производительностью, удобством в эксплуатации и высочайшей надежностью. Они широко применяются как для сложных аналитических задач, так и для поточного анализа в лабораториях. Топовые модели линейки ААС ***Agilent 240FS/280FS*** - самые быстродействующие и высокопроизводительные ААС с пламенным атомизатором в мире. ***Agilent Duo*** - уникальный, единственный в мире приборный комплекс, позволяющий проводить истинно параллельный анализ методами пламенной и электротермической атомизации.

## Оптико-эмиссионные спектрометры

Оптические эмиссионные спектрометры с индуктивно-связанной плазмой (ИСП-ОЭС) ***серии 710*** фирмы Agilent обладают превосходными характеристиками. Они предназначены для лабораторий поточного анализа со средним пробопотоком. ИСП-ОЭС ***серий 720 и 730*** фирмы Agilent отличаются превосходными рабочими параметрами, быстродействием и адаптабельностью. В соответствии с аналитическими задачами возможен выбор оптимизированной осевой (710/720/730) или радиальной (715/725/735) конфигурации.

## ИК-Фурье микроскопы/ИК-Фурье спектрометры

Совершенный оптический дизайн ИК-микроскопов, в сочетании с высокой светосилой спектрометров Agilent, образуют непревзойденную по возможностям и чувствительности комбинацию. ***Cary 640 FTIR*** – доступный по цене ИК-Фурье спектрометр с улучшенными характеристиками, выпускаемый с двух версиях: для работы в ближней и средней ИК области. Серия ИК-спектрометров ***Agilent Cary 660/670/680*** FTIR изготовлена на базе интерферометра Майкельсона с динамической юстировкой и может перекрывать широкий спектральный диапазон при наличии соответствующих источников, светоделителей и детекторов.

## Портативные ИК-Фурье анализаторы

Портативные ИК-фурье анализаторы ***4100 Exoscan*** и ***4200 Flexscan*** обладают высокой производительностью, устойчивостью к внешним воздействиям и могут использоваться в полевых условиях при анализе материалов, поверхностей, молекулярном анализе камней, минералов, грунтов и твердых веществ. Интерфейс на основе диффузионного отражения не требует предварительной подготовки образца. Для анализаторов доступна геофизическая базы данных коэффициентов диффузионного отражения, что позволяет проводить быструю идентификацию состава образца.

## УФ-Вид спектрофотометры

Линейка УФ-ВИД спектрофотометров включает в себя приборы различных классов. ***Cary 60*** - уникальный по своим техническим характеристикам прибор для самого широкого круга спектрофотометрических задач от рутинного анализа до уникальных специфических анализов. Спектрофотометры ***Cary100/300*** с двухлучевой схемой предназначены для рутинной лабораторной работы. Спектрофотометр ***Cary 5000*** с инновационной технологией PbSmart, позволяющей расширить спектральный диапазон в ближнюю ИК область до 3300 нм.

**ООО “Реолгрейд Сервис”**
**630559 Россия, Новосибирская обл., Наукоград Кольцово ул. Вознесенская, 4 офис 53**
**тел/факс: (383) 306-37-97, 291-71-05**
**web: www.reolgrade.ru, e-mail: ovking@yandex.ru, service@reolgrade.ru (сервисная служба).**

Reolgrade service

Agilent Technologies

*Авторизированный дистрибьютор*

**ООО “Реолгрейд Сервис” (г.Новосибирск) – аналитическое и лабораторное оборудование**

## Спектрофлуориметры

***Cary Eclipse*** - спектрофлюориметр с двумя сверхбыстрыми сканирующими монохроматорами, построенный на основе пульсирующей ксеноновой лампы и оптики Шварцшильда. Cary Eclipse обеспечивает работу в режимах измерения флюоресценции, фосфоресценции, хеми- и биолюминесценции. Сочетание мощности светового импульса лампы с оптикой Шварцшильда обеспечивает максимальную чувствительность прибора, повышает светоотдачу более чем в 100 раз и создает световую иммунность к комнатному освещению при открытом кюветном отделении.

## Хроматографическое оборудование

Серия хроматографов ***Agilent 1200*** имеет модульную конструкцию, позволяющую формировать конфигурации, наиболее подходящие по требованиям прикладных задач любой сложности. Жидкостные хроматографы Agilent – это превосходные завершенные системы, рассчитанные на самую высокую производительность с одновременным улучшением качества хроматографических результатов. В списке оборудования представлены линейка высокоэффективных газовых хроматографов от микро- до потоковых промышленных хроматографов.

## Расходные материалы для Хроматографии

В компании “Реолгрейд сервис” представлены расходные материалы для газовой и жидкостной хроматографии.

Это капиллярные колонки для газовой хроматографии, колонки для жидкостной хроматографии для аналитического или препаративного применения, предколонки, держатели предколонок, фитинти, сорбенты, стандарты, тестовые смеси, шприцы для ввода проб, виалы и прочие товары.

RENISHAW apply innovation™

## Рамановский микроскоп ReniShaw inVia

Конфокальный рамановский микроскоп Renishaw inVia – инструмент, позволяющий решать широкий круг аналитических задач. Renishaw inVia обеспечивает высокую скорость сканирования и получение рамановских и фотолюминесцентных спектров в диапазоне от 10 до 10000 $см^{-1}$. Конфокальный режим позволяет снимать спектры с объектов, находящихся в толще матрицы, без их разрушения. Комбинация прибора с атомно-силовым или электронным сканирующим микроскопом, позволяет проводить спектрохимическое картирование образца с высочайшим пространственным разрешением.

DAIHAN Scientific

## Лабораторное оборудование Daihan Scientific

В ассортименте компании “Реолгрейд сервис” представлено общелабораторное оборудование фирмы Daihan Scientific, Корея. Перечень оборудования включает в себя: автоклавы, бани водяные и термостаты, бани масляные, ванны ультразвуковые, вортексы и шейкеры, гомогенизаторы, дистилляторы, бидистилляторы, инкубаторы, климатические камеры, лопастные и магнитные мешалки, печи муфельные, плитки, термостаты и криотермостаты циркуляционные, шкафы сушильные.


ООО “Реолгрейд Сервис”
630559 Россия, Новосибирская обл., Наукоград Кольцово ул. Вознесенская, 4 офис 53
тел/факс: (383) 306-37-97, 291-71-05
web: www.reolgrade.ru, e-mail: ovking@yandex.ru, service@reolgrade.ru (сервисная служба).

# Современный рентгеновский анализ в промышленности


## Рентгенофлуоресцентный волнодисперсионный спектрометр S8 TIGER

- Определение химического состава материалов
- Простая и быстрая пробоподготовка
- Анализ элементов от бериллия до урана
- Диапазон измеряемых концентраций от долей ppm до 100%
- Воспроизводимость 0,05 % отн.
- Быстрый обзорный анализ и получение полуколичественных результатов без использования стандартных образцов
- Современное программное обеспечение SPECTRA$^{PLUS}$

## Настольный рентгеновский дифрактометр D2 PHASER

- Качественный и количественный фазовый анализ
- Определение степени кристаллличности
- Характеристики фазы (параметры ячейки, размер кристаллитов, микронапряжения)
- Определение кристаллических структур
- Широкий спектр прободержателей стандартного промышленного размера (Ø 51.5 мм) для различных задач

## Рентгеновский дифрактометр D4 ENDEAVOR

- Фазовый анализ большого количества проб
- Быстрый анализ при помощи позиционно-чувствительного детектора
- Интегрирование в производственные линии
- Дифрактометр D4 ENDEAVOR специально разработан для автоматизированной системы контроля качества в промышленности

Innovation with Integrity

XRF/XRD

www.bruker.ru

**ООО Брукер**
Москва, 119017,
Пятницкая ул. 50/2 стр. 1
Тел.: +7 (495) 517-92-84
+7 (495) 517-92-85
e-mail: xray@bruker.ru

Санкт-Петербург Тел.: +7 (812) 323-46-09
Екатеринбург Тел.: +7 (343) 345-85-92
Казань Тел.: +7 (843) 290-81-89
Новосибирск Тел.: +7 (983) 121-63-89

BRUKER

# aurora Elite –
## самый чувствительный ИСП-МС в мире

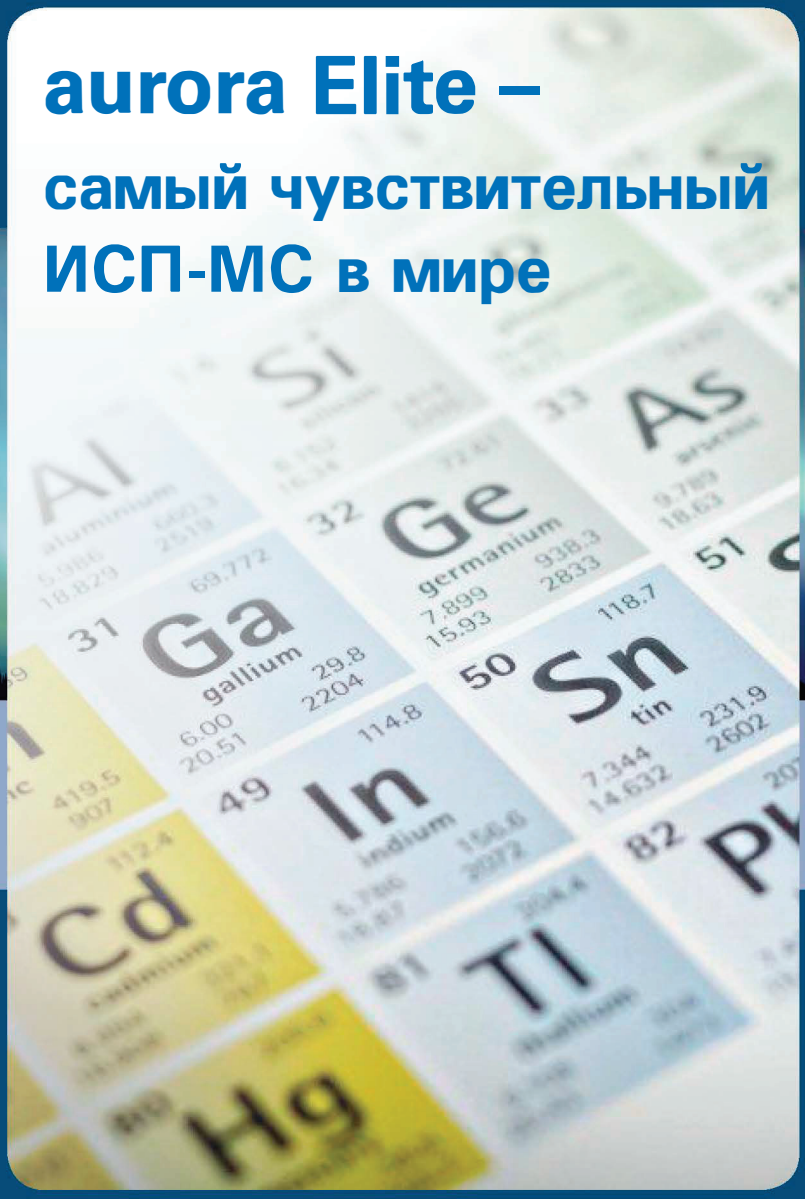



www.bruker.com

- **Непревзойденная чувствительность**
- **Низкий уровень оксидных помех**
- **Эффективное подавление интерференций**
- **Полностью цифровой детектор с динамическим диапазоном более 9 порядков**

Новейший масс-спектрометр aurora Elite компании Bruker позволяет проводить ультраследовой элементный анализ без особых усилий. Независимо от Ваших требований, с нашей системой ИСП-МС Вы легко и быстро справитесь с любой задачей!

Для получения более подробной информации и демонстрации систем обращайтесь к нам!

ООО „Брукер“
г. Москва
8(495) 517-9284
8(495) 517-9285

г. Новосибирск
8(383) 319-0789
8(383) 333-2241

ms@bruker.ru
www.bruker.com

ICP-MS

Innovation with Integrity

BOOK OF ABSTRACTS

Second International School-Conference
“Applied Nanotechnology & Nanotoxicology”

Editor: Dr. Aleksey A. Vedyagin

Most abstract are reproduced as presented camera-ready texts for which the authors bear full responsibility. Some abstracts underwent minor technical editing.

Compiled by: Aleksey A. Vedyagin
Irina V. Tokareva

Подписано в печать 01.08.2013. Заказ №48.
Формат 60x84/8. Усл. печ. л. 24. Тираж 140 экз.
Отпечатано в Издательском отделе Института катализа СО РАН.
630090, Новосибирск, просп. Академика Лаврентьева, 5.
http://catalysis.ru/